THESIS SUBMITTED FOR THE DEGREE OF

DOCTOR OF PHILOSOPHY

AT THE UNIVERSITY OF OXFORD

STELLAR ABUNDANCES AND NUCLEOSYNTHESIS

Richard S. Ellis

Wolfson College

Trinity Term 1974

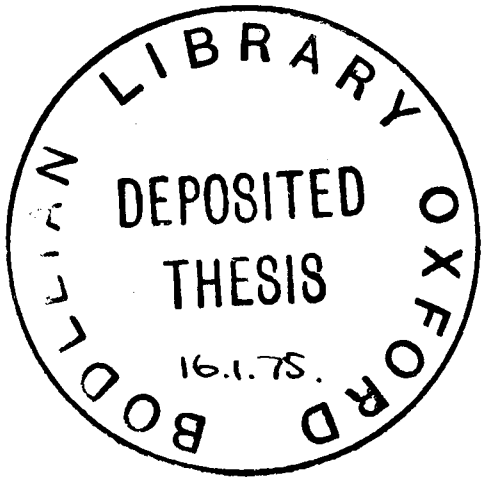

DEDICATION:

To little Derek and his
blissful ignorance of
stellar astrophysics

PERSONAL COMMENT:

Derfydd aur, a derfydd arian
Derfydd melfed, derfydd sidan,
Derfydd pob dilledyn helaeth;
Eto er hyn ni dderfydd hiraeth.

from 'Hen Benillion'
(ed. T.H. Parry-Williams)
Author unknown

CONTENTS

CONTENTS (continued)

CONTENTS (continued)

Abstract

Stellar abundances are essential parameters for many branches of astronomy. They are also particularly important as tests for theories of nucleosynthesis. Despite the encouraging results from band photometry, detailed spectroscopic analyses are still important in furthering knowledge of physical processes occurring in a variety of stellar objects. This thesis presents the first of a series of absolute abundances for the late-type giant Arcturus. The broader aim of the investigation is to make Arcturus a reliable standard star, and also it is hoped that equilibrium assumptions in its atmosphere can be scrutinised.

An essential prerequisite to a model atmosphere is the continuum flux curve. Certain discrepancies near the flux maximum prompted the construction of a spectrum scanner which was used to obtain fluxes of Arcturus at the Wise Observatory, Israel. All known flux results have been collated for Arcturus, and the continuum flux curve is presented for the region 3800 Å to 13 microns.

Ways of measuring the effective temperature are discussed. The only adequate method for Arcturus and other cool stars involves comparing the relative energy distribution with model predictions. As all present models fail to account for the flux below 5000 Å, this method is not as accurate as it could be. A value of $4450 \pm 50^{\circ}K$ is adopted for Arcturus; most of this error is due to the unrealistic nature of the models.

Using this temperature a grid of line-blanketed models with different gravities has been constructed. The suggested gravity-indicator requires a precise value for the microturbulence, and for this preliminary analysis a model with log g = 1.7 was selected. This value, reported by several investigators, is later shown to be fairly realistic.

Uncertain oscillator strengths continue to plague abundance work in astronomy, though the Oxford furnace is now producing precision values for several elements. Using this furnace a series of neutral titanium lines of direct astrophysical interest have been measured, and they are accurate to at least $\pm$0.03 dex(7%) on a relative scale. Considerable effort is still needed in establishing accurate absolute scales however; these results have been made absolute by referring to theoretical and observational lifetimes.

The internal consistency of the Ti I values has been verified by studying the solar abundance of titanium. By restricting the analysis to good quality weak lines, uncertainties in damping and microturbulence have been avoided. A log abundance of 4.81 ± 0.03 is reported (on the log H = 12.00 scale).

For the Arcturus analysis, a few iron lines have also been included. In this star the abundances are very sensitive to the value assumed for the microturbulence. The empirical nature of this parameter is emphasised. A value of 2.1 ± 0.2 km sec^{-1} was found by demanding an unique abundance for all lines. Using this velocity gave absolute abundances of:-

$$\log\ n(Ti) = 4.42 \pm 0.15$$

$$\log\ n(Fe) = 7.37 \pm 0.10$$

With suitable solar abundances these imply $[Ti/H] = -0.39 \pm 0.07$, $[Fe/H] = -0.33 \pm 0.10$.

Theories accounting for the origin of iron-peak elements are discussed. Explosive Silicon burning cannot account for all the observed isotopes, and the equilibrium process has been re-introduced to explain some anomalies. These theories are examined in relation to supernova models and Galactic evolution, and also with regard to the broader purpose and prospects for measurements of stellar abundances.

CHAPTER 1

INTRODUCTION

1.1 Abundances of chemical elements

A great deal of effort has been directed towards the accurate measurement of chemical abundances in the Universe. As the results are usually presented as an 'ultimate answer' their relevance is not always self-evident. This is demonstrated by the large volume of literature reporting abundance peculiarities in isolated, perhaps insignificant, astronomical objects. As this thesis might be criticised as an example of such ill-directed research, it is pertinent to ask at the outset; Why bother to measure abundances?

Quite apart from wishing to quantitatively understand the Universe, its material and its history, abundances are necessary input data for scientific disciplines as diverse as cosmology and seismology. Accurate astronomical abundances, more germane to this thesis, are vital for determining structures of stellar atmospheres and interiors, and as these affect evolutionary models, the seemingly insignificant abundances become quite indispensable.

Of even greater importance is the role that astronomical and terrestrial abundances play in furthering knowledge concerning the origin and distribution of the chemical elements, and how the nucleosynthesis theories can be connected to Galactic history. In this context therefore an abundance curve is the ultimate test for a nucleosynthesis theory. As these theories themselves may rely on stellar models, one can see that the topic of abundances envelopes almost every aspect of astronomy.

1.2 Stellar abundances

Nucleosynthesis predictions are usually compared with solar-system abundance curves (e.g. Suess and Urey 1956, Cameron 1963,

1963, 1974) derived mainly from meteoritic, lunar and terrestrial rock samples. Stellar abundances have been regarded as 'second-best' for this purpose because of large uncertainties attached to the results. Yet it is clearly desirable to continue measuring stellar abundances, not only to investigate ways of reducing these uncertainties, but also to find out whether the solar-system abundance mix is representative of that in other regions of the Galaxy. Despite the lack of precision, stellar atmospheres are far more homogeneous than rock samples, which show staggering differences from place to place. It should therefore be noted that the composite abundance curves of Cameron, based mainly on meteoritic data, depend critically on the way these inhomogeneities are allowed for.

This is not the place to describe in detail the procedures adopted for extracting abundances from stellar spectra and this cursory introduction must necessarily use terminology defined in later chapters. Nevertheless a brief criticism of present methods is needed to explain the purpose of this thesis.

Classical abundance investigations (e.g. Menzel 1936) used a unified theory known as the 'curve of growth'. This curve relates the strength of an absorption line to the product Nf, where N is the abundance of the relevant atomic energy level for the element, and f is a quantity called the oscillator strength or f-value needed to explain selective absorption. As the shape of the curve of growth (c.o.g.) can be predicted according to various theories of line-formation (v.der Held 1931), a comparison between the observational and theoretical curves yields, among other things, the abundance N.

It was quickly realised that the scatter on the observed c.o.g. made it very difficult to describe the curve with any certainty. Although line measurements were spoilt by poor spectra, inaccurate f-values were mainly to blame. These f-values, sometimes estimated theoretically but more usually measured in the laboratory, have hindered

direct astronomical abundance work for many years. A great deal of effort has been directed towards their accurate measurement but it is still quite evident that what had been thought of as reliable f-values even very recently, are in fact hopelessly in error.

For these reasons astronomers have preferred to perform differential analyses. Given a solar abundance, a differential c.o.g. can be used that avoids f-values altogether. Of course any error in the solar analysis (which will have used f-values) is transferred, but even so the method is at first sight quite plausible. It does have some limitations however. The curve of growth is not unique: lines of different excitation not only form in different regions of the atmosphere but are broadened to different extents. The ideal solution would be to calculate a curve of growth for each line using a physical model of the stellar atmosphere, though this demands accurate f-values. As the average astronomer does not have the patience to plough through the mass of published f-values (nearly all of which disagree with one another) differential analyses are still in favour.

With f-values of increased precision now available from careful work (e.g. Blackwell et al 1974a), and also with the provision of several good model atmosphere programs, it is perhaps time that line-by-line methods were used to establish abundance standards of different spectral types with which simple differential analyses can be quickly yet accurately compared.

All above methods require good quality high dispersion spectra and are referred to as 'detailed analyses'. It would be unfair to omit to mention the exciting and useful work made through narrow and intermediate bandpasses, isolated either spectroscopically or with interference filters. These methods (reviewed by Strømgren 1974) can offer quick yet reliable results for many stars. As examples one can cite the extensive surveys of Williams (1971ab) Griffin and Redman (1960), and more recently the work of Osborn (1973) using the David

Dunlap System described by McLure (1973). Such studies are also invaluable in providing information for stellar classification schemes (see Morgan and Keenan 1973). From the point of view of nucleosynthesis and Galactic evolution, the relevance of the band results is already well known (Spinrad and Taylor 1969, Williams 1971b).

Notwithstanding these remarks there is still a need for detailed analyses, to check and calibrate these band systems and also to investigate and understand the many aspects of stellar spectroscopy and line theory that detailed analyses unavoidably involve.

1.3 Arcturus and the aims of this thesis

"I name this standard Arcturus,
God bless her, and all who sail in her"

The need for standard abundance stars has been emphasised. To avoid unnecessary accumulation of errors arising from long chains of differential analyses, it is desirable to use absolute f-values and perform an absolute abundance analysis for each standard star.

As all standards should have good spectra, the choice is immediately restricted to a handful of bright stars. In the hotter domain, work is progressing with models for Sirius (Fowler 1974) and Procyon (Strom and Kurucz 1966, Darius 1974) though abundance results have not yet been given.

The position with cool stars is slightly more complicated. The lower temperature results in a confused line spectrum making model construction a difficult task. For giants with low pressures and extended atmospheres many of the conventional assumptions of line and model theories may be invalid. Nevertheless a start must be made somewhere and cool stars are not only challenging in the above respects, but are also important in understanding the later stages of stellar evolution.

For this work the star Arcturus αBoo K2III (m_v =-0.1) has been chosen. This bright nearby giant is in many ways an ideal standard. Griffin (1968) obtained an excellent spectrum of dispersion 1-1.5 Å/mm, which is widely available and was in fact intended to serve as a standard reference. The only other bright cool star under detailed study is Betelgeuse MI (m_v = +0.7) (Faÿ and Johnson 1973) whose lower temperature introduces many molecular bands making model construction even more difficult. Furthermore as it is variable and fainter than Arcturus, its flux curve will be more uncertain, and its spectrum will not match the quality of Griffin's.

As one might expect Arcturus has already been studied extensively (e.g. Gasson 1966, Griffin and Griffin 1967, Upson II 1973) though nearly always differentially with respect to the sun. There is certainly a demand for absolute abundances for this star, particularly for the iron group (Wegner 1974) and the main aim of this work is to provide these using f-values determined in the absorption furnace at Oxford. It will also be possible, eventually, to test assumptions such as thermodynamic equilibrium, which may not hold in the lower density regions of the atmosphere of this star.

For this thesis the main objective is to set out the groundwork for the above research. In particular:-

1. A model atmosphere is needed for Arcturus. This demands an observed energy distribution for the star which the model should accurately reproduce.

2. A start must be made on the enormous task of measuring precision f-values for the iron-group elements. Titanium was chosen as the first of a large number of elements now under investigation. The lines to be measured should be closely tailored to abundance work in cool stars, and an accurate absolute scale for these f-values is also needed.

3. A preliminary set of absolute abundances for Arcturus can then be established using the available f-values. An error analysis would be particularly helpful in showing where future investigations should be performed with greatest care.

As the Titanium f-values will hopefully be the best available, a solar Titanium abundance would also be of interest. This would enable a comparison with other Arcturus/solar abundances in the literature.

CHAPTER 2

SCANNER OBSERVATIONS OF ARCTURUS

2.1 The importance of stellar fluxes

In the measurement of radiation the terms 'intensity' and 'flux' have several connotations. Of interest here, however, is the specific intensity I_λ, which is the radiant energy crossing a unit area oriented normal to the beam, into unit solid angle, in unit wavelength interval & unit time. Thus if θ is the angle between the normal to a surface $d\sigma$ and the direction of a solid angle $d\omega$, then the energy dE_λ in time dt and wavelength interval $d\lambda$ is generally given by:

$$dE_\lambda = I_\lambda (z, \theta, \phi) \; d\sigma \; \cos\theta \; d\omega \; d\lambda \; dt \qquad (2.1)$$

where the spatial variation of I_λ is given by two angles (θ, ϕ) and a distance z from some reference level. In stellar atmospheres the assumption is usually made that the plane-parallel layers are homogeneous, and thus there will be no azimuthal (or ϕ -) dependance. Therefore for a given level I is a function of θ only.

The flux is defined as the net rate of energy flow across unit area, obtained by integrating dE_λ over all solid angles, viz:

$$\mathcal{F}_\lambda = \oint I_\lambda \cos\theta \; d\omega \qquad (2.2)$$

A quantity sometimes called flux or astrophysical flux leads to confusion, and is here referred to as the surface mean intensity. This weights the intensity according to the area projected and is defined by:

$$F_\lambda = \oint I_\lambda(\theta) \; \cos\theta \; dw \Big/ \oint \cos\theta \; dw \qquad (2.3)$$

thus for z-axis symmetry $\mathcal{F}_\lambda = \pi F_\lambda \qquad (2.4)$

In this thesis when referring to 'flux' the quantity $\mathcal{F}_\lambda$ is implied and written as πF_λ in all equations to avoid any possible confusion. The total flux over all wavelengths is then:

$$\mathcal{F} = \pi F = \int_0^\infty \pi F_\lambda \; d\lambda \qquad (2.5)$$

Deep inside a star the density of material is high enough for thermodynamic equilibrium, and the specific intensity is given by the

Planck function for a black body:

$$I_\lambda = B_\lambda(T) = \frac{2hc^2}{\lambda^5} \frac{1}{(e^{hc/\lambda kT} - 1)} \qquad (2.6)$$

where T is the temperature and h,c,k are fundamental constants. Because of the high density the photons emitted are soon absorbed by various processes. Towards the surface the temperature and density drop and thermodynamic equilibrium is no longer possible. However if the atmosphere is stratified in temperature it may be possible to assume a local thermodynamic equilibrium (LTE) for each layer and temperature. The intensity of emitted radiation at that level can then still be given by (2.6) using the relevant temperature.

If photons of all wavelengths escaped from the same level then the radiation would approximate to a black body distribution at the appropriate temperature, but the material in the atmosphere absorbs more at certain wavelengths and where the absorption coefficient or 'opacity' is greater the photons originate higher up in the atmosphere where T and $B_\lambda(T)$ are less. Consequently the flux at that wavelength is reduced. In the absence of LTE B_λ is replaced by an analogous function S_λ called the source function. The argument still generally holds however, and the detailed equations are discussed under the construction and use of model atmospheres in Chapter 4.

The distribution of flux with wavelength is called the flux curve and it depends basically on two parameters, temperature and opacity. A comparison between theory and observations can yield useful information about both quantities, though the important absorbers are generally understood and the main aim of measuring stellar fluxes has been to determine quantities related to the distribution of temperature in the atmosphere. Of particular significance is the effective temperature T_e, related to the total flux $\mathcal{F}$ by Stefan's law

$$\pi F = \mathcal{F} = \sigma T_e^4 \qquad (2.7)$$

This quantity is more useful than say, the surface temperature, as it is the most important parameter of a model atmosphere defining the total flux the model must produce. It is shown in Chapter 4 that T_e

can be determined by several methods including the use of equation 2.7; all methods depend on an accurate knowledge of the flux curve however.

At this point a distinction must be made between the continuum flux and the observed flux. For a cool star these will not be the same because of the many absorption lines present in the spectrum which absorb a significant proportion of the energy thereby reducing the emerging flux. Since the model atmospheres generally predict continuum fluxes ie. without lines, this effect known as 'line-blanketing', must be allowed for. This can be done by using a high dispersion spectrum of the star and measuring the energy blocked by the lines in the wavelength regions where comparisons are to be made.

Although the determination of T_e (or a related temperature index), has been the main motive for measuring stellar fluxes, detailed features in the flux curves of various stars have led to important findings in many branches of astronomy. Generally if the bandwidths $\triangle\lambda \leqslant 50$ Å then the photometry is termed 'narrow-band' photometry and although such work gives more precise information the method is only suitable for the brighter stars where there is plenty of energy available. For fainter stars wider bands are necessary and although detail may be lost, the broad band (> 500 Å) photometry of Johnson et al (1967) for example, has given general information about many faint stars.

In this chapter and that following, the flux curve of Arcturus is discussed. For Arcturus the results of narrow-band photometry are more important, though the broad-band work will also be used. This chapter deals mainly with the results obtained by the author and co-workers at the Wise Observatory, Israel using a spectrum scanner built and designed at Oxford. The need for these observations is also discussed. Establishing a flux curve for Arcturus based on all the observations (including the author's), and correcting the flux curve for line blanketing is discussed in the next chapter.

2.2 Previous measurements of the flux from Arcturus

As Arcturus is bright and cooler than the Sun, the flux curve has been studied extensively, usually with the aim of establishing the

absolute flux outside the Earth's atmosphere. Such spectrophotometric standards are useful in that absolute fluxes of other stars can then be obtained directly by comparison.

Altogether the region 3300 Å to 13 microns has been studied, although most effort has been concentrated in the visible region where the flux is greatest and most important for determining the effective temperature. Table 2.1 lists the various data available, the wavelength range considered, and the bandwidths used.

Detailed scanner observations are restricted to the region 3300 - 9000 Å, and beyond 2 microns the only detailed measurements are those of Gillett et al (1968). However, the spectrum has been fairly comprehensively covered apart from the difficult region between 1.4 & 1.8 microns. Here ground-based observations are severely hampered by extensive water-vapour absorption in the Earth's atmosphere. The only measurement here at present is due to Walker (1969), but with the current interest in space astronomy there is hope that our knowledge of this region may be supplemented in the near future. The importance of the region lies in the fact that theory predicts a sub-maximum at this point in the flux curves of cool stars because of the minimum in the absorption coefficient of the negative hydrogenion. This point is quantitatively investigated in the next chapter.

In the visible region the fundamental scanner measurements are due to Willstrop (1965), who has reduced his observations to absolute values without the use of another standard. Such 'primary' results usually involve calibrating the flux at the Earth's surface with a standard lamp to allow for instrumental absorption, and meticulously correcting the results for atmospheric extinction. Willstrop's results initially cover the region 4000 - 6500 Å but he has kindly supplied additional unpublished data extending the range to 3300 and 6900 Å. The internal consistency in the published data is quite good; results on different nights differ by less than 4%. The quality of the unpublished results is not so good.

The other scanner results are secondary measurements; that is, absolute fluxes have been found by using a primary standard. Komarov &

Table 2.1

Fluxes of Arcturus

Source	Wavelength region	Bandwidth etc.
This work	3697 - 8817 Å	24--48 Å
Willstrop(1965)	3300 - 6900*	50
Komarov & Pozigun (1970)	4000 - 9000	50
Kharitonov & Knyazeva(1969)	3450 - 7250	15--20
Johnson(1963,1965), et al(1966)	0.36 - 10.2 μ	U-N colours
Walker(1969)	0.36 - 2.21	7 colours
Johnson et al(1967)	0.33 - 1.10	13 colours
Gillett et al(1971)	3.50 - 11.0	4 colours
Gehrz & Woolf(1971)	3.50 - 11.0	4 colours
Gillett et al(1968)	2.80 - 13.0	

* range includes unpublished results

Pozigun (1970) for example, used αLyr, η U Ma, and β Ari as standards. They scanned beyond Willstrop's fluxes to 9000 Å and are the main source of narrow band fluxes in the near infra-red. Kharitonov and Knyazeva (1968) used α Lyr and γ Ori as standards and scanned notably in the ultraviolet to 3450 Å. The secondary data is not as detailed as that of Willstrop; Kharitonov & Knyazeva present fluxes for every 100 Å in the range considered, Komarov & Pozigun for every 50 Å, whereas Willstrop scanned at intervals of 25 Å.

Stickland (1970, 1971) has drawn attention to possible errors incurred in the use of current spectrophotometric standards. The favourite standard would appear to be αLyr (Vega) and although this star must surely be a poor choice with such a large Balmer discontinuity it has been repeatedly studied in the last decade (see Oke & Schild (1970) for a review). Despite the efforts there are still notable discrepancies between different observers (see Hayes 1970). Indeed, Willstrop's measurements of αLyr are 6% higher than those of Oke & Schild (1970), but since similar discrepancies are seen between other reliable observers it is not clear who has the best fluxes for this star and the author decided not to alter Willstrop's results.

The broad-band results cover the entire measured spectrum but are mainly of use in defining the flux curve in the far infra-red. Johnson (1963, 1965, et al 1966) gives the magnitudes on the Arizona system (U through to N), and these are extended further with the data of Gillett et al (1971) and Gehrz & Woolf (1971). These results overlap considerably and the more detailed fluxes of Gillett et al (1968) are most useful in the region 2.8 to 13 microns. In the near infra-red the fluxes of Walker are useful, these have been calibrated using a black body. High resolution spectra of Arcturus have been obtained by Johnson & Mendez (1970) as far as 2.5 microns, but as they are not presented on an absolute scale they are not used here.

Of particular interest is the 13 colour data of Johnson, Mitchell and Latham (1967) with its absolute calibration based on standard reference stars as described by Mitchell & Johnson (1969). These measurements are made with smaller bandwidths than those of the Arizona

system, ($\sim$ 300 - 500 Å) and are confined to the region 0.33 to 1.10 microns. Together with the Arizona system they offer a crude definition of the flux curve for a star for which there is no narrow-band data available.

The range of bandwidths used for all these observations makes it difficult to compare measured fluxes obtained by different observers. Discrepancies are properly shown only by a comparison of continuum fluxes, where the line-blanketing effects have been removed. In the visible region, where such corrections are largest and different observations overlap considerably, the broad-band data is difficult to use. Over such large bandwidths the line absorption and continuum flux may change a great deal thus blanketing corrections are difficult to apply correctly.

The continuum flux of Arcturus and the necessary blanketing corrections are discussed in Chapter 3, but the results are anticipated here in order to explain why it was felt necessary to supplement the already existing flux data. In Fig 2.1 the continuum fluxes in the visible region are shown. The precise way in which these results were derived from the observed fluxes is described in the next chapter.

It is evident from this comparison that the agreement is generally fairly good, particularly in the region 5000 - 6000 Å. However for 6300 Å - 7250 Å is a serious disagreement of about 20% between the Russian authors. For this important region Willstrop's fluxes are either poor or non-existent and a check on the results in the vicinity of the maximum flux at 6500 Å is needed. Furthermore if the reason for the discrepancy is due to an error in the fluxes of Komarov & Pozigun, then their values out to 9000 Å may similarly be suspect. These discrepancies and uncertainties in an important region as far as effective temperature is concerned, promted a new investigation in order to fix the flux curve, and therefore the value of T_e, more precisely.

2.3 The Oxford spectrum scanner

The instrument described below was not built solely for investigations of Arcturus, but has been used for determining effective

Fig. 2.1

Blanketed scanner fluxes

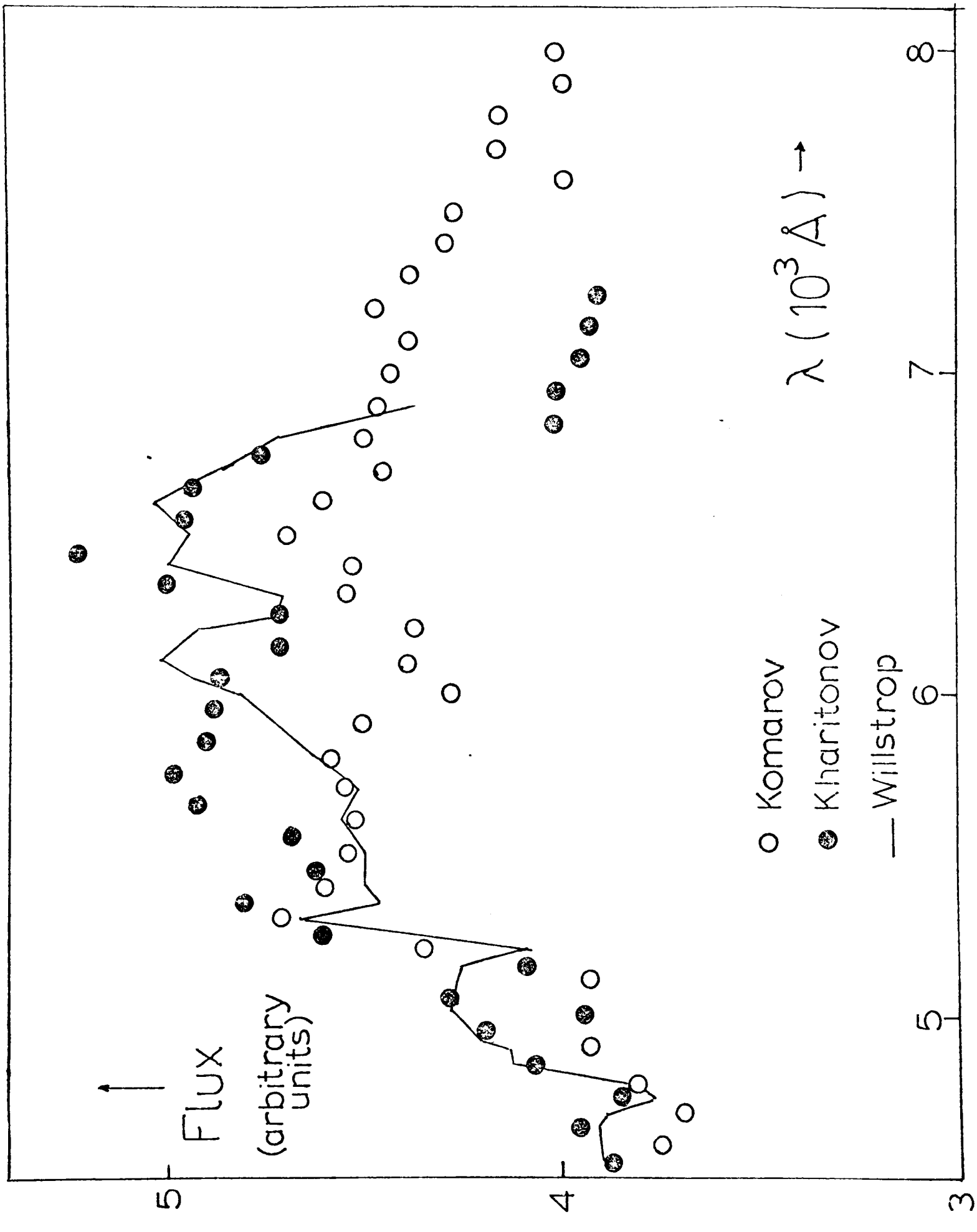

temperatures of other moderately bright ($m_v < 6$) stars of various spectral types. As the apparatus has been used by others a detailed description will be given elsewhere (Willis 1975?). In order to clarify the observing procedure however, a basic outline is provided. In particular, a description is included of that part of the design which was influenced by the requirements of the Arcturus measurements.

A plan of the instrument is given in Fig. 2.2, and reference will be made to this diagram. The optical arrangement is that of a Czerny-Turner monochromator (Czerny & Tumer 1930) and closely resembles that used by Willstrop (1965). Light from one of a selection of entrance apertures (1) is collimated into a diffraction grating (2) which is mounted on a rotating table driven by a stepping motor. The diffracted light is focused onto an exit slit (3) whose width determines the bandwidth used. In order to follow changes in the atmospheric transparency a small glass plate (4) reflects 25% of the white light to a 'monitor' channel; the diffracted light enters the 'object' channel.

Each channel consists of a photomultiplier, an electronic pulse-counter, and a digital display. Both channel signals are simultaneously integrated for a pre-selected interval and then displayed together. For this work the photomultipliers were both EMI Modified S-20 with quartz windows, chosen for their extended infra-red sensitivity. In order to reduce the dark currents, both photomultipliers are Peltier-cooled to -20°C during observation periods.

The grating is positioned using calibrated settings on a digital voltmeter. The calibration can be checked periodically by using a small mercury lamp (5) brought onto the optical axis with the manual rod (6). To simplify the observing procedure an eyepiece (7) and microscope (8) are included. (See inset Fig. 2.2) The eyepiece, used in conjunction with a prism, is primarily for guiding purposes, whereas the microscope which drops in place behind the entrant aperture (1) is used for centring and assessing image quality.

The Bausch-Lomb grating is ruled at 600 lines/mm and is blazed at $n\lambda = 16000$ Å so that observations are made in $n = 3$ for $\lambda < 5000$ Å and $n = 2$ for $\lambda > 5000$ Å. A setting accuracy of 1 Å was chosen; a

Figure 2.2

The Oxford Scanner - plan & cross-section (not to scale)

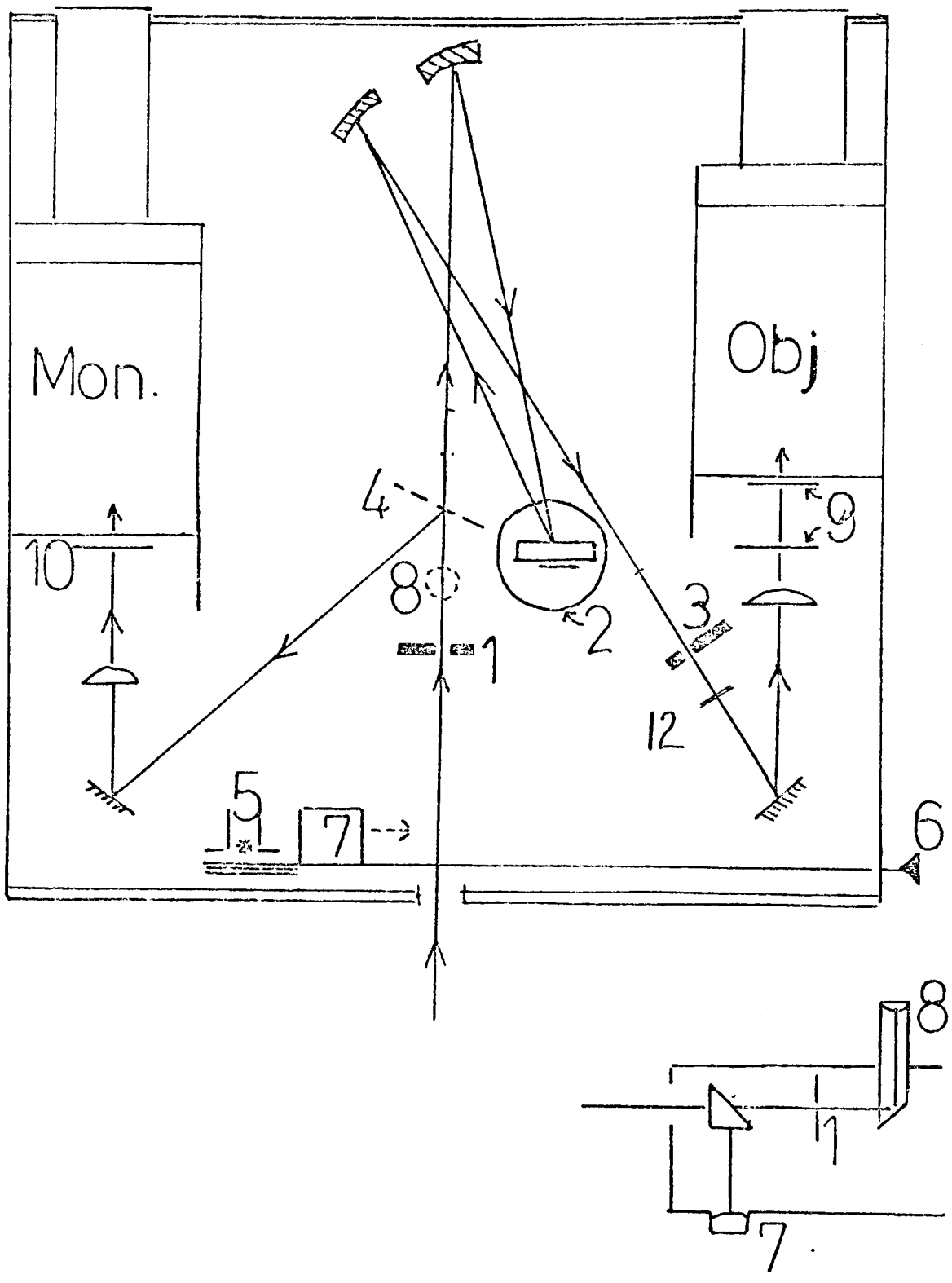

greater error would introduce significant uncertainties in the blanketing corrections. This constraint leads to an angular resolution of 14".1 for the grating, and the stepping motor was constructed appropriately. The dispersion is 12 Å/mm in n = 2 and 8 Å/mm in n = 3, thus since the exit slit can be set to 0.01 mm, this corresponds to an error of less than 0.12 Å in the bandwidth; the large dispersion means the exit slit is much larger than the corresponding stellar image ($\sim$ 0.07 mm) thus ensuring a near-rectangular transfer function.

The electronic counting system has a 'dead-time' of about 10^{-7} secs, thus a counting rate of less than 10^6 is desirable to maintain linearity. On the other hand the rate must be high enough for a reasonable low noise level. The instrument was designed mainly for use with the 40-inch telescope at the Wise Observatory, Israel, and for a zeroth magnitude star using this telescope the theoretical count rate (assuming no instrumental losses) is 1-5 10^8 sec^{-1} for a 50 Å bandwidth. Thus the problem of this astronomer is one of too much energy! The rate was reduced by introducing two neutral density filters (9), one of which can be removed for observations of fainter stars without opening the instrument. The monitor channel has an interference filter (10) of bandwidth $\sim$ 160 Å centred at 5189 Å placed over the photomultiplier window, thereby reducing the count rate and defining a constant wavelength for the channel.

To avoid light from other orders entering the object channel, a series of colour filters (12) are incorporated. Choice of such filters in the region $\lambda < 4500$ Å is extremely difficult with the present grating, since the range $3800 < \lambda < 4500$ in n = 3 corresponds to $5500 < \lambda < 7500$ in n = 2, a region where the filter should have a transmission of less than 0.01 % to avoid contamination. Only one such filter (Ilford 621) could be found.

For Arcturus it was decided that rather than duplicate the detailed scanner work of Table 2.1, a few high quality relative fluxes at carefully chosen wavelengths would satisfy the needs mentioned in the last section. In choosing these wavelengths several criteria were drawn up:

1) The regions must, as far as possible, avoid large atmospheric features so that there will be no time variations or residual effects in comparing Arcturus and the standard star.

2) The blanketing corrections for the region should be known accurately. For this reason the ends of the bands should be free of large absorption features which, in the case of a setting error, would change the correction. Furthermore the blanketing should be minimised to avoid uncertainties introduced by inaccurate continuum levels and scattered light.

3) There should be plenty of regions in the range $6000 < \lambda < 9000$ Å.

The choice is further limited at the short wavelength end by the lack of suitable colour filters, and also by the uncertain blanketing corrections. At the long wavelengths the choice is limited by the end of the Griffin atlas (1968) (used for criterion 2) at 8825 Å, which almost coincides with the fall in the photomultiplier sensitivity at 9000 Å. For criterion 1 the solar atlas of Moore et al (1966) was used and it was generally found that 35 Å was the maximum bandwidth satisfying this and other criteria. A constant bandwidth of 24 Å was eventually adopted wherever possible, this corresponds to about 2 mm on the exit slit in the second order.

The 17 regions chosen are listed in Table 2.2 together with the approximate percentage line-absorption and the expected flux according to the results of Table 2.1. In addition the regions are grouped according to the use of the colour filters for isolating the relevant orders.

2.4 Observing procedure

For the purpose of resolving uncertainties in the flux curve of Arcturus, and also for the purposes of other research conducted in this department, observing time was obtained at the Florence & George Wise Observatory of the University of Tel-Aviv, Israel. This relatively new observatory is situated at longitude $34^{\circ}\ 37'$ E and latitude $30^{\circ}\ 30'$ N at a height of ~ 900 m in the Negev desert. The telescope is a 40-inch Boller & Chivens reflector, and the Oxford scanner was attached to the f/15

Table 2.2

Regions for observations of Arcturus

	λ	$\Delta\lambda$		n	η %	πF_λ $\cdot 10^{-14}$
1	3697	12	⌐		62	63
2	4002	12			54	110
3	4513	12		3	31	280
4	4620	24			22	292
5	4947	24	=		16	334
6	5299	24			17	391
7	5566	24		2a	10	404
8	5835	24			6	428
9	6045	24	⌐		4	415
10	6388	24			6	424
11	6695	24		2b	6	428
12	6813	24			3	430
13	7476	24	=		3	413
14	7766	24			4	407
15	8077	24			4	391
16	8482	24		2c	5	365
17	8636	24	⌐		6	365

Col 1: Band number
2: Central wavelength in Ångstroms
3: Bandwidth in Ångstroms
4: Spectral order and colour filter scheme (abc)
5: Percentage line blocking (approx.)
6: Observed flux at Earth in Watts cm^{-2} $micron^{-1}$

Cassegrain focus. The observations of Arcturus were made on 4 moonlit nights during April 1973.

As mentioned before, for this investigation the Arcturus measurements need only be relative, and thus absolute extinction corrections are not necessary. As the star will be generally observed at various zenith distances however, differential atmospheric extinction is important. If the star has been observed over a large range of zenith distances, the observations can be used to define an observed extinction curve which then provides the necessary corrections. The zenith distance is easily found from the sidereal time given by a digital clock incorporated in the Oxford scanner.

In order to allow for the different colour filters used for isolating various orders, reference to a standard star is necessary. The observed ratio of the test star (Arcturus) to the standard star is then used together with the known standard star fluxes to give fluxes for the test star. The choice of such standards is mainly limited by the requirement that these stars should also be observed over a suitable range of zenith distances. It was fortunate in this instance that during April, when Arcturus transits close to midnight, both α Leo and α Lyr are also favourably placed. For various reasons given later, the primary measurements of Hayes (1970) were chosen for the reduction. An investigation of possible errors in interpolating these fluxes revealed that it was sufficient merely to observe the standard stars at the 17 wavelengths reserved for Arcturus.

The general procedure therefore was a series of readings for a set of bands in the test star, followed by the same series observed in the standard star. Each reading consisted of 3-5 measurements of the object and monitor channels with a specified integration time, 1 second in this instance. In order to minimise possible errors introduced by time variations in the atmospheric extinction, one should interchange between the stars for each band. Such a procedure is impracticable however, and in the reduction such time dependances have been ignored.

Before observing commenced the photomultipliers were cooled to -20°C or so; in the meantime the grating calibration was usually checked.

Even at such low temperatures the dark current during the first few nights was sometimes as high as 200 counts sec^{-1}, but the rate dropped (albeit somewhat erratically) to only 5 sec^{-1} on the last nights. The count rates for the stars were generally between 10^4 and 10^5 sec^{-1} for the object channel, and about 5.10^5 sec^{-1} for the monitor channel. Thus, even at its worst the dark current represents only 2% of the signal.

The entrance aperture was kept at 21".3 for all these observations. Normally apertures are limited by sky background troubles but for Arcturus and other bright stars this is no problem. Enlarging the aperture reduces scintillation effects which were usually about 2-3". Thus light from the full image always entered the apparatus and as the dispersion is fairly high the effective change in wavelength across the exit slit because of scintillation amounts to less than 0.2 Å. The sky signal was quite small and consisted almost entirely of dark current, thus no wavelength dependence or variation with sky position would be important. The sky background was measured every 4 or 5 scans by temporarily allowing the telescope to drift off the star.

The observing record is given in Table 2.3, together with the traditional vague comments on the observing conditions (see Observatory No. 1000). On all 4 nights the sky quality was good, though on the last night there was discernable cirrus. Although the site is good for its clear skies, its position in a large complex of sand and stone deserts (particularly to the south) leads to a significant dust content in the lower atmosphere. In these regions winds of 60 kph are quite frequent and the turbulence and scattering caused by these dust clouds could seriously affect any astronomical observations made from this observatory.

2.5 Reduction of data

This section is intended to give an outline of the procedure adopted for the reduction of the Israel data; emphasis has been placed particularly on the assumptions made and the possible alternative methods. It is worth remarking that the data has been reduced independently without significant differences.

The recorded data consists basically of an object reading termed

Table 2.3

Observing record

Night	Date	Order	Comments
1	15-16th	A(1-7),V(1-9),A(10-15);	Seeing good 1-2"
2	16-17th	R(1-17),A(1-17),R(1-17), A(1-17),R(1-17),V(1-17), A(1-17);	ditto
8	22-23rd	R(1-17),A(1-17),R(1-17), A(1-17),V(1-17);	Seeing poor 3-4"
9	23-24th	R(1-17),A(1-17),V(1-17)	Cirrus, seeing moderate 2-3"

Col 2: April 1973

Col 3: A = Arcturus (α Boo)

R = Regulus (α Leo)

V = Vega (α Lyr)

Bracketed numbers refer to bands observed (see Table 2.2)

'a', a monitor reading 'b', and the sidereal time τ . The set of observations for one star is then simply (a_i , b) $i = 1,..17$, where the subscript i refers to the band number and hence a wavelength. To simplify the discussion further, λ will be used for wavelength, and z for zenith distance.

In accordance with the suggested 'dead-time' (of $t_d \sim 1.2\ 10^{-7}$ sec), for the electronic counting system, the large count rates can be corrected for non-linearity using the first order relation:

$$a_i^o = a_i \ (1 + a_i t_d) \quad i = 1,..17$$
$$b^o = b \ (1 + b\ t_d) \qquad (2.8)$$

Typically $a_i \leqslant b \sim 5.10^5$ sec^{-1} and so the correction is $\leqslant 6\%$. The precise value of t_d is not important as an error of 20% in t_d leads to only 1% error in the corrected reading.

It was revealed in the last section that the sky count was largely dark current, and that it was therefore impossible to include an explicit λ or z term when subtracting. The dark current, and therefore the sky background, did vary quite erratically with time however, and intermediate values were found by interpolating from sky-time graphs constructed for each night. A typical such curve is given in Fig. 2.3 where the plotting has been performed using a procedure written in Algol 68-R (Woodward & Bond, 1971). This procedure, kindly supplied by P.G. Craven is useful for astronomical functions with discontinuities, as the plotting interval is varied according to the second derivative. In this case discontinuities have been allowed when the telescope was moved onto a different star. Subtracting the sky count gives:-

$$a_i^1 = a_i^o - sky_a \ (\tau) \quad i = 1,..17$$
$$b^1 = b^o - sky_b \ (\tau) \qquad (2.9)$$

Generally sky counts lay between 20 and 400 sec^{-1} and thus were only important for the weakest object channel readings.

In monitoring changes in the atmospheric transparency, it has been assumed here that fluctuations in b (at $\lambda 5189 \pm 180$ Å) can be applied directly to a_i for all λ_i. In other words, the assumption is

FIG. 2.3

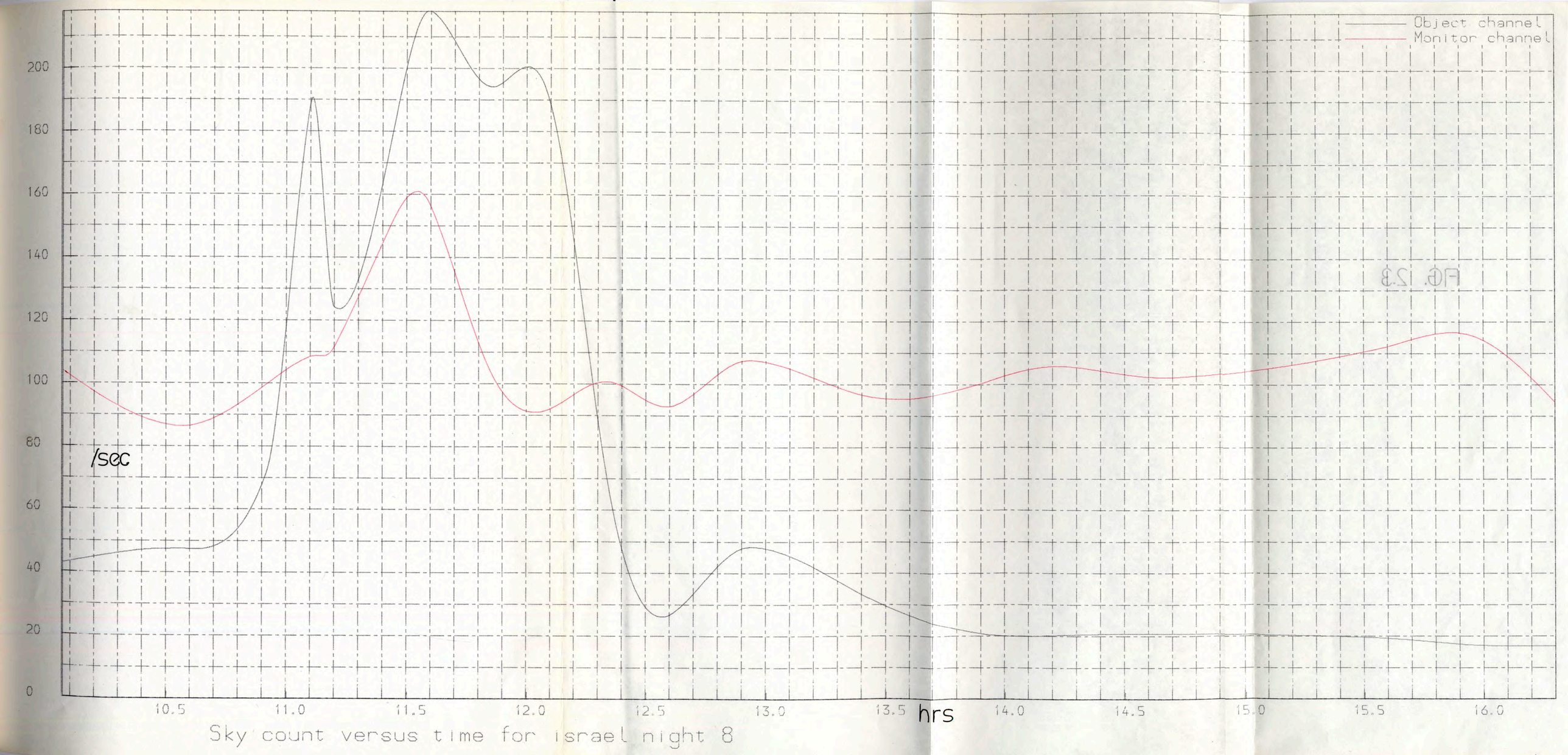

FIG. 2.3

Sky count versus time for Israel night 8

that changes in transparency have no λ-dependence, and that a cloud or dust-particle is a 'grey' absorber. To improve upon this one effectively wishes to reduce the wavelength difference $|\lambda_a - \lambda_b|$ between the two channels. An alternative method is to introduce a series of colour filters for the monitor channel that roughly keep in step with the grating setting, but a large number of quite narrow-band filters would be needed to avoid the assuption altogether. Willstrop (1965) used several broad-band monitor filters in his apparatus and his electronics output the ratio a/b directly. For relative measurements requiring reference to a standard star such a method introduces the need for transmission curves for these filters. This is because in referring to the standard star the ratio $(a/b)_{test}/(a/b)_{std}$ introduces difficulties for the quantity b_{test}/b_{std} which will vary from one monitor filter to another in a complex manner. In our simple analysis monitoring is effected by taking the ratio of a to b, setting

$$R_i = a_i^1 / b^1, \; i = 1,..17 \qquad (2.10)$$

where an average over the 3-5 measurements constituting each ith reading has now been performed.

Differential atmospheric extinction is corrected by reducing all the ratios R_i to the same zenith distance, in this instance $z = 0$. Two different methods were used: firstly a theoretical investigation utilising published absorption coefficients, and secondly an experimental investigation using the values of R_i observed at different z.

In the theoretical investigation the relation

$$R_i (z) = R_i(z=0)\, e^{-\sec z(\kappa_i - \kappa_b)} \qquad (2.11)$$

was used, where κ_i is the exponential absorption coefficient for the ith band in the object channel, and κ_b that for the monitor band. The relation assumes a plane-parallel atmosphere and also that κ is independent of z. For these observations z was less than 40° and both assumptions are reasonable. The coefficients, taken from Allen (1973), include the effects of molecular scattering, water vapour, ozone and dust absorption. They were weighted against the transmission curve $\phi(\lambda)$, for the interference filter of the monitor channel, since κ_λ changes appreciably

across 160 Å. Across the narrow bandwidth of the object channel (12-24 Å) wavelength variations in K_λ are negligible.

Thus for each value of $R_i(z)$ a value for $R_i(z=0)$ was found using equation 2.11, and those results for which $z \sim 0$ were weighted in determining a mean value. R-values, $S_i(0)$, $T_i(0)$ can be found for the standard and test star respectively, and the ratio for the test to standard at $z = 0$ is then written as $T_i(0) / S_i(0)$ $i = 1,..17$

The experimental method also employs equation 2.11, but here the results of both test and standard stars were combined to define a curve $\log_e(T_i / S_i)$.vs. sec Z. for each i. By using a least-squares program the curve using one standard star was shifted to join that for the other standard, thus utilising all the results in one extinction curve for that night. The ratio $T_i(0)/S_i(0)$ can, in fact, be found immediately for both standard stars from the intercept of the curve with the sec $z = 1$ axis, and the shift needed to bring the two curves together. The advantage of the least-squares method is that it is easy to estimate the errors in such a program. As is seen from Table 2.3, the observational curve for a given night is defined by between 3 and 7 points in the range $1.0 \leqslant \sec z \leqslant 1.3$. A typical error analysis is summarised in Table 2.4 in which it will be seen that the standard deviation on the observations is usually less than 0.02 dex(5%), leading to an implied error of about 0.03dex(7%) or less, in the final ratio T(0)/S(0). Generally this method is quite successful and would be particularly useful for many points spread over a larger range of sec z since a reasonable estimate of K_λ could then be obtained.

It is encouraging to find that the theoretical and experimental values for T/S agree to within 0.02dex(5%) for most of the 17 wavelengths. The mean ratios for the two methods gives the following information:

$$T_i(z = 0) / S_i(z = 0) \quad i = 1,17 \quad \text{for} \quad S = \alpha\,\text{Lyr} \;\&\; \alpha\,\text{Leo}$$

It now remains to introduce the fluxes $\pi F_s(i)$ for the standard star. The Arcturus fluxes are then simply given by:

Table 2.4

Error analysis of experimental extinction method

(Night 8)

Band	λ	$\log(A/R)_{z=0}$		$\log(A/V)_{z=0}$		σ
1	3697	-0.265	± 0.028	-0.752	± 0.023	0.022
4	4620	-0.206	0.010	-0.884	0.008	0.008
9	6045	+0.254	0.020	-0.082	0.017	0.017
13	7476	+0.489	0.019	+0.186	0.015	0.015
17	8636	+0.595	0.018	+0.290	0.015	0.015

Notes:

Col. 3 & 4: Ratios of test to standard at zero zenith distance using notation of table 2.3

Col 5: σ Standard deviation on the observations

$$\pi F_T(i) = \pi F_S(i)\ (T_i(0) / S_i(0)) \quad i = 1,..17 \qquad (2.12)$$

Fig. 2.4 shows the flux curves of α Lyr obtained using the data of Oke & Schild (1970) and Hayes (1970). Oke and Schild's results are based on detailed calibrations against a standard tungsten lamp and various black-body sources (Lee 1969), whereas Hayes only used a standard lamp. The agreement is very good (to within $0^m.02$) but because of slight irregularities in the data of Oke and Schild (1970) at short wavelengths and also because their secondary data for α Leo (Schild 1971) does not cover the entire wavelength region required here, the values of $\pi F_s(i)$ have been interpolated from the results of Hayes for both αLyr and αLeo. On Fig. 2.4 the 17 wavelengths at which interpolation was made are marked, the vertical scale is in magnitudes relative to 5556 A.

In order to reduce the final fluxes to continuum fluxes, the results must be de-blanketed and this procedure is described in detail in Chapter 3 since this correction must be applied to all observed fluxes before useful comparisons can be made.

2.6 Final results

The flux curves for Arcturus for the four nights are given in Fig. 2.5. For greater clarity these curves have been separated in the y-axis, but the relative scales are the same. It is again emphasised that it is not possible to compare with other published results until line-blanketing corrections have been made. The purpose of this section is to discuss the reliability of these results and to produce one averaged flux curve for use in Chapter 3.

The four curves are all encouraging in that they predict a maximum flux at 6500 Å, and the results for $\lambda > 5000$ Å differ little from one night to another. However it is immediately apparent that the results for $\lambda < 5000$ Å are not only variable but must be in error. The clear discontinuity between these two parts will be worse in the flux curve for the continuum because the blanketing correction generally increases with decreasing wavelength. This disturbing feature present in all 4 curves can only therefore arise from instrumental or reduction errors.

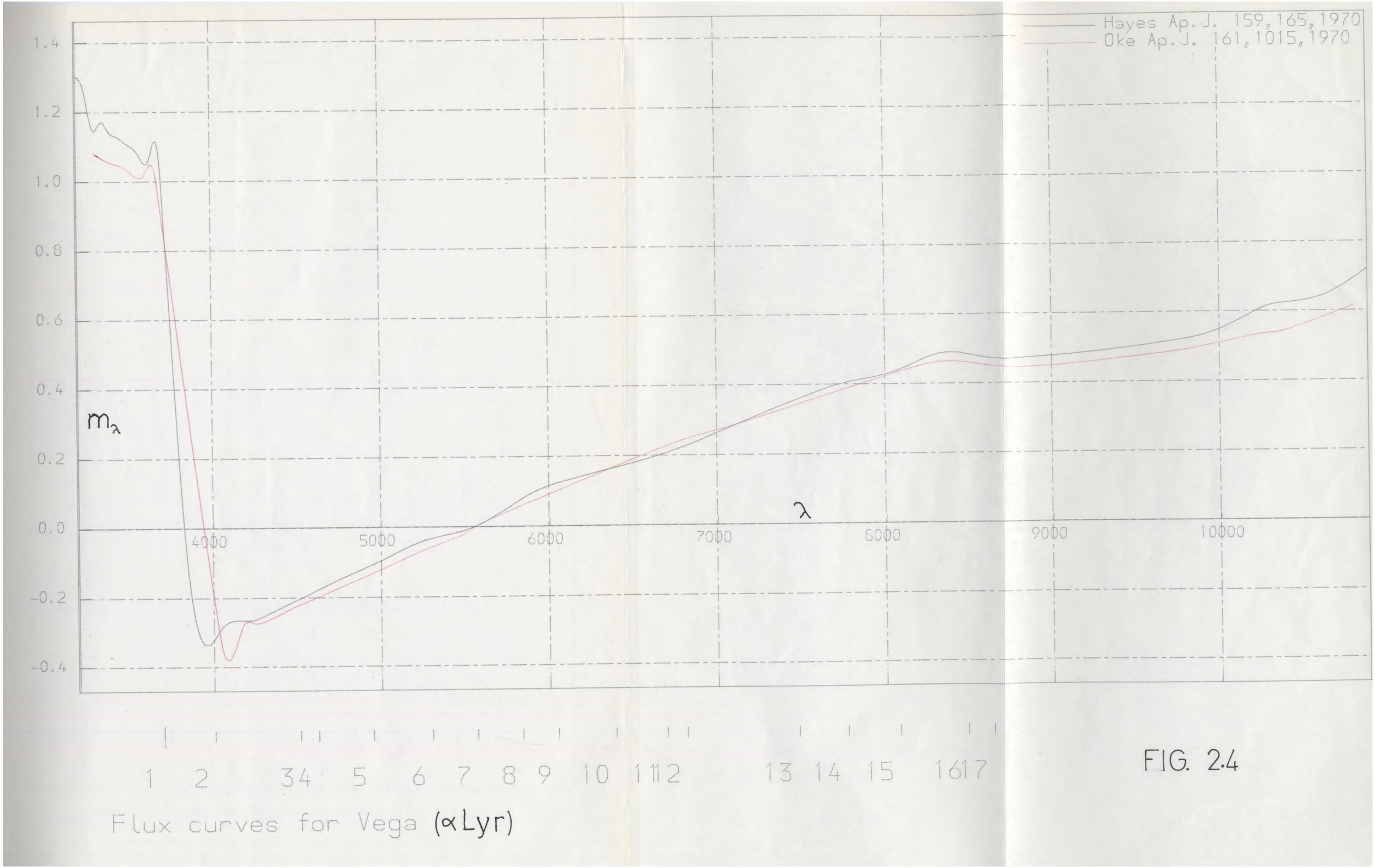

Flux curves for Vega (αLyr)

FIG. 2.4

Figure 2.5

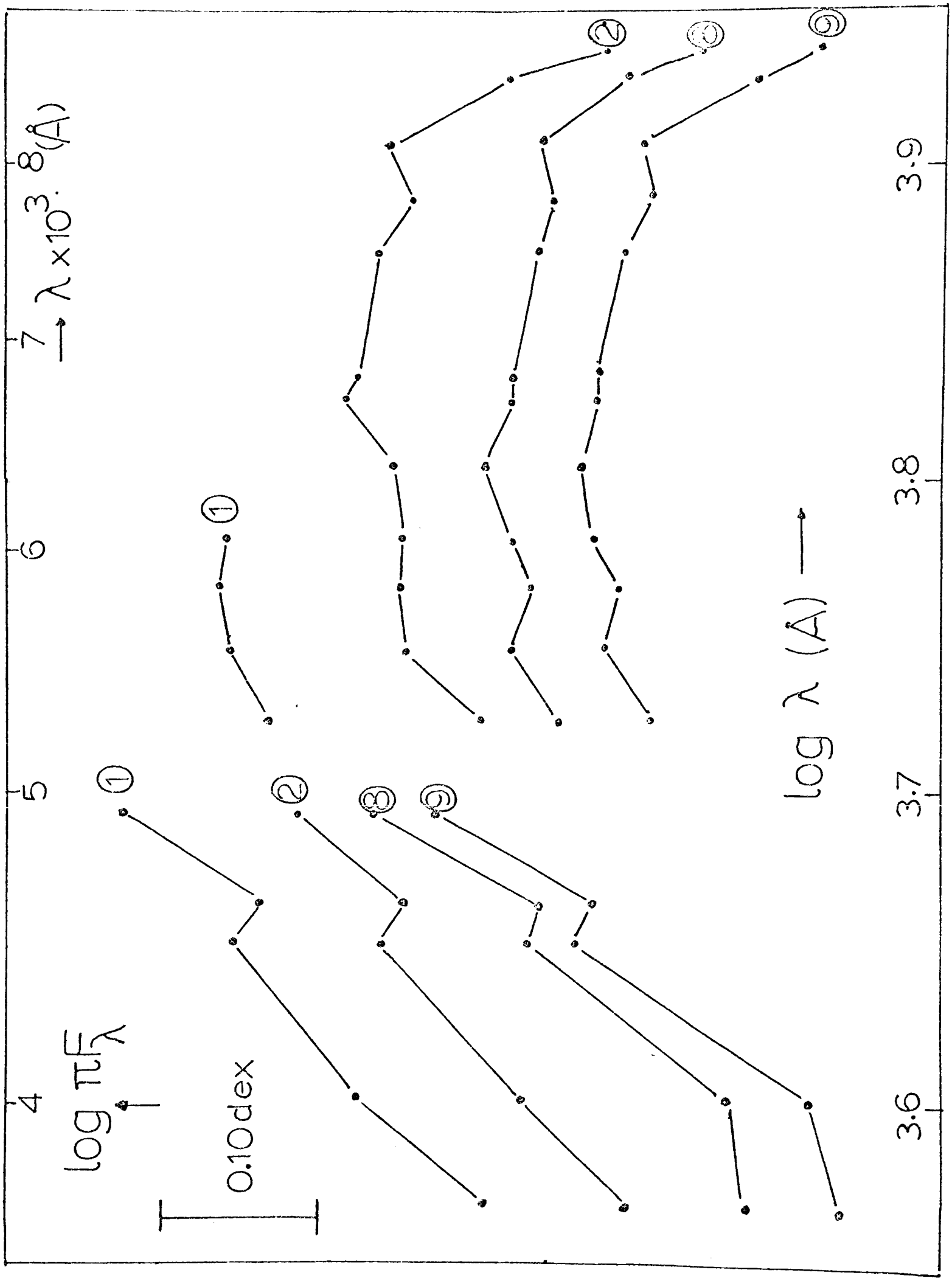

Observed fluxes for Arcturus on different nights

Useful knowledge of the reproducibility of the reduction procedure is given by the good agreement of 0.025 dex(6%) between fluxes reduced via αLyr and αLeo. A further assessment of the reliability of the Israel measurements can be obtained from a study of the comparison α Leo/ α Lyr with that given by Hayes. Such a comparison is shown in Fig. 2.6 from which it will be seen that the maximum discrepancy in slope over the useful wavelength range is about $0^m.3$ or only 0.015 dex(4%).

In attempting to place an error on the final fluxes a distinction must be made between instrumental and reduction errors. Assessment of the instrumental error would require a detailed investigation, and for this thesis such an error is ignored. The photon statistics however imply an error of less than 1% for all counts. In the reduction program appreciable errors could arise at 3 stages: in the monitoring correction, the extinction corrections, and in the standard star correction.

For a 'normal' atmosphere Allen (1973) shows that the transmission changes by 12% from λ_b(=5189) to 8600 Å. Thus the grey-absorber assumption used in applying monitor corrections, could lead to large errors for the bands at long wavelengths. Across a set of 17 measurements however, allowing for sec z variations, the monitor variations were less than 5% and so 12% errors in such corrections lead to negligible errors in the final fluxes. It is interesting to note that increasing the dust-content of the atmosphere will, all other things being equal, reduce the wavelength dependence of the total absorption coefficient. This is because the wavelength dependence of dust absorption is much less than that of Rayleigh scattering by molecules, or that of water vapour and ozone absorption. Doubling the dust content in fact reduces the change in transmission from 12% to 2%. Such experimenting is not rigorous, of course, and the term 'normal atmosphere' is as vague as the weather conditions given in Table 2.3. It would nevertheless appear that the monitoring assumption holds remarkably well for dusty conditions.

The extinction correction is always the most uncertain part of such reduction programs, and absolute results will depend critically on a knowledge of the extinction coefficient. For established observatories

Figure 2.6

Standard star ratios c.f. Hayes (in magnitudes)

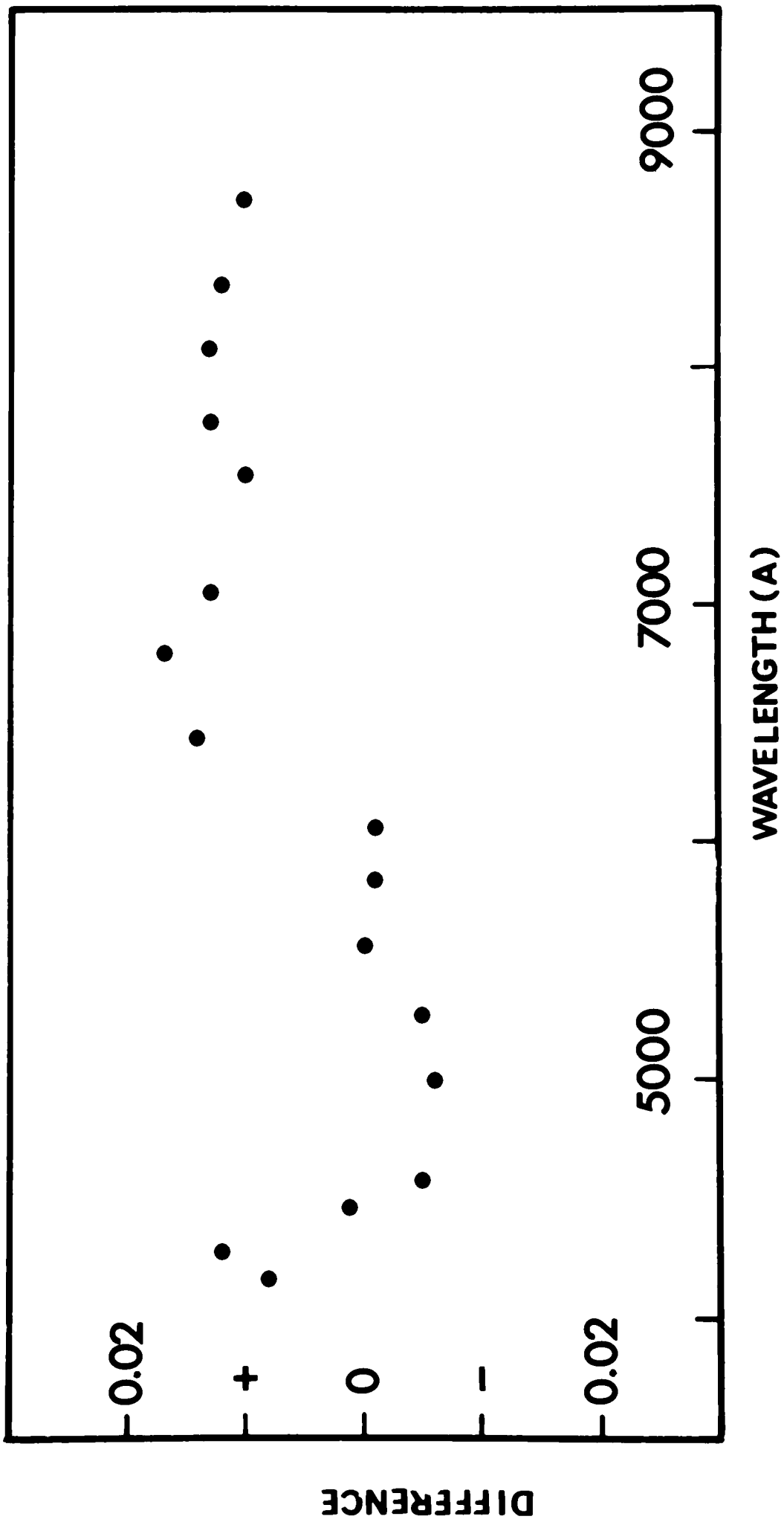

standard atmospheric extinction coefficient have usually been determined by detailed investigations (eg. Oke 1965 for Palomar); but for the Wise Observatory no data is available yet. Although great accuracy is claimed in such general tables, users would appear to employ gross approximations in referring to them. The corrections are critical even for relative fluxes and the author maintains that the detailed treatment of section 2.5 is quite essential. It seems, in fact, that this treatment for relative fluxes is more rigorous than methods often adopted for absolute fluxes. Although these relative results using theoretical coefficients will depend on the dust and ozone contents the agreement of less than 5% between the two methods described in section 2.5 is encouraging, and to avoid a lengthy analysis this is taken as the likely error for this stage.

As the standard star fluxes of Hayes (1970) and Oke & Schild (1970) differ by less than $0^m.02$ (0.008 dex) (see Fig. 2.4) a final error of about 0.02 (5%) is claimed. The above error analysis is hardly rigorous, but can be used as a guide when comparing continuum fluxes in Chapter 3.

The erroneous results obtained for $\lambda < 5000$ Å were all observed using the blue colour filter, Ilford 621. It was mentioned in section 2.4 that this filter was the only one that would prevent the stronger flux in the second order from entering the object channel. The observed discontinuity in Fig. 2.5 could arise when changing from one filter to another at 5000Å. Normally such discontinuities are eliminated by referring to the standard star, but a residual would remain if the filter transmitted a small amount of light at longer wavelengths. A leak of a few percent for $\lambda > 6000$ Å would contaminate the region 4000-5000 Å observed in n = 3. It would be possible to calibrate this filter and correct the observations below 5000 Å, but this is unnecessary as the main interest in these results lies in the region > 6000 Å. For future work the best answer is a grating blazed at a shorter wavelength. Perhaps the moral of this story is simply not to believe the manufacturer's data sheets! Scattered light could introduce a further error. As the flux curves of test and standard stars are quite different there

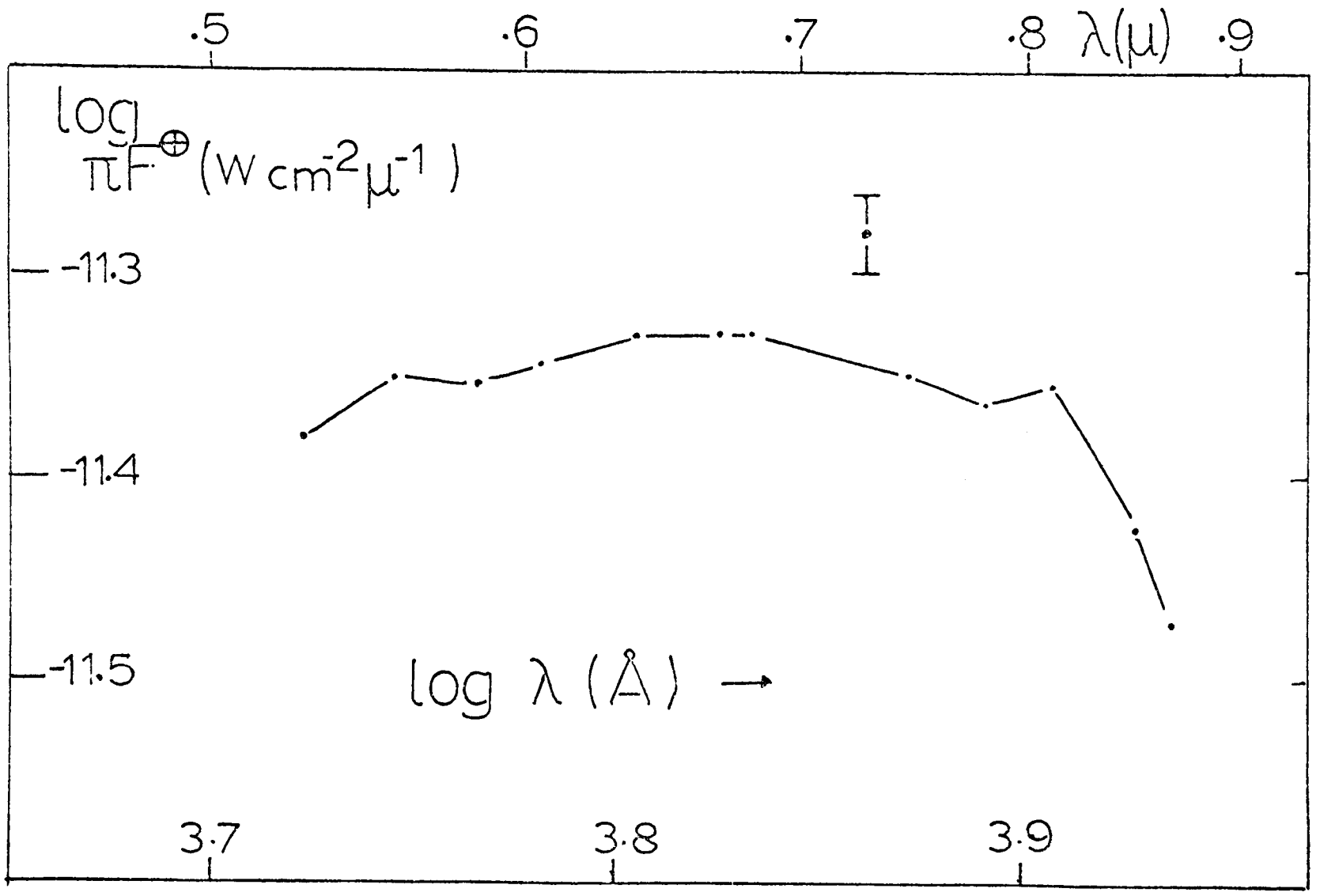

Figure 2.7

Mean observed flux curve for Arcturus (before de-blanketing)

could be a residual affecting the short wavelength values.

CHAPTER 3

THE CONTINUUM FLUX FROM ARCTURUS

3.1 Introduction

By defining the continuum flux curve this chapter finalises the first set of observation material for Arcturus. Although the motive for producing this curve is a precise determination of the effective temperature, it may also be the starting point for several other investigations, and the curve therefore represents a result in its own right. It is possibly the first time that stellar fluxes from such diverse methods have been collated, and the discussions in section 3.4 are of value in a broader sense for all cool stars. Inasmuch as fluxes eventually lead to abundances, the discussions are therefore important for many branches of astronomy.

It has been emphasised that the distribution of the continuum flux with wavelength is required in order to make useful comparisons between the results of various observers and also for matching observations with calculated fluxes from model atmospheres. This chapter deals firstly with a description of the procedures for removing the line-blanketing, and discusses the uncertainties that the correction introduces.

Two further modifications are necessary before comparisons with theoretical models are possible. Firstly the fluxes are reduced to values at the stellar surface. This transformation is effectively a change in units, and involves a knowledge of the angular diameter that Arcturus subtends at the Earth. This quantity is known only to a limited precision, and thus errors are introduced by converting to a stellar flux scale. It is relevant to point out at this stage that stellar fluxes are only required if an absolute comparison with theory is intended; fluxes at the Earth are sufficient for relative comparisons.

The second modification to the flux curve involves the possible effects of interstellar extinction and reddening. Interstellar matter in the form of dust particles called 'grains' could reduce the flux received and thus effectively alter the stellar scale. More important perhaps is that if these absorptions are strongly wavelength dependant the shape of the flux curve would be changed. This effect is briefly

discussed in section 3.3.

The final continuum flux curve is presented in section 3.5, the various modifications having been previously discussed. The curve is tabulated in a numerate form for the convenience of others who may wish to utilise the curve for various purposes.

3.2 Blanketing corrections

To allow for line-absorption which reduces the emitted flux, it is necessary to refer to a photometric tracing of a high dispersion spectrum. An integration of the line spectrum across the relevant bandwidth e.g. with a planimeter, is normally sufficient to give the correction. If the continuum flux is $\pi F_c(\lambda)$ and the observed (line) flux $\pi F_l(\lambda)$, then the blanketing coefficient, normally defined as the fraction of energy blocked by the lines is

$$\eta = 1 - \frac{\int \pi F_l(\lambda)\, d\lambda}{\int \pi F_c(\lambda)\, d\lambda} \qquad (3.1)$$

where the integrations are performed across the bandwidth. The observed flux is then multiplied by a factor $\eta' = \{1/1-\eta\}^{-1}$ to obtain the continuum flux.

For line-blanketing in the visible region of the Arcturus spectrum, Griffin's atlas was used; this covers the important region 3600-8875 Å. The main source for the infra-red is the spectrum of Connes et al (1970) which covers the region 1.0-2.5 microns. For the intermediate region the blanketing coefficients of Edmonds (1973) were used; these are derived from tracings obtained by Griffin (1964).

The corrections increase generally as one proceeds to shorter wavelengths, and exceed 50% for $\lambda < 4000$ Å. For wavelengths longer than 6000 Å the coefficients are less than 7%, and thus do not critically affect the observations. In the region 7000-9000 the atomic lines are gradually replaced by molecular bands, and at longer wavelengths the coefficient occasionally increases considerably e.g. in the region $\lambda > 2.3$ microns where the bands of CO are particularly intense, though

sufficiently far apart in wavelength for the average coefficient across a band of 100 Å to be less than 7%.

The Connes spectrum is not in the form of a tracing, but lists the features present and their equivalent widths. The resulting coefficients, found by summing the equivalent widths, will therefore be a lower limit, since the table omits numerous weak features. Such errors are not important because the coefficients themselves are so small. The lack of spectra beyond 2.5 microns is similarly not a great handicap.

It is worth mentioning that planimetering between 20 and 100 bands for the results of each of 7 observers is a long and tedious business. It is therefore of interest to investigate possible approximate methods. Both Warren (1970) and Edmonds (1973) have measured blanketing coefficients for Arcturus in the manner described above in steps of 100 Å, though they were concerned with constructing line-blanketing statistics for model atmospheres rather than correcting observed fluxes. Nevertheless interpolation in their values would be far quicker and could give results bearing on approximate methods for stars for which high dispersion spectra are not available.

Fig. 3.1 shows the variation of η with wavelength for Arcturus in 100 A steps. Also included is the variation in the values over the quarter-intervals; this sometimes amounts to as much as 40%. It is therefore quite evident that to maintain the high accuracy of the observed fluxes, blanketing corrections must be determined using the correct bandwidths. The rapid variation of η with wavelength also means that the corrections at any wavelength are probably peculiar to the Arcturus specrum and cannot be transferred accurately to another star.

In planimetering the scanner observations, the transmission function can be regarded as a rectangular block, (Willstrop 1965) but for the intermediate and broad-band results the filter transmission must be taken into account as the bandwidth becomes rather a vague term. A detailed analysis weighting η_λ against the transmission ϕ_λ for small intervals across the entire filter was compared with a relatively

Figure 3.1

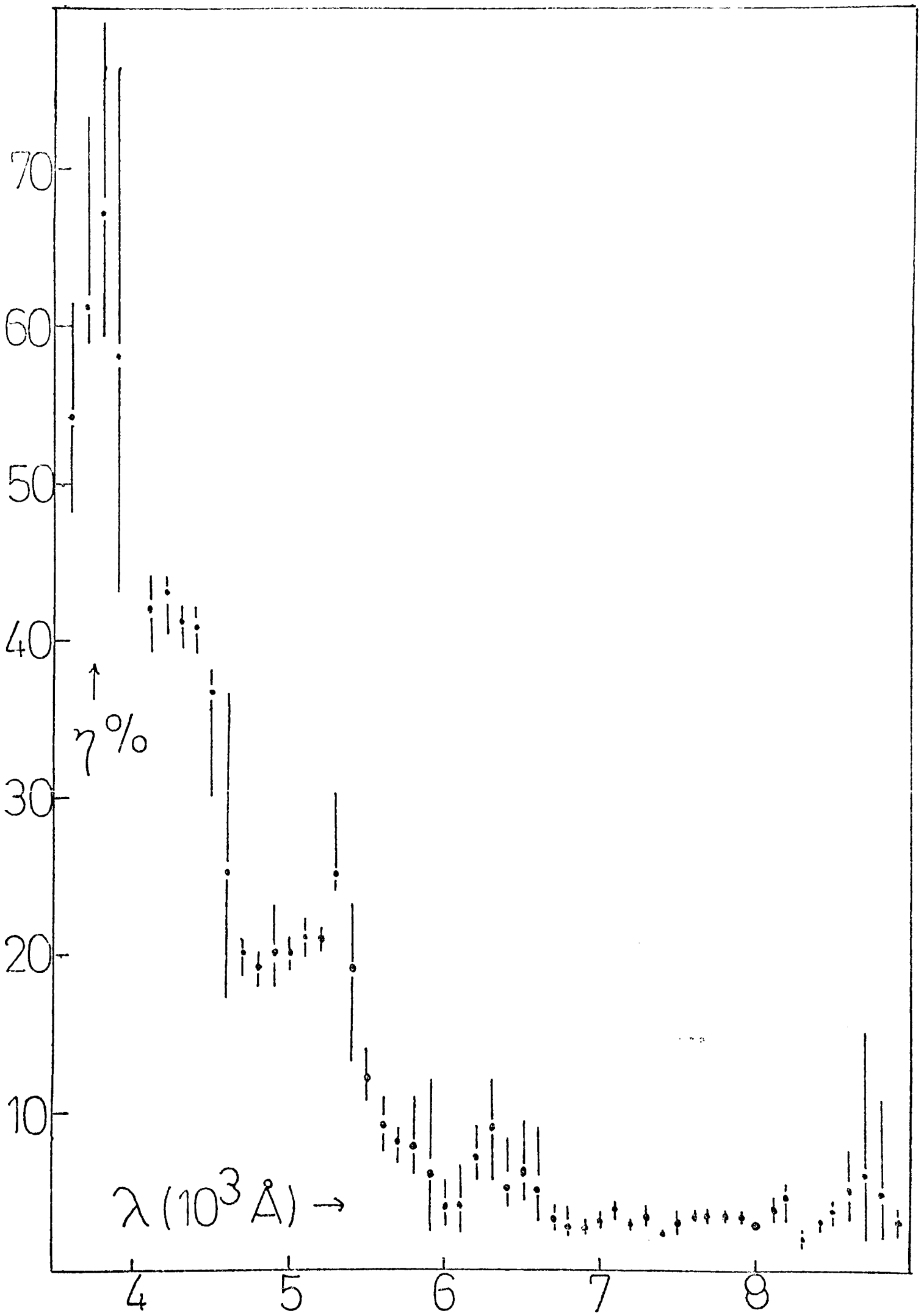

Line blocking coefficients and quarter interval dispersion

straightforward mean blanketing coefficient at the 'effective wavelength' of the filter (see below). For the 13 colour system both methods agreed to within 5%.

For the broad-band results a further complication arises. Even in a star with no absorption lines the continuum flux may change appreciably across such broad bandwidths, and thus the coresponding wavelength at which the flux is valid need not necessarily be the centre of the band. For this reason Johnson (1965) has established a set of effective wavelengths for the U-N system, and in constructing the curves these have been used. The appropriateness of effective wavelengths, determined essentially by weighting $\phi(\lambda)$ against λ, was confirmed by King (1952). As continuum slopes change with effective temperatures these wavelengths are not valid for all stars, but in the far infra-red where the broad-band results are of most use, such effects are quite small.

Although the blanketing corrections are largest for $\lambda < 4500$, they are also most uncertain here. As the size of η and its rapid variation with wavelength would suggest, the lines here are so crowded that it becomes impossible to determine the position of the continuum with precision. Griffin states in his atlas that the continuum so drawn is only well-defined for $\lambda > 5200$, and is most uncertain for $\lambda < 4300$. A typical error of 2% in the continuum level could alter the correction by as much as 5%, so no great weight should be placed on continuum fluxes for $\lambda < 4300$. Methods for determining effective temperature that rely on accurate fluxes for this region should therefore be avoided wherever possible. Elsewhere, errors in the continuum are much less and the error in the resulting correction is mainly due to measurement and is probably less than 1%.

3.3 Interstellar reddening

The extinction of radiation (absorption plus scattering) in interstellar space is attributed to dust particles called grains. The best way of determining the extent of the effect, and particularly its

wavelength dependance, is by comparing the observed fluxes of O and B stars at various distances. Hot stars are chosen because of the absence of line-blanketing effects which could vary appreciably from one star to the next.

The classical work of Stebbins et al (1940) showed that the extinction is generally $\sim 1^m$/kpc in the visible region of the spectrum, and that it increases as $1/\lambda$. The effect of this '$1/\lambda$ - law' is to redden starlight by an amount depending on the distance of the star. The reddening is, in fact, determined more accurately than the total extinction, which requires a knowledge of the true flux for a close, supposedly unreddened star.

More recent measurements (summarised by Wickramasinge, 1967; and Johnson, 1968) show that there is no universal reddening law. The extinction curve is usually specified by a parameter R_V defined by

$$R_V = A_V / (A_B - A_V) \qquad (3.2)$$

where the A_B, A_V are extinctions in magnitudes for the wavelengths in the broad-band system of Johnson. The quantity $A_B - A_V$ is the B - V colour excess, more commonly written E_{B-V}. Johnson has shown (1968) that R_V lies between 3 and 6, being most for the direction $\ell^{II} = 100\text{-}200^\circ$, and the value of A_V has been determined for 207 different directions by Neckel (1967). The possiblility of extinction affecting the continuum flux from Arcturus, and its distribution with wavelength, can therefore be investigated using the above results, and corrections can be made if necessary.

The proximity of Arcturus (11 pc) suggests at first that it is unlikely that interstellar material could significantly alter the flux curve, although near stars are not necessarily unreddened. Münch and Unsöld (1962) for example, found evidence for reddening in α Oph, which is only 20pc distant.

For the region in which Arcturus lies, Neckel gives an extinction measured over 3 kpc of only $0^m.3$. This amounts to only $0^m.001$ for Arcturus, thus it is quite evident that total extinction and reddening are both negligible for any reasonable value of R_V.

3.4 Discussion of the continuum flux results

Fig. 3.2 shows the continuum flux results for Arcturus obtained by de-blanketing the observed fluxes discussed in Chapter 2. To avoid the graph becoming too confused not all the scanner data has been included, and the visible region 3800Å - 1 micron has been drawn separately on Fig. 3.3.

For the region < 6000 Å blanketing corrections are important and it is pleasing to note that the resulting curve is smoother than that obtained by using the raw observed fluxes. Also, where the corrections are most accurate, the discrepancies between the results of different observers have been reduced.

The spread of results for $\lambda<4800$ is generally twice that for λ 5500-6500 Å and this is primarily due to uncertainties in the blanketing corrections caused by the absence of a clear continuum level. However the internal consistency of, for example, Willstrop's fluxes is much worse at these short wavelengths. The Griffin atlas begins at 3600 Å and thus it is not possible to measure blanketing for all the results of Willstrop and of Kharitonov and Knyazeva that extend to 3400 Å. For completeness however, an attempt has been made to include these results, though the correction (determined by extrapolation), would appear to have been overestimated as the flux curve does not have the same slope at these wavelengths. For $\lambda<4500$ Å an error of about 0.08 dex(20%) is claimed for these fluxes, this being the sum of the mean difference between various observers on Fig. 3.3 and the likely error in the blanketing corrections determined in section 3.2. This is an average error across the region $3400<\lambda<4500$; for the shortest wavelengths the error might be as much as twice this value.

The Israeli data is in good agreement with the fluxes of Willstrop, and emphasises the divergence between the Russian results. It is now clear that the fluxes of Kharitonov and Knyazeva are probably incorrect by 0.08dex(20%) for 6850-7250. Komarov has found a similar discrepancy for other stellar fluxes published by Kharitonov and Knyazeva. With one exception the Israeli results agree to their claimed error of 0.25dex(6%) with the other scanner data, and the resulting curve is now

Figure 3.2

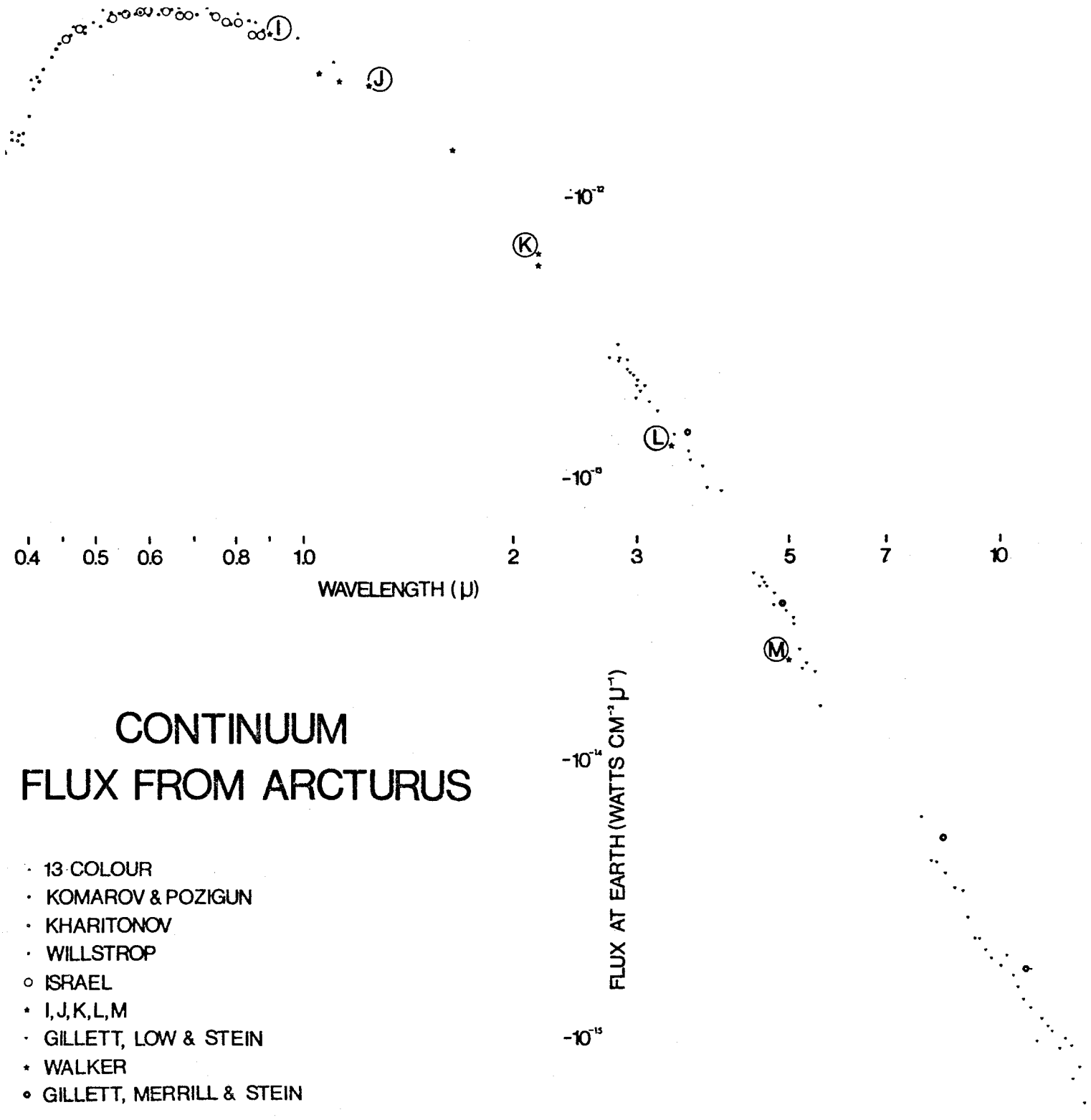

CONTINUUM FLUX FROM ARCTURUS

- 13 COLOUR
- KOMAROV & POZIGUN
- KHARITONOV
- WILLSTROP
- ISRAEL
- I, J, K, L, M
- GILLETT, LOW & STEIN
- WALKER
- GILLETT, MERRILL & STEIN

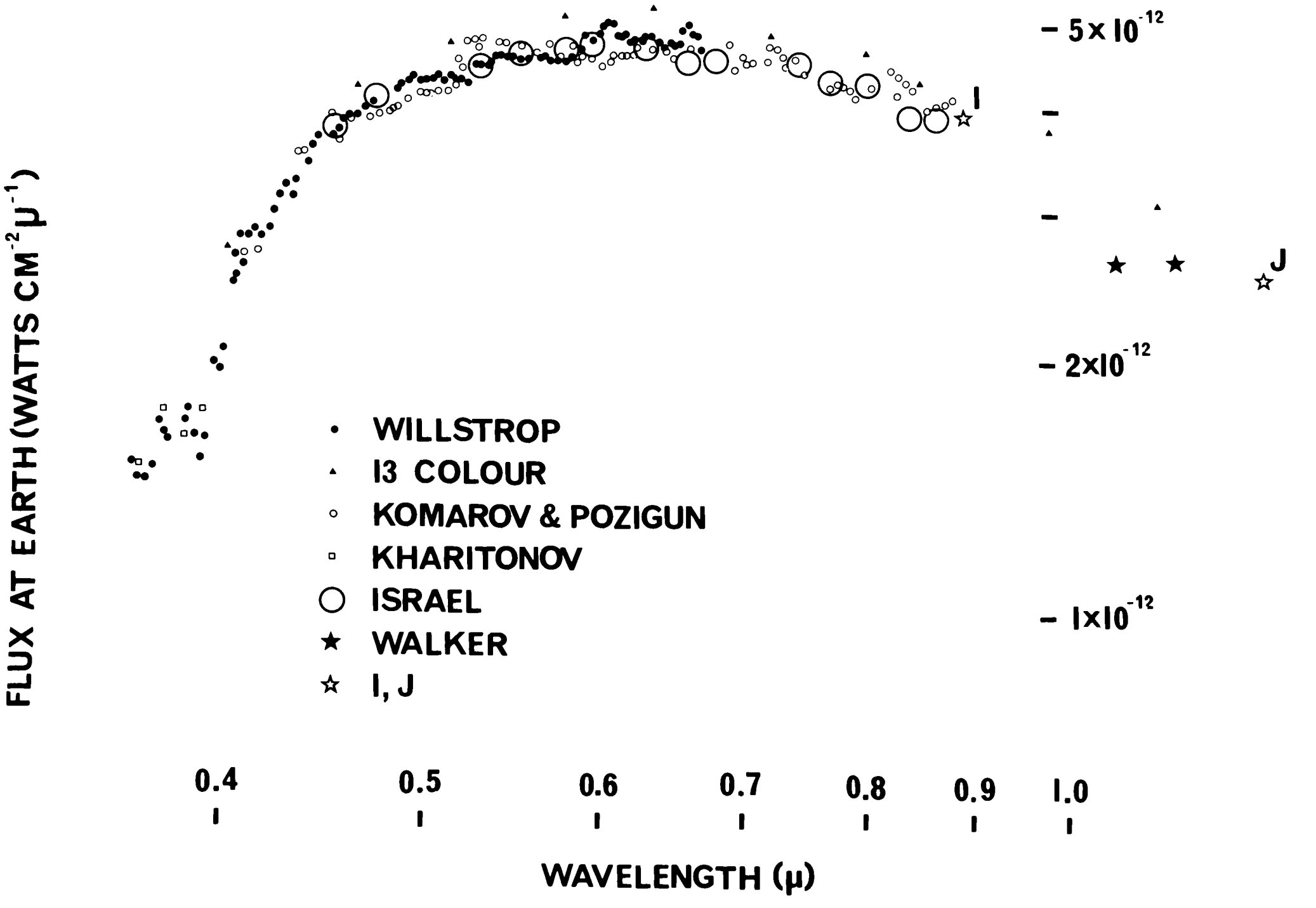
FLUX AT EARTH (WATTS CM$^{-2}\mu^{-1}$)
WILLSTROP
I3 COLOUR
KOMAROV & POZIGUN
KHARITONOV
ISRAEL
WALKER
I, J
5×10^{-12}
2×10^{-12}
1×10^{-12}
I
J
0.4
0.5
0.6
0.7
0.8
0.9
1.0
WAVELENGTH (μ)

Figure 3.3

remarkably well defined, particularly around the maximum. Using a similar error analysis, a figure of 0.035(8%) is obtained for the flux error in the region $4500 < \lambda < 9000$.

The 13 colour results by themselves define the flux curve only fairly well, the results being often 0.05dex(12%) too high, which could arise from an error of that amount in the calibration. The relative calibration of the system (i.e. with wavelength) relies on the standard stars αLyr and αCMa, for which the results of 5 different authors were averaged; these included Hayes and Millstrop but not Oke and Schild. The absolute calibration for the entire scale comes from the work of Labs and Neckel (1967). As the maximum possible error in the calibration of the 13-colour system is only 0.01dex(2%), the observed discrepancy is not understood.

Turning to the near infra-red (0.8-2.5 microns), (Fig. 3.2), it is seen that the curve is not so well defined, and it is here in particular that future work should be directed. The results of Walker are particularly decisive, and yet where comparisons can be made, his fluxes are down by about 0.04dex(10%). The K-magnitude for example, has been measured, together with its calibration, several times (Johnson 1962, 1964 et al 1966) and the flux here would therefore appear to be well established, yet Walker's value is 0.04dex less. It is nevertheless difficult to believe that Walker's absolute calibration (based on a black body source) could be in error by such a large amount. Furthermore, the error in the effective wavelength of his filters would have to be as much as 400 Å to account for the discrepancies. Walker states that his results give evidence for a brightening at 1.6 microns, consistent with the minimum in the H^- opacity at this wavelength. However when the results of other observers are included, the author finds that this effect is quite small unless Walker's points are all raised by about 0.04 dex(10%). The results then coincide elsewhere, and give a brightening at 1.6 microns which is roughly consistent with model predictions. This region is unfortunately quite important, and thus emphasises the need for more results. For the purpose of assessing errors in T_e an error of 0.04dex(10%) is placed on the fluxes in the region 0.9-2.5μ.

For the far infra-red, > 2.5 microns, the results are not important for determining the effective temperature. The infra-red spectrum of Gillett et al (1968) is invaluable in this region, and together with the broad-band magnitudes of Johnson et al. (1966), Gehrz and Woolf (1971), and Gillett et al (1971), the flux curve is fairly well defined. Beyond 7 microns there is considerable scatter however, and Gillett warns that such variations do not necessarily represent any features. There are conspicuous gaps in Gillett's spectrum where atmospheric absorption considerably reduces the flux at the Earth's surface. Between 4 and 4.5μ there are strong CO_2 bands, and between 5 and 7μ water vapour is the main absorber. The region $17\text{-}30\mu$ is in fact the last infra-red window, and it is therefore necessary to use orbiting instruments to determine the flux for the intermediate regions.

The far infra-red results are particularly useful for investigating the possibility of infra-red emissions from circumstellar grains (Gillett et al 1971). It was proposed by Hoyle and Wickramasinghe (1962) that stars could form an extensive envelope of graphite or silicon grains which would be heated to a few hundred degrees by the stellar radiation, and would then emit a black body spectrum in the far infra-red. Many such infra-red emissions have since been detected (see review by Spinrad and Wing 1969); and most occur in the spectra of cool stars at $10\text{-}11\mu$, corresponding to a grain temperature of about 250°K. Gillett revealed, using his broad-band photometry at 11μ, that the emission is dependant on the luminosity, being most prominent for M-type supergiants.

Gillett et al (1968) compared the detailed infra-red spectrum of Arcturus with that of a black body at 4000° K in order to investigate the possibility of long-wavelength emission. Beyond 5μ the observations are below the black body curve by about 0.11dex(30%), though the shape from $7.5 - 13\mu$ is very much the same. Gillett's calibration was initially based on the L-N magnitudes of Johnson et al (1966) but has been verified independently by Gehrz and Woolf (1971). Thus for Arcturus there is clearly not an excess of flux at any wavelength in the far-infrared and Gillett concluded there was no evidence for any circumstellar material.

It is interesting to note that there is also a similar depression, with respect to a black body curve at 4000°K, of about 0.10dex(25%) for λ4.5-5.5μ . Such troughs have been explained as being due to extensive band absorption by the molecule CO (Solomon and Stein 1966). This is quite an important point because although Spinrad and Wing (1969) have recently said that CN is the most important band opacity in the far infrared, the work of Yamashita (1962) on CO prompted an investigation by Alexander and Johnson (1973) which has produced some interesting model atmospheres. These are discussed in Chapter 4.

3.5 Final continuum flux curve

For easier comparisons with the predicted flux curves of model atmospheres, it was decided to reduce the many observations given in Fig. 3.2 onto one curve. This curve is given in Fig. 3.4 together with the flux errors at various parts of the spectrum as determined in the last section.

For the visible region, $\lambda < 9000$ Å, fitting the curve was quite straight forward because of the wealth of scanner data now available. The 13 colour results were excluded here because of the puzzling discrepancy with the scanner results; their removal does not however increase the error of the curve.

In the near infra-red the problem is much worse. There is only one result between 1.2 and 2.2μ , and it has been demonstrated that this point (due to Walker) may be considerably in error. The points of Walker were all adjusted by +0.04 dex as suggested before; this is quite arbitrary and apart from matching the fluxes with other results in the neighbourhood there is little justification for such manipulation. It does however introduce a sizeable brightening at 1.6μ , and the curve was fitted in this region with the help of theoretical fluxes from model atmospheres at 4000° and4400°K (see inset to Fig. 3.4); this fitting is not sensitive to the model used.

For the remaining region, $\lambda > 2.5\mu$, the curve closely follows a Rayleigh-Jeans law. The gradient of the log flux - log λ curve here is in fact roughly that of a blackbody at about 4000 - 4200 K, as can be inferred from Gillett's (1968) comparison. No attempt has been made to

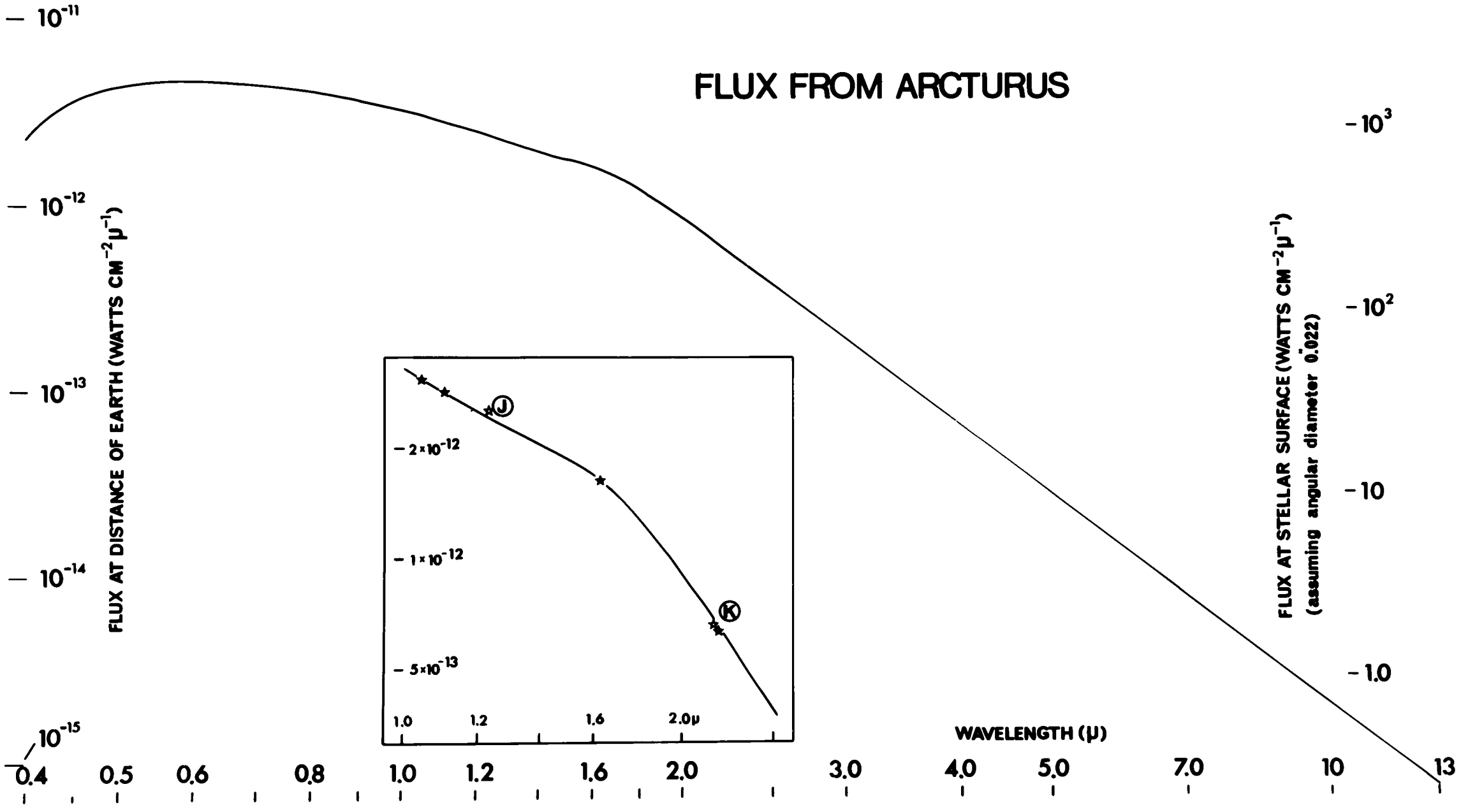
FLUX FROM ARCTURUS
FLUX AT DISTANCE OF EARTH (WATTS CM$^{-2}\mu^{-1}$)
FLUX AT STELLAR SURFACE (WATTS CM$^{-2}\mu^{-1}$)
(assuming angular diameter 0.022)
WAVELENGTH (μ)
10^{-11}
10^{-12}
10^{-13}
10^{-14}
10^{-15}
10^{3}
10^{2}
10
1.0
0.4
0.5
0.6
0.8
1.0
1.2
1.6
2.0
3.0
4.0
5.0
7.0
10
13
J
K
2×10^{-12}
1×10^{-12}
5×10^{-13}
1.0
1.2
1.6
2.0μ

Figure 3.4

fit the possible depression at 4.5 - 5.5μ as no suitable model fluxes for this region were available. It is therefore suggested that anyone interested in using such a curve for the far infra-red would do better using the full results given in Fig. 3.2.

It is fairly easy to reduce these fluxes at the Earth to those at the stellar surface and thereby permit absolute comparisons with model predictions. In fact,

$$\pi F_\lambda^* = \frac{4 \pi F_\lambda^\oplus}{\theta^2} \qquad (3.3)$$

where superscripts * and ⊕ refer to stellar and terrestrial-based fluxes respectively, and θ is the angular diameter in radians. It is thus evident that the stellar flux scale is particularly sensitive to errors in θ.

For Arcturus there are two published values of θ. The classical determination using Michelson's interferometric method (Pease, 1931; Michelson and Pease, 1921) gives θ = 0" .020, and a recent measurement by Gezari et al (1972) using the new technique of speckle interferometry on the 200-inch at Mount Palomar gives a slightly higher value of θ= 0" .022 $\pm$ 0.003. A third value of 0" .026 $\pm$ 0.005 from Currie (reported by Upson II 1973) has not been published and is not used in this thesis. As Pease does not include any errors, and also because of overwhelming advances in instrumentation over the last 50 years, the value of Gezari has been chosen. (The fact that Pease's value comes within Gezari's error is nevertheless a tribute to his outstanding experimentation). Fig. 3.4 therefore includes a stellar flux scale based on this diameter. The uncertainty in this scale, from the error in θ, is $\pm$ 0.10dex(26%) and further uncertainties are introduced if this value is to be corrected for limb-darkening. Thus the scale in Fig. 3.4 is very approximate, but future values of θ can be readily incorporated in it by using equation 3.3.

For general convenience, the flux at the earth at various representative wavelengths has been determined from fig. 3.4 and is tabulated in Table 3.1.

Table 3.1

The continuum flux from Arcturus at the Earth

$\lambda(\mu)$	$\log \pi F_\lambda$	λ	$\log \pi F_\lambda$
0.40	-11.640	1.6	-11.772
0.45	-11.438	1.8	-11.900
0.50	-11.362	2.0	-12.050
0.60	-11.322	2.5	-12.390
0.65	-11.315	3.0	-12.685
0.70	-11.338	4.0	-13.160
0.80	-11.374	5.0	-13.540
0.90	-11.420	7.0	-14.080
1.0	-11.481	10.0	-14.700
1.2	-11.588	13.0	-15.140
1.4	-11.700		

Fluxes are in Watts cm^{-2} $micron^{-1}$ and are subject to the following uncertainties :

	$\lambda <$ 4500 Å	> 0.08 dex(20%)
4500 $\leqslant$	$\lambda \leqslant$ 9000	0.035 dex(8%)
	$\lambda >$ 9000	0.04 dex(10%)

CHAPTER 4

MODEL ATMOSPHERES

"O what a load of misery and pain
Each Atlas-line bore off! - a shine of hope
Came gold around me, cheering me to cope
Strenuous with hellish tyranny."

Endymion: John Keats (1817)

4.1 Introduction

The discussion so far has been restricted to the continuous energy distribution and its determination. The line spectrum (also originating in the outer layers of the star) contains a wealth of information about many atomic species, but in order to utilise this spectrum it is necessary to know the physical conditions in the region of its formation. Such information can generally come only from a theoretical solution of the equations determining the structure of the outer layers. It is possible to parameterise the theoretical solution by considering the continuum flux and also by studying the profiles of certain lines in a way described later. Once these parameters are known the theoretical solution can be found and applied to the line spectrum.

In this chapter the assumptions and construction of model atmospheres are discussed quite generally, though the main motive is a model for Arcturus consistent with the continuum flux curve presented in the last chapter.

4.2 Assumptions

Early investigations showed that a single temperature and pressure, determined for example from the continuum flux, led to inconsistencies when regarding the excitation and ionisation of atoms in the line analysis. A more realistic representation of the atmosphere is a series of stratified layers each with its own

temperature and pressure. The model atmosphere problem is then simply to determine the run of such physical variables with depth. As the energy source for the star is in the central regions far below the atmosphere, the problem is basically a solution of the transfer of this energy through the outer layers. The radiation will be absorbed, scattered and emitted according to the conditions at each layer, and a general solution of the equations would be a very difficult task. Many mathematical and physical approximations are therefore necessary to make the problem tractable. Some of these assumptions and approximations were initially introduced to avoid tedious calculations by hand and have been removed with the advent of high-speed computers, whereas others reflect inadequate knowledge of the physical processes concerned. The usual assumptions are listed below and discussed in turn.

1) The atmosphere is plane-parallel: This is realistic if the atmosphere is thin relative to the stellar radius. For extended atmospheres this may not be valid and although the transfer equations can be easily written in circular geometry they require a value for the stellar radius, an uncertain quantity for this type of star.

2) The atmosphere is homogeneous except in the normal direction: This is not so easy to justify as there is considerable evidence to the contrary for the sun. As such two-dimensional effects may also be time-dependant it follows that the model can only give some crude average representation at each level. It is also assumed that the relative abundances are specified and constant with depth.

3) The atmosphere is in hydrostatic equilibrium: For no net acceleration pressure balances gravity i.e.

$$\frac{dP}{dx} = -\rho g \qquad (4.1)$$

where ρ is the density, and g, the gravity, is assumed constant over the atmosphere. (4.1) means that all large scale velocity fields are ignored.

4) The atmosphere is in a steady state: i.e. effects such as pulsations, expanding envelopes etc. are not included.

5) The atmosphere is in energy equilibrium: No energy is generated in the atmosphere thus the total flux is constant with depth. In the general case where energy can be transported by modes other than radiation, this means that for each level -

$$\pi F^{total} = \int \pi F_\lambda^{rad} d\lambda + \pi F^{other} = \sigma T_e^4 \quad (4.2)$$

For a prescribed T(x) this will generally not be true, and an important function of the model is to alter T(x) until (4.2) holds reasonably well for all levels.

An additional assumption sometimes made is that the atmosphere is in LTE, i.e. that each layer can be given one temperature valid for excitation and ionisation as well as for the radiation field and the velocity distribution of the atoms. For low densities where collisions will not maintain a steady-state population, this will not be justified and detailed equilibrium calculations must be made for each species. Such non-LTE calculations have represented the frontier of progress in studies of model atmospheres for many years. They are no longer limited by the size and speed of the computer, but are hindered by the need for detailed equilibrum rates and atomic constants, many of which are most uncertain.

By restricting studies of the spectrum to those lines which originate in the higher density regions it has always been hoped that non-LTE calculations can be avoided. It is possible to

examine the validity of such an assumption by determining abundances from lines in various stages of excitation and ionisation. Such investigations have so far been restricted to the sun where the density is not so critical.

4.3 Constructing a model

The following discussion attempts to bring together the many relationships used in constructing model atmospheres. In practice the sequence of operations is complicated by the inter-dependance of many quantities; for this reason the final procedure is described at the end of the discussion.

The radiation field at any depth can only be determined by solving the equation of transfer, which is merely a conservation of energy across the atmosphere. The energy change in the radiation of intensity I_λ, passing through an element of material (see Fig. 4.1), equals the energy the element emits minus that it absorbs, i.e. in time dt

$$dI_\lambda \, d\lambda \, d\omega \, d\sigma \, dt = j_\lambda (\rho \, d\sigma \, ds) \, d\omega \, d\lambda \, dt - k_\lambda I_\lambda (\rho \, d\sigma \, ds) \times d\lambda \, d\omega \, dt \qquad (4.3)$$

where j_λ and k_λ are the emission and total absorption (or extinction) coefficients per gram of material. In the plane-parallel case, $dz = \mu \, ds$ (where $\mu = \cos\theta$) and so

$$\frac{\mu}{\rho} \frac{dI_\lambda}{dz} = j_\lambda - k_\lambda I_\lambda \qquad (4.4)$$

It is more convenient to replace z by the optical depth τ_λ,

$$d\tau_\lambda = -\rho k_\lambda \, dz \qquad (4.5)$$

which is a direct measure of the opacity at that wavelength. In addition the quantity j_λ / k_λ is defined as the Source function

Figure - 4.1

An elemental cylinder in a stellar atmosphere (see text)

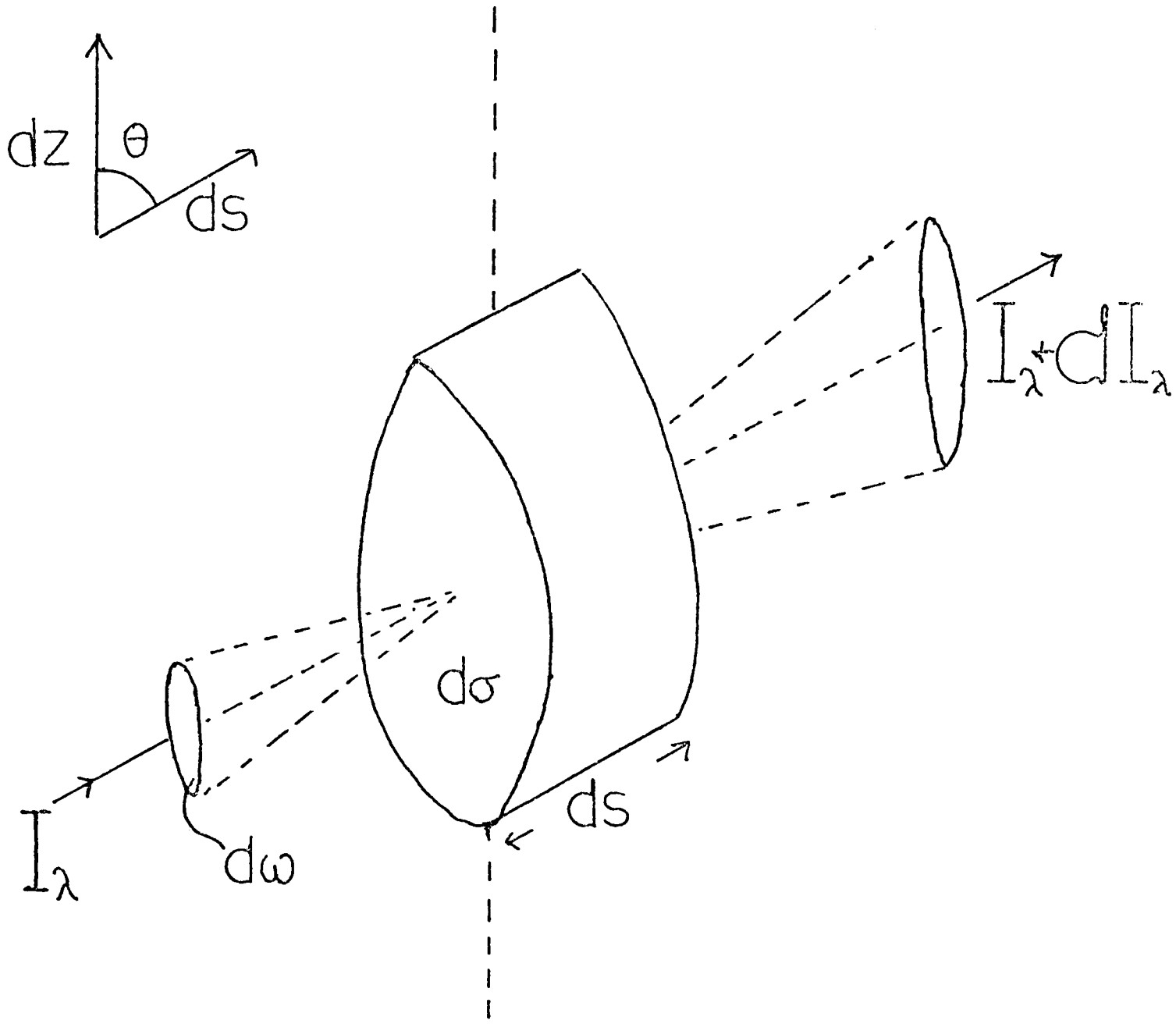

S_λ, Therefore (4.4) becomes:-

$$\mu \frac{dI_\lambda}{d\tau_\lambda} = I_\lambda - S_\lambda \qquad (4.6)$$

It is useful to introduce S_λ because it renders many equations such as (4.6) valid for several different physical approximations. Similarly k_λ represents the total extinction coefficient which may include scattering and line opacities, as well as those of pure absorption. S_λ and k_λ are given below for three important cases:

1) LTE emission plus coherent isotropic scattering:

$$S_\lambda = \frac{\kappa_\lambda B_\lambda}{\kappa_\lambda + \sigma_\lambda} + \frac{\sigma_\lambda J_\lambda}{\kappa_\lambda + \sigma_\lambda} \quad ; \quad k_\lambda = \kappa_\lambda + \sigma_\lambda \qquad (4.7)$$

2) LTE emission and no scattering:

$$S_\lambda = B_\lambda \quad ; \quad k_\lambda = \kappa_\lambda \qquad (4.8)$$

3) Coherent isotropic scattering only:

$$S_\lambda = J_\lambda \quad ; \quad k_\lambda = \sigma_\lambda \qquad (4.9)$$

where κ_λ, σ_λ represent the true absorption and scattering coefficients, B_λ is the Planck function (see eqn. 2.6), and J_λ is the mean intensity over all solid angles:

$$J_\lambda = \frac{1}{4\pi} \oint I_\lambda(z,\mu)\, d\omega = \frac{1}{2} \int_{-1}^{1} I_\lambda(\mu)\, d\mu \qquad (4.10)$$

In solving the transfer equation (4.6) two boundary conditions are imposed; firstly for $\mu < 0$ there is no incident radiation at $\tau_\lambda = 0$, viz.

$$I_\lambda = -\int_0^{\tau_\lambda} S_\lambda e^{-(t-\tau_\lambda)/\mu} \frac{dt}{\mu} \quad ; \quad \mu < 0 \qquad (4.11)$$

and secondly, for $\mu > 0$ the intensity contribution from infinity is zero, i.e.

$$I_\lambda = \int_{\tau_\lambda}^{\infty} S_\lambda e^{-(t-\tau_\lambda)/\mu} \frac{dt}{\mu} \quad , \quad \mu > 0 \qquad (4.12)$$

Using these solutions it follows that at τ_λ

$$J_\lambda = \frac{1}{2} \int_0^\infty S_\lambda(t) E_1 |\tau_\lambda - t| \, dt \qquad (4.13)$$

and
$$\pi F_\lambda = -2\pi \int_0^\infty S_\lambda(t) E_2 |\tau_\lambda - t| \, dt \qquad (4.14)$$

where $E_n(x) = \int_1^\infty \frac{e^{-xz}}{z^n} dz$

To summarise therefore, a knowledge of S_λ and k_λ at various wavelengths enables a determination of the radiation field at each level in the atmosphere. If scattering is to be included the solution is complicated by the inter-dependance of S_λ and J_λ, (4.7), though this can be bypassed either by iteration or using a method of integration matrices (Kurucz 1969).

In order to correlate the different optical depths it is useful to have a fixed depth scale. This can be either the optical depth at a standard wavelength or some suitable mean optical depth. Here the Rosseland depth will be used as it will feature prominently in future discussions. Various other mean depths have been discussed by Chandrasekhar (1950). The Rosseland depth is defined by:-

$$\int \pi F_\lambda \, d\lambda = \frac{4\pi}{3} \frac{d}{d\tau_{Ross}} \left(\int B_\lambda \, d\lambda \right) \qquad (4.15)$$

so that if
$$d\tau_{Ross} = -\kappa_{Ross} \rho \, dz \qquad (4.16)$$

then
$$\frac{1}{\kappa_{Ross}} = \frac{\int_0^\infty \frac{1}{K_\lambda} \frac{dB_\lambda}{dT} d\lambda}{\int_0^\infty \frac{dB_\lambda}{dT} d\lambda} \qquad (4.17)$$

The introduction of a standard optical depth has the advantage that the equation of hydrostatic equilibrium can be written in a density-independant form. Combining (4.1) and (4.16) gives:

$$\frac{dP^{total}}{d\tau_{Ross}} = -\frac{g}{\kappa_{Ross}} \qquad (4.18)$$

where the total pressure includes components of radiation, turbulence and gas pressures. Electron pressure is normally contained in the gas pressure term. If g is specified and a preliminary κ is assumed, it is possible to integrate (4.18) to give P total (τ).

Improving the initial estimate of P and also determining τ_λ for many λ^s requires evaluation of the opacities. These in turn require a knowledge of the number densities, which are found by writing down equations for conservation of charge, number and abundance (for each species).

$$\left.\begin{aligned} \text{Abundance:} \quad & \sum_{\substack{\text{all species} \\ \text{containing the atom}}} n = X_{atom}\, n_A \\ \text{Charge:} \quad & \sum_{\text{+ve ions}} n - \sum_{\text{-ve ions}} n - n_e = 0 \\ \text{Number:} \quad & \sum_{\text{all species}} n + n_e = P^{total}/kT \end{aligned}\right\} \qquad (4.19)$$

where X is the atomic abundance for that species, and n_A is the total number density.

Each term in (4.19) can be written as a function of the neutral atom and electron number densities using the Saha equation relating adjacent stages of ionisation. There are then as many equations as unknowns and all the number densities can be found. These equilibrium equations are not linear however, and their

solution requires an interative process such as that described by Carnahan et al (1969 p.240). In practice it is easier to assume an electron number density and then correct it using the solutions.

The astute reader will realise that the entire model calculation so far assumes a temperature distribution. The main aim is to produce the radiation field at each depth and obtain an improved temperature distribution. Knowing n_e and T it is then easy to add up all the opacities for each wavelength and level:

$$\kappa_\lambda = \sum \kappa_\lambda (P_e, T) \qquad (4.20)$$

$$\sigma_\lambda = \sum \sigma_\lambda (P_e, T)$$

and thus produce S_λ, k_λ and solve the equation of transfer for $\pi F_\lambda (\tau_\lambda)$.

In cases where convective transport is important it is necessary to calculate the convective flux. Unfortunately, convection is not well-understood and most workers resort to a crude first-order approximation known as the mixing-length theory, reviewed by Cox and Guili (1968). Simple calculations (Biermann 1948) show that the convection in the Sun is turbulent, and although detailed hydrodynamical calculations of the interacting eddies have successfully reproduced the observed polygonal pattern of the solar convective granules (Fromm 1966), the incorporation of such theory into a general model atmosphere program would be a hopelessly difficult task.

The mixing length theory assumes that convective elements are bubbles of diameter 1 which rise a distance 1 and radiate before merging into the background. As 1 will vary with depth, the ratio 1/h is usually specified, where $h = P_{total} / \varrho g$ is the 'scale-height'. Typical analyses have used 1/h = 1 or 2, though there is little

evidence for any particular value.

Schwarzschild found that if the temperature gradient exceeds that corresponding to an adiabatic gas, the region is convectively unstable, and bubbles will rise carrying energy to cooler regions. In fact radiative losses bring the bubble gradient closer to the background gradient. Writing

$$\nabla = d\log_e T / d\log_e P$$

the convective flux is (Mihalas 1970 p202)

$$\pi F^{conv} = \frac{1}{2}\left(\frac{\ell}{h}\right) \rho C_p T v_{conv} \left[\nabla_{backgnd} - \nabla_{bubble}\right] \qquad (4.21)$$

where C_p is the specific heat at constant pressure, found by considering the total energy per unit mass at various depths, and v_{conv} is the bubble velocity found by considering its equation of motion.

The radiative and convective fluxes are combined and compared, at each depth, with the value required by the effective temperature. There are two criteria to satisfy:

i) The flux error should be zero:

$$\Delta(\pi F) = \sigma T_e^4 - \int \pi F_\lambda d\lambda - \pi F^{conv} = 0 \qquad (4.22)$$

ii) The flux derivative should be zero:

$$\frac{d(\pi F)}{d\tau} = 0 \qquad (4.23)$$

Gingerich (1961) showed that temperature corrections based on (4.23) alone could lead to convergence to unreal situations. In fact, for deep layers where the flux originates, (4.22) is more sensitive and using temperature corrections derived from $\Delta(\pi F)$ it is possible to integrate (4.23) providing corrections for the

higher layers. There are now several good temperature correction procedures available for model programs; in particular Avrett and Krook (1963) devised a method which allows a perturbation in both T and τ thus speeding up convergence considerably. The method has been extended to include convection (Kurucz 1970), though this slows convergence considerably. Fig. 4.2 shows the convergence for a solar model using an Avrett-Krook scheme. In favourable cases it is possible to obtain convergence to 1% in 8 iterations without convection, and in 15 iterations with convection, though speed of convergence will vary from one program to another, and (perhaps surprisingly) from one set of parameters to another.

To recap the procedure used in constructing a model, a flow diagram of the program ATLAS (Kurucz 1970) is given in Fig. 4.3. This programme in fact, uses a fixed mass depth scale rather than a Rosseland depth scale. The merits of this and other details will be considered in a later section.

4.4 Model atmospheres for cool stars

An appropriate way of testing a model is to try and reproduce and observed flux curve. Such a comparison is quite sensitive to the temperature distribution $T(\tau)$ used, and can reveal important information about the opacities. For stars of spectral type earlier than F5 the models are quite realistic (Peytremann and Parsons 1973). As an example, the fluxes of Hayes (1970) for the standard star α Lyr are reproduced remarkably well by the model of Woolf and Ney (1968). For cool stars (cooler than the sun, $T_e \leq 5800^{\circ}K$), however, these simple models have to be modified for several reasons.

A glance at the spectrum of Arcturus reveals that lower temperatures generally induce a more complex line spectrum. The absorption lines have two important effects. Firstly they block

Figure 4.2

Convergence of the Avrett - Krook scheme for a solar model

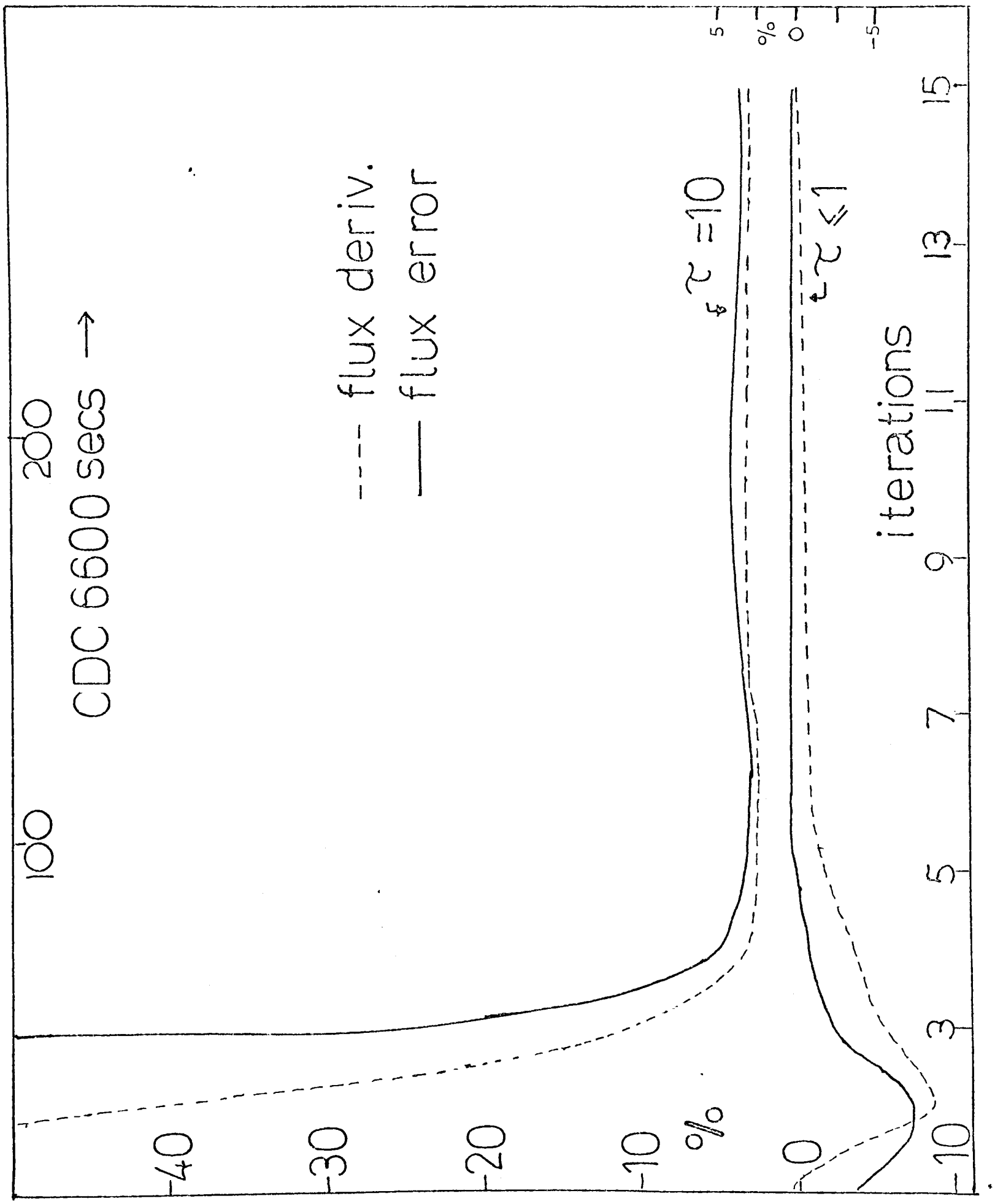

Figure 4.3

Flow diagram for ATLAS (Kurucz 1970)

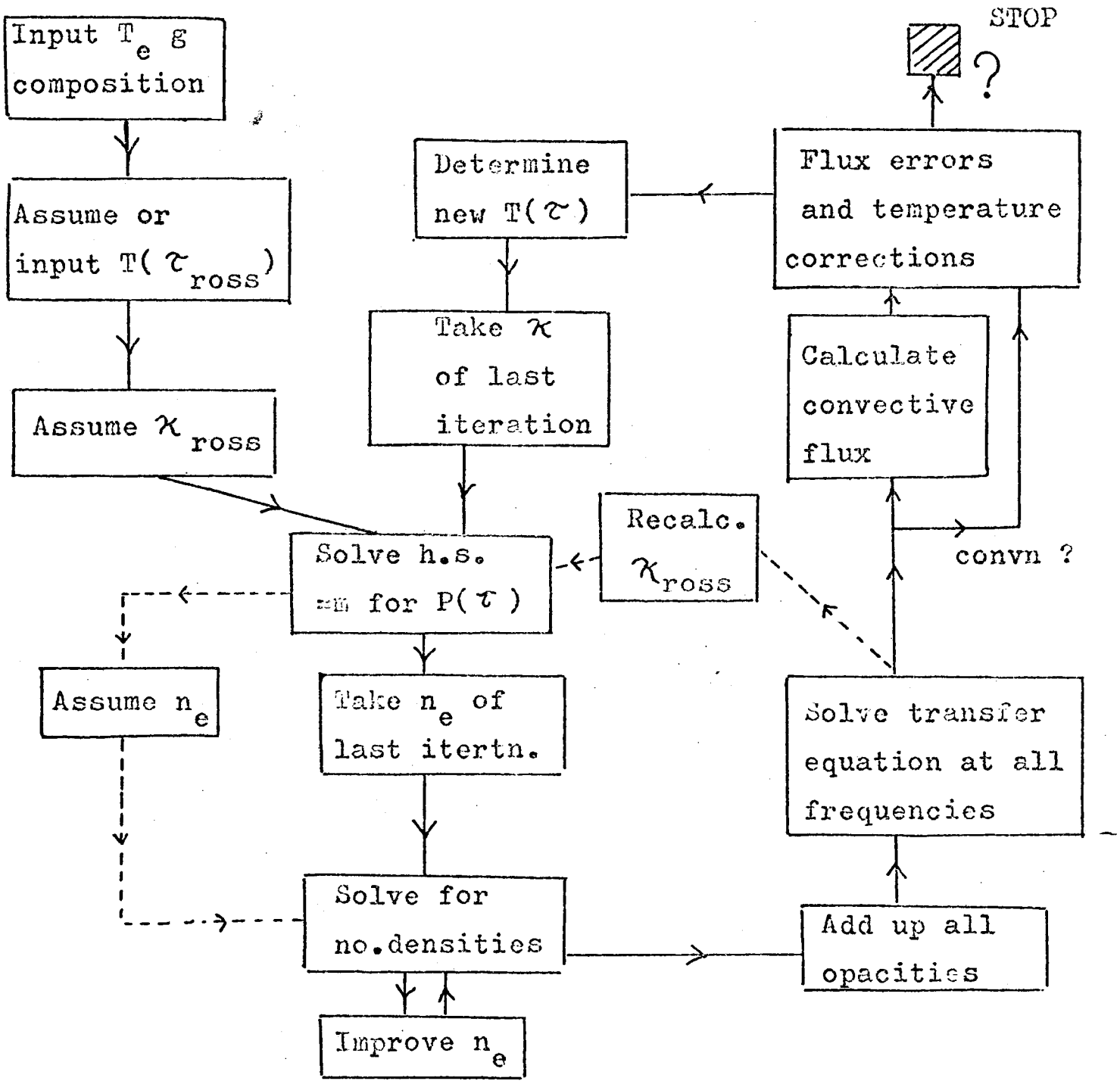

Notes:

---- first iteration only

▨ if converged satisfactorily (or ran out of computer time) program halts here.

radiation and affect the flux measured in photometric bands; this effect was discussed in the last chapter and can be allowed for using a high dispersion spectrum and an accurate continuum reference. From energy considerations however, the absorption will, for a given total flux, mean an increase in the adjacent continuum flux corresponding to a rise in the local temperature. This effect known as 'backwarming', means that the $T(\tau)$ is changed such that for $\tau \lesssim 1$ there is a rise in temperature, whereas the boundary temperature, T_o, drops. Thus line-blanketing can seriously affect interpretations of the line-spectrum.

To take account of backwarming, it is necessary to include the line absorption coefficient 1_λ in the Source function. Mihalas (1969) has shown that it is usually safe to assume the lines form by LTE absorption and that a non-LTE line-blanketing theory (e.g. Mihalas 1970 p.432) will only change small details. Thus in LTE the source function becomes:

$$S_\lambda(\tau_\lambda) = \frac{\kappa_\lambda + \ell_\lambda}{\kappa_\lambda + \ell_\lambda + \sigma_\lambda} B_\lambda(\tau_\lambda) + \frac{\sigma_\lambda}{\kappa_\lambda + \ell_\lambda + \sigma_\lambda} J_\lambda(\tau_\lambda) \quad (4.24)$$

and the problem in a nutshell is to calculate and incorporate $1_\lambda(\tau_\lambda)$.

It is possible to calculate 1_λ in a detailed fashion using an extensive list of lines and their atomic parameters and thus to generate a synthetic spectrum (see Bell 1972). This approach has been successful for hotter stars (Morton and Mihalas 1965, Hickock and Morton 1963), but to represent the millions of weak lines present in a cool star would not only require several hours of computer time for each iteration but would also demand accurate line data that is just not available at present. It is therefore desirable to investigate possible approximations to ℓ_λ.

The picket fence approximation of Chandrasekhar (1936),

developed by Münch (1946), replaces 1_λ by blocks or pickets of suitable width and spacing. This first order approximation can in some instances be worse than no blanketing at all (Carbon 1974).

A more elaborate approach (originally suggested by Labs) has been developed by Mihalas (1969). Here, 1_λ is transformed to a smooth distribution function which can be easily represented in (4.24). If $f_o(1)$ is the fraction of some interval for which $1_\lambda = 1 + \Delta 1$ then defining

$$f(l_\lambda) = \int f_0(1)\, dl \qquad (4.25)$$

and inverting the function to obtain $1_\lambda(f)$, it is seen that this function, with end points $1_\lambda(1) = f_{max}$, $1_\lambda(0) = f_{min}$, is well-behaved. Using 1000Å intervals Strom and Kurucz (SK, 1966) incorporated line-blanketing into a model of Procyon ($T_e \sim 6500^o$K) by this method; to define 1_λ data from 30,000 lines was used. Kurucz (1974) has since produced a staggering list of 1,860,000 lines for use with models of solar type stars, and he proposes to extend this list further thereby slowly working his way to later type stars. For $T_e \leqslant 4000^o$ molecular bands will be important and computer storage will indubitably limit his progress.

The above method ignores any depth-dependance $1_\lambda(\tau_\lambda)$. If the line spectrum changes appreciably over an interval $\Delta\tau_\lambda < 1$ the distribution functions could be unrealistic. Calculating 1_λ at various depths would return to the computing problems associated with the synthesis programs.

It is possible to estimate the depth-dependance empirically by fitting profiles of suitably chosen lines. Carbon and Gingerich, (CG, 1969) used an extended picket fence model and separated the λ and τ dependances, thus

$$l_\lambda(\tau_\lambda) = f_1(\lambda)\, f_2(\tau) \qquad (4.26)$$

The lines were split into wing and core, and both pickets were adjusted to match the observed blocking. Three spectra were used for constructing a grid of blanketed models - Arcturus ($4000^{\circ} < T < 5000^{\circ}$), the Sun ($5000^{\circ} \leqslant T \leqslant 6000^{\circ}$) and Procyon ($6000^{\circ} < T \leqslant 10000^{\circ}$).

Despite the impressive line list used by SK, their fluxes for Procyon are in fact poorer with respect to the observations of Bahner (1963) than those of CG (see Fig. 4.4). Peytremann (1974) has repeated the SK analysis using an edited list of 6000 strong lines, this time including convection. His $T(\tau)$ is almost identical to that of CG and confirms that a detailed line list does not necessarily improve upon the empirical approach of CG.

All methods require accurate line statistics and such data is badly needed for a whole range of spectral types. The solar statistics of Mutschlecner and Keller (1970, 1972) are now adequate, and Edmonds (1973) is presently collecting data for 10000 lines from the Griffin Arcturian atlas. For stars without high dispersion spectra however, interpolating these statistics is the only present solution (see Natta and Ranieri 1972), and will be a poor approximation in the region $T \lesssim 4000^{\circ}K$ because of the appearance of many different molecular bands. These contribute to 1_{λ} in the same way as the atomic lines and some models have attempted to include their effects, though usually in a primitive fashion e.g. Auman (1967,1969a b). A large number of molecules such as CO, CN, contribute significantly in the infra-red and have been reviewed by Spinrad and Wing (1969, 1970). In particular Johnson (1973) has constructed models that include the molecule CO according to calculations by Querci et al (1971) and finds the boundary temperature of a 4000° model is reduced by 1000 degrees.

As with bound-bound opacities, so different continuous opacities such as C^{-} may be important for cool stars (see Vardya

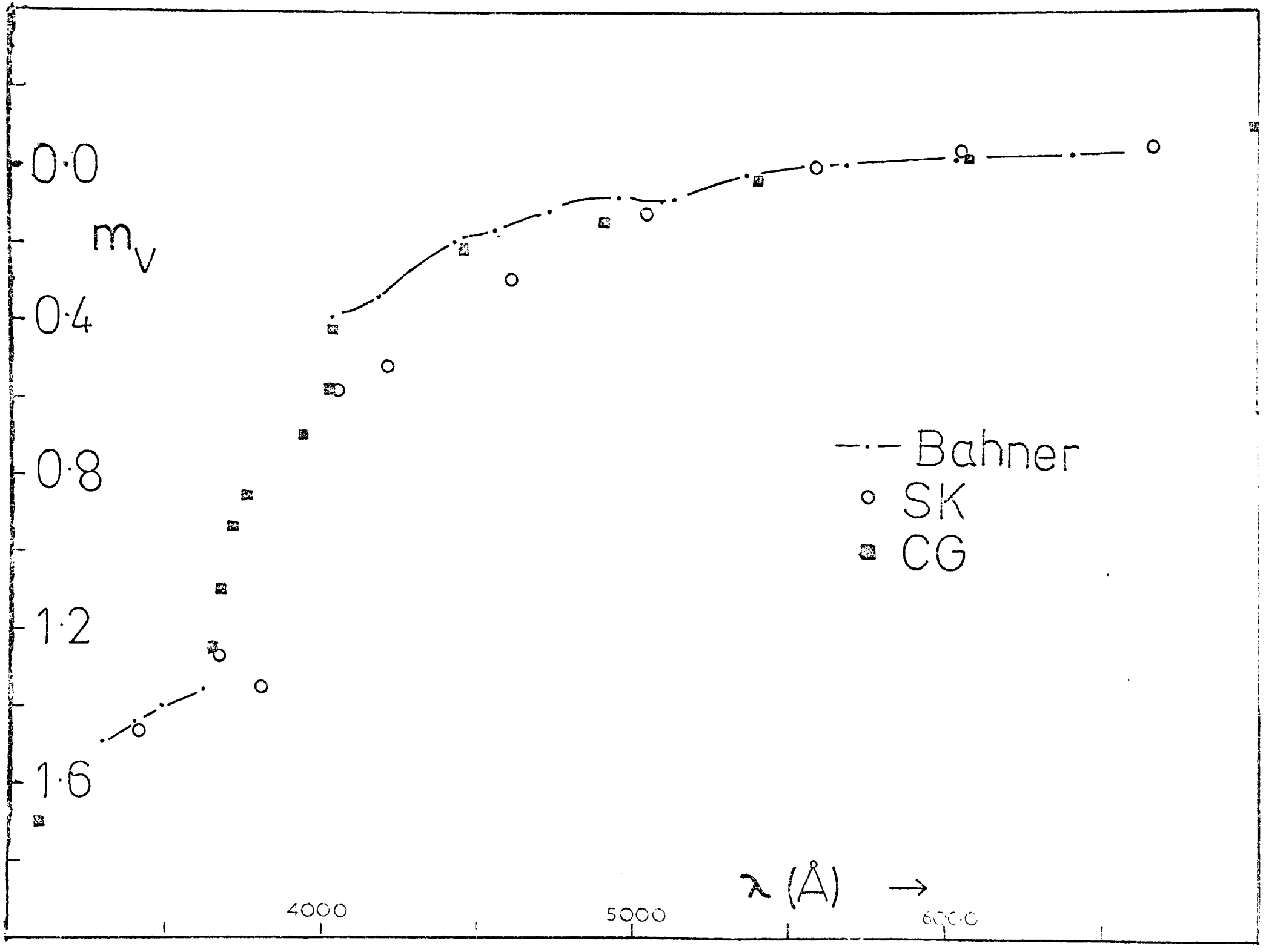

Model fluxes for Procyon (after CG 1973)

Figure 4.4

1970 for a review). Many possible cool opacity sources have not been investigated and those that have, e.g. FeI (Travis and Matsushima 1968) contain gross uncertainties "even for astronomers". At short wavelengths scattering may replace H^- as the dominant opacity, thus Rayleigh scattering by H, H_2, He and possibly even C, should be included. The fact that all flux curves for cool stars, (including the sun), are less than theory predicts for $\lambda < 4000$ Å warrants further investigation of cool ultra-violet opacities.

The difficulty of constructing line-blanketed models explicitly has led to widespread use of 'scaled atmospheres'. These are models for stars of different T_e but supposedly identical in all other respects, obtained by scaling $T(\tau)$ as $T_e(\text{new})/T_e(\text{old})$; pressures can be recalculated if necessary using this new distribution. Various investigators have attempted to demonstrate that over large ranges of T_e scaled blanketed distributions are accurate to within $\pm$ 10 degrees at most depths (e.g. CG 1969). The principle of scaling can be investigated by considering the Rosseland depth. From (4.15), (4.17) and integrating the Plank function

$$\int \pi F_\lambda d\lambda = \frac{4\pi}{3} \frac{d}{d\tau_{Ross}} \int B_\lambda d\lambda = \frac{4\pi}{3} \frac{d}{d\tau_{Ross}} \left(\frac{\sigma T^4}{\pi}\right) = \frac{16\sigma T^3}{3} \frac{dT}{d\tau_{Ross}} \qquad (4.27)$$

Thus in a purely radiative model

$$\sigma T_e^4 = \frac{16\sigma T^3}{3} \frac{dT}{d\tau_{Ross}}$$

$$\text{whence} \quad T(\tau_{Ross}) = T_e \left(\frac{3}{4}\tau_{Ross} + C\right)^{1/4} \qquad (4.28)$$

and $T(\tau_{Ross})$ should scale as T_e.

Scaling will therefore only be valid on a τ_{Ross} depthscale in a model without convection. In fact many workers have used scaled

solar models for $T_e \sim 4000^\circ$ (Upson II 1973, Gasson 1966). For solar models $\tau_{Ross} \sim \tau_{5000}$, but at 4000° K an appreciable flux in the near infra-red makes $\tau_{Ross} \sim \tau_{1\mu}$. This shifting Rosseland scale will lead to a small error over large ranges of T_e. Changes in convective equilibrium are also important. Fig. 4.5 shows the error at various depths found by scaling different models in the CG grid (which includes convection) down to 4000° K. It is remarkable that even over small changes in T_e errors of 100° deg are common; this is contrary to the findings of CG at 6000° K. The importance of convection in the region 4000° - 4500° K makes a scaled model $6000^\circ \rightarrow 4000^\circ$ only slightly worse than one from $4500^\circ \rightarrow 4000^\circ$. Fig. 4.6 shows a similar graph for models scaled to 4500°, including the solar model of Gingerich et al (1971). Even here scaled models are unlikely to be correct to within 100 deg. at important depths. Similar errors were found in interpolated models. A crude abundance analysis has shown that this error corresponds to 0.08 dex in the derived metal abundance.

Perhaps even more surprising is that a scaled solar blanketed model at 4000° may be worse than an unblanketed model. Since

$$\sigma T_e^4 = \int_0^\infty \pi F_\lambda^{line} \, d\lambda$$

then defining a continuum temperature $\sigma T_c^4 = \int_0^\infty \pi F_\lambda^{c} \, d\lambda$

and so

$$\frac{T_c}{T_e} = \left(\frac{1}{1 - \eta_{total}}\right)^{1/4} \qquad (4.29)$$

where η_{total} is the total line-blocking coefficient. As an illustration $\eta = 0.10$ for Arcturus hence $T_c - T_e \sim 100^\circ$, which is about the same as the error introduced by scaling. Thus in the case where $T(\tau)$ is not affected by the lines, the method could be used to produce a blanketed model from an unblanketed one. For cool stars where η is large however, backwarming changes $T(\tau)$ considerably as Fig. 4.7 shows.

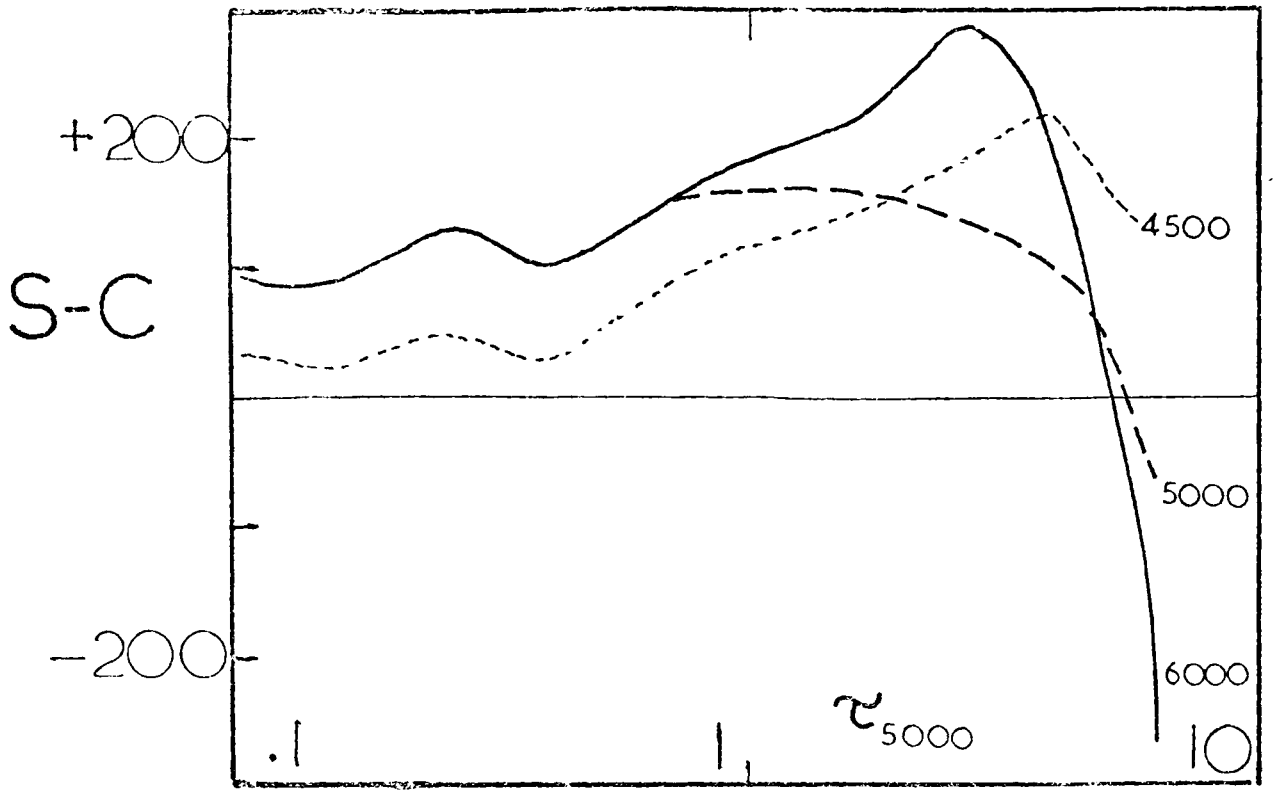

Figure 4.5

Scaled & calculated models at 4000 K (log g = 3)

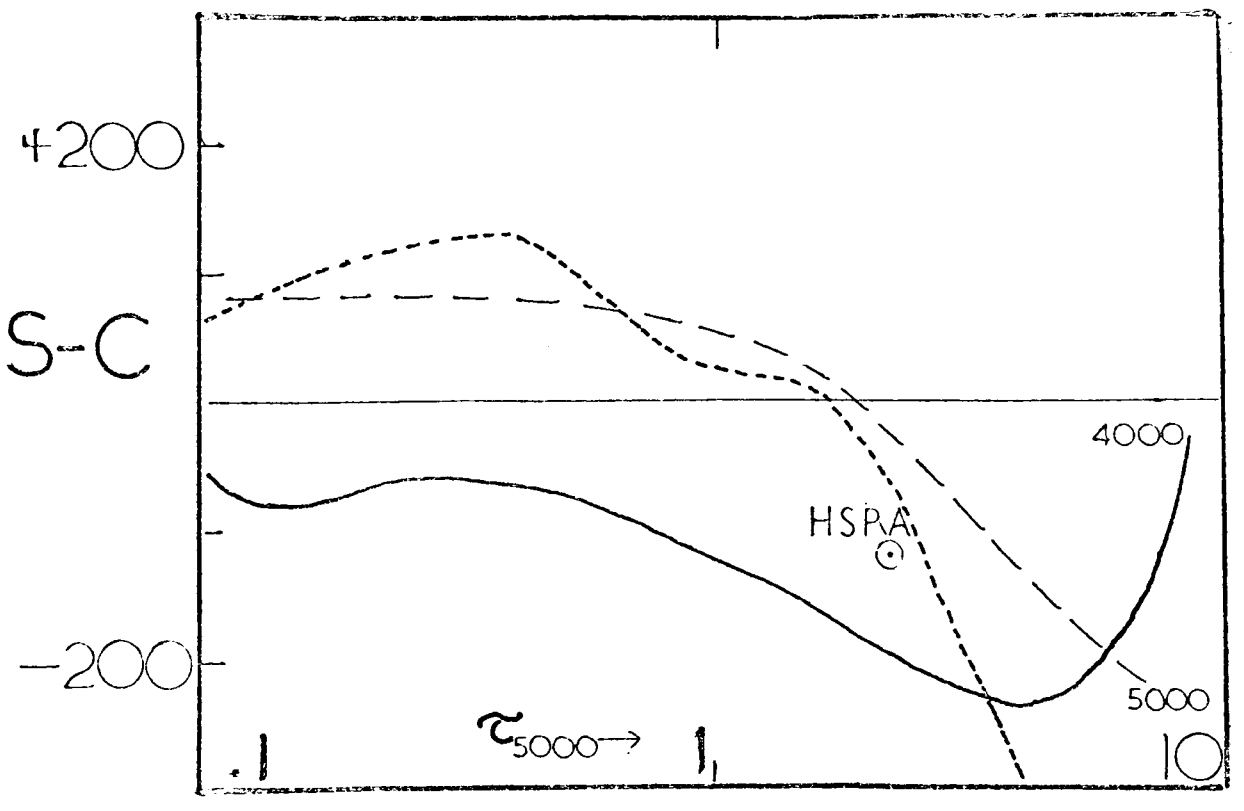

Figure 4.6

Scaled and calculated models at 4500 K (log g = 3)

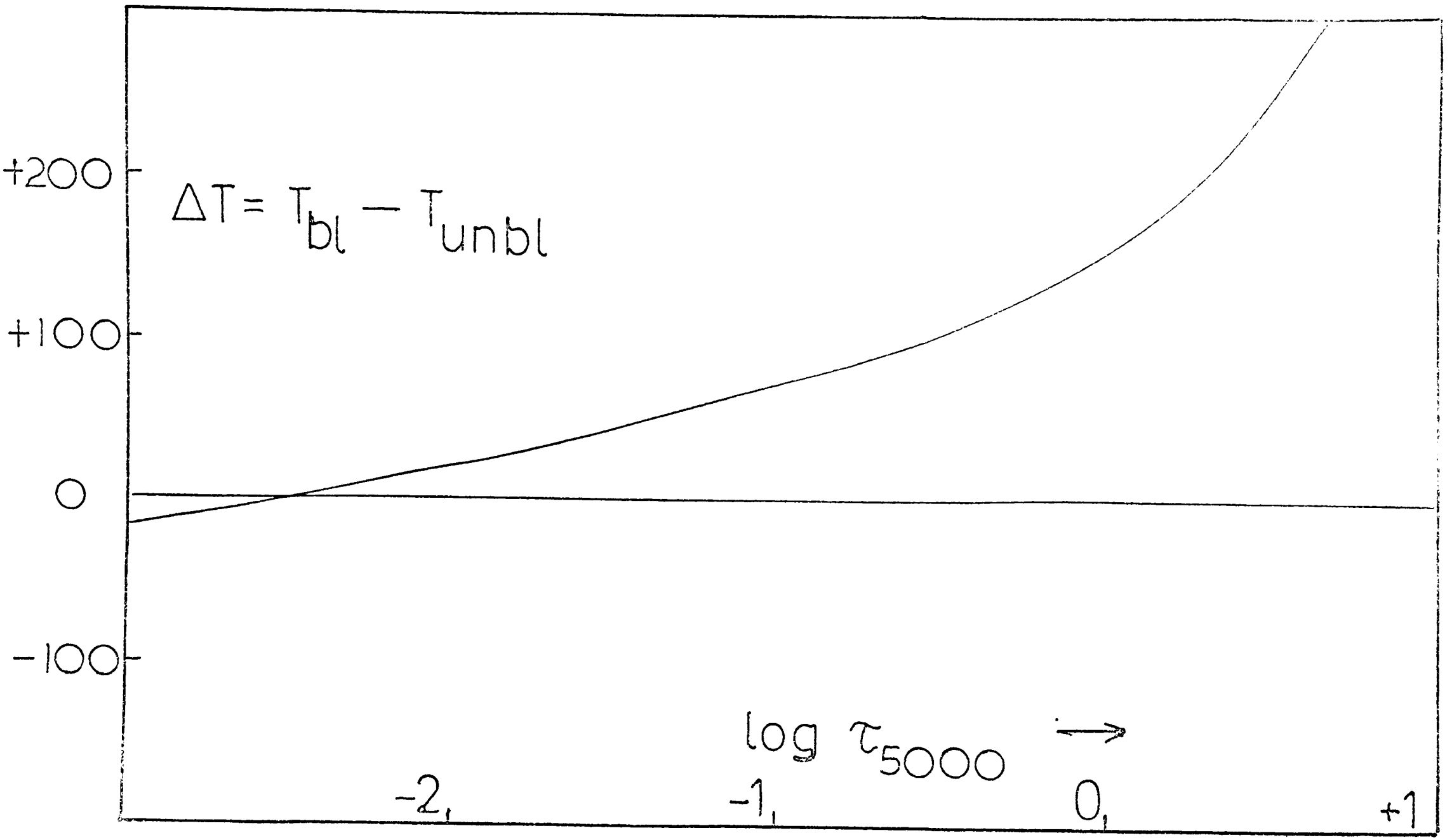

Figure 4.7

Blanketed and unblanketed temperature distributions at 4000 K

It has already been shown that convection may be important in disrupting scaled models for T = 4000 - 4500° K. The opacity rises sharply at the H ionisation zone and the temperature gradient becomes steep enough for convection. This is increasingly important for later spectral types, and particularly for giants and supergiants. Unfortunately 1/h affects T(τ) considerably for the deepest regions though the flux carried does not change much. Convection is possibly the worst problem in studying of cool stars since not only is the mixing length theory inadequate, but 1/h is also unknown.

It is of interest to compare the continuum fluxes of various blanketed models for a standard case: T_e = 4000° log g = 2.0. Fig. 4.8 compares the following models:-

1) Auman (1969) — 1b=atomic + H_2O
2) CG (1969) — 1b=empirical atomic (Arcturus), convection
3) Johnson (1973) — 1b=atomic (solar) + molecules, convection, molecules in equation of state.
4) ATLAS — no 1b, convection

(1b=line-blanketing.)

Johnson claims his model at T_e = 3300°K reproduces the flux curve for α Ori Betelgeuse (Faÿ and Johnson 1973) yet his flux curve shows several features absent in other curves here on Fig. 4.8. There is a displacement of u-v flux to the near infra-red which suggests his blanketing in the u-v may be too strong. The fact that even the unblanketed ATLAS curve comes closer to a typical observed curve at this temperature (e.g. Arcturus Fig. 3.4) implies Johnson's statistics are less realistic than those of Auman and CG, whose curves are similar to that of ATLAS. Johnson included CO in his models and it is interesting to note that in the far infra-red they predict a trough at 4.5-5.5 microns ( ) shown on Fig. 4.8) consistent with the remarks made in section 3.4. He agrees (private communication 1974) that his models are at present rather unreal-

Figure 4.8

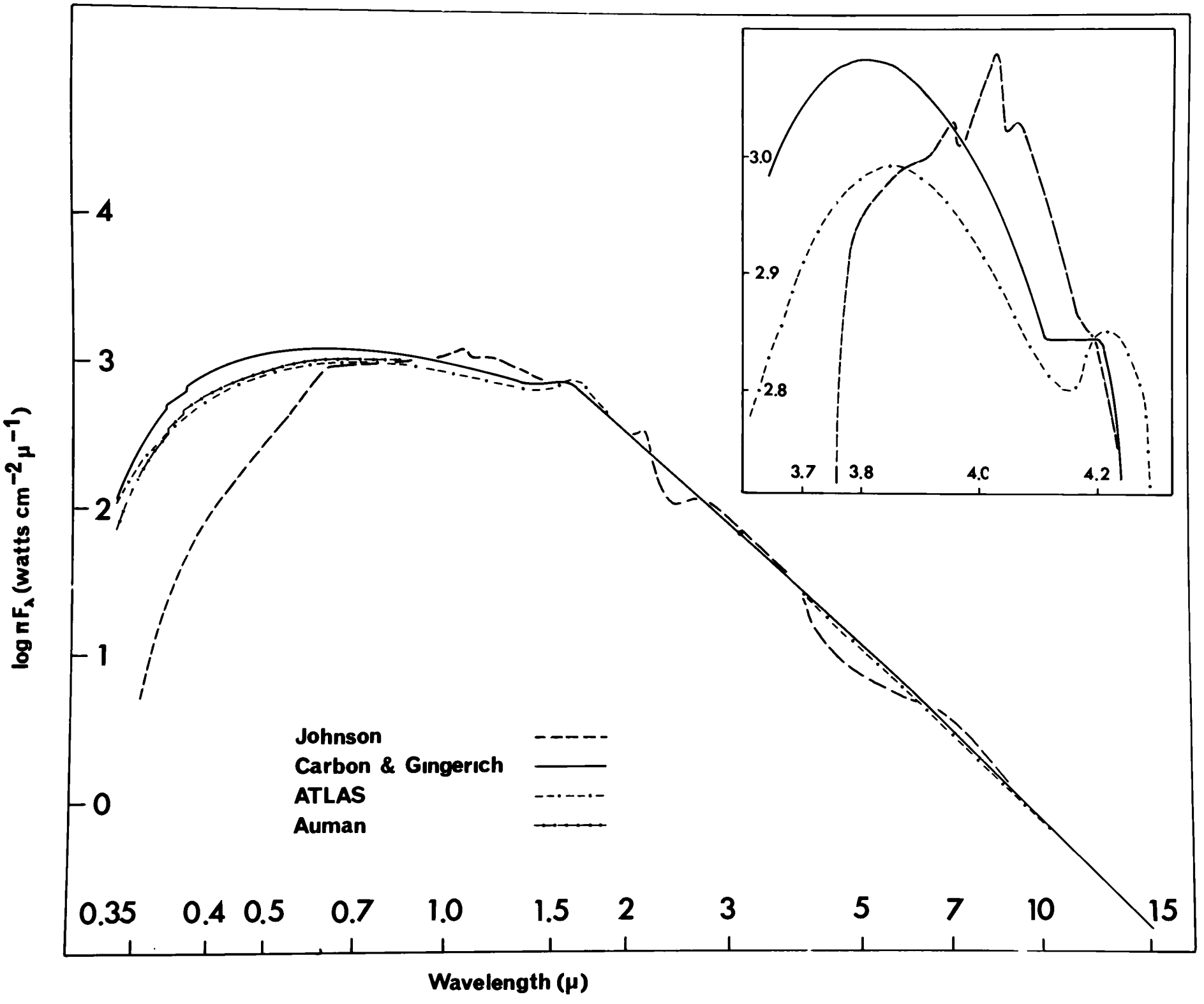
log πF_λ (watts cm^-2 μ^-1)
4
3
2
1
0
Johnson
Carbon & Gingerich
ATLAS
Auman
0.35
0.4
0.5
0.7
1.0
1.5
2
3
5
7
10
15
Wavelength (μ)
3.0
2.9
2.8
3.7
3.8
4.0
4.2

istic, and is attempting to rectify this by adding TiO and other more exotic molecules. His approach, whilst instructive, has its shortcomings at present, possibly because the incorporation of the molecular opacities as a straight mean is unrealistic.

The above models were all calculated in LTE. For lower temperatures and densities non LTE will be important and much work is needed in this direction, Simon (1971) has investigated the chromosphere of Arcturus attempting to fit strong line profiles; he found a temperature reversal was necessary. Yet Peytremann and Avrett (1974) revealed that the CaII-K line was fitted better by a LTE model. It would appear therefore, that like line-blanketing, a non-LTE analysis depends critically on the way it is incorporated.

4.5 A model atmosphere for Arcturus

A model can be crudely represented by four parameters: effective temperature (T_e), surface gravity (log g), composition and opacity, all of which are important though in different ways and to varying extents. T_e is the most important parameter as it will affect subsequent observational determination of all other parameters. It can be found by studying the flux curve which, for cool stars, is fortunately more or less independent of gravity and composition. The opacity includes line-blanketing which can alter the flux curve considerably as Fig. 4.8 has already demonstrated. It therefore simplifies matters considerably to regard the flux curve as a way of distinguishing between models in which line-blanketing has been incorporated in different ways, and then one can proceed to fix T_e from a grid of the most realistic models.

For Arcturus the models of CG are the most encouraging and the determination of T_e was performed using a grid of their models. For cool stars, the gravity must come from considerations of the

line spectrum, and it is therefore desirable to consider a grid of models with various gravities and a fixed $T(\tau)$ appropriate to a determined T_e and line-blanketing.

4.5a Effective temperature

Previous determinations of T_e for Arcturus, given in Table 4.1, are of interest in tracing a steady rise in the value as new astronomical techniques have developed. The extent of the revision may be seen from a comparison of the value of 3810^o K for a K2III star given by Keenan and Morgan (1951) with that of 4250^o K given by Allen (1973). As later studies of Arcturus, using the model to be determined here, will investigate the existence of equilibrium in the atmosphere, methods for determining T_e that rely on ionisation and excitation equilibria must be avoided. The continuous opacity in Arcturus is mainly due to H^- (see later), and as Lambert and Pagel (1968) have satisfactorily shown this is formed in equilibrium, methods involving the use of the continuum flux curve are preferable. In Table 4.1 the two distinct methods for determining T_e have been separated.

In principle T_e can be obtained directly from the total flux.. Combining (3.3) and (4.2) gives

$$\mathcal{Y}^{\oplus} = \pi F^{\oplus} = \frac{\sigma T_e^4}{4} \theta^2 \qquad (4.30)$$

This method has the advantage that no allowance for line-blocking is necessary. In addition it does not depend on a model atmosphere. Griffin and Griffin (1967) obtained a value of 4163^o by integrating Willstrop's fluxes alone. A large contribution to the flux will come from the near infra-red however, where Willstrop did not measure Arcturus. Williams (1970) has included Walker's fluxes and the broad band colours to obtain higher values of about 4300^o (see Table 4.1 for details).

Table 4.1

Previous T_e for Arcturus

Author	Method	Value
Kuiper(1938)	Radiometric data(Pettit & Nicholson 1928)*	4074
Griffin[2](1967)	Willstrop's fluxes	4163
Williams(1970)	Willstrop & Walker's fluxes	4280
Williams(1970)	Broad band data	4370
Williams(1971)	RIK colours	4338
Simon(1971)	Willstrop plus CG models	4250
Gasson(1966)	T_{ex} for Fe relative $\odot$	4720
Conti et al(1967)	Forbidden O I lines	4150
Warren(1971)	T_{ex} for Ti relative $\odot$	4350
Warren(1971)	T_{ex} for Fe relative ε Vir	4305
Mean values:	Warren(1971)	4300 ± 50
	Linsky & Ayres(1973)	4250 ± 250

Notes: Top portion refer to methods using the flux curve, generally using ϑ of Pease(1931)
Other methods involve equilibrium assumptions

*Pettit E.,Nicholson S.B. 1928; Ap. J. 68, 279

Although the large infra-red contribution is now known with good accuracy from the Russian and Oxford scanner results, the great disadvantage of this method is the need for an angular diameter, θ . Previous determinations have used Pease's value which has now been replaced by the speckle interferometric measurement of Gezari et al (1972). To demonstrate that T_e is particularly sensitive to errors in θ , the calculation has been repeated using the comprehensive set of observed fluxes discussed in Chapters 2 and 3, together with the new θ . The total flux at the Earth from Arcturus is

$$\mathcal{F}^{\oplus} = \pi F^{\oplus} = 5.08 \pm 0.03\ 10^{-12} \text{ Watts cm}^{-2}$$

and was obtained by integrating the raw fluxes (before deblanketing). Gezari claims that $\theta = 0''.022 \pm 0.003$; this value should be corrected for limb-darkening. For Arcturus the correction is about 10% when measured with an intensity interferometer (Hanbury-Brown et al 1974). The precise value of the correction is not important for this discussion; the main concern is the uncertainty in θ (whether corrected or not) and the subsequent error in T_e. Applying a rough 10% correction gives a true diameter of $\theta = 0''.024 \pm 0.003$. Thus in (4.30):-

$$T_e = 4213^{\circ} \begin{matrix} +321^{\circ} \\ -261^{\circ} \end{matrix} \quad \text{, using } \theta = 0''.022$$

$$T_e = 4035^{\circ} \begin{matrix} +277^{\circ} \\ -231^{\circ} \end{matrix} \quad \text{, using } \theta = 0''.024$$

Using Pease's value with a 10% correction gives $T_e \sim 4200^{\circ}$ with an unspecified error.

Even with the improved diameter measurement the uncertainty of the total flux method is evidently very great. This is particularly so if the additional uncertainty introduced by the limb-darkening correction is also considered, the minimum error then would be at

least $\pm$ 300 deg.

Ideally the accuracy to which T_e is known should match that to which a subsequent abundance analysis is required. Numerical experiments show that a 5% accuracy in an abundance analysis demands T_e to $\pm$ 30 deg and whence θ should be known to 3% for this method. Thus even in the favourable case of Arcturus, a nearby giant, the uncertainty introduced by the interferometric method is still an order of magnitude too great for a reasonable determination of T_e by the total flux method.

Utilising the relative distribution of the continuum flux with wavelength has the advantage of being independent of θ. This is an elaboration of the more commonly used, but less fundamental, method based on colour differences (described for example by Williams 1971a). The continuum fluxes will be unreliable shortward of 4800 Å because of inaccurate blanketing corrections, but it is possible to compare the region $\lambda > 5000$ Å with models at different temperatures. The CG model $T_e = 4500^o$, log g = 3.0 was scaled to various effective temperatures in the range 4200-4500° K and fluxes were obtained for each model. Fortunately the adopted T_e is fairly close to 4500° and thus large errors in scaling will not affect the conclusions. The fluxes produced by these models were shown to be virtually independent of gravity and input abundance, in agreement with the findings of Auman (1969a).

The sensitiveity of the predicted flux curve to changes in T_e is greatest in the region 4500-6500 Å and drops for shorter wavelengths. This is explained by the importance of neutral hydrogen as an opacity source in this wavelength region. Fig. 4.10 shows the various opacity contributions at $\tau_{5000} = 1$ for 4400°K, and Fig. 4.11 shows the increased temperature at $\tau_{5000} = 4$ has introduced a Balmer discontinuity of about 0•4dex. This substantial increase in the total opacity at short wavelengths is much greater than the corresponding increase at 5000 Å (where the opacity is almost

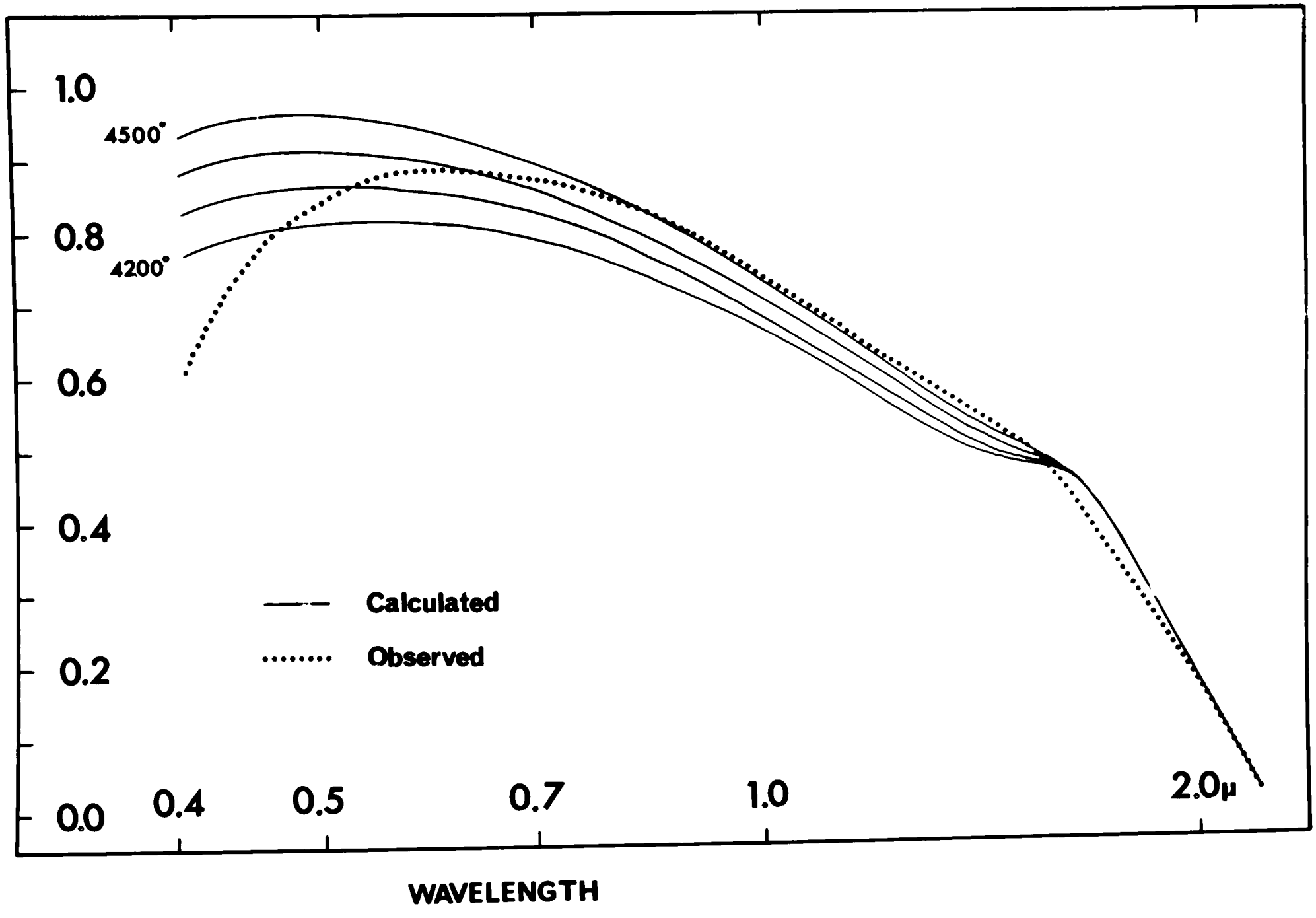
1.0
0.8
0.6
0.4
0.2
0.0
LOG F$_\lambda$/F$_{2.2\mu}$
4500°
4200°
Calculated
Observed
0.4
0.5
0.7
1.0
2.0μ
WAVELENGTH

Figure 4.9

FIG. 4.10

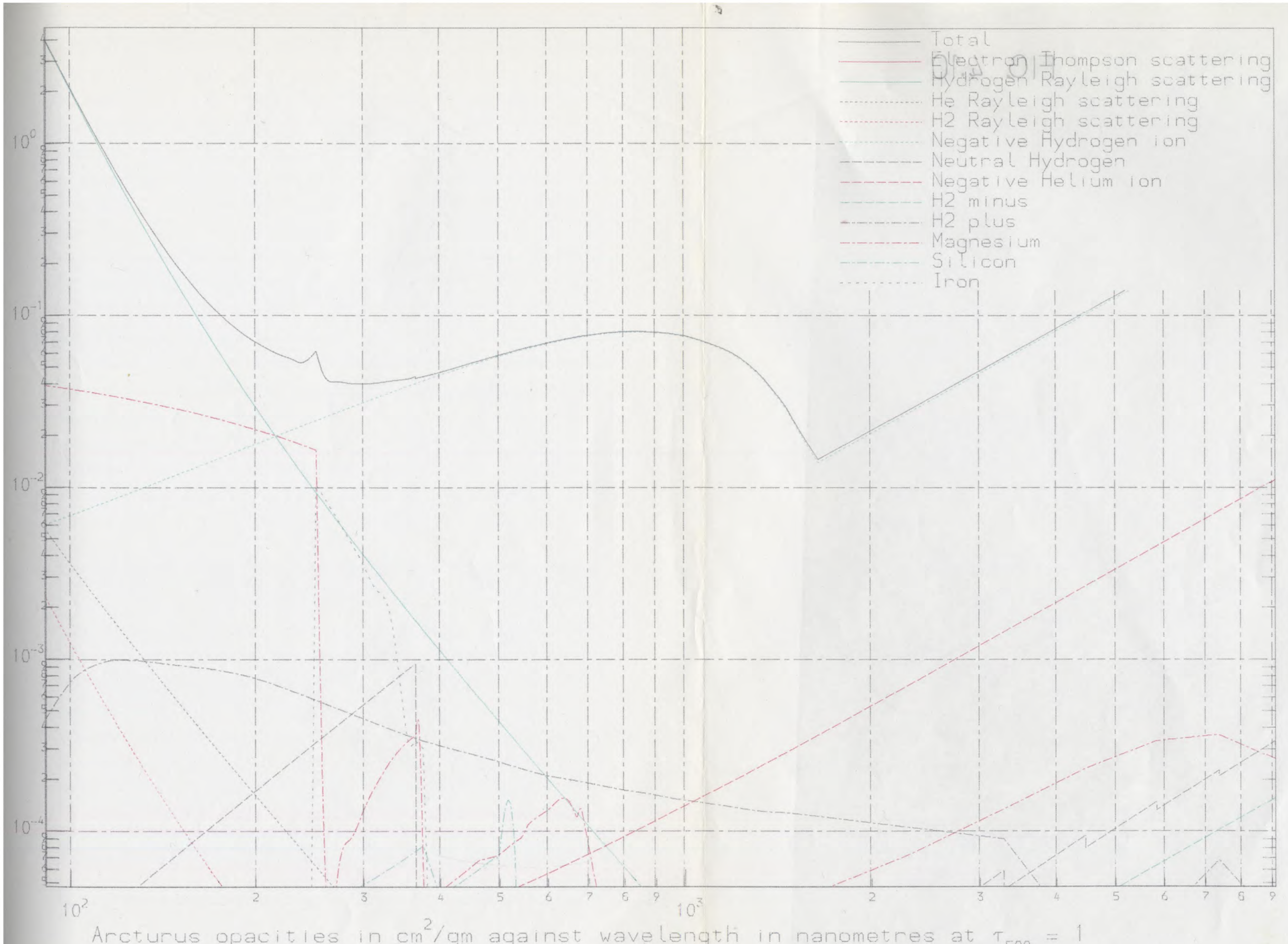

Arcturus opacities in cm^2/gm against wavelength in nanometres at $\tau_{500} = 1$

FIG. 4.11

FIG. 4.17

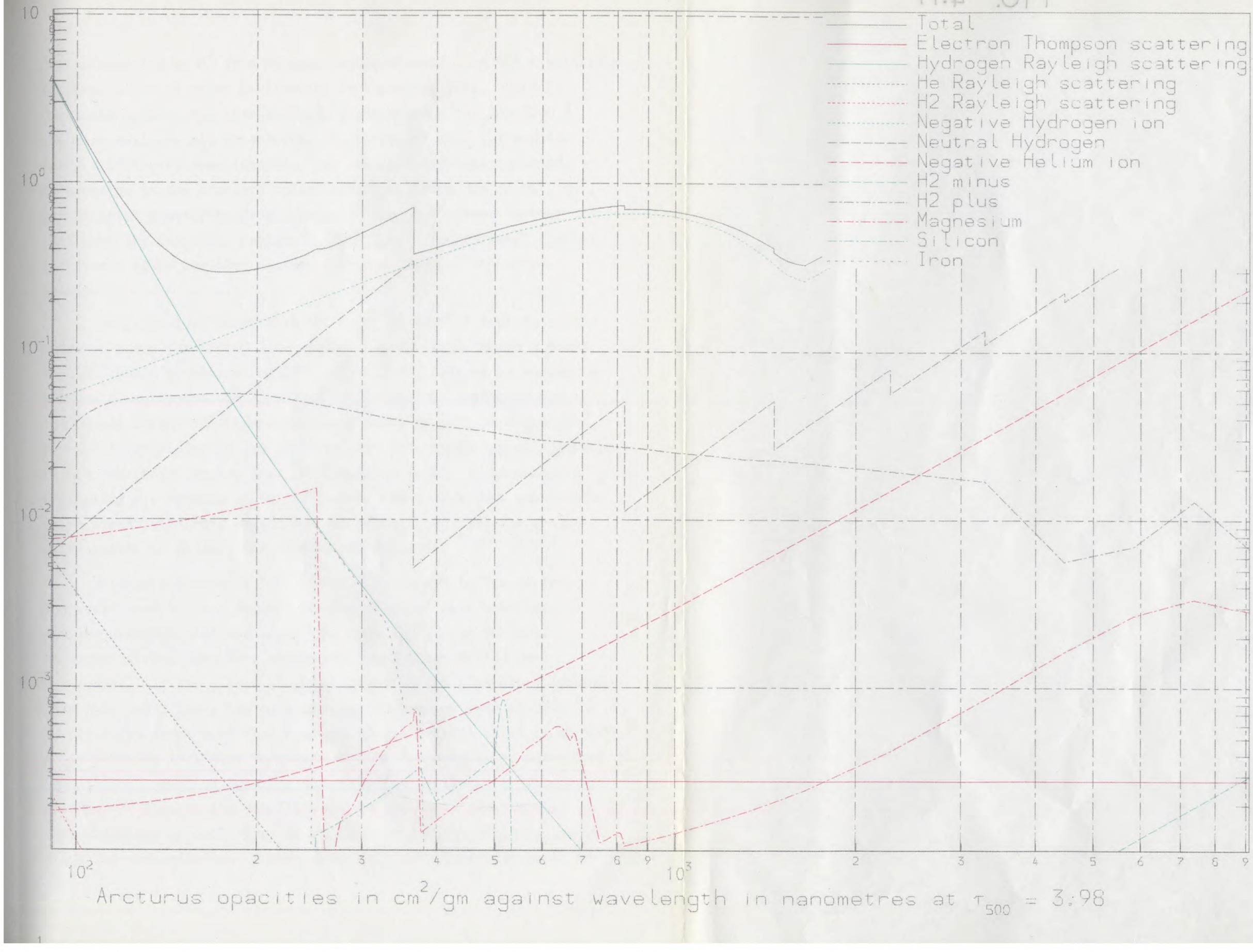

Arcturus opacities in cm^2/gm against wavelength in nanometres at $\tau_{500} = 3.98$

exclusively due to H^- even at solar temperatures), and the sensitivity to temperature at short wavelengths is therefore less. This is fortunate because the line-blanketing corrections for $\lambda > 5000$ Å are more reliable and in matching the curves of Fig. 4.9 results for $\lambda < 4800$ have been ignored. The calculated fluxes included, in addition to the standard solar opacities, those due to He^-, H_2^-, and Rayleigh scattering from He atoms. Fig. 4.10 shows however that over the important region λ 5000- 2μ, H^- and Rayleigh scattering from H atoms together account for some 99.6% of the total opacity.

The comparison shows that the model at 4500° K reproduces the observed shape for $\lambda > 6000$ Å to within 0.04 dex(10%) though a model at 4400° would be better for $5000 < \lambda < 6000$ Å. There is however a serious disagreement for $\lambda < 5000$ Å which could be partially due to inaccurate fluxes and blanketing corrections as well as due to an incomplete knowledge of the opacities at these wavelengths. Although it was concluded earlier that circumstellar reddening is probably negligible for Arcturus, the '$1/\lambda$-law' could make such extinction quite sizeable in this region and yet perhaps not heat the grains sufficiently to produce a far-infra-red emission.

This poor agreement for $\lambda < 5000$ Å is clearly quite serious and would seem to be a general problem for cool star analyses; similar discrepancies are noted by Kurucz (1974) for the sun, by Morgan (1970) for εVir, and by Faÿ and Johnson (1973) for Betelgeuse. If the source of error lies with the blanketing corrections this would imply the continuum is 20% too low even at 4500 Å. As the first stretch of flat spectrum in the Griffin atlas is at 5500 Å it is possible that many thousands of weak features (e.g. molecular transitions) could be lowering the effective continuum by this amount. If this is the case it would be a serious blow to all investigations of cool stars as it would be a formidable problem to allow for such effects. A more optimistic solution would be to say

that the models are simply unrealistic at short wavelengths. Quite apart from possibilities of molecular blanketing there may be missing continuous opacities. It would be beneficial to study the same method for another star of roughly this effective temperature (Betelgeuse is unfortunately not a good choice for reasons described earlier). These uncertainties necessitate using only the region 5000-2μ in fixing T_e, and from Fig. 4.9 a value of

$$T_e = 4450^\circ \pm 50^\circ \text{ K}$$

is adopted. The error is due to the quality of the fit obtained, taking into account the accuracy of the observations.

This value is slightly higher than other values obtained by flux comparisons, which give $T_e \sim 4250^\circ$ (e.g. Williams 1971a). They often rely on scaled solar models however, which will not only introduce large scaling errors of 150 deg or so (see last section) but also assume that backwarming has the same effect on the solar $T(\tau)$ as it does for Arcturus. This is a poor approximation as Fig. 4.6 has shown.

Perhaps more disturbing however is that the value obtained from the shape of the flux curve is a good deal higher than that obtained from the total flux, even after allowing for the error in θ . Yet it is quite evident that a model at 4250° for example, would give serious flux inconsistencies at all wavelengths. Further evidence for the higher T_e comes from the size of the sub-maximum at 1.6μ which decreases with increasing temperature because of the reduced H^- abundance. Not only is there evidence for such a brightening in the observed curve but the bump is within 5% of that expected at 4400° K. At 4250° K the bump would be twice as large and quite inconsistent with Walker's fluxes. The adopted higher T_e could mean that the angular diameter used in the total flux calculation is too high, either because the limb-darkening correction is much less than 10% or because Gezari's error analysis is

too optimistic; Pease's value may be more accurate after all!

It is possible to determine T_e from the stellar monochromatic flux although this requires both a model and an angular diameter. Whereas the total flux is proportional to the fourth power of T_e, the monochromatic flux depends on a higher power and thus the error introduced by θ can be offset by an increased sensitivity to T_e. It is essential to choose a wavelength where the opacity is well-defined, and this restricts the method to $\lambda\lambda 5000 - 1\mu$. The precise T_e obtained in this case will depend on wavelength since one model cannot fit the observed curve even over this limited wavelength range. Using Gezari's θ with the 10% correction gives:

$$T_e = 4130^\circ \pm 170^\circ \quad \text{at} \quad \lambda 5556 \text{ Å}$$

$$T_e = 4400^\circ \pm 130^\circ \quad \text{at} \quad \lambda 1\mu$$

The error (solely due to uncertainties in θ) is thus a little less than for the total flux method, though still too large for serious application of this method. A further error will of course be introduced if the model is unrealistic at the chosen wavelength.

For almost every other cool star, the angular diameter is known with even less precision, if at all, and both monochromatic and total flux methods become quite inadequate. The only hope is to use the relative distribution and the present error of $\pm$ 50 deg could be reduced if more realistic models were available.

4.5 b Gravity

The surface gravity, g, affects the equation of hydrostatic equilibrium (4.13) and hence the pressure structure of the atmosphere. Thus whereas $T(\tau)$ depends on T_e but hardly on g, the rest of the model requires a precise value for g. The electron pressure is particularly important since it determines the degree of ionisation needed for abundance analyses.

The flux curve is pretty well independent of gravity for cooler stars. This is a direct corollary of the independence of $T(\tau)$ to changes in g, and can be verified experimentally by inspecting the fluxes and $T(\tau)$ of models in the CG grid. Physically this is explained by the dominance of H^- as an opacity source at these temperatures. Although the actual opacity at any λ changes with electron pressure (and hence gravity), the shape of $\hat{\kappa}_\lambda$, which determines the relative flux curve, does not. This is fortunate in one respect as it renders the previous determination of T_e independent of g, but it also means that features of the flux curve normally used as gravity indicators are not present and resort to the line spectrum has to be made. Consider for example the Balmer discontinuity at λ3647 Å which has been used fairly successfully in determining gravities for hotter stars (Underhill 1972). Fig. 4.10 shows that at 4500° K there is no discontinuity, and even if there were, the continuum in this region would be difficult to establish.

The disadvantage of using line features as opposed to continuum features for gravity determinations, is that a host of other quantities are immediately needed. For detailed work a model atmosphere is required, though once T_e has been established a grid of models can be constructed. Line profile analyses, however, require abundances and atomic constants and depend critically on velocity fields, all of which can be uncertain.

The simplest and perhaps most common spectroscopic method used for cool stars involves the ionisation equilibrium of Saha's equation. By determining the abundances of elements in different stages of ionisation a mean electron pressure can be found, g then follows from an approximate theory of Pagel (1964). Dividing the elements into hydrogen and metals gives an electron pressure

$$P_e = P_H \left(x_H + \sum x_m \right)$$

where x is the degree of ionisation. Then for H^- opacity alone (4.13) becomes:

$$dP = g m_H / \alpha(H^-) \rho_e$$

and differentially with respect to another star these equations give:

$$[g] = [\rho_e] - [\chi_H + Z\chi_M] + [\alpha(H^-)] \qquad (4.31)$$

where the [] notation denotes logarithmic ratio.

The method is not always used differentially though it then requires atomic oscillator strengths (see Chapter 5) which could contain systematic errors for ionised species. A mean electron pressure is used despite the fact that p_e varies rapidly with depth. Such gravities can therefore only be regarded as rough estimates. In this thesis the method is not desirable as it assumes LTE for ionisation. Although this may be so, the eventual need is for an Arcturus model to test such an assumption.

The relationship between spectroscopic g-indicators and element abundances is unfortunate since it makes any detailed analysis an iterative procedure. Gravity indicators used in narrow-band photometry also rely on some abundance for their calibration. Ideally we require indicators that are independent of abundance and velocity fields. Spinrad and Taylor (1969) claim they have such a system though this is refuted by Gottlieb and Bell (1969). Narrow-band methods are successful only where average abundances are meaningful (e.g. in large samples); in an individual study a more exacting indicator is sought.

Despite the good quality spectrum there is no reliable gravity for Arcturus. Griffin and Griffin (1967) used Pagel's equation (4.31) with respect to the sun and ε Vir and obtained values of 50 and 100 cm sec^{-2} respectively. They concluded that $g \leqslant 100$, though an

independent error analysis of their results gives $37 \leqslant g \leqslant 150$.

Upson II (1973) has developed an ingenious indicator for late giants and applied it to Arcturus. As these stars show a strong gravity effect in the formation of molecules (through the appropriate partial pressures), it follows that the observed ratio of OH/O I line strengths can be used to discriminate between models of different gravities. The O/H abundance ratio is required and Upson determined this separately. Using a spectrum synthesis program he concludes g is "about" 50 and "is not" 125. Unfortunately his models were scaled solar ones reproduced at the low T_e of 4100° K. This may mean his gravity interpretations are in error by as much as 0.3dex.

As a check on these values it is possible to estimate g from the luminosity of Arcturus. This is defined as

$$L = 4\pi R^2 \sigma T_e^4 \qquad (4.32)$$

and since

$$\frac{M}{M_\odot} = \frac{g}{g_\odot}\left(\frac{R}{R_\odot}\right)^2 \qquad (4.33)$$

a determination of the mass from a mass-luminosity relation gives g. R must come from the parallax and angular diameter. Using Gezari's diameter gives

$$g = (45 \pm 10)\frac{M}{M_\odot}$$

and the mass-luminosity relation of Harris et al (1963) for $T_e = 4500^{\circ}$ gives $M = (2.2 \pm 1.2)M_\odot$ ie. $45 \leqslant g \leqslant 153$

Williams (1971a) determines L from the parallax and the Wilson-Bappu effect (Wilson and Bappu 1957). This empirical relationship (between L and the core profile of the CaII-K line), has been shown to be dependent on the metal abundance of the star (Pagel and Tomkin 1969), though Helfer (1969) has attempted to salvage a

relation by including a metal abundance term. Williams uses the Iben (1967) mass-L relation to get g = 125, a value specifically excluded by Upson II. Williams value is probably only accurate to about 0.30 dex however.

A method avoiding equilibrium and abundance assumptions has been suggested by Professor Blackwell and R.B. Willis, and involves comparing strong and weak lines originating from the same lower level. For the sun, where g is accurately known, the abundance of the level is found using the weaker line and applied to the stronger line to give a damping constant consistent with its wing profile. A similar analysis for Arcturus with the known damping constant can distinguish between models of different gravities. The method requires a good oscillator strength for the weaker line, and the fact that both lines must be clear and unblended limits the choice considerably. In investigating wing profiles uncertainties in continuum levels and instrumental functions will be important.

It is proposed that this method be applied to a variety of late-type stars including Arcturus, though in this research it has not been performed for two reasons. Firstly, for reasons given in Chapter 7, the level population can only be determined accurately if a weak line is used and at present there are no good oscillator strengths for such lines in the Arcturian spectrum, though using techniques described in Chapter 6 these values will be shortly available. Secondly, all line profile analyses and the majority of spectroscopic gravity-indicators are sensitive to the velocity field. It is necessary, at first, to assume a gravity and determine the field from a preliminary abundance analysis. The non-thermal velocity field is conventionally divided into two components; microturbulence - a small scale field affecting abundance interpretations (discussed in Chapters 7 and 8), and macroturbulence - a large scale field which affects only the profile of the line.

For this preliminary investigation a value of g = 50 is assumed; this corresponds to a mass of $\sim 1.2\ M_{\odot}$. The micro-turbulence derived in the abundance analysis can be used to redefine g more precisely, if required, using the above method.

4.5 c Results and discussion

The previous sections gave $T_e = 4450 \pm 50^{\circ}$ K and g $\sim$ 50 for Arcturus. It is now relatively straightforward to construct a model from these parameters. It was hoped, at the inception of this research, that a detailed grid of models could be constructed using ATLAS with the preliminary line-blanketing statistics of Edmonds (1973). This program was made operational on the University of London CDC7600 but is not amenable, in its present form, for calculating cool models.

ATLAS uses a fixed mass-depth scale, conveniently termed RHOX ($= \int \rho\, dx$), rather than a optical depth scale. This cuts computer time by about $\frac{1}{3}$ since iteration on the opacities in solving for pressure is eliminated. The temperature correction procedure is less efficient however. As RHOX and p are slower functions, with respect to T, than τ_{Ross} and τ_{λ}, a small correction ΔT implies a large $\Delta\tau$ and a negligible ΔRHOX. This makes such corrections unstable on a RHOX scale and it is perfectly possible for ATLAS to deconverge a flux-constant model! The situation is worst for cool stars because of the convective flux included in the temperature corrections. Using a patched version the author has obtained convergence to within 0.1% in 30 iterations for $T_e \sim 4000^{\circ}$K, but this is clearly uneconomical. Other users of this code (e.g. Faÿ and Johnson (1973), Simon (1971) etc.) run older versions of the program with a conventional τ_{5000} depth-scale. Their models converge in about 10 iterations, each iteration takes 3 times as long! There is clearly a need for a faster convergence procedure for cool stars

with convective zones.

By preserving the blanketed $T(\tau)$ from the CG model, temperature corrections are unwanted in this work. A couple of iterations with this $T(\tau)$, and a specified T_e, g gives the entire Arcturus model. The only free parameters left are composition, opacities and turbulence. The composition hardly affects the model at all and nominal values of n(He)=0.11n(H) and metals at $\frac{1}{3}$ solar abundances were adopted. Turbulence (consisting of micro plus macro) can contribute a significant pressure via.

$$P_{turb} = \frac{1}{2} \rho v_{turb}^2 \qquad (4.34)$$

For $p_{turb} \sim 0.1\ p_{total}$ this requires $v_{turb} > 3\text{km sec}^{-1}$ and in these models turbulence has been ignored. The opacities were decided by reference to Fig. 4.10, and convection was included with (l/h)=1 consistent with the CG models (once $T(\tau)$ is fixed this has little effect).

The final models are given in Tables 4.2 and 4.3; the convective boundary is marked. The entire models cover only 2.10^5 km which is $< 2\%$ of the Arcturus radius thereby justifying the plane-parallel geometry used. Both models have log g = 1.7 (g = 50.1) and the effects of uncertainties in this value are depicted in Figs. 4.12 and 4.13 showing $p(\tau)$ and $p_e(\tau)$ for a grid of models at 4500°K with $1.5 \leqslant \log g \leqslant 2.5$. Once the microturbulence has been established this gravity-grid could be used to determine a more accurate model for Arcturus.

Table 4.2

ARCTURUS MODEL TEFF = 4400° LOG G = 1.7

TAU5000	TEMP	PRESSURE	PE
1.000E-3	3547.4	6.129E+1	1.321E-3
1.585E-3	3561.1	9.893E+1	1.990E-3
2.512E-3	3571.8	1.469E+2	2.772E-3
3.980E-3	3585.5	2.091E+2	3.738E-3
6.310E-3	3604.1	2.906E+2	4.978E-3
1.000E-2	3627.6	3.950E+2	6.562E-3
1.585E-2	3655.9	5.313E+2	8.649E-3
2.512E-2	3690.1	7.054E+2	1.140E-2
3.981E-2	3735.1	9.296E+2	1.522E-2
6.310E-2	3791.8	1.211E+3	2.051E-2
1.000E-1	3863.2	1.564E+3	2.803E-2
1.585E-1	3958.0	2.003E+3	3.906E-2
2.512E-1	4097.9	2.540E+3	5.622E-2
3.981E-1	4259.2	3.203E+3	8.002E-2
6.310E-1	4515.4	4.061E+3	1.217E-1
1.000E+0	4832.2	5.191E+3	2.276E-1
1.585E+0	5242.8	6.624E+3	6.948E-1
2.512E+0	5761.1	7.912E+3	2.908E+0
3.981E+0	6409.3	8.606E+3	1.334E+1
6.310E+0	7044.9	8.993E+3	4.606E+1
1.000E+1	7474.1	9.251E+3	9.498E+1
1.585E+1	7794.8	9.499E+3	1.555E+2
2.512E+1	8069.6	9.750E+3	2.303E+2
3.981E+1	8319.9	1.003E+4	3.226E+2
6.310E+1	8556.5	1.036E+4	4.363E+2

Line marks convective boundary.

Other parameters for this model:

/ LTE / He:H = 0.11 / metals = 0.33 solar / (l/h) = 1 /
no turbulence /

Table 4.3

ARCTURUS MODEL TEFF = 4500° LOG G = 1.7

TAU5000	TEMP	PRESSURE	PE
1.000E-3	3628.0	5.922E+1	1.422E-3
1.585E-3	3642.1	9.556E+1	2.168E-3
2.512E-3	3653.5	1.415E+2	3.044E-3
3.981E-3	3667.2	2.009E+2	4.129E-3
6.310E-3	3686.4	2.784E+2	5.519E-3
1.000E-2	3710.0	3.778E+2	7.294E-3
1.585E-2	3739.7	5.075E+2	9.627E-3
2.512E-2	3774.5	6.734E+2	1.269E-2
3.981E-2	3820.1	8.87[illegible]E+2	1.690E-2
6.310E-2	3878.1	1.159E+3	2.267E-2
1.000E-1	3951.3	1.502E+3	3.077E-2
1.585E-1	4048.0	1.931E+3	4.246E-2
2.512E-1	4191.6	2.467E+3	6.025E-2
3.981E-1	4356.2	3.140E+3	8.526E-2
6.310E-1	4618.4	4.029E+3	1.345E-1
1.000E+0	4942.1	5.200E+3	2.856E-1
1.585E+0	5362.0	6.573E+3	9.445E-1
2.512E+0	5892.7	7.654E+3	3.935E+0
3.981E+0	6555.0	8.236E+3	1.758E+1
6.310E+0	7205.4	8.553E+3	5.908E+1
1.000E+1	7644.2	8.767E+3	1.198E+2
1.585E+1	7972.8	8.971E+3	1.935E+2
2.512E+1	8253.1	9.181E+3	2.833E+2
3.981E+1	8509.0	9.417E+3	3.925E+2
6.310E+1	8751.6	9.688E+3	5.252E+2

Notes as for Table 4.2

Figure 4.12

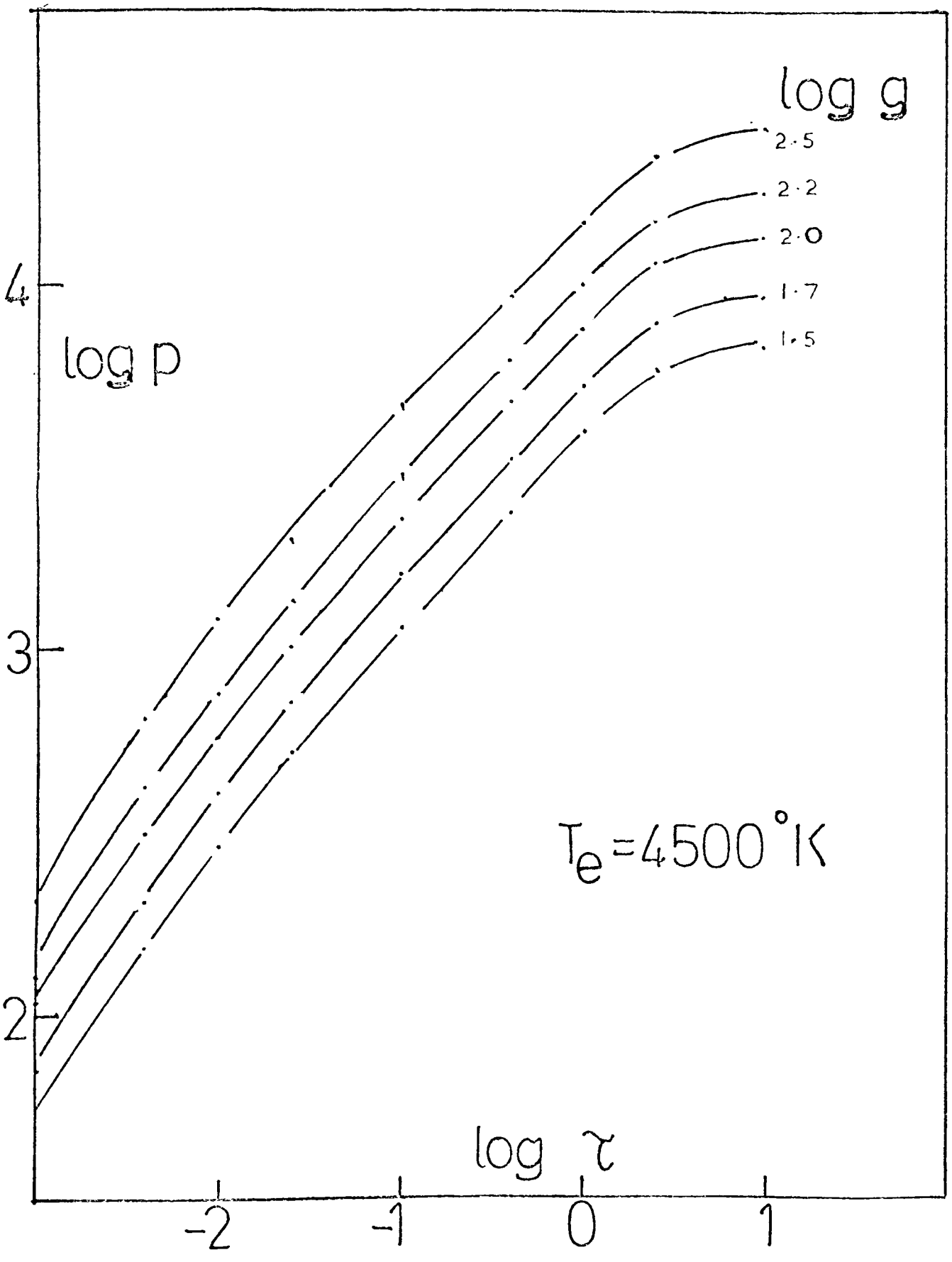

Pressure structure for a gravity grid at 4500 K

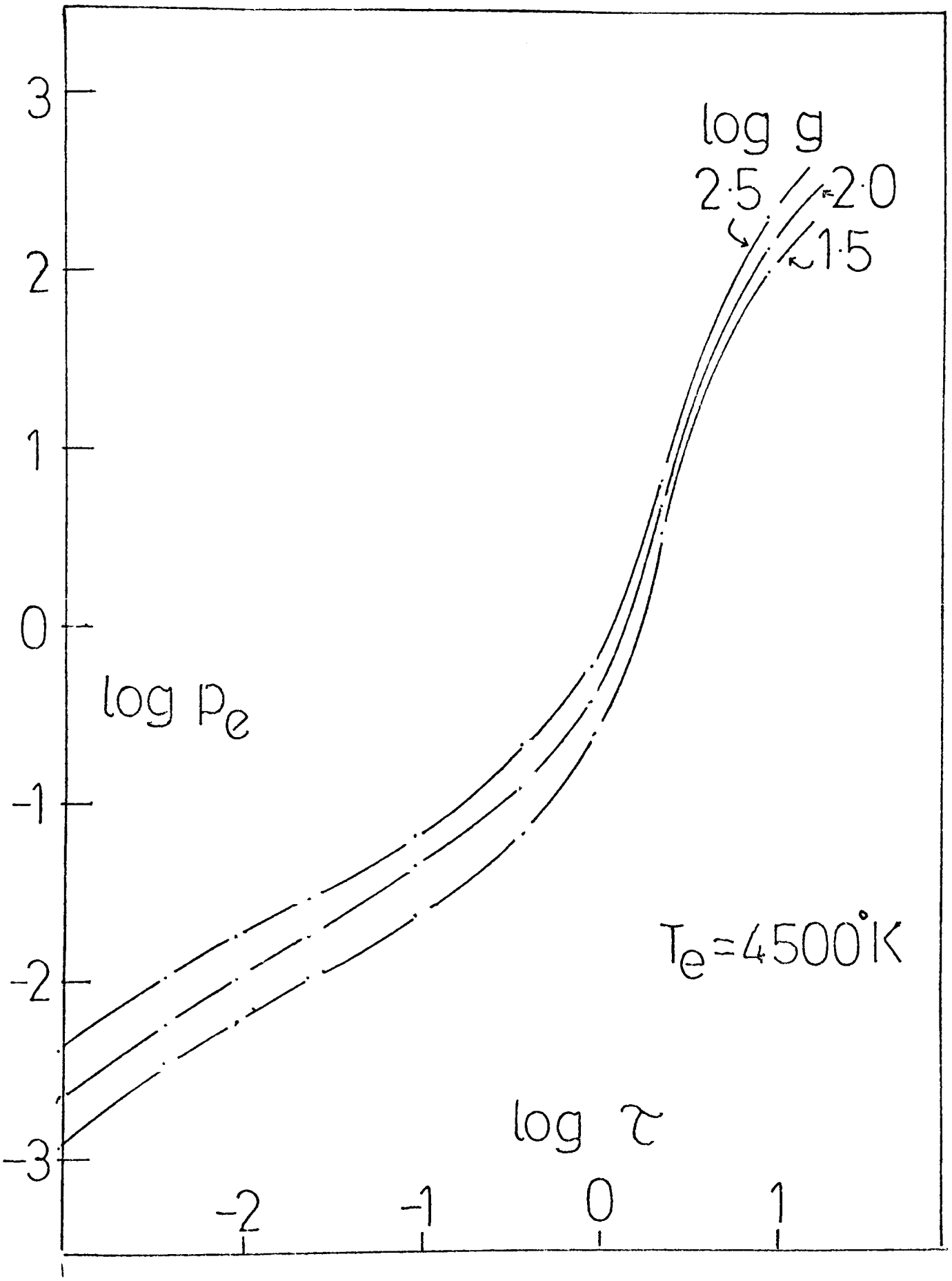

Figure 4.13

Electron pressure structure for gravity grid at 4500 K

CHAPTER 5

DETERMINATION OF OSCILLATOR STRENGTHS AND THE OXFORD FURNACE

5.1 Introduction and definitions

Of all the physical quantities required by the astronomer the oscillator strength is surely the most abused. In education for example, the treatment of the subject is usually restricted to its definition and use in procuring abundances; the outstanding difficulties in its determination are rarely mentioned. Astronomers therefore have a habit of taking the published results at face-value (despite the clarity with which large uncertainties are shown), or generally the attitude seems to be that a large quantity of poor quality results when averaged will give the right answer. This approach is dangerous, for systematic differences of 0.30dex in oscillator strengths are fairly common, and these lead to abundance differences of the same amount. Indeed, it is almost entirely because of changes in the oscillator strengths that the solar abundances of iron-group elements have been revised by factors of up to 10 during the last decade (Takens 1970). The precision for the lighter elements is generally sufficient for astrophysical purposes, but despite the recent revision there is evidence (Blackwell and Collins 1972) that there are systematic errors still present in some modern results for the iron-group elements.

The purpose of this chapter is therefore to briefly discuss the advantages and disadvantages of the various methods for determining oscillator strengths. The discussion does not pretend to be exhaustive, and there are several general reviews(e.g. Foster 1964) which are more complete. However, although oscillator strengths are useful in many branches of physics, the concern here will be for accurate values for abundance work in cool stars. The emphasis will also be for the iron-group elements, where a great deal of accurate work still needs doing. It is shown later that the only useful lines for such abundance work are weak lines originating from low-lying levels; also for cool stars like the Sun and Arcturus the blending of lines at short wavelengths limits accurate stellar measurements further. Thus although general

points will be made in the ensuing discussion, the orientation will be very much for the purposes of this thesis.

The Oxford furnace is dealt with separately, and the absorption method used is explained. Since the last complete description of the apparatus (Collins 1970) there have been a few modifications, which are described in more detail. In order to define an oscillator strength and introduce many relations needed for the discussion, first the basic nature of line emission and absorption must be considered.

A spectrum line occurs when an atom changes its energy state. For an emission line, the intensity across the profile of the line is given by:

$$I_{ab} = \int_{line} I_\nu \, d\nu = \frac{1}{4\pi} N_a A_{ab} \, 1 \, h\nu \qquad (5.1)$$

where A_{ab} is the transition probability, or Einstein A- coefficient, per second for an atom to spontaneously change from state a to state b. N_a is the number density of atoms in state a, and 1 is the thickness of the emitting layer. In (5.1) it is assumed there is no other form of decay from a to b, and that state a is not fed from another state. It is thus immediately apparent that the intensity of lines originating from state a will depend on A_{ab}.

Suppose now that there are many allowed transitions from a to lower states. The population N_a will decay according to:

$$\frac{d N_a}{d t} = - N_a \sum_b A_{ab} \qquad (5.2)$$

The solution of (5.2) is a simple exponential function, which leads to the definition of the lifetime τ_a of state a as being the interval over which N_a drops to 1/e th its starting value. Hence

$$\tau_a = 1 / \sum_b A_{ab} \qquad (.3)$$

Again repopulation of a, and induced emission from a, are ignored.

For absorption lines the atom in a lower energy state b absorbs sufficient energy from a radiation field (such as a continuous spectrum)

to allow it to jump to a higher energy state a; this is therefore not analogous with the case of emission lines where spontaneous transitions are possible. If the absorbing atoms in state b are uniformly distributed in length 1, then across an element dl the change in the radiation intensity is:

$$dI_\nu = -\frac{1}{4\pi} I_\nu B_{ba} N_b h\nu \, dl \qquad (5.4)$$

where B_{ba} is the Einstein absorption B- coefficient and I_ν the radiation intensity.

Using a simple extinction formula of the type

$$I_\nu = I_\nu (1=0)\exp(-\kappa_\nu 1) \qquad (5.5)$$

it is easy to relate the exponential absorption coefficient κ_ν to the Einstein absorption B-coefficient.

$$\int_{line} \kappa_\nu \, d\nu = \frac{1}{4\pi} B_{ba} N_b h\nu \qquad (5.6)$$

where integration over the line gives the total intensity as in eqn (5.3).

To introduce the oscillator strength, an equation analogous to (5.6) is produced by assuming that the atom behaves like a classical oscillating dipole. When such an atom is placed in a radiation field, it vibrates with the frequency of the radiation. If this frequency lies close to the natural frequency of the atom, the oscillations may attain considerable amplitude. In this way it is possible to explain the rudiments of line absorption. The derivation is quite lengthy, although simply involves solving the equation of motion of the electron in an oscillating electric field with the help of Maxwell's equations. Foster (1964 p. 473) gives a clear summary, the unexpurgated version appears in Woolley and Stibbs (1953). For this classical approach

$$\kappa_c = \int_{line} \kappa_\nu \, d\nu = \frac{\pi e^2}{mc} N_c \qquad (5.7)$$

where e,m,c are the fundamental constants, and N_c is the number density of classical oscillators. Thus collecting (5.6) and (5.7) and taking

the ratio gives:

$$f_{ba} = \frac{N_c}{N_b} = \frac{mc}{4\pi e^2} B_{ba} h\nu \qquad (5.8)$$

where the ratio N_c/N_b is called f_{ba}, the absorption oscillator strength for the transition b to a. It is therefore the number of classical oscillators corresponding to one atom in quantum state b. The name derives from the concept of the atom having different strengths, or f-values, at different frequencies, thus explaining selective absorption whilst retaining the simple classical picture.

It is sometimes more useful to represent absolute line intensities by a parameter S_{ba}, the line strength, related to f_{ba} by

$$g_b f_{ba} = \frac{3\pi^2 m\nu}{3he^2} S_{ba} \qquad (5.9)$$

where g_b is the statistical weight of state b.

For induced emission there is a similar argument leading to an Einstein B-coefficient for emission, and an emission oscillator strength f_{ab}. It is easily shown that:

$$g_a B_{ab} = g_b B_{ba} \qquad (5.10)$$

and

$$g_a f_{ab} = - g_b f_{ba} \qquad (5.11)$$

hence the emission f-value is always negative.

Finally f can be related to the spontaneous transition probability A_{ab} by

$$g_b f_{ba} = -g_a f_{ab} = \frac{mc^3}{8\pi^2 e^2 \nu^2} g_a A_{ab} \qquad (5.12)$$

It is stressed that generally the transfer of radiation must consider all 3 forms of transitions to and from state a, and then (5.5) is no longer valid. In particular (5.3) becomes

$$\frac{1}{\tau_a} = \sum_a A_{ab} + \sum_b B_{ab} I_{ab} + \sum_\alpha B_{a\alpha} I_{a\alpha} \qquad (5.13)$$

where the last term sums the transitions by induced absorption from a to higher levels α . The product gf is symmetric and occurs so frequently in these relations, that it has become customary to quote results as gf-values in the form $\log_{10}$ gf.

It is therefore seen that any absolute abundances based on line measurements (line strengths or integrated profiles) require absolute f-values. It may be mentioned at this stage that it is generally considerably more difficult (for a given accuracy) to measure absolute values, than it is to measure f-values relative to one another. Relative f-values are internally more accurate, and can be placed on an absolute scale, either by doing one measurement absolutely, or by referring to a well-established absolute scale. This is in some ways convenient because absolute methods are usually accurate for a restricted set of lines that do not include ones of astronomical interest. It is therefore sufficient merely to measure one of these lines relative to all the ones of astronomical interest in order to establish a complete absolute scale. The disadvantage, however, is that the accuracy of the final abundances contains at least the error in the absolute scale; furthermore, comparisons between many relative scales become very complex, particularly when there is no clearcut 'best' absolute scale to use.

It has been said earlier that it is possible to avoid using f-values by studying abundances of one star relative to a standard star, usually the Sun. The final abundances are only as good as those for the standard however, and the approximations made when comparing the same spectrum lines in both stars introduce further errors. These errors can be limited by performing a detailed analysis of star/standard using relative f-values however; nevertheless there is a great need for accurate absolute f-values and damping constants, particularly for the astronomer, whose fear of doing absolute analyses is hindering our knowledge of processes occurring in a wide variety of stars.

5.2 Methods for determining oscillator strengths

5.2 a) Approximate methods

Theoretical estimates of f-values can be found by manipulating

tabular material concerning line strengths (Allen 1973, Bates and Damgaard 1949) as well as from detailed quantum mechanical calculations. Such tables are calculated on the assumptions of LS-coupling, and Coulomb's law, and give the radial integrals necessary for converting relative line strengths in a multiplet into absolute f-values. The method is fairly successful for light elements, but for the iron-group elements deviations from LS-coupling occur and intermediate coupling must be considered.

Although the relative line strengths can be calculated in such coupling, the radial integrals must come from a solution of the appropriate wave equations. A discussion of the various possible approximations at this stage is beyond the scope of this discussion and the interested reader is referred to Garstang (1955); more recent calculations are described by Stewart and Rotenberg (1965), Naqvi (1964), Siddall (1969), and are reviewed by Crossley (1969).

Despite the collapse of LS-coupling and Coulomb's law for complex atoms, attempts have been made to establish an absolute scale for experimental relative f-values by using a sum -rule. Insofar as the f-value can be regarded as the effective number of electrons per atom at that wavelength, it follows that the sum of the absorption f-values for any one series is the number of electrons that give rise to the spectrum (not necessarily the atomic number). i.e.

$$\sum_a f_{ba} = Z' \qquad (5.14)$$

This rule is known as the Thomas-Kuhn-Reiche sumrule, and the descriptive argument above has been verified rigorously by Bethe and Salpeter (1957). It is only strictly applicable where LS-coupling holds, and thus its use in complex systems is questionable (see Prokof'ev 1969, for discussion).

5.2 b) Emission methods

These methods rely on the relationship between the emitted intensity and the f-value, which is derived by solving the equation of transfer for the gas. A rigorous derivation of 5.1 is now given; this introduces other equations of importance as well as clarifying the assumptions

involved.

For a change of intensity dI(x) from an element of gas at x, thickness dx, per unit area and solid angle:

$$dI(x) = \frac{1}{4\pi} \left\{ A_{ab} h\nu N_a + I(x) \left[B_{ab} N_a - B_{ba} N_b \right] \right\} dx \quad (5.15)$$

This is completely general and includes all forms of radiative transitions between levels a and b. If the plasma is in LTE then N_a and N_b can be related using Boltzman's equation.

$$N_a = N_b \frac{g_a}{g_b} \exp\left\{ -\frac{(E_a - E_b)}{k T(x)} \right\} \quad (5.16)$$

Where T(x) is the local equilibrium temperature at x.

Substituting (5.16) in (5.15) and using (5.8), (5.10) and (5.12) gives a transfer equation:

$$\frac{dI}{dx} = A(x) - I(x)B(x) \quad (5.17)$$

where

$$A(x) = \frac{1}{4\pi} A_{ab} N_a h\nu$$

$$B(x) = \frac{1}{4\pi} A_{ab} N_a h\nu \frac{c^2}{2h\nu^3} \left[e^{h\nu / k T(x) - 1} \right] \quad (5.18)$$

This can be solved if N_a and T are independent of x:

$$I(1) = \frac{A}{B} (1 - e^{-Bl}) = \frac{A}{B} (1 - e^{-\tau}) \quad (5.19)$$

where τ is the optical depth. Inoptically thin conditions where $\tau \ll 1$ this reduces to (5.1)

$$I(1) = \frac{A}{B} \tau = \frac{1}{4\pi} A_{ab} N_a h\nu \ell \quad (5.20)$$

(5.20) is thus the basis of the emission methods. Although intensities can be measured fairly accurately, the assumptions are often not valid in practice and this has led to results of poor quality.

The source for the emitted radiation is normally an electric arc or a luminous shock tube. The arcs are of two basic types, those that

are stabilised by some means and those that burn freely in air.

The general procedure with arcs is to measure, photographically or electronically, the intensities of many emission lines in the arc spectrum. The element under investigation can either be introduced into a 'doped' arc with Cu electrodes, or can itself form the electrodes for the discharge. In both cases the relative intensity scale is given by using eqns.(5.12) and (5.16) in (5.20):

$$\frac{I_{ab}}{I_{a'b'}} = \frac{A_{ab}}{A_{a'b'}} \frac{g_a}{g_b} \frac{\nu_{ab}}{\nu_{a'b'}} \exp\left\{-\frac{(E_a - E_{a'})}{kT}\right\} \qquad (5.21)$$

thus requiring a 'mean' temperature for the arc. It is the determination of this mean temperature that has aroused much controversy, yet has also prompted considerable improvements in the emission technique.

With the free-burning arc of Allen and Asaad (1957) elements were introduced in known concentrations between Cu electrodes. For an optically thin layer, (5.20), (5.12) and (5.16) give

$$I_{ab} = \frac{2\pi e^2 h}{m}\left(\frac{N}{Z(T)}\right) g_a f_{ab} \frac{l}{\lambda^3} \exp\left\{-\frac{E_a}{kT}\right\} \quad .. \quad (5.22)$$

where N is the total number density in all states, and Z(T) is the atomic partition function. Taking logs gives:

$$\log\left\{\frac{\lambda^3 I_{ab}}{g_a f_{ab}}\right\} = C - \left(\frac{E_a}{kT}\right) \qquad (5.23)$$

and a plot of the left-hand-side of (5.23) against E_a for lines of known relative f-values gave a mean temperature for their arc. A comparison of the resulting f-values in (5.21) with known absolute values gave an absolute scale for the results of Allen and Asaad.

The mammoth investigation of Corliss and Bozman (1962), involving some 25000 lines from 70 elements was carried out in a similar fashion. To allow for temperature variations in the arc, the constant C in (5.23) was allowed to be a function of E_a. A lengthy discussion of the derived arc temperature, its likely errors, and the various form of $C(E_a)$ is given by Takens (1970). He shows that corrections of as much as x100(2 dex) are sometimes necessary, though generally the absolute scale is accurate to about 0.30dex. The sheer volume of data

produced by Corliss and Bozman should not inspire statistical confidence, particularly as there is evidence (Wolnik & Berthel 1973) that there are systematic errors; unfortunately for lack of alternative data, these values have been used extensively for detailed work in astrophysics.

To reduce instabilities of temperature and density during the observations arcs have been stabilised in various ways, and it is possible to operate such arcs under carefully controlled conditions. They usually consist of a rotating tube observed end-on to reduce self-absorption, and by observing the intensity variation of, say, some hydrogen lines, a temperature and density can be assigned to each distance from the axis. The relative intensities derived using these distributions can be made absolute by reference to another method. Using such vortex arcs far higher temperatures ($\sim$15000^{o} K) can be reached than for the free-burning arc ($\sim$ 5000^{o} K) and consequently lines of higher excitation can be studied.

The stabilised arcs are a considerable improvement on the free-burning arc, and the results of Garz and Kock (1969) for iron-group elements for example, are claimed to 0.10dex on an absolute scale. However, temperature errors are still possible, and systematic errors in the work of Garz and Kock have been reported by several investigators (see Blackwell and Collins 1972). To determine absolute f-values directly, a knowledge of the number of emitting atoms is required and although various attempts have been made (Tatum 1961a), the results show the method to be unsuitable for absolute values.

The other main source of emission is the shock tube, described by Laporte and Wilkerson (1960). This method has also been used occasionally in absorption. A discharge sends a shock wave along the tube and this excites the specimen vapour long enough for thermal equilibrium to be set up. The temperatures and densities can be calculated from the known composition of the gas and the shock wave hydrodynamics. The shock condition lasts for less than 10^{-3} secs thus rapid electronic recording is essential. The method has been studied by Grasdalen et al (1968) and they claim 0.06dex for their relative values of FeI and II. There is a great deal of controversy concerning the reduction procedure

however, particularly with regard to the hydrodynamics. The line broadening mechanisms are also uncertain, though large damping wings are seen and these present observational problems. Wolnik and Berthel (1973) found that adsorption of certain elements on the shock tube walls could alter experimental values by as much as 1 dex. By flushing the tube prior to firing, a reduced error of 0.08dex is claimed for their Ti I and Ti II absolute f-values.

A serious drawback with all emission measurements is that the central intensity of the line can be absorbed by the cooler regions. This effect, termed 'self-reversal' is particularly important for ground state lines observed in arcs. The main advantage of the methods, is the relative ease with which such a wealth of data can be obtained. Furthermore the restrictions are few and astrophysically important lines can be readily observed; but the complex nature of the sources often leads to errors in temperature, and deviations from LTE are possible, thus systematic errors in the f-values are likely.

5.2 c) Absorption methods

These methods study the influence of the gas on a continuous spectrum. If the gas is cooler than the source an absorption spectrum is formed. Absorption regions such as furnaces can be extended and thus it is much easier to study thermal equilibrium and line-formation than in the confined regions of arcs.

In the simplest absorption method, first attempted by King and King (1935, 1938), the element under investigation is placed in an electrically heated furnace. At temperatures of about 2000° K sufficient vapour is present for detailed measurement of the absorption spectrum. In absorption work where there is a clear continuum reference, it is convenient to express the absorbed energy as an equivalent width W_λ. This is simply the width of a line of infinite photographic density which removes the same amount of energy from the spectrum, i.e. over the line profile,

$$W_\lambda = \int \frac{I_c - I_\lambda}{I_c} \, d\lambda \qquad (5.24a)$$

The general solution of the transfer equation (5.17) for N and T independent of x with a boundary condition $I = I_c$ at $x = 0$ is (Collins 1970):

$$I(x) = \frac{A}{B} - \left(\frac{A}{B} - I_c\right)e^{-Bx} \qquad (5.24b)$$

Thus use of exponential absorption is justified since from (5.18) even at $T=3000^{\circ}K$, $\lambda = 5000$ Å, $A/B \sim 10^{-12}$ and the stimulated emission factor $e^{-h\nu/kT}$ (from B_{ba}) is only 10^{-5}. Viz.

$$I(\tau) = I_c e^{-B\tau}$$

where $B = \frac{1}{4\pi} N_b B_{ba} h\nu = \int_{line} \kappa_\nu \, d\nu$ (from 5.6)

and thus in an optically thin plasma for any point on the line profile, $\tau_\nu (= \kappa_\nu \ell) << 1$ and

$$I_\nu = I_c e^{-\kappa_\nu \ell} \doteq I_c(1 - \kappa_\nu \ell) \qquad (5.25a)$$

where ℓ is the absorbing path length, and from (5.7) and (5.8)

$$\int_0^\infty \kappa_\nu \, d\nu = \frac{\pi e^2}{mc} N_b f_{ba}$$

thus
$$W_\nu = \int_0^\infty \kappa_\nu \ell \, d\nu = \frac{\pi e^2}{mc} N_b f_{ba} \ell \qquad (5.25b)$$

hence
$$W_\lambda = \lambda^2 \frac{\pi e^2}{mc^2} N_b f_{ba} \ell$$

$$= \lambda^2 \frac{\pi e^2}{mc^2} \frac{g_b f_{ba}}{Z(T)} N \ell e^{-E_b/kT} \qquad (5.26)$$

where Boltzman's equation has been used to give the total number N over all levels.

Thus in an optically thin gas W_λ is proportional to Nlf for a given temperature T. The precise relationship between W_λ and Nlf for all τ as the line strengthens is known as the curve of growth (after van der Held 1931). For lines with $dI/I \lesssim 10\%$ the curve departs from linearity and this must be corrected for by considering the precise form of the curve of growth.

Considering the rudimentary nature of the apparatus and photometry used by King and King, their relative f-values for Ti and Fe are remarkably useful, and have formed the basic material for several other scales (Prokof'ev 1969). The method is particularly suited to relative values of weak lines originating from low-lying levels. These are also lines of astrophysical interest, and the iron-group elements are at present under study at Oxford using an improved absorption furnace. Although the procedure adopted at Oxford is basically that above, several major modifications make it desirable to discuss this method separately in the next section.

Attempts to measure absolute f-values by this method (Estabrook 1951) require a value for N_b, which is usually taken from the vapour pressure corresponding to the measured temperature. As the pressure must be low to avoid broadening, it usually means that the temperature of the gas is near to its melting point where vapour pressure data is imprecise.

Accurate absolute f-values have been measured by the atomic beam method first described by Kopferman & Wessel (1951). The principle of the method is as follows: The specimen is placed in a crucible with a small orifice at the top, which is then placed in an absorption furnace. The atomic beam emanating from the orifice absorbs continuous radiation passing through the furnace, and the spectrum is analysed as before. For weak absorption W_λ gives Nlf, and N can, in this method, be determined directly by measuring the increase in weight of a collecting pan (enclosed in the furnace), on which the atoms condense. The temperature, measured with a pyrometer as for the furnace method, is used to give the velocity distribution in the beam, and hence the absorbing length l. The observations of Bell et al (1958) on the iron resonance lines show very good agreement with other absolute measurements and they claim an accuracy of 0.04dex. The method is difficult to perform accurately, and in order to avoid multiple collisions in the beam the density of gas must be kept low, which results in very weak absorption (generally $W_\lambda \sim 8$ mÅ) and so only the strong resonance lines have been measured. Although these are not usually of astrophysical interest the method has

the advantage that the number density N can be determined with relative certainty and it has proved useful for establishing absolute scales.

The technique has been recently improved (Bell and Tubbs 1970) by using a chopped atomic beam giving a signal independent of continuum fluctuations. The absorption is still necessarily weak, and significant errors could arise in the instrumental profile of the spectrograph used.

An ingenious method avoiding photometric errors was devised by Rozhdestvenskii (1912) and is particularly in favour with other fellow comrades. With this method extensive relative measurements have been accumulated, and a few absolute measurements have been made.

The method relies on the property of anomalous dispersion of radiation. In section 5.1 the classical oscillator was used to give the line absorption coefficient. The velocity of the radiation in the medium is given by $c/\sqrt{\epsilon}$ where ϵ is the dielectric constant, in general a complex number of the form.

$$\epsilon = \mu - i\kappa \quad (i = \sqrt{-1}) \qquad (5.27)$$

where κ is the absorption coefficient and μ, the refractive index.

Equation (5.7) was obtained by solving the equation of motion for the oscillator and taking the imaginary part. The corresponding real part gives μ in terms of N_c the number of classical oscillators, and hence relates μ and f. This relation is (Woolley and Stibbs 1953)

$$\mu_\lambda - 1 = \frac{e^2}{4\pi m c^2} N_b \frac{\lambda^3_{ba}}{\lambda - \lambda_{ba}} f_{ba} \qquad (5.28)$$

Thus in the region $\lambda \sim \lambda_{ba}$ a plot of $(\mu_\lambda - 1)$ against λ shows a pattern similar to the cross-section of a breaking sea-wave. A study of this pattern gives f_{ba}.

The apparatus is essentially a Jamin-Mach interferometer, one arm of which is a King furnace. The fringes observed depend on the optical path difference and hence the refractive index. To make the pattern clearer, a thick plate is normally introduced into the compensating arm, thereby producing a retardation which tilts the fringes to form

'hooks' on either side of the spectrum line. The separation of the two hooks Δ is related to f_{ba} by

$$f_{ba} = \frac{\pi mc^2}{e^2} \frac{\Delta^2}{\lambda_{ba}^3} \frac{K_\lambda}{N_b \ell} \qquad (5.29)$$

where K_λ is the constant of the apparatus and ℓ is the length of the interferometer arm. It is usually assumed that the hooks are isolated from the hooks of other lines. For complex spectra this is a severe limitation since Δ is usually about 2-3 Å, and although it is possible to allow for superimposition of hooks (Ostrovsky and Penkin 1957) the accuracy of the results is then reduced.

The hook method is capable of giving very accurate relative f-values. There are no photometric errors and the accuracy is limited only by the measurement of Δ and a knowledge of K_λ. The Russian authors usually claim less than 0.01dex(2%) for their relative values.

In order to allow simultaneous photographic measurements of hooks surrounding many lines the spectrographic dispersion has been kept relatively low, and so for Δ^S of reasonable magnitude only the resonance lines with large f values have been observed. Again therefore, astrophysical lines have not been measured.

It is possible to use the hook method to determine absolute f-values, by simultaneously measuring the equivalent width W_λ. (Ostrovsky and Penkin 1957).

For a strong line

$$W_\lambda = \frac{\lambda^2}{c} \left(\frac{e^2 \Gamma}{mc} N_b \ell f_{ba} \right)^{1/2} \qquad (5.30)$$

where Γ is the damping constant, which is the reciprocal mean lifetime for a resonance level (Foster 1964). Thus combining (5.29), (5.30) and (5.8) gives

$$f_{ba} = R \frac{g_a}{g_b} \frac{\lambda}{K_\lambda} \left(\frac{W_\lambda}{\Delta} \right)^2 \qquad (5.31)$$

where R is a conglomeration of fundamental constants.

(5.31) thereby enables f_{ba} to be found without needing N_b or T. It is an extremely difficult procedure in practice, requiring the use of two spectrometers, and photometric errors are naturally introduced in

measuring W_λ. To produce a measurable separation Δ, Nlf must be large, yet N_b must be small enough for collision damping to be negligible; in practice this means l must be very large.

The absorption methods all offer a reasonable means for determining relative f-values. Temperature control is far greater than for the arc methods. Both the atomic beam and the hook methods can give reasonable absolute values, but are restricted at present to resonance lines which are too strong for direct use in astrophysical investigations of cool stars. There is incidentally no reason why the hook method could not be adapted for weaker lines by increasing the dispersion.

5.2 d) Lifetime methods

By measuring the lifetime of levels it is possible to produce an absolute scale for existing relative oscillator strengths. This method has the advantage that no knowledge of the temperature or density is required. The principle is to excite the upper level a in some way, and observe the subsequent decay in the population $N_a(t)$.

By definition

$$N_a(t) = N_a(0)\, e^{-t/\tau_a} \qquad (5.32)$$

and for spontaneous decays from level a to lower level b it follows from (5.3) and (5.12) that

$$\frac{1}{\tau_a} = \sum_b A_{ab} = \frac{8\pi^2 e^2}{mc\, g_a} \sum_b g_b f_{ba}/\lambda^2 \qquad (5.33)$$

where it has been assumed there is no repopulation of level a. Generally τ is of the order of 10^{-8} secs so direct measurements have been limited in the past by the speed at which recordings can be made.

The simplest method for measuring τ consists of exciting the atoms by electron bombardment, removing the electron current in a time much shorter than τ, and observing the decay in intensity of a transition from the level with a fast oscilloscope. Holzberlein (1964) has used this technique for levels in helium. To achieve sufficient intensity however, electron energies greater than the excited energy of the level are necessary, and thus cascading from higher levels can

occur. This can be allowed for, but the uncertainty is then much greater.

A similar though more accurate technique is that of 'delayed coincidence', which has been widely employed for many elements (Bennett, 1961). To illustrate the method the apparatus of Heron et al (1956) is described.

The electron gun, used for excitation, is pulsed for 2.10^{-8} secs duration at a frequency of 10kHz and the light emitted by the decaying atom is detected by a photomultiplier. The arrival of a photon produces a negative voltage at the cathode and this is applied, together with the delayed pulse of the gun, to a coincidence circuit. By varying the gun pulse delay a graph of log coincidence rate against delay time is drawn, and the slope gives τ. The method claims an accuracy of 5%, though higher accuracy is now possible with recent advances in pulsed electronic circuitry (Corney 1970).

The time dependant decay of atoms can be converted into a spatial decay of intensity by exciting a moving beam. Such methods were originally limited to levels with long lifetimes so that a sufficiently long beam would result. However the discovery by Bashkin (1964) that ions in the beam of a Van der Graaff accelerator, travelling at velocities of around 10^9 cm sec^{-1}, were strongly excited by passing through a thin carbon foil, has made this the principle of the 'beam-foil' method for determining τ. It has produced accurate lifetimes for many highly ionised atoms, though in practice there are several difficulties. In particular the unselective nature of the excitation leads to cascade problems, and the data must then be analysed as the sum of several exponential decay curves. Usually the line intensities are weak and thus require integration over a long period. This means that the beam must be very stable.

The technique is also applicable for neutral atoms. A gas target replaces the foil and is bombarded with ions such as H^+ and the subsequent decay in intensity from the target atoms is studied. However uncertainties arise because the energy of the emitted foil atoms and their angular distribution is unknown. It is better to use a conventional

foil and use the fact that a significant portion of the beam contains neutral atoms, particularly if low particle energies are used. This method has been used for iron group elements such as Ti I and Fe I (Whaling et al 1969, Andersen et al 1973), but is restricted by its nature to fairly strong lines. The developments in this rapidly expanding field are summarised by the proceedings of three international conferences (Bashkin 1968, Martinson 1970, Bashkin 1974).

The 'phase-shift' technique is much older (Mitchell and Zemansky 1961) and uses the fact that the response of the population of a level to a periodic excitation process is shifted in phase with respect to the excitation. The phase lag is determined by the lifetime τ and the frequency of the excitation process, which is normally several times greater than τ^{-1}.

If $I_e(t)$ is the intensity of the exciting resonance radiation, and $I_s(t)$ that of the scattered radiation, then for optically thin conditions

$$I_s(t) = C\int_0^\infty I_e(t-t')e^{-t'/\tau}\,dt' \qquad (5.34)$$

where C is a constant depending on the number of absorbing atoms, their f-values etc.

If $I_e(t)$ is modulated according to

$$I_e(t) = A + B\cos\omega t$$

then integration of (5.34) gives

$$I_s(t) = \tau C\left[A + \frac{B}{(1+\omega^2\tau^2)^{1/2}}\cos(\omega t-\theta)\right] \qquad (5.35)$$

where $\tan\theta = \omega\tau$. Thus measurement of the lag in phase, θ at a given ω yields τ.

The use of modulated light for excitation has been described by Ziock (1957) and reviewed by Jones (1964). Ziock used a Kerr cell operating at 1 MHz for measuring lifetimes in Fe I to 10%, whereas Demtroder (1962) has used the diffraction of light in a standing ultrasonic wave to modulate light at 18 MHz thereby achieving an accuracy of 1-5%. In this form the method is possibly the most accurate available, though is restricted in application to the few levels with strong

electric dipole transitions to the ground state. The optical modulators limit the wavelength range to 2000-8000 Å. Lawrence (1965) has developed a modulated electron beam however, which extends the application of the phase-shift technique considerably.

Nearly all the methods described above suffer from problems of cascading. The corrections applied require observations of all the transitions in the cascade; this can only be done for a few atoms.

The measurement of the Lorenz width for a series of spectrum line profiles will allow a determination of the natural or radiation damping constant Γ_a, and hence the lifetime τ. For a line a-b

$$\Gamma_{ab} = \Gamma_a + \Gamma_b = \frac{1}{\tau_a} + \frac{1}{\tau_b} \qquad (5.36)$$

Normally the line profiles are dominated by thermal Doppler broadening, although this can be reduced or corrected for. A technique of high resolution spectroscopy has been used by Kuhn and Vaughan (1963) to study emission line profiles and lifetimes for inert gases. The Doppler effect can be substantially reduced by inducing the signals with a radio frequency (rf) magnetic field. These methods known as 'resonance fluorescence' methods are carried out at low densities to limit pressure broadening effects. Of particular interest in this field is the results of optical double resonance technique which has been used by Hese (1972) to measure lifetimes for levels of direct astrophysical interest.

This method, first applied by Brossel and Bitter (1952) is capable of very accurate lifetimes for resonance levels. Polarised light is applied to atoms in a resonance cell such that the $\underline{E}$-vector of the radiation is parallel to the constant magnetic field $\underline{H}$ in the cell. The radiation stimulates only $\Delta m_J = 0$ electric dipole transitions which decay emitting π-polarised light. If the atoms are subjected to a strong rf field $\underline{H}_1$, perpendicular to $\underline{H}$, then magnetic resonance can occur. When the Larmor frequency ν_L, of the excited atoms in $\underline{H}$ approaches the angular frequency of the rf field $\underline{H}_1$, atoms are transferred to $m_J = \pm 1$ states by stimulated magnetic dipole transitions. Decays from $m_J = \pm 1$ levels are thus σ-polarised. The photomultiplier is arranged

to detect only π-polarised light so at resonance the intensity recorded decreases. A curve of signal versus $\underline{H}$ shows two peaks surrounding the resonance value. The shape of the curve for various $\underline{H}_1$ gives the lifetime directly. The full analysis is given by Corney (1970).

The selective nature of the optical excitation used in resonance fluorescence experiments makes these methods extremely accurate for there are no cascading troubles. For short lifetimes however, impracticably large rf fields are necessary to produce resonance. An accuracy of 3-5% is claimed for resonance lines; for nonresonance lines 10% is possible.

Thus combined with good relative f-values from absorption or emission methods, accurate lifetimes are invaluable for determining the absolute scale. Although most emphasis at present seems to be with the beam-foil methods, the species investigated by this method are generally too highly ionised for direct relevance in studies of cool stars. The cascading difficulties also limit the accuracy of these experiments, (though several values for neutral iron-group elements are claimed to 5% even after cascade corrections). Resonance fluorescence is a particularly attractive technique though has not been used very much. Nevertheless the work of Hese for example, is perhaps as exciting for astrophysicists as the discovery of Bashkin was for the beam-foil spectroscopists.

5.3 The Oxford Furnace

The method adopted at Oxford is still essentially that used by King and King, and has already been described in section 5.2 b. Many of the King's assumptions have since been shown to be unjustified. This was mainly because of the limitations of their apparatus and experimental technique and it does not reflect any general disadvantages for the absorption method. By using an improved furnace and a more refined technique it is now possible to measure relative oscillator strengths at Oxford to a precision of at least 2% (Blackwell *et al* 1974a), whilst also quantitatively justifying the assumptions necessary.

Before describing the instrument in detail, it is desirable to briefly mention the technique used at Oxford, thus placing each part of

the apparatus in a broader context. The element under investigation is vapourised in a heated carbon tube. Continuous radiation from a high pressure xenon arc is passed through the tube, and observed with two identical low-noise spectrometers, one for each of two lines to be measured. By scanning across the two line profiles simultaneously, the equivalent widths are found. The curve of growth is then used together with equation (5.26) to give the ratio of the gf-values for those lines. In this way many such comparisons can be used to build a scale of relative oscillator strengths.

5.3 a) Description of furnace

The history of the Oxford furnace has been well-documented. The original design described by Peach (1966, 1969) was replaced by a refined version described by Collins et al. (1970). It is the latter design that is now under discussion, and a more copious description has been given by Collins (1970).

Fig. 5.1 shows a simplified view of the apparatus. The element to be studied is placed on a carbon tray (1) inside the cylindrical carbon heater tube (2). This tube is 122cm long with an internal diameter of 5cm, and is approximately three times longer than the original graphite tube used by King. This provides a more uniform temperature distribution along the column of absorbing vapour, and thus the absorption takes place in a well-defined region. The increased length also gives greater absorption and thus weaker lines can be examined. The carbon tube is installed in a steel cylindrical vacuum chamber (3) to avoid possible oxidising reactions at higher temperatures.

The tube is heated by current passing through two copper busbars (5 & 6) which are connected to the tube via two sets of carbon blocks (7). These complete the electrical circuit by carrying the current through a compression joint. Power is provided by a transformer capable of an output of 42.5V and 5000 amperes.

Cooling the apparatus effectively raises the temperature at which the furnace may be safely used. Both busbars are internally water-cooled (8) and the vacuum chamber is surrounded by a jacket (4) through which water flows continuously. In the apparatus described by Collins the furnace

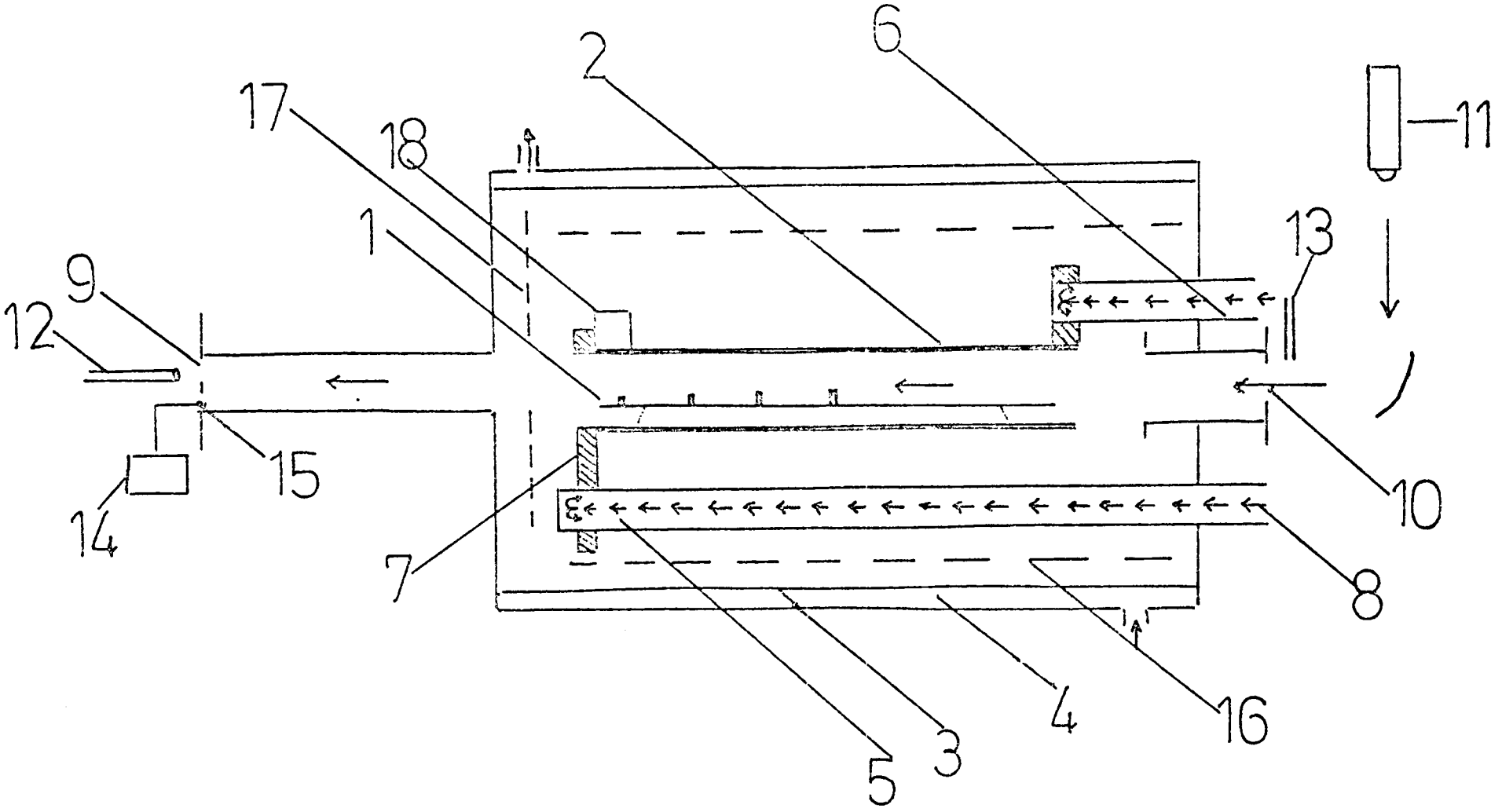

Figure 5.1

The Oxford furnace - a simplified view

was cooled by the mains water supply, and this limited operation to temperatures below 2500°K. An improved cooling system has now been installed, in which water is pumped in a closed circuit via an air cooling tower outside the department. This allows safe operation to at least 3000°K. In the event of a pump failure, cooling is transferred to the mains water supply.

The vacuum chamber is closed at two ends by quartz windows (9 & 10) through which the continuous radiation from a high pressure xenon arc (11) is directed. The windows are 150 cm and 70 cm from the ends of the heater tube (2) thus minimising any deposit on the windows. This is particularly important for the more distant window (9), through which accurate temperature measurements are made with a disappearing filament pyrometer (12). In practice such deposits have been found to be insignificant even over 100 hours of normal operation.

The temperature at various points along the tube can be measured by sighting the pyrometer (12) onto carbon blocks mounted along the tray (1). An accurate temperature distribution is essential when excited lines are being investigated, for the line profile is calculated according to the vapour pressure and Boltzman factor, $\exp(-E_b/kT)$, along the entire tube. This pyrometer has been calibrated by the National Physical Laboratory and is accurate to between $\pm$ 7-10 deg K for temperatures below 2600°K. These measurements necessitate blanking off the arc light with a mechanical shutter (13). A continuous, though less accurate, record of temperature is obtained with a photoelectric pyrometer (14) which monitors the central wall temperature for the tube through an auxiliary quartz window (15).

This accurate temperature distribution is possibly one of the most important modifications to the technique used by the Kings, who simply measured the central wall temperature at glancing incidence. The uniformity of the distribution is increased further by two extensive carbon heat shields (16) surrounding the heater tube. Other heat shields are situated by the carbon end blocks (18), and at the entrance to the 'top-hat' (17). Collins et al showed the temperature is constant to within the error of measurement over a length of 50 cm (approximately

40% of the tube length). Even 15 cm from the ends of the tube the temperature is still 95% of that at the centre.

The furnace is normally filled with inert gas at a pressure sufficient to keep the absorbing vapour in the heated tube (Peach 1969). Pressures of 10 to 70 torr are sufficient for all but the very weakest lines, and ensure that collisional excitation maintains thermal equilibrium. Extremely low pressures ($\sim$ 0.1 torr) could result in undesirable non-equilibrium effects (Blackwell & Collins 1972), whilst pressures above 2-300 torr produce damping wings, (particularly for lines of high excitation potential), which affect equivalent width measurements and curve of growth interpretations. These and other uncertainties are discussed under the reduction procedure in section 5.3c.

5.3 b) Optics and spectrophotometry

The continuous radiation from the 900 Watt xenon arc is rendered parallel by an off-axis paraboloid. This mirror ensures that the beam passing through the furnace is collimated at all wavelengths. The emerging light is directed to a half-silvered beam splitter where it is equally divided between two identical spectrometers. Such an arrangement is necessary for studying detailed line profiles of two lines of different wavelengths because the range of each spectrometer for a given grating position is only about 5 Å.

An important conclusion in section 5.2 was that, together with errors in temperatures, photometric problems have presented the greatest uncertainty in the determination of accurate oscillator strengths. Accurate photometry is essential in many branches of astronomy, and considerable progress has been made in reducing such errors in stellar and solar spectroscopy as well as for more general observations of distant objects. In spectroscopy accurate photometry particularly demands both a high quality diffraction grating and a low-noise detection system.

Observations made by several workers show that there are wavelength dependent errors in the Fe I f-values of King and this strongly suggests that the quality of the grating used in this early work was

poor. To remain on a region of the curve of growth where corrections for non-linearity are small one must use narrow lines. A poor grating instrumental profile with extended wings would change the effective continuum position and thus reduce the measured equivalent width. Griffin (1969a,b,c) has discussed this effect quantitatively and suggested that the uses of single-pass spectrometers are thus severely limited. However Blackwell et al (1971) have in turn demonstrated that the considerable effort in improving grating performances over the last 20 years has resulted in modern echelles of excellent quality and that Griffin's remarks are relevant only to the older Babcock gratings. They studied the instrumental profile of one of the Oxford gratings using a helium-neon laser technique similar to that employed successfully by Gurtovenko and Fedorenko (1969). The resulting profile shows a remarkably symmetrical core with a width at half intensity of only 10.9 mÅ. The width at 1% peak intensity is 43 mÅ and there are no conspicuous features or 'ghosts' to intensities much less than 1% even using the full grating aperture. These measurements thus satisfy the first requirement of accurate photometry.

The second requirement is a low-noise detection system. King used photographic plates, which would give a typical noise level of 1-2% on the microphotometer tracings. For lines of 25% depth this amounts to an error of 8% in the equivalent width W_λ. When the line is not on the linear portion of the curve of growth, a small change in W_λ could lead to an increased error in the derived gf-value and so this effect could be quite serious for strong lines.

A low noise level is also essential in comparing two lines of different strengths. The stronger line must be limited to avoid an undesirably large curve of growth correction so the capability of the entire system, i.e. the negotiable ratio $W_{\lambda_1} : W_{\lambda_2}$. depends on the smallest equivalent width that can be accurately measured. The initial investigations of the present low-noise spectrometers were carried out by Peach (1966) who demonstrated that noise levels of 0.1% are quite feasible, and this corresponds to an error of only 1% in an equivalent width of 1.5 mÅ.

The main factor in the improved detection system described by Blackwell et al (1967) is the use of a photomultiplier of high quantum efficiency; this introduces an insignificant noise in comparison with the intense arc radiation. Other sources of noise such as continuum fluctuations are eliminated by chopping alternately between the continuum and line signals at a frequency greater than that of the fluctuations. The difference between the two signals is proportional to the line absorption even when the photomultiplier gain is controlled in such a way as to keep the mean d.c. output constant.

The photoelectric noise can be further reduced by increasing the integration time, though this is eventually limited by the response of the electronics to fluctuations in the increased signal.

The discussion of the optics will now be completed. Both spectrometers are preceded by prism monochromators which isolate the required orders. One entrance slit serves both monochromators and is followed by the beam splitter. The prisms are rotatable and their positions set and calibrated using a digital voltmeter. The monochromator entrance slit is normally reduced to 2mm width to limit the effects of scattered light. Too narrow a slit results in a curved continuum which would lead to difficulties in interpreting and measuring equivalent widths, and by setting the entrance slits of the spectrometers to 150 microns or so, the transfer function of the monochromators becomes rectangular to a good approximation.

The spectrometers are mounted above each other and housed in a closed light-tight tunnel to reduce possible air turbulence effects. Both gratings are Bausch and Lomb replica blazed echelles recently ruled from the same master. They have a focal length of 9.6 metres, are ruled at 300 lines mm^{-1} and give a dispersion of 5 mm/Å at 5100 Å in 10th order.

Each spectrometer has three exit slits; the outer reference slits are fixed 40 mm apart and are normally placed on the continuum, whereas the central scanning slit is free to move at various speeds in the intermediate region. The chopper allows light from the reference and then scanning slits to fall on the photomultiplier cathode. When

the scanning slit is set on the continuum the reference slit widths are adjusted to produce a net zero difference signal; this is termed 'balancing'.

From the human point of view the console offers the experimenter a dazzling variety of integration intervals (in 2^n secs), scanning speeds (2^n steps/point), and scan lengths (10n points). Here, 'step' refers to a count registered by the electronics, and 'point' refers to a total count which is recorded on punched paper tape. Typically a step is 0.5 mÅ, so with settings of 1 second, 8 steps/point and 80 points, the scanning speed would be 4 mÅ/sec and the recorded line profile would consist of 80 points each 4 mÅ apart.

There is a separate electronic counting system for both spectrometers, thus enabling simultaneous recording of two lines. The recorded counts are displayed digitally and monitored with a pen recorder as well as being stored on paper tapes for subsequent reduction on a departmental Nova computer.

5.3 c) Reduction procedure

The reductions are performed in two stages with the aid of a computer display, thus enabling the user to monitor various effects. The first stage fits a continuum and then determines an equivalent width from the line profile calibrated by the decided continuum and the signal measured for zero intensity.

The second stage places the observed equivalent widths for each scan on a curve of growth calculated for each line. From (5.25a)

$$W_\nu = \int_0^\infty \kappa_\nu \, l \, d\nu = \int_0^\infty N_b \alpha_\nu \, l \, d\nu$$

and writing this to allow a variation of N(x) and T(x)

$$W_\nu = \frac{g_b}{Z} \int_0^l N(x) e^{-E_b/KT(x)} \int_0^\infty a(\nu, x) \, d\nu \, dx \qquad (5.37)$$

where $a(\nu, x)$ is the atomic absorption coefficient. The form of N(x) is important, although King ignored any such variation. In this method it is assumed that N(x) is proportional to the vapour pressure at the T(x). This is reasonable if there is sufficient inert gas to prevent

streaming motions, but there is no guarantee that the vapour temperature is identical to that measured on the carbon blocks. The assumption is necessary, though unfortunate because vapour pressure tables (e.g. Nesmayanov 1963) are notoriously unreliable. For this method, however variation of pressure with temperature is more important than the absolute values, and this variation is now fairly well-established.

The curve of growth effect mentioned earlier arises from the shape of $a(\nu)$ which is calculated for several points along the tube. Calculating a curve of growth removes the restriction that the line must be optically thin. Contributions to $a(\nu)$ could come from thermal Doppler broadening, natural damping, pressure broadening and Stark broadening.

The electron pressure is too low for significant Stark broadening, and natural damping will only be important for lines of high excitation. In this case Doppler broadening and damping from pressure broadening are the only significant contributors, and

$$a(\nu) = a_o H(\alpha, v) \qquad (5.38)$$

where

$$\alpha = \frac{\gamma}{4\pi} \frac{c}{\nu_o} \left\{ \frac{M}{2KT(x)} \right\}^{1/2} ; \quad v = \frac{(\nu - \nu_o)}{\nu_o} c \left\{ \frac{M}{2KT(x)} \right\}^{1/2} \qquad (5.39)$$

and

$$a_o = \frac{\sqrt{\pi} e^2 f}{m \nu_o} \left\{ \frac{M}{2KT(x)} \right\}^{1/2} \qquad (5.40)$$

The Voigt function H has been tabulated by Allen (1973) and presented as a computer subroutine by Armstrong. For all pressures under 100 torr observations by Dr. G. Smith show that pressure broadening affects the curve of growth by less than 2% and (5.38) thus reduces to

$$a(\nu) = a_o H(0, v) = a_o e^{-v^2} \qquad (5.41)$$

Inserting (5.41) into (5.37) and integrating along the furnace length l for various gf-values gives a curve of growth for the line. Interpolating with the observed equivalent width gives a quantity proportional to the absolute gf-value. The ratio for the two spectrometers therefore

gives gf_1/gf_2 and a relative scale is constructed.

An analogue to self-absorption occurs in the absorption method. At high temperatures a detectable line emission could be present; this would tend to reduce the absorption at the line centre and hence reduce the observed equivalent width. This effect can be checked by observing the furnace spectrum without the continuum source. The effect is less than 0.1% of the arc light though could become important for strong lines of high excitation.

As a refinement it is possible to remove the assumption that the continuum is independant of wavelength across the line. Observing the arc with a cooled furnace gives a correction to the observed equivalent width which is normally about 0.5-1%.

To reduce the effects of scattered light the lines can be reversed between the spectrometers. If scattering is independent of wavelength, then the true equivalent width is always a constant S for that spectrometer times the observed value. It can then be shown the true ratio is

$$\frac{W_1}{W_2} = \left\{ \left(\frac{W_1}{W_2}\right)_a \left(\frac{W_1}{W_2}\right)_b \right\}^{1/2}. \qquad (5.42)$$

where a, b refer to the two possible arrangements. Dr. P.A. Ibbetson has determined S to be less than 1% in both spectrometers at many wavelengths by observing suitable solar lines already measured with a double-pass spectrometer (Pierce 1969). Thus any discrepancy in reversing should be less than 1%. However it has been found (Blackwell et al 1974a) that significant differences of up to 0.03dex(7%) can result. The effect is not systematic and the average discrepancy over many reversals is only 0.001dex(0.2%). The reason for this effect is not at present understood.

CHAPTER 6

OSCILLATOR STRENGTHS FOR NEUTRAL TITANIUM

"Some of the people can be part-right all of the time, and all of the people can be all-right part of the time, but all the people can't be all-right all of the time."

adapted from an original idea of
Abraham Lincoln

... or perhaps simpler...

"Well Brian, my brain hurts"

6.1 Introduction

Titanium is possibly one of the most important elements in the iron-group. With an atomic number of 22, and 5 stable isotopes it is the 18th most abundant element. Together with other iron-group elements it is a member of the first transition series. The electron shells up to and including the 3p shell are filled, leaving 4 electrons which distribute themselves between the 3d, 4s, and 4p shells. This shell competition gives a fairly complex line spectrum.

Experimentally the spectrum has been extensively analysed; the detailed work of Russell has formed the groundwork for later investigations (e.g. Moore 1949). Theoretical studies have been performed by Many (1946), Rohrlich (1948) and by Siddall (1969).

A simplified term diagram is shown in Fig. 6.1. As there are several low-lying levels, the spectrum is fairly well populated even at low temperatures. In the visible region there is however a conspicuous gap in strength between two sets of transitions. The stronger set includes all the ground state a^3F and y^5G^o; the weaker set consists of other a^5F transitions and all the lines originating from a^1D, a^3P and higher levels.

Figure 6.1

A simplified term diagram of astrophysical interest for Ti I

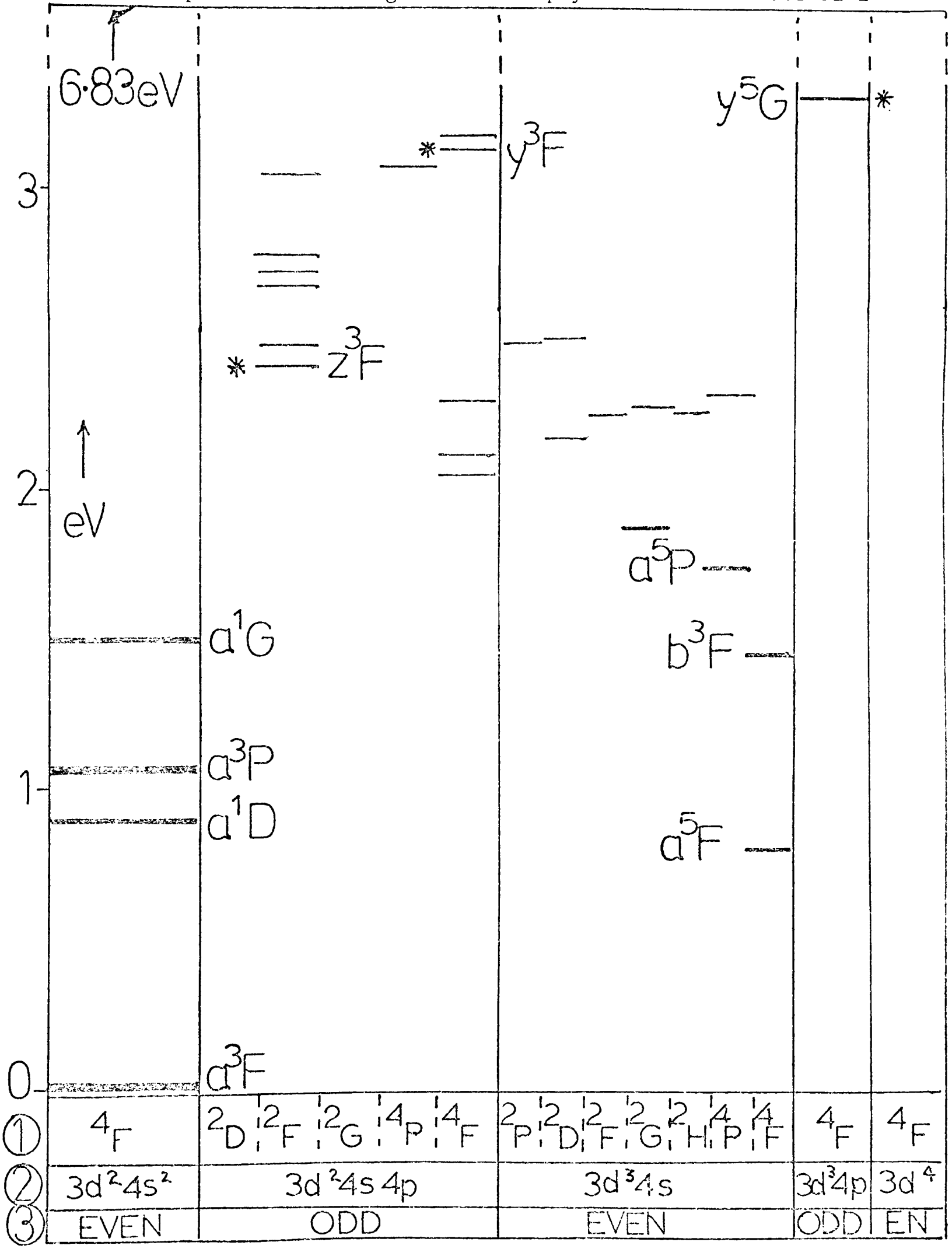

① Series limit ② Confign. ③ Parity

* Lifetimes available

At a given temperature there is a factor of at least 15 in equivalent width between the two sets of lines, and this would seem to present a formidable problem in any attempt to measure oscillator strengths for lines of the weaker set using the absorption method described in section 5.3. Similar intervals are present in the spectra of other metallic elements and it will be demonstrated that such 'jumps' are within the capability of the Oxford furnace, and can be regarded as a useful test of its versatility.

It might be noted here that titanium is not the ideal experimental metal. Although it is cheap and easy to handle, it reacts at high temperatures with nitrogen, and to a lesser extent with carbon; it also oxidises at room temperature.

Astrophysically, titanium is quite important in the understanding of the origin of the iron-peak. Ti^{48} is underproduced by the current theories of explosive nucleosynthesis (see Chapter 9), and thus abundances of this element are most useful. Accurate oscillator strengths are of course an essential prerequisite to such investigations.

6.2 Published oscillator strengths of Ti I

With the sole exception of iron there are more oscillator strengths available for neutral titanium than for any other iron group element. To review critically the many observations would take far too long and is unnecessary as there are several good summaries available (Miles and Wiese 1970, Siddall 1969). In particular, Prokof'ev (1969) has analysed all the data up to 1963 and discussed extensively the various merits of individual results.

Since then there have been several new investigations and the aim of this section is to consider the relevant conclusions of Prokof'ev in the light of the newer results. In particular a set of good relative gf-values is required for comparing with the Oxford measurements. Discussion of the absolute scale is postponed until section 6.5.

Table 6.1 lists the sources of Ti I gf-values published before June 1974. The third column indicates whether the results are relative or absolute. Often relative values are brought onto an absolute scale by another method and this is shown appropriately. There is clearly a wealth of data to consider, but only three studies are really extensive, namely those of King and King (1938), Corliss and Bozman (1962), and Prokof'ev (1969), (whose review article encompasses the other two). These three studies are briefly described.

The first detailed measurements on Ti I were carried out by King and King using a electrically heated graphite furnace. The absorption technique was used. Temperatures between 1300 -2600° C or varying amounts of titanium supply were used to bring the absorption lines onto the linear part of the curve of growth, and the Boltzmann distribution was used to determine the relative level populations. The assumptions were tested and found to hold to within the quoted error of 10%. The furnace was considered capable of negotiating the 15:1 interval mentioned in the last section, yet in such a comparison the weaker line measurements would be greatly spoilt by the microphotometer noise and the stronger lines would have appreciable curve of growth corrections. It is also evident that the grating used was of poor quality and that instrumental and scattering effects were present, yet were ignored. For these reasons the King scale is expected to be accurate to 10% only for the strongest lines.

Despite these criticisms there is good evidence that the Ti I gf-values obtained by King are in better agreement with subsequent results than their Fe I gf-values obtained at the same time. This could be because the inevitable interval in iron is even larger and close to 25:1. At any rate a high opinion seems to have formed in the literature concerning the King Ti I values and Prokof'ev bases his comparisons on their scale. Transfer formulae of the form.

$$\Delta_i = (\log gf)_i - (\log gf)_{King} = A_i + B_i \chi \qquad (6.1)$$

Table 6.1

Oscillator strengths for Ti I

Reference	Method	Abs/Rel	Lines	λλ Å
Allen(1934)	Solar lines	Rel	172	4060-6556
King[2](1938)	Furnace	Rel	227	3123-6743
Stekelenbg. (1948)	AC arc	Rel	29	3186-5192
Mitrofanova (1952)	AC arc	Rel	169	3717-6098
Ostrovsky (1956)	Hook	Rel	56	3200-5200
Boyarchuk (1960)	Stellar lines	Rel,abs(1)	91	3904-6743
Hefferlin (1960)	DC arc	Rel	46	3925-6575
Goldberg (1960)	Review	Rel,abs(2)	51	4272-6556
Tatum(1961a)	Vortex arc	Rel,abs(2)	98	3199-4981
Tatum(1961b)	Review	Rel,abs(1)	98	3199-4981
Corliss & Bozman(1962)	Arc	Rel,abs(1)	734	2272-8766
Morozova (1964)	Arc	Rel,abs(1)	10	3729-3998
Reinke(1968)	Arc	Abs	3	3635-3654
Boni(1968)	Shock tube	Abs	3	3635-3958
Siddall(1969)	Theory	Abs	221	3123-6743
Prokof'ev (1969)	Review	Rel,abs(2)	737	2272-8778
Wolnik(1973)	Shock tube	Abs	97	3858-5703
Klemt(1973)	Arc	Rel,abs(1)	139	3598-15118

Notes: Col 1: Abbreviated authors

Col 3: Rel = relative, abs = absolute determined by (1) comparisons, (2) the sumrule.

were constructed, where χ is the upper excitation potential in eV and A_i, B_i are constants to be evaluated. For each set of results, i, Prokof'ev took all lines for which $|\Delta_i - \bar{\Delta}_i| \leqslant 0.30$ and determined a mean value for A_i and B_i. These and other transfer formulae are given in Table 6.2.

Corliss and Bozman (C & B) measured 25,000 relative gf-values for 70 elements and reduced them to an absolute scale using published values. The elements were placed in 0.1% number density between copper electrodes. The arc emission spectrum was photographed, and by using the same 200 copper lines all intensities were measured on the same relative scale. The effective arc temperature was found to be $5100 \pm 110^{\circ}$ K by using lines with known relative gf-values. A table of relative gf-values can thus be deduced from the photographed line intensities. The absolute scale and its notorious errors are not of interest here and the reader is referred to Takens (1970) for further details. An independent estimate of 50% (Siddall (1969)) is fairly realistic for the error of the relative scale.

These results agree only fairly well with the King values, the scatter is sometimes large though Prokof'ev finds no energy (or B) term is needed.

An energy or a B-term could indicate a temperature error e.g. in an arc or a stellar atmosphere. Prokof'ev found large B-terms for several emission results, implying temperature errors of up to 30%. Allen's astrophysical values for example, are based on a solar temperature of 5600° K which, according to Prokof'ev, is 800 degrees too high. Similar large temperature errors are suggested for the water-stabilised vortex arc measurements of Tatum, the d.c. arc results of Hefferlin and the astrophysical f-values of Boyarchuk and Boyarchuk.

For some results, such as for the arc measures of Mitrofanova no B-term is needed; but the scatter is so large that eqn. (6.1) cannot be fitted successfully. Of course the presence of the B-term

Table 6.2

Relative gf values compared

Standard	Source	Transfer formula	Error
King	C&B	+2.97	±0.11
	Ostrovsky	-0.87 - 0.28	.06
	Allen	-0.02 + 0.14	.17
	Morozova	+3.70	.04
	Stekelenburg	-0.19	.03
	Boyarchuk	+3.35	.19
	Tatum	+2.73 + 0.16	.19
	Hefferlin	+1.45 - 0.37	.19
	Mitrofanova	+0.07	.21
Wolnik	C&B	+0.36 - 0.20	?
	Tatum	+0.03	?
Klemt	King	-2.82 - 0.09	±0.11
	Tatum	+0.17 - 0.01	.15
	C&B	+0.38 - 0.15	.12
	Wolnik	+0.17	.06

Notes:

Col 1: Standard comparison source

2: C&B = Corliss & Bozman(1962)

3: Formulae are of the form:-

$$\Delta_i = \lg f_{std} - \lg f_{srce}$$

$$= A_i + B_i \chi \quad (\chi \text{ in eV})$$

4: Mean error(logarithmic)

can also imply that the King results are energy dependant.

Of the higher quality results there are three outstanding. Morozova and Startsev measured relative gf-values by the same method as C & B. No attempt was made to correct for ionisation or self-reversal in the arc and consequently the absolute scale is poor, but the relative scale agrees with King to a remarkable dispersion of less than 0.04dex.

Even better agreement is found for the small set of lines measured by v. Stekelenburg using a carbon arc. In this arc self-absorption was minimised by introducing limited quantities of titanium. The arc temperature was determined by the intensities of the CN bands, and an accuracy of 10% is quoted for these relative values.

Although the anomalous dispersion results of Ostrovsky et al contain a large B-term the values agree well with those of King. The method involved the use of a cigar-shaped graphite kiln to ensure uniformity in temperature along the furnace tube. The strong dependance indicates a temperature error of 10% and as Prokof'ev favours this method, he recalculated the data of Ostrovsky et al with the new temperature.

Therefore to sum up: Prokof'ev found that only Ostrovsky, Morozova and v. Stekelenburg have gf-values which agree to within 0.06 dex with those of King. Instead of basing the final means on these three scales however, all sets were included. Thus the Prokof'ev results contain all the errors inherent in the above discussion. Also of course, the analysis can be criticised as it relies on the King scale, but such criticisms can always be made when comparing relative scales, and Kings' scale is certainly the best extensive list. It would have been instructive to repeat Prokof'ev's analysis for just the high quality data, but recent results have rendered such an investigation redundant.

Since 1963 there have been further investigations of the Ti I spectrum. Reinke (1963) has studied the three resonance lines $a^3F_{2,3,4} - y^3G^o_{3,4,5}$ using an atomic beam, Using the linear part of the curve of growth the absolute values are given to a quoted accuracy of 15%, Over the 3 lines, the agreement with Prokof'ev's final table is excellent, even on an absolute scale.

There have been two shock tube measurements since 1963. Boni (1963) has measured 3 resonance lines $a^3F_4 - y^3D^o_3$, $x^3F^o_4$, z^5P^o, but the values are a factor 10 down on other absolute values, and even relatively the results are very poor. As the Ti II gf-values in the same article are between 2 and 4 orders of magnitude too low, the general opinion is that Boni's measurements are fundamentally in error (see Klemt 1973, Siddall 1969).

In contrast Wolnik and Berthel (1973) have produced an extensive and useful list. Each line was measured by the shock tube method 10-15 times and the scatter is less than 20%. Their results reveal a large χ dependence in the work of C & B (see Table 6.2). The fact that Prokof'ev failed to detect such a trend could mean there are serious systematic errors in the King scale. As other workers have found that C & B iron and chromium scales show strong χ dependences, contrary to Prokof'ev, it is clear that the C & B scale is quite poor even on a relative scale.

Finally Klemt (1963) has measured 139 relative values using a triple chamber arc burning in argon. $TiCl_4$ was introduced into the centre and the emission spectrum was observed end-on to minimise self-absorption. The arc temperature came from absolute Ar I line intensities, and also by using known Ti I relative f-values. The final accuracy quoted is 20-40%. Agreement with Wolnik is good, to within 0.17dex absolutely with little dispersion, and no energy dependence is detected. Klemt also reports strong energy terms when comparing with King and

C & B (see Table 6.2).

Concluding therefore, one can see here a prime example of the confused world of oscillator strengths. Intercomparisons without reference to an absolute scale make it very difficult to know where fresh measurements are most needed. In order to assess the Oxford results, good extensive relative gf values are needed. For this purpose the author chose the lists of King, Prokof'ev, Wolnik and Klemt.

6.3 The Oxford Measurements

Despite the many gf-values available, there are only a few of high quality. For Ti I the precision work of Reinke, v.Stekelenburg and others is restricted to strong lines in the ultraviolet. For abundance work in cool stars such values are useless as line measurements in these regions are severely hampered by blending and the lack of a clear continuum reference. Absolute values can, of course, be at any wavelength provided there are relative values common to both regions, but at present there is a severe shortage of good relative values for weak lines of astrophysical interest. The results that follow are a preliminary attempt to rectify this situation. It must be stressed that these results are only the beginnings of an extensive survey of Ti I, and that work at Oxford is continuing with other iron group elements. In this chapter the particular aim is to obtain gf-values suitable for abundance studies in the sun and Arcturus. Precision work is desirable and will eventually be achieved, but these preliminary results, although accurate to $\leqslant 0.03$ in log gf throughout, are currently being improved by various checks and elaborations to provide values with accuracy as high as 0.01.

6.3 a Choice of a line list

In choosing suitable lines to measure in the furnace a list of 5 criteria was constructed, and the lines chosen satisfy some or all of these conditions.

1) There should be plenty of clear and unblended lines in the spectra of both Arcturus and the sun.

2) There should be plenty of weak lines on the linear portion of the stellar curves of growth where damping and microturbulence uncertainties are small.

3) For comparison purposes lines from the 4 surveys chosen in the last section should be included.

4) A few lines for which good absolute gf values are available should also be included.

5) The lines should be suitably grouped in strength for accurate comparisons in the furnace.

For 1) the Utrecht and Griffin atlases were used together with the solar wavelength table of Moore et al (1966). Curves of growth of Griffin and Griffin (1967) and Goldberg et al (1960) were consulted for 2). For 5) a strength ordering program was written. This calculates an arbitrary parameter F_T, which is related to the equivalent width in that it contains the gf-values and a Boltzmann factor for a given temperature T.

viz: $$F_T = 10 + \log gf - (5040/T)\chi_l \ldots \qquad (6.2)$$

χ_l is in eV. The program orders the lines in decreasing F and was run for T = 2000° and 2300° K using the gf values of Corliss and Bozman. This led to some errors in the fifth criterion where some of the gf-values of C & B were clearly incorrect; no great significance should thus be placed on such a preliminary order.

It is impossible to satisfy criterion 2) for Arcturus without extending the line list at least 5 orders of magnitude further down in F from the strongest resonance lines included in the list. Excellent lines of 5-20 mÅ in the sun are often 100-200 mÅ in Arcturus and this preliminary list does not include any very weak lines for Arcturus. It is perfectly possible to reach such lines with the

Oxford furnace, but to satisfy criterion 5) this would involve many comparisons each having an associated error. The author therefore decided it was better from the abundance point of view to have a few moderate lines of 50-100 mÅ with good gf-values than to spend an inordinate length of time reaching weaker lines for which many checks would be needed to achieve the same accuracy.

The first list drawn up included many lines with wavelengths shorter than 4000 Å, but identification problems and uncertainties in the furnace led the author to abandon these lines. Generally this will not be the case, and it has since become de rigueur at Oxford to assign a separate tube for each element, thus minimising the likelihood of contaminating lines being present.

The final line list is shown in Table 6.3 together with the strength parameter of eqn 6.2, which was calculated using the gf-values of Corliss and Bozman. Also listed are the solar equivalent widths of Moore et al, a rough indication of the line quality in the Griffin Arcturus atlas, and whether or not an absolute gf-value is available.

6.3 b Observational Procedure

Titanium is available in granules or in a 99% pure roll form. The impure granules were used almost exclusively, and although lines of other elements were encountered shortward of 4000 Å, these were attributed to the results of using the tube for more than one element. The purer titanium, 20 times as expensive, did not reduce the confusion at short wavelengths and these observations are currently being repeated with a new tube. Unlike iron, Ti does not impregnate the tube and fresh samples were loaded into the furnace on carbon trays for each run.

The comparisons fall into 3 hierarchies:

1) lines originating from the same level

$$\text{e.g. } a^3F_2 - z^3F^o_2,\ a^3F_2 - z^3G^o_3$$

Table 6.3

A Ti I line list

χ_l eV	Transition	M	λ	F	f	⊙	∝Boo
0.000	a^3F_2 - z^3F_2	4	5173.75	8.94	*		
	z^3G_3	6	4675.47	8.85		55	*
	z^3F_3	4	5147.48	8.29	*		b
0.021	a^3F_3 - z^3D_2	5	5039.95	8.99	*	66	
	z^3F_3	4	5192.98	8.99	*	80	
	z^3G_4	6	4667.59	8.88	*		
	z^3F_4	4	5152.20	8.22	*	38	
	z^3F_2	4	5219.71	8.05		25	**
	z^3D_3	5	5009.65	7.89		24	**
	z^1D_2	7	4562.63	7.67		8	*
	z^5D_3	3	5426.26	7.47		6	**
0.048	a^3F_4 - z^3D_3	5	5064.66	9.01	*	79	*b
	z^3F_4	4	5210.39	8.98	*	80	*
	z^3G_5	6	4681.92	8.89	*	64	
	z^1G_0	9	4112.71	8.84	*	43	
	z^3F_3	4	5252.11	7.86			
	z^5D_4	3	5460.51	7.52		9	**
	z^3G_4	6	4715.30	7.28		15	**
0.813	a^5F_1 - y^3F_2	35	5389.18	6.26		5	**
0.818	a^5F_2 - y^5G_3	38	5007.21	8.26		96b	*
	y^5G_2	38	5024.84	7.47		62	*
	x^3F_3	39	4926.16	6.23		6	**

Table 6.3(contd.)

χ eV	Transition	M	λ	F	f	⊙	∝Boo
0.818	$a^5F_2 - y^3F_3$	35	5366.65	6.05		3	*
0.826	$a^5F_3 - y^5D_4$	38	4999.51	8.30		104	*
0.848	$a^5F_5 - y^5D_4$	37	5238.58	6.67		15	**
	y^5G_4	38	5045.41	6.37		10	*b
0.899	$a^1D_2 - y^1D_2$	37	4840.87	7.26	*	60	*
	z^1D_2	38	6743.12	6.31		19	**
1.046	$a^3P_0 - z^3S_1$	69	6064.63	6.20		7	**
1.053	$a^3P_1 - z^3S_1$	69	6085.23	6.23		40b	*
1.066	$a^3P_2 - y^3D_3$	72	5866.46	6.77		40	*
	x^5D_3	77	4675.12	6.21	*	30	**
	z^3S_1	69	6126.22	6.20		20	**
	x^3D_3	74	5295.79	6.06		10	**
1.749	$a^5P_3 - w^5D_4$	145	4617.27	6.30	*	49	**

Notes: Col 3: M = Multiplet number(Moore 1949)

Col 5: F = strength parameter at 2000°K(see text) using C&B gf-values.

Col 6: f indicates whether an absolute value is available for this line.

Col 7: Solar equivalent width(mÁ) from Moore et al

Col 8: Quality in Arcturus atlas

b = slightly blended

2) lines originating from different levels in the same term

e.g. $a^3F_2 - z^3F^o_2$, $a^3F^o_3 - z^3D^o_2$

3) lines originating from different terms

e.g. $a^3F_2 - z^3F^o_2$, $a^5F_1 - y^3F^o_2$

The equivalent width ratios for the first hierarchy are almost entirely independent of temperature, a small effect present only in the curve of growth corrections. Similarly, the energy differences in the second hierarchy are always less than 0.05eV and so differential excitation effects prove to be negligible. A substantial error in temperature of 25-50 degrees is shown in the next subsection to produce a negligible error in the final gf-ratios for comparisons of the first two types. These comparisons were done first in order to decide which lines were best for linking up the different terms.

Generally each comparison consisted of 30 to 40 good scans at a stable temperature. The standard deviation on these scans is a good indicator of the furnace stability. Instability arises from either voltage or pressure fluctuations. A servo system is now under development which will greatly improve the stability of the instrument. The furnace and electronics were always allowed a statutory 2 hour warming up period. There was little trouble in maintaining the stability in temperature except during a period of national emergency when, even on the 3 days a week that work was permitted, the voltage fluctuations were sometimes 5%. However all such effects were immediately apparent by monitoring the scans on the pen recorder; these faulty scans could be omitted or accounted for in the subsequent reduction. The lines themselves are very sensitive to small temperature changes and are thus the best indicators of the stability of the furnace.

The temperature profile was measured every 10 or 20 scans for the first two hierarchies, and at least every 5 scans for the third set of comparisons. Calibrations of the difference signal for 100% absorption were taken before and after each series of scans, the

values never varied by more than 0.8% over 40 scans.

Before recording the scans, long scans at afast scanning rate were made to investigate the wavelength region and sort out any identification problems. Typically these preliminary scans would cover a region of 5Å at 50 mÅ/sec. Each recorded scan consisted of 80 points each integrated for a second; this would cover roughly 300 mÅ at 4 mÅ/sec thus allowing plenty of continuum reference points either side for even the strongest lines.

Generally lines were brought to between 5 and 12 mÅ (though for large 'jumps' this was not always possible) and these correspond roughly with absorption depths of between 12 and 30% respectively. For a 0.2% noise level, these lines will give less than a 1.5% error in the final equivalent width (Collins 1970). The monochromator entrance and exit slit widths were 2mm and 150μ respectively in accordance with the suggestions of Chapter 5.

Various argon pressures were used; generally between 50 and 100 torr was found to be high enough to keep the vapour in the hot region of the tube. This high pressure also reduced the likelihood of other reactions occuring in the tube. As mentioned earlier, titanium is quite reactive and a certain amount of difficulty was encountered at temperatures between 1700 and 2100°C. A thick mist sometimes formed which decreased the light throughput considerably thereby effectively masking the lines. This mist is still not fully understood, but as it appears only with titanium samples it is possibly the oxide burning off at various parts of the tube. Pressures of 200-300 torr tend to inhibit such outgassing though damping effects would then be significant; no scans were attempted until the mist had completely resettled.

Background scans with no furnace current were taken for several strategically important comparisons in order to investigate the continuum curvature. These background corrections to the equivalent widths are discussed later.

Wherever possible the comparisons were arranged in closed loops thus enabling a check on the reproducibility of the results and on the accumulative error theory. Despite the small differences known to exist between the 2 spectrometers the lines were not reversed in this study. The reasons for this, and a more detailed error analysis follows.

6.3 c Data reduction, errors and results

As mentioned in Chapter 5, scans were recorded on paper tapes, one for each spectrometer, for subsequent reduction on a departmental computer. The reduction method has been described before and the aim here is to demonstrate the sensitivity of the results to various parameters in order to justify some simplifications made in the observing procedure, as well as to determine the errors present in the final results.

For the first part of the reduction, where a continuum is fitted and the normalised scan is integrated to give an equivalent width, the only uncertain parameter is the calibration level. A variation of more than 0.3% was never seen over a series of 40 scans and this corresponds to less than 0.6% in the equivalent width W_λ . The only other possible source of error in this part is due to the fitting of the continuum. Scans which, for some reason or other, have poor continua can be identified on the computer display and dealt with accordingly. Thus taking the 1.5% error in W_λ introduced by the noise level, an error of less than 2% in the final W_λ is quite realistic. Of course by taking the ratio of the W_λ's such errors are reduced considerably.

In the second part of the reduction the equivalent widths are fitted onto curves of growth for each line and the ratio of the gf-values found for each scan. This program is sensitive to two parameters in particular: temperature and continuum background correction.

The temperature effect is much more pronounced for lines from

different terms because of the differential excitation involved. For lines from the same term, an exaggerated error of +50 degrees for each point on the 4-point temperature profile produces an error in the gf-ratio of less than 0.2%. Thus for these lines temperature accuracy presents no problems.

For the comparisons where the lines originate from different terms a detailed anlysis of the temperature effects was performed. For the worst cases of linking a^3F to a^5F ($\Delta\chi$ = 0.8eV), and from a^3P to a^5P ($\Delta\chi$ = 0.7eV), the cooler 2 points on the profile do not contribute significantly to the total vapour pressure. This is verified by considering the vapour pressure curve of Nesmayanov (1963) in Fig. 6.2, where four typical temperatures on the profile are marked. But for an accuracy of 1% in the gf-ratio the central temperatures must be known to $\pm$ 7 degrees.

The accuracy to which the temperature is known depends on the accuracy of the pyrometer calibration and also on that of a correction made for absorption by the quartz window at the end of the top. The pyrometer has been calibrated by the N.P.L. and in the region of 1700-2300°C is accurate to between $\pm$ 7 to $\pm$ 10 degrees. The window absorption was taken as 15 degrees, this was later confirmed by measurements of R.B. Willis. Thus the largest 'jumps' in χ will be correct only to 1½%. However these are the worst cases, and generally the error introduced by temperature uncertainties will be less than 0.2%.

Larger effects are seen with the background corrections, and whenever possible these were included. As the curvature of the arc continuum can be in either direction, so the residual equivalent widths with the furnace off can be positive or negative. Unforturnately the dispersion around the corrections is often larger than the corrections themselves. Typically corrections of $\pm$0.04 mÅ were found; for a weak line-strong line comparison this could change the

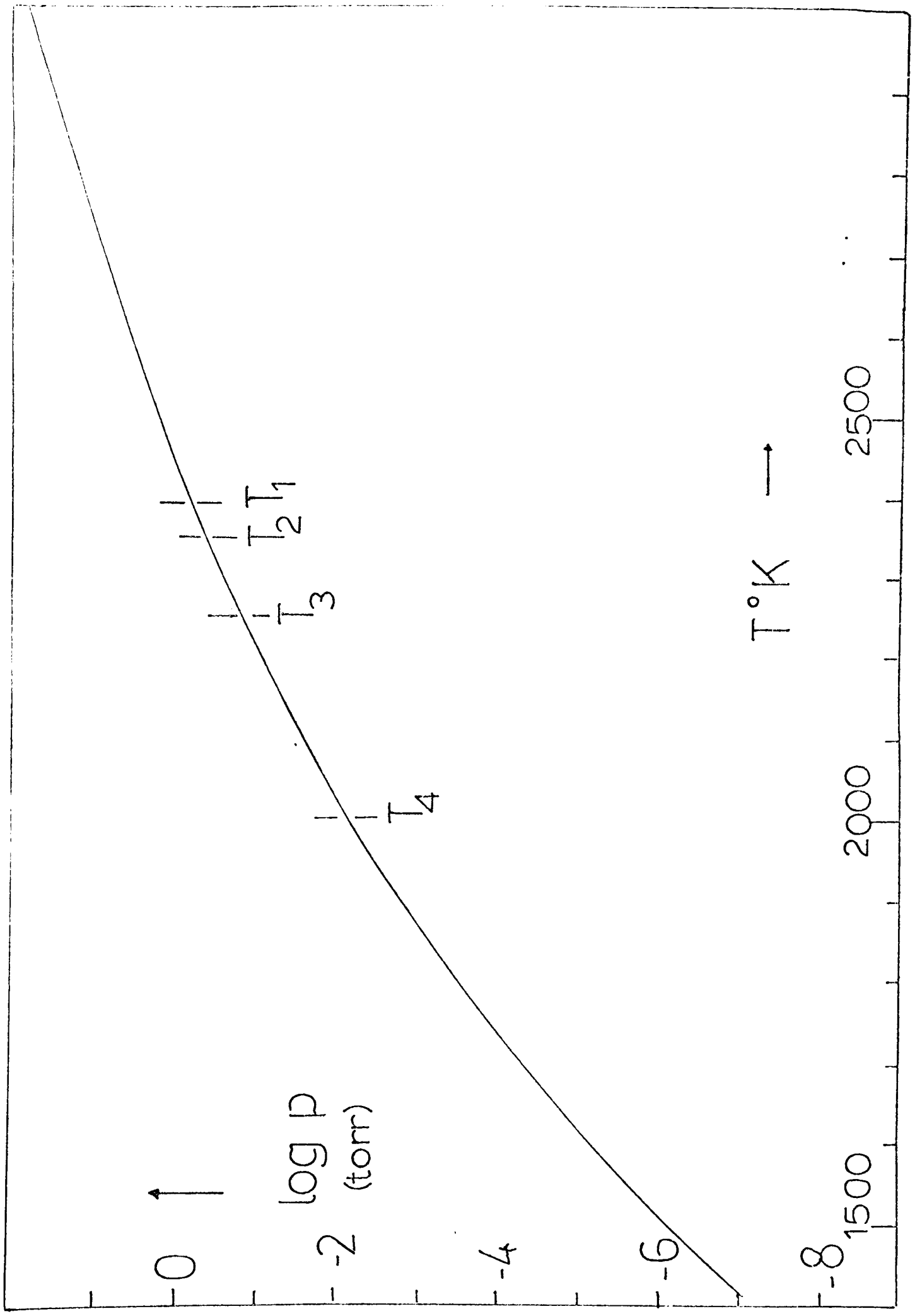

Figure 6.2

Vapour pressure curve for Titanium (from Nesmayanov 1963)

gf-ratio by up to 3%. To determine the correction accurately however, at least 40 background scans are needed, thus halving the effective work rate. As the corrections produce changes far less than the standard deviations, they were only included for strategically important comparisons, and then only if they could be accurately determined.

The problem of line-emission was discussed in Chapter 5. A more serious problem at high temperatures is that of blends, particularly those due to lines of C_2 and carbon impurities. The most difficult region $\lambda < 4000$ Å was avoided for this reason though it is still possible that some of the weaker lines elsewhere are affected. Blackwell et al (1974a) have shown the effect is less than 5% even for the weakest lines.

Various investigators at Oxford report the curious differences seen when the lines are reversed between the two spectrometers. This might arise if the scattered light in the two spectrometers was different, though detailed work has shown this is not the case. As the effect is smaller than 2%, and not systematic it has been ignored in this investigation.

All closed loops check to within 0.03dex and most agree to 0.015. This justifies the assumptions made above. The standard deviation on all comparisons is less than 0.025 dex and generally lies between 0.005 and 0.020dex. It is possible to find the cumulative error on a given line by summing the squares of the standard deviations, i.e. in comparing lines 1 and 2 if the deviation is σ_{12} then:

$$\sigma_2^2 = \sigma_{12}^2 + \sigma_1^2 \qquad (6.3)$$

A certain amount of trouble was taken to achieve an accurate result for the important link of the terms a^3F and a^5F. The comparison 5147.43($a^3F_2 - z^3F_3$) / 5007.21($A^5F_2 - y^5G_3$) proved to be most satisfactory. Both lines had more or less the same equivalent width of 12 mÅ and the background effects cancelled. Furthermore

there was a standard deviation of only 0.009dex for this comparison.

Coping with the 15:1 interval proved to be more difficult. Consulting table 6.3 it is seen that the comparison 5238(a^5F_5 - y^5D_4) / 4840(a^1D_2 - y^1D_2) implies a ΔF_t of only 0.6dex, and this seemed to be the best way of linking the weak and strong sets of lines. However the Corliss and Bozman gf-values are clearly incorrect for these lines, as a difference of 1.6 dex was found. A better comparison proved to be 4840(a^1D_2 - y^1D_2) / 6743(a^1D_2 - z^1D_2) for which C & B predict a difference of 0.95dex, and in fact a difference of 1.3dex was observed. Both comparisons give gf-values for λ 4840 which agree to 0.015dex, which is pleasing agreement for such large jumps.

The isotope effects of titanium are now briefly considered. The five stable isotopes and their nucleas parameters are given in Table 6.4. It is seen that Ti^{47} and Ti^{49} exhibit a nuclear spin and therefore one might expect to see a significant hyperfine splitting of lines, both in the laboratory and in stellar spectra. Although no-one, to the author's knowledge has investigated this possibility, it is important to justify such neglect. The only hyperfine (hf) data available for Ti is that of Channappa (1965) who has measured the magnetic and electric-quadrupole hf constants A and B for the levels $3d^24s^2\ ^3F$ (J = 2,3,4), i.e. the ground state term. Assuming no splitting in the other levels, (for lack of any other information), the author calculated the splitting expected in the 5173.75 Å resonance line (a^3F_2 - $z^3F^o_2$) on which the above relative scale is based. This line is split into 5 components in both isotopes, all contained within 7 mÅ and the strongest components are within 2 mÅ of the single line. In view of such small splitting and because of the small abundances of Ti^{47} and Ti^{49} relative to the main isotope, hf structure was ignored in all subsequent work with titanium.

The final oscillator strengths are given in Table 6.5, and the standard deviation associated with each gf-value as calculated by equation 6.3 is given alongside. The scale is normalised for comparison

Table 6.4

Isotopes of Titanium

A	%	N(A)	I	μ
46	7.93	182	-	-
47	7.28	168	5/2	-0.79
48	73.94	1700	-	-
49	5.51	127	7/2	-1.10
50	5.34	123	-	-
total	100.00	2300	-	-

Notes: Col 1: Atomic weight

2: Percentage abundance

3: Actual abundance relative to Si=10^6

from Cameron(1968)

4: Nuclear moment

5: Magnetic moment in nuclear magnetons

Table 6.5

Oxford oscillator strengths

χ_{eV}	λ	lgf	σ	King	P'ev	Wlnk	Klt
0.00	5173.75*	2.000	.000	2.000	2.00	2.000	2.00
	4656.47	1.759	.016	1.715	1.76		
	5147.48*	1.112	.018	1.037	1.16	1.234	
0.02	5039.95	2.246	.013	2.000	2.03		1.84
	5192.98*	2.112	.011	2.125	2.15	2.133	
	4667.59	1.863	.016	1.829	1.93	1.954	1.78
	5152.20*	1.094	.023	1.028	1.18	1.234	
	5219.71*	0.820	.024	0.756	0.94	1.137	1.04
	5009.65	0.866	.026	0.819	0.96		
	4562.63	-0.044	.032	0.426	0.56		
	5426.26	-0.347	.029	0.276	0.37		
0.05	5064.66	2.058	.018	2.125	2.19	2.109	1.95
	5210.39*	2.232	.014	2.250	2.23	2.234	
	4681.92	1.872	.027	1.990	2.03	2.133	1.87
	4112.71	1.279	.023	1.472	1.52	1.456	
	5252.11*	0.678	.020	0.551	0.78		
	5460.51	0.256	.017	0.438	0.55		
	4715.30	0.320	.020	0.250	0.40		
0.81	5389.18	0.434	.033	0.829	1.08		1.01
0.82	5007.21	3.222	.020	3.192	3.34		2.95
	5024.84	2.504	.024	2.482	2.54		
	4926.16	0.824	.033		1.22		
	5366.65	0.368	.034	0.911	1.02		0.62
0.83	4999.51	3.329	.025	3.368	3.44		3.01
0.85	5238.58	1.037	.030	1.361	1.55		
	5045.41	1.030	.031		1.36		
0.90	4840.87	2.580	.025	2.532	2.52	2.57	2.38
	6743.12	1.247	.028	1.551	1.60		
1.05	6064.63	1.150	.031	1.347	1.61		
1.06	6085.23	1.500	.029	1.676	1.83		
1.07	5866.46	2.180	.029	2.293	2.41		2.26
	4675.12	1.678	.030	1.721	1.90	1.862	
	6126.22	1.582	.033	1.783	1.85		
	5295.79	1.436	.034	1.702	1.71		
1.75	4617.27	3.414	.027	3.401	3.50	3.359	3.21

* used in determining the absolute scale(section 6.4)

purposes by setting log gf(5173) = 2.00.

As the standard deviations are considerably larger than the errors given by the analysis above, they can be regarded as pessimistic limits on the accuracy of the scale as a whole. Thus the entire scale is accurate to within $\pm$ 0.03dex, but the accuracy of a small set of comparisons is of course much greater.

6.4 The results compared

Table 6.5 lists the log gf values, on a normalised scale, for the four chosen surveys. There are too few common lines for a detailed comparison and therefore it is difficult to measure energy dependances. A large range of lower excitation potentials χ_l have been studied however, and Figs 6.3 a-d show the four sets of results compared individually with those of the author. The differences are plotted against χ_l even for the comparisons with emission methods, this is in order to test for systematic errors in the author's work.

The scatter on these graphs is quite large, but more encouraging is the lack of any systematic trend with χ_l on Figs. 6.3 b-d. In particular, the following points emerge:

1) Apart from the points at 1.75eV, there appears to be a slight energy dependance in the work of King. This is also reported by Klemt.

2) The agreement with Wolnik is generally to within $\pm$ 0.10dex with the exception of a few ground state lines.

3) The agreement with Prokof'ev is poor, and it is suggested that his values are contaminated by the poorer results mentioned in section 6.2.

4) The scatter with Klemt's values is the largest and many of his gf values are too low (with respect to all other results) by 0.2 dex.

Thus except for Wolnik, the comparison is disappointing. Nevertheless there are only four lines for which the author's values are consistently

Figure 6.3a

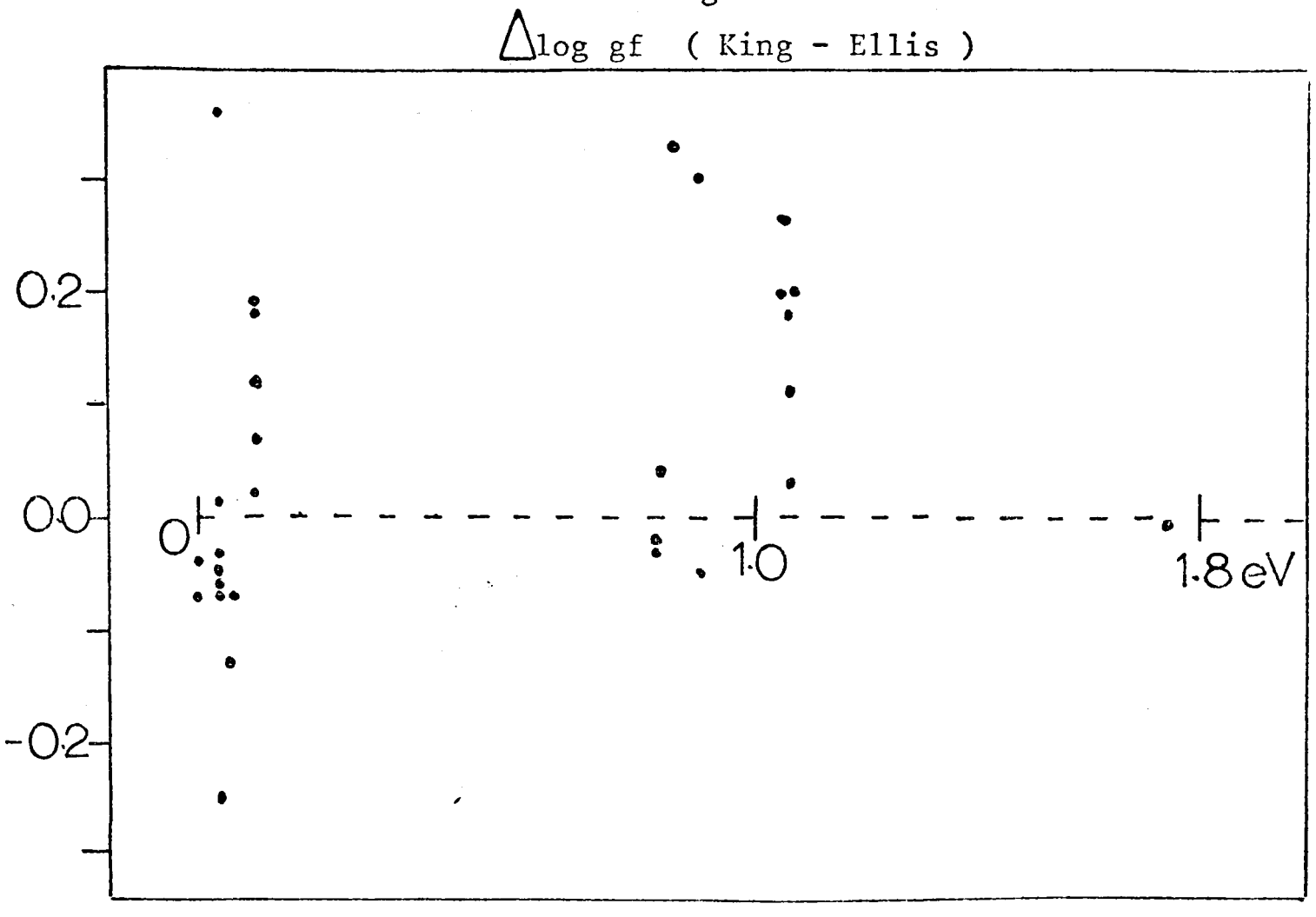

Figure 6.3b

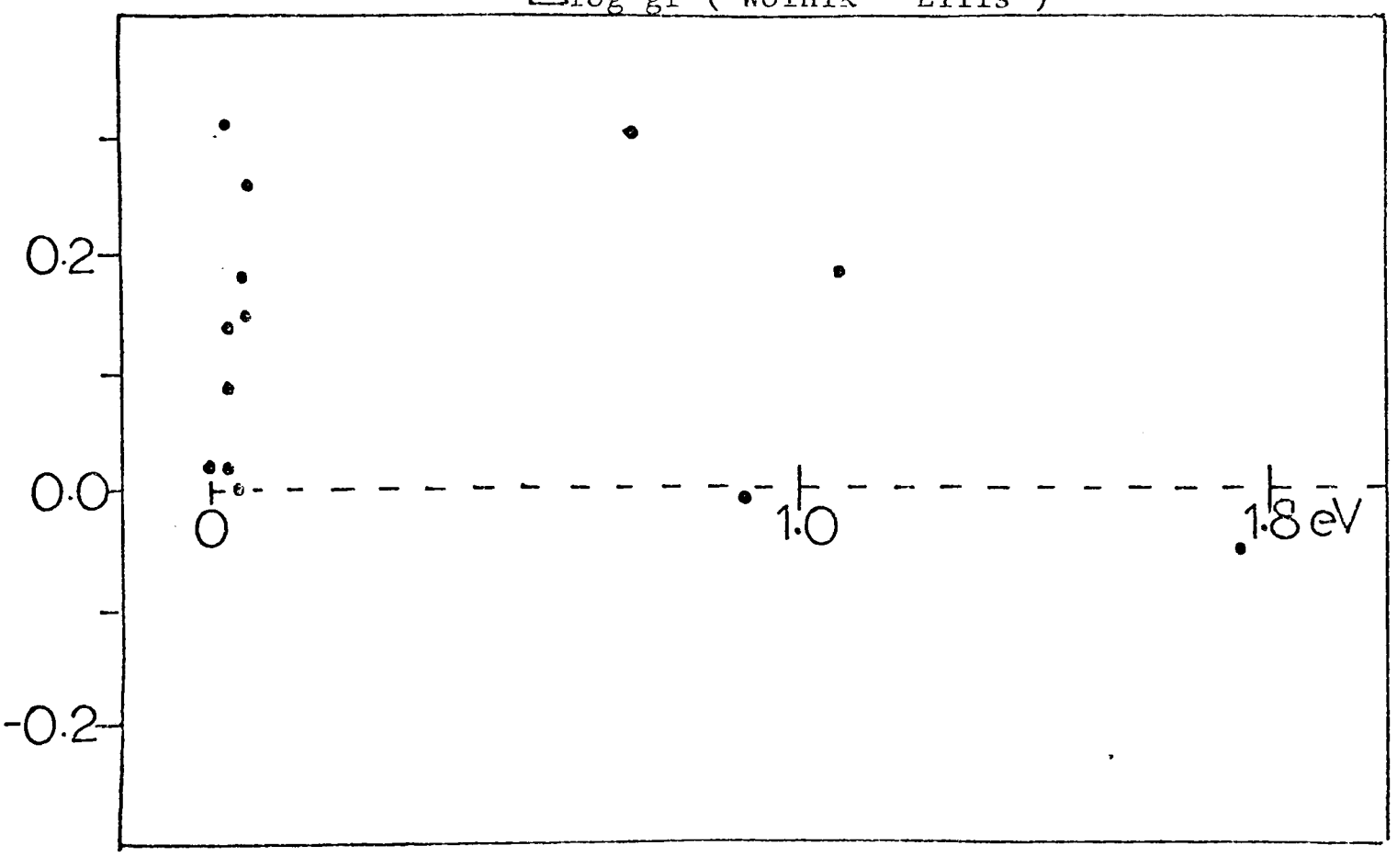

Figure 6.3c

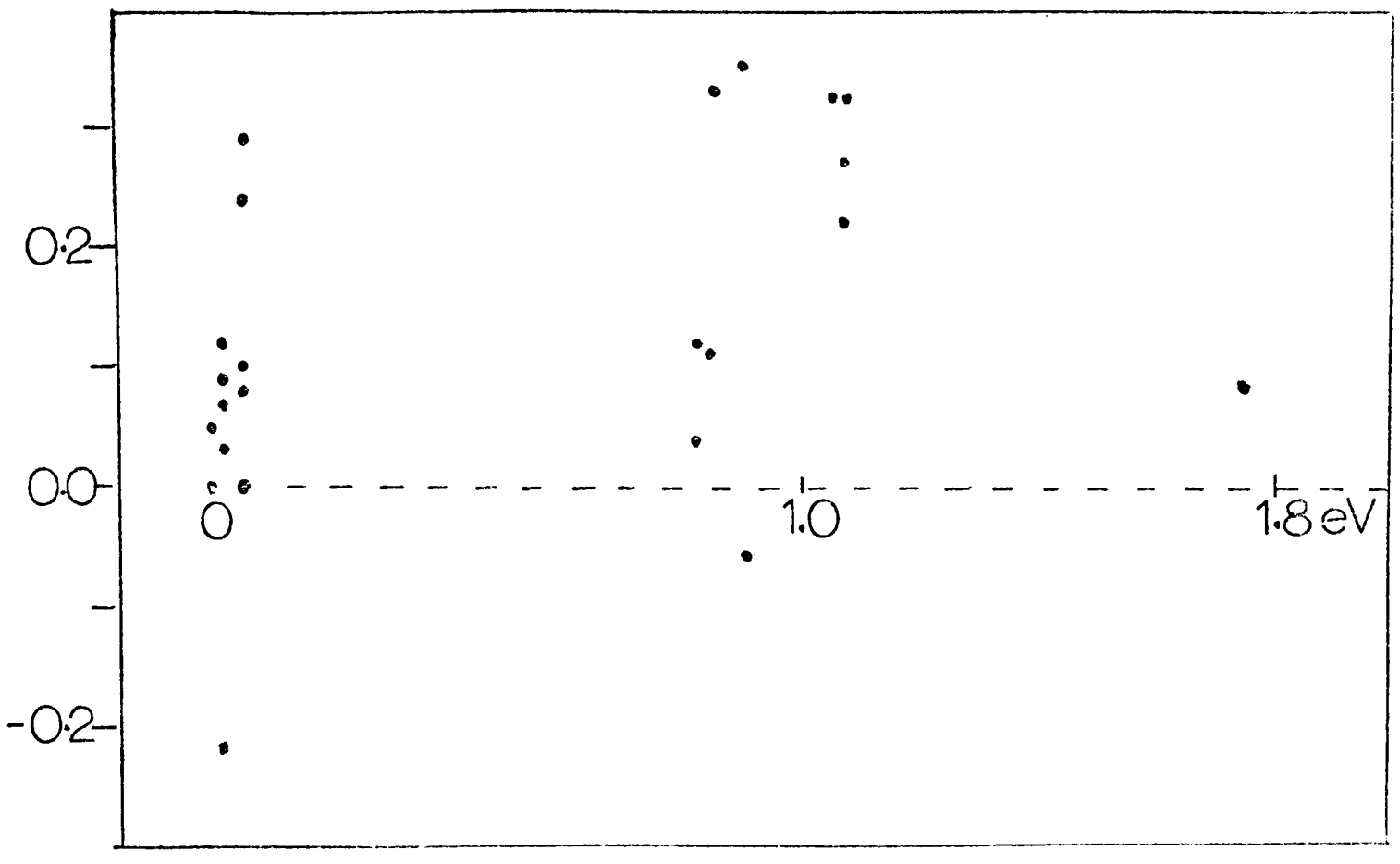

Figure 6.3d

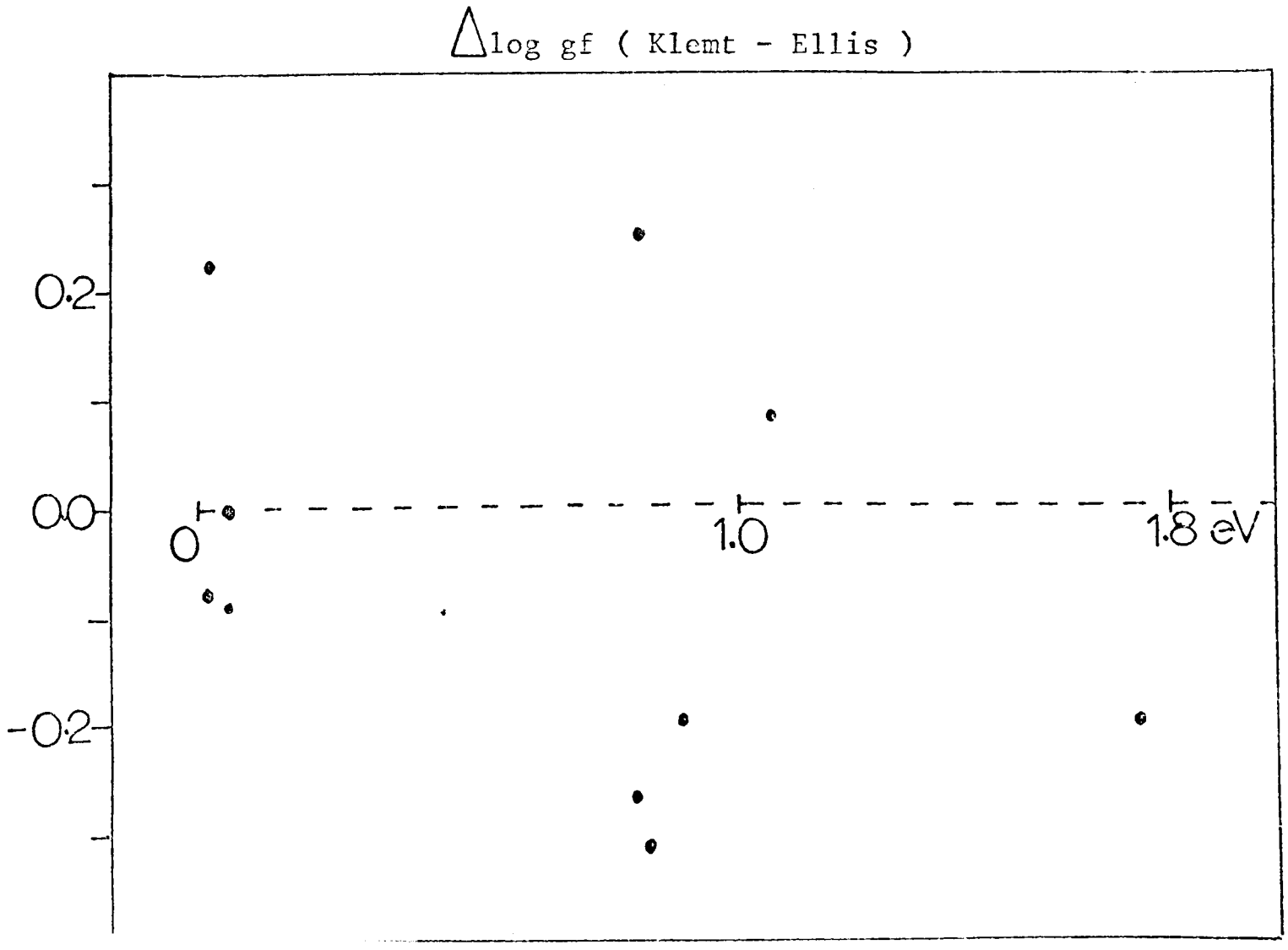

different, and from the abundance point of view only two of these are important lines. These lines have been remeasured, and no change in the values is found necessary. In justifying the use of the author's scale for abundance work, it must be remembered that the scatter between the other results is even larger than that in Figs. 6.3. In fact, because of the pleasing agreement in closed loops and remeasurements, and the low standard deviations on all comparisons, it is still maintained that the author's scale is accurate to at least $\pm$ 0.03 dex. The internal scatter on Wolnik's results is quoted as $\pm$ 0.03 dex, thus if we ignore the odd ground state lines in Fig. 6.3b, the agreement to $\pm$ 0.10dex confirms this assertion.

Further evidence is drawn from the absolute values of Siddall (1969). These values were calculated theoretically using a central-field model. The work was semi-empirical in that the transition integrals used assumed an experimental one-electron ionisation energy. This so-called 'scaled Thomas-Fermi' method will be incorrect only for the highest energies. In Fig. 6.4 the difference between the absolute and relative scales is plotted against χ_ℓ, and it is clear that the spread for the 1eV lines is much larger than for the ground spread around the mean difference (indicated by the line on the figure) is again only $\pm$ 0.10 dex.

The agreement with Siddall is particularly encouraging because it confirms the author's values for the two uncertain lines mentioned above. These lines are marked on the figure 6.4.

Plots of log gf_1 vs. log gf_2 abound in the literature. Such plots should be regarded with suspicion. In order to accommodate all the points, the scale must be small. Therefore agreement looks remarkably good. An example of such a plot is given in Fig. 6.5 where the Siddall-Ellis comparison appears to be excellent.

Thus good agreement of $\pm$ 0.10 dex between the relative scale of the author and the two absolute scales of Wolnik and Siddall enables the determination of the mean transfer coefficient, which

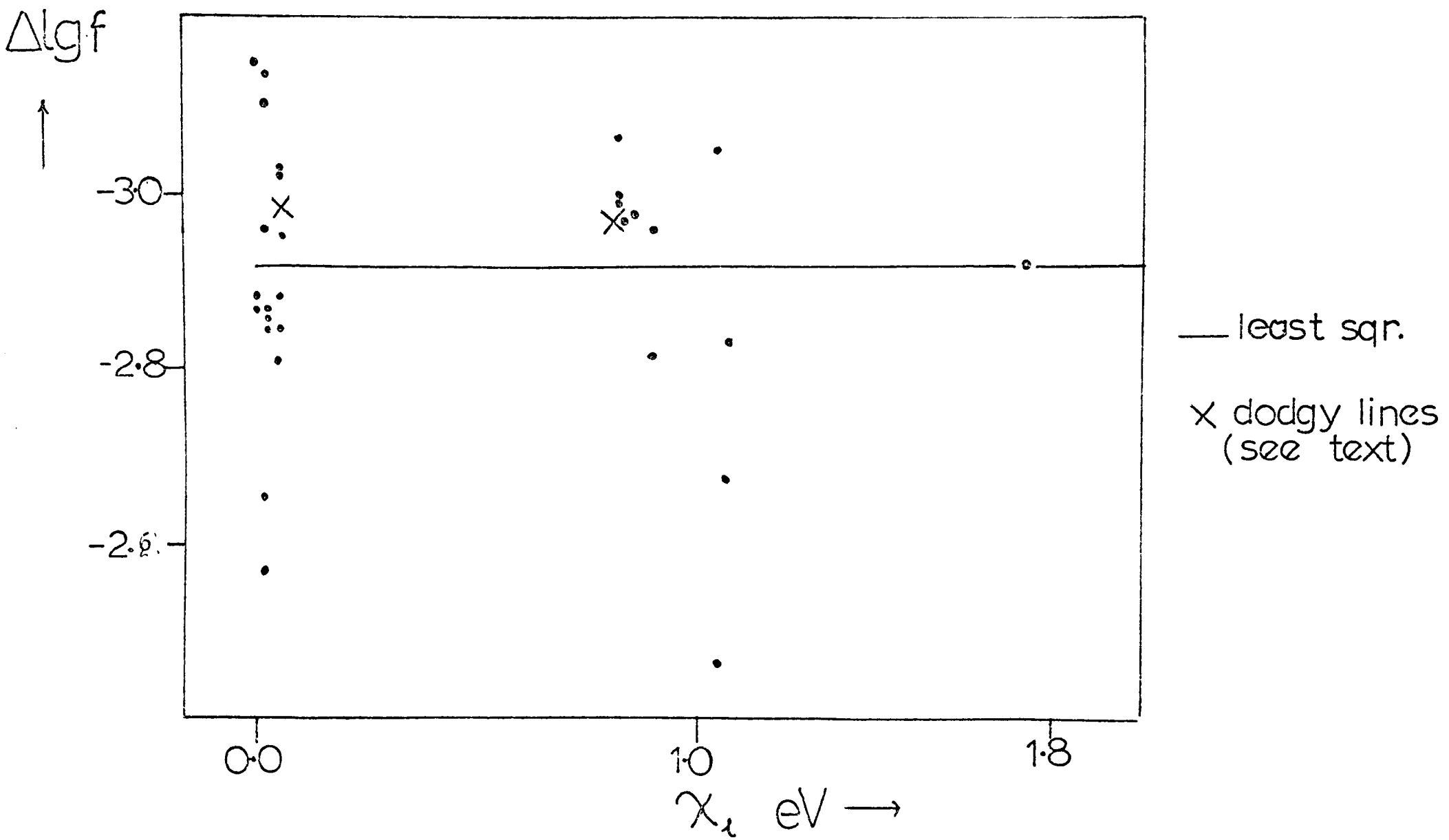

Figure 6.4

△log gf (Siddal - Ellis)

Figure 6.5

log gf(Ellis-furnace). vs. log gf(Siddall-theory)

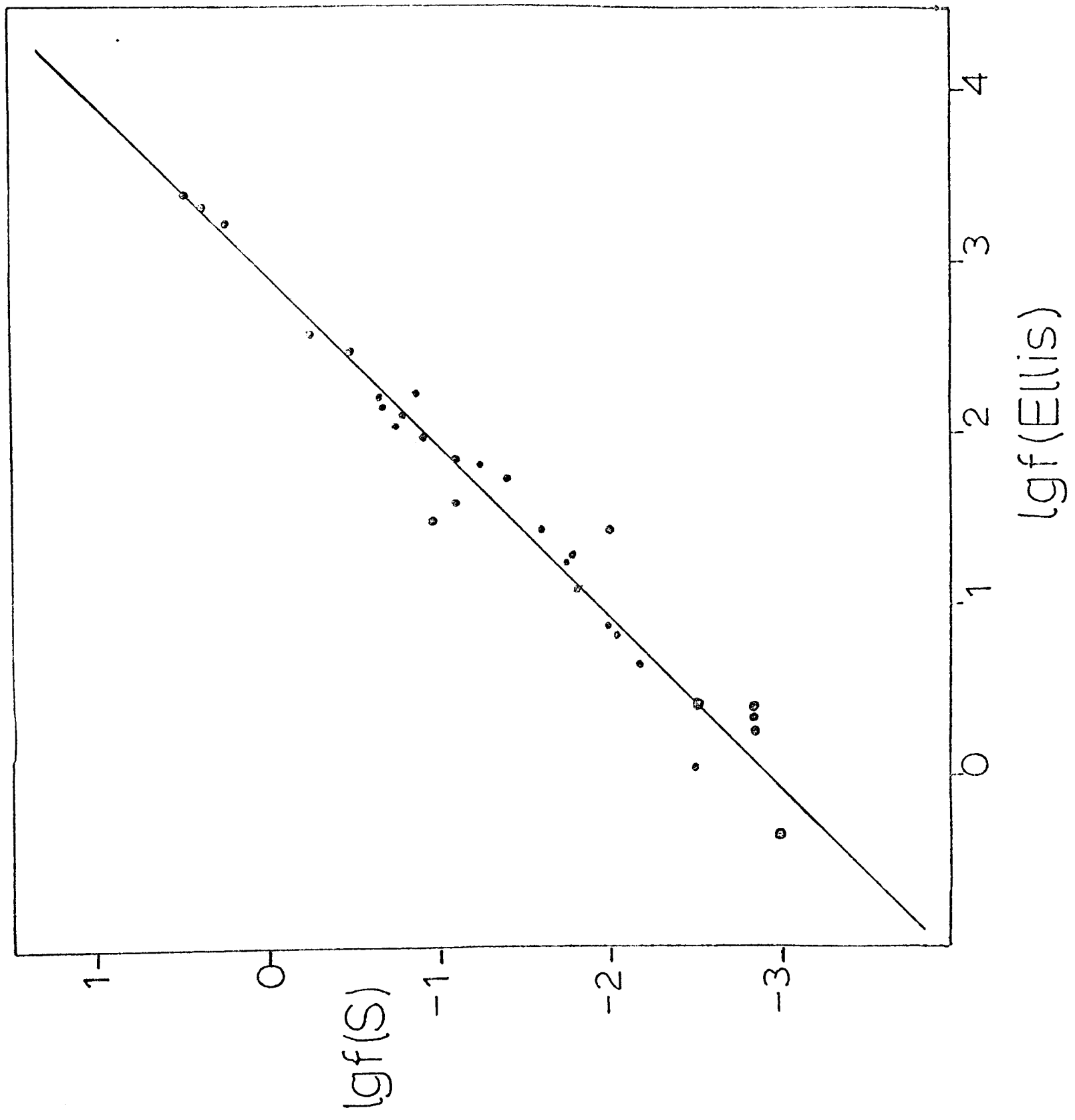

places the author's gf-values on an absolute scale.

6.5 Absolute oscillator strengths

The position regarding absolute gf-values is even worse than that for relative ones. This is because one cannot arbitrarily shift scales to meet and so all errors become embarrassingly obvious. There are many so-called 'absolute' values for Ti I in the literature; they are not all reviewed here. Most are from emission or absorption methods and rely on a knowledge of the absolute number density of titanium in the apparatus. Such results do not even agree on a relative scale, and on the absolute scales the spread is often several orders of magnitude. Provided good relative values are available, the best way of getting absolute values is from the lifetime of a level. These methods, if performed carefully, do not need to assume any number densities, a knowledge of the relative decay rate is sufficient.

For a level a the lifetime τ_a is related to the transition probability by (see Chapter 5):

$$\frac{1}{\tau_a} = \sum_b A_{ab} \qquad (6.4)$$

A_{ab} is related to the absorption oscillator strength on an absolute scale by

$$A_{ab} = \frac{8\pi^2 e^2}{mc\, g_a} \left(\frac{g_b\, f_{ba}^{abs}}{\lambda^2} \right) \qquad (6.5)$$

thus

$$\frac{1}{\tau_a} = \frac{8\pi^2 e^2}{mc\, g_a} \sum_b \left(\frac{g_b\, f_{ba}^{abs}}{\lambda^2} \right) \qquad (6.6)$$

therefore if we relate the relative scale to the absolute one by a transfer coefficient X then

$$\log gf_{ba}^{rel} = \log gf_{ba}^{abs} + X \qquad (6.7)$$

thus in eqn (6.6)

$$\log X = 9.176 - \log \tau_{ns} - \log \left\{ \frac{1}{g_a} \sum_b g_b f_{ba}^{rel} / \lambda^2 \right\} \qquad (6.8)$$

enabling a determination of X. In (6.8) τ is in the conventional units of nanoseconds. To determine X one therefore requires good relative gf-values for all allowed transitions from a.

There are two lifetime measurements for Ti I. The first is by Andersen et al (1973), who have measured lifetimes for the $3d^2 4s4p\ y^3F^o$, y^3D^o and $3d^3 4p\ y^5G^o$ terms using the beam-foil technique. There are, however, many allowed transitions from each one of these levels and gf-values are not available for all of them. Thus it is unfortunately not possible to use these lifetimes at the moment, but an attempt to measure these branching ratios may be included in the future Oxford program.

The second set of lifetimes is for Hese (1972) who has measured the $3d^2 4s4p\ z^3F^o$ (J = 2,3,4) term using an optical double resonance method (see Chapter 5). His results, together with other comparisons, are given in table 6.6. There are two sets of transitions allowed, $a^3F - z^3F^o$ (multiplet 4 in Moore's scheme) and $a^5F - z^3F^o$ (multiplet 34). The second multiplet has never been observed; no intensities or gf-values are available. It was therefore assumed that these gf-values are negligible in comparison with those of the resonance lines of multiplet 4.

Using the author's gf-values and the lifetimes of Hese in eqn 6.8 gives a coefficient X_j for each J level in the term. The results are shown in Table 6.6. The mean value is

$$X_{Hese} = -2.93 \pm 0.07$$

Although the spread is quite large this agrees closely with the

Table 6.6

Lifetimes and transfer coefficients for the $3d^2 4s4p\ z^3F^o$ term

Level	C&B	Siddall	Hese	X_{Hese}
$^3F_4^o$	252	147	205	-3.011
$^3F_3^o$	205	145	140	-2.862
$^3F_2^o$	200	143	155	-2.915

(lifetimes are in nanoseconds)

Table 6.7

Transfer coefficients for the Ellis scale

Author	Method	X
Hese	lifetime	-2.93 ± 0.07
Siddall	theory	-2.92 0.08
Wolnik	shock tube	-3.16 0.08
Klemt	arc emission	-2.86 0.14
Prokof'ev	sumrule	-3.26
Reinke	atomic beam	-3.21

mean coefficient determined from Siddall's results on Fig. 6.4.

$$X_{Siddall} = -2.92 \pm 0.03$$

The error here is a standard deviation. Various other coefficients are given in Table 6.7, as derived from their absolute gf-values for the normalising line λ5173. The total spread is $\pm$ 0.20 dex.

The work at Oxford could be extended to include the absolute values of Reinke, who has measured 3 resonance lines between $\lambda\lambda$ 3635 - 3654 Å. Reinke's scale agrees to within 0.04dex of Prokof'ev's however, and since the X value of Prokof'ev is slightly higher than the others in Table 6.7, this places some doubt on these two scales.

The chosen X is the mean of the values for Hese and Siddall, viz.

$$X = -2.925 \pm 0.03$$

This error encompasses the results Klemt but not those of Prokof'ev or Wolnik. It is suggested that Prokof'ev's absolute scale, determined by the sumrule, is 0.30 dex too high.

The accuracy of the final absolute results depends not only on the error in X, but also on the errors in the gf-values used in eqn 6.8. The lines used in the reduction are marked in Table 6.5; they all have standard deviations of less than 0.025 dex. The final absolute gf-values are listed in Table 6.8.

It has therefore been shown that gf-values for weak, astrophysically important lines can be measured by the Oxford furnace to a relative accuracy of at least $\pm$0.03 dex(7%). These results have been placed on an absolute scale which is accurate to $\pm$ 0.03 dex (20%).

Table 6.8

Absolute Ti I gf-values

λ	χ_{eV}	lgf_{abs}	σ_{rel}
4112.71	0.048	-1.656	.023
4562.63	0.021	-2.881	.032
4617.27	1.749	+0.489	.027
4656.47	0.000	-1.166	.016
4667.59	0.021	-1.062	.016
4675.12	1.066	-1.247	.030
4681.92	0.048	-1.053	.027
4715.30	0.048	-2.605	.020
4840.87	0.899	-0.345	.025
4926.16	0.818	-2.101	.033
4999.51	0.826	+0.404	.025
5007.21	0.818	+0.297	.020
5009.65	0.021	-2.059	.026
5024.84	0.818	-0.421	.024
5039.95	0.021	-0.679	.013
5045.41	0.848	-1.895	.031
5064.66	0.048	-0.867	.018
5147.48	0.000	-1.813	.016
5152,20	0.021	-1.831	.023
5173.75	0.000	-0.925	-
5192.98	0.021	-0.813	.011
5210.39	0.048	-0.933	.014
5219.71	0.021	-2.108	.024
5238.58	0.848	-1.888	.030
5252.11	0.048	-2.247	.020
5295.79	1.066	-1.489	.034
5366.65	0.818	-2.557	.034
5389.18	0.813	-2.491	.033
5426.26	0.021	-3.272	.029
5460.51	0.048	-2.669	.017
5866.46	1.066	-0.745	.029
6064.63	1.046	-1.775	.031
6085.23	1.053	-1.425	.029
6126.22	1.066	-1.347	.033
6743.12	0.899	-1.678	.028

CHAPTER 7

THE SOLAR ABUNDANCE OF TITANIUM

7.1 Introduction

A determination of the solar titanium abundance using the Oxford f-values is of interest not only for its own sake, but also in providing a means of examining the internal consistency of the relative f-values. By treating the sun as another absorption furnace the observed equivalent widths should be consistent with one abundance. Such investigations have already shown for other elements (Garz et al 1969, Collins 1970) that abundance variations of 0.50dex are sometimes seen despite claimed relative f-value errors that are considerably less. It is therefore expedient to produce an independent estimate of the error in the relative scale by studying the solar abundance from line to line.

The method however assumes the physical processes of solar line formation are perfectly understood; uncertainties in the theory for stronger lines severely limits this test. With weak lines, ($W_\lambda \sim 35$mA) however, uncertainties in microturbulence and damping constants will not seriously affect interpretation of the results, and thus deficiencies in the line theory can be avoided somewhat. Despite the criteria set out in choosing the lines, there are few weak unblended lines in the solar spectrum that have been measured in the furnace. Thus a detailed investigation of possible abundance variations with wavelength or excitation potential is unfortunately not possible.

7.2 Solar models

The determination of a solar model atmosphere is an essential prerequisite to all studies of solar line formation, and as this is obtained in a slightly different manner to that outlined in Chapter 4, it merits a brief mention.

As the solar disk can be resolved it is possible to observe the limb-darkening relation at various wavelengths and hence establish an empirical temperature distribution. A solution of the transfer equation in LTE gives (cf Chapter 4)

$$I_\lambda(\tau_\lambda = 0, \mu) = \int_0^\infty B_\lambda(\tau_\lambda)\, e^{-\tau_\lambda/\mu}\, \frac{d\tau_\lambda}{\mu} \qquad (7.1)$$

thus the limb-darkening relation becomes

$$\phi_\lambda(\mu) = \frac{I_\lambda(0,\mu)}{I_\lambda(0,1)} = \int_0^\infty \frac{B_\lambda(\tau_\lambda)}{I_\lambda(0,1)}\, e^{-\tau_\lambda/\mu}\, \frac{d\tau_\lambda}{\mu}$$

$$= \int_0^\infty b_\lambda(\tau_\lambda)\, e^{-\tau_\lambda/\mu}\, \frac{d\tau_\lambda}{\mu} \qquad (7.2)$$

Assuming $b_\lambda(\tau_\lambda)$ can be represented in a power series e.g.

$$b_\lambda(\tau_\lambda) = \sum_K a_K \tau_\lambda^K \qquad (7.3)$$

then in (7.2)

$$\phi_\lambda(\mu) = \sum_K a_K K!\, \mu^K \qquad (7.4)$$

By judicious choice of a relation (7.3) and fitting to the observed ϕ_λ at various wavelengths it is therefore possible to determine $b_\lambda(\tau_\lambda)$. An absolute value for $I_\lambda(0,1)$ then gives $T(\tau_\lambda)$ for various τ_λ. Furthermore since at a given T

$$\frac{(d\tau_\lambda/dT)_{\lambda_1}}{(d\tau_\lambda/dT)_{\lambda_2}} = \frac{\kappa_{\lambda_1}}{\kappa_{\lambda_2}} \qquad (7.5)$$

it is then possible to determine the absorption coefficient empirically. With a knowledge of κ_λ and $T(\tau)$ the equation of hydrostatic equilibrium can be integrated to give the pressure and complete the model.

Such empiricalsolar models are quite successful, though are constantly being revised as new observations are made. The most recent model is the Harvard Smithsonian Reference Atmosphere (HSRA, Gingerich et al 1971) which utilises the ultraviolet rocket observations of Parkinson and Reeves (1970) and the absolute energy distribution of Labs and Neckel (1970). The model replaces the earlier Bilderberg Atmosphere (Gingerich and Jager 1968), which failed to reproduce the observed limb-darkening in the visible region. An intermediate model after Elste (1968) meets this requirement but is based only on observations up to 1968.

The observed limb-brightening at short wavelengths is represented in the empirical models by a temperature reversal in the lower chromosphere ($\tau_{5000} \sim 10^{-4}$). In the HSRA non-LTE calculations in this region were made using the departure coefficients of Noyes and Kalkofen (1970). A further advantage of using weak lines in abundance analyses therefore is that they are formed lower down in the atmosphere where uncertainties in non-LTE are smaller.

A preliminary theoretical LTE model has recently been published by Kurucz (1974). Comparison between the HSRA and this model can yield useful information regarding energy transport and equilibrium in the sun. The temperature distributions of this model and the HSRA are shown in Fig. 7.1; the model of Elste (1968) is also included. The agreement with the HSRA is encouraging, and Kurucz shows that the central intensities in the visible and infra-red are consistent with observations. It is therefore likely that future solar models will benefit greatly from theoretical comparisons of this nature.

7.3 Theory of line formation

The mechanism of line formation in a stellar atmosphere is by no means fully understood although many of the rudimentary

Figure 7.1

Comparison of empirical and theoretical(Kurucz) solar models

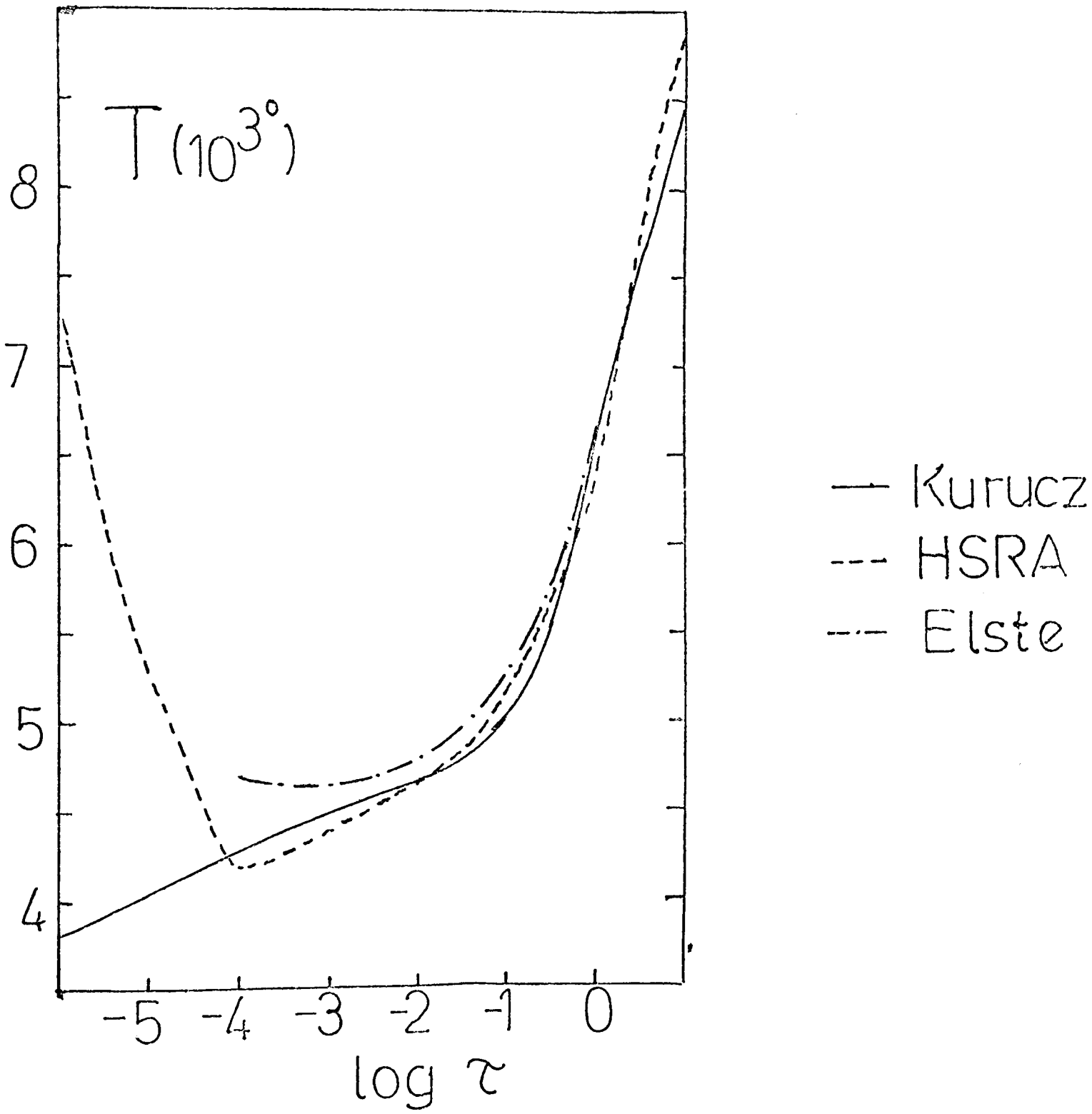

investigations of Minnaert are still applicable. A computer program has been developed in this department for the calculation of a line profile in LTE from a model atmosphere, and this section essentially describes the features and facilities of the program. The program, conveniently termed STARLINE, was written by Professor Blackwell and has been recently overhauled by R.B. Willis.

The model provides T, p_e, p_g, and κ_{λ_o} as a function of τ_{λ_o}, the optical depth at the standard wavelngth λ_o. The continuous absorbers are then combined for each level j in the atmosphere:

$$\kappa_\lambda^j = \sum_{\text{all}} k_\lambda (T^j, p_e^j) \qquad (7.6)$$

the corresponding optical depth at λ is then given by

$$\frac{d\tau_\lambda}{d\tau_{\lambda_o}} = \frac{\kappa_\lambda}{\kappa_{\lambda_o}} \qquad (7.7)$$

Table 7.1 shows the opacities included in STARLINE. For the solar spectrum in the region $4500 < \lambda < 6000$ Å, the H^- opacity accounts for 93% of the total. Below 4500 Å however there is disagreement between the theoretical total and that derived empirically from observations. This has led to the suggestion of a missing ultra-violet opacity (Gingerich 1964).

In the absence of scattering the total absorption coefficient is analogous to that used in the furnace curve of growth (see eqns 5.58-40). i.e.

$$\ell_\lambda = N_r \alpha_\lambda = N_r \alpha_o H(a, v) \qquad (7.8)$$

where N_r is the number of absorbing atoms (found in LTE by applying the Saha ionisation and Boltzman excitation formulae), H is the Voigt function, and a , α_o , and v are as in equations (5.39).

The treatment of damping in the solar atmosphere is more

Table 7.1

Opacities in STARLINE

Source	Remarks
H	Gaunt factors of Karsas & Latter(1961)
H^-	
H_2^+	Gingerich(1964)
H_2^-	Somerville(1964)
He, He^-, He^+	Carbon et al(1968)
Fe, Mg, Si	Travis & Matsushima(1968)
Scattering:-	
H Rayleigh	Dalgarno(1962)
H_2 Rayleigh	Dalgarno & Williams(1962)
He Rayleigh	Dalgarno(1962)
Electron	

detailed than in the case of the furnace. The important mechanisms are summarised in Table 7.2. Natural damping is generally included at its classical value for lack of sufficient accurate f-values. For low lying levels this form of damping is usually negligible. Collision damping with hydrogen is usually predominant, and it is assumed here that the interacting forces obey van der Waal's law (i.e. $\propto r^{-6}$). Laboratory work has shown that this representation is not physically correct, and Cowley et al (1969) have suggested arbitrary enhancement (i.e fudge-) factors of between 1.8 and 7.4 for levels in Fe I, the exact value depending on excitation. Similar corections will apply for collision damping with helium, though the reduced abundance makes this form of damping less important. The Stark broadening constant also depends on accurate f-values and introduces a further uncertainty. Blackwell et al (1972) have shown that for the sun, uncertainties in abundance interpretations of more than 10% can only be avoided by using lines with equivalent widths less than a 'safe' value. For uncertainties from damping alone, the 'safe' value is 75mÅ for groundstate lines and only 35 mÅ for lines of high excitation.

For the case of microturbulence the uncertainties are greater and affect even weaker lines. A discrepancy between observed and calculated profiles has unfortunately led to the permanent incorporation of this fitting parameter in most abundance analyses. Yet Worrall and Wilson (1972) have shown that forcing agreement in this way could be necessary because of deficiencies in the line theory and that there is no experimental or theoretical justification for microturbulence. The velocity field has its effect through the Doppler part of the Voigt profile. The parameter v consists of components of the thermal velocity and the turbulent velocity. Including the velocity therefore broadens the line and changes the curve of growth. Velocities of between 0.5 km s^{-1} (Foy 1972) and

Table 7.2

Damping constants (Allen 1973)

Mechanism	Constants for transitions from level b to level a
Natural	$\gamma_n = C_n \gamma_c \qquad C_n = 3 \sum_i \frac{g_i}{g_b} f_{bi}$ $\gamma_c = 0.2223 / \lambda^2_{cm}$
Collisions with	
a) Hydrogen	$\gamma_6 = 17 C_6^{0.4} V^{0.6} N_H$ $C_6 = 1.61E\text{-}33 (13.5 Z)^2 \left[(\chi' - \chi_b)^{-2} - (\chi' - \chi_a)^{-2} \right]$
b) Helium	$\gamma_{6he} = 17 C_{6he}^{0.4} V^{0.6} N_{He}$ $C_{6he} = 0.50E\text{-}33 (\chi_{he} Z)^2 \left[(\chi' - \chi_b)^{-2} - (\chi' - \chi_a)^{-2} \right]$
Stark effect	$\gamma_4 = 38.8 C_4^{0.67} V^{0.33} N_e$ $C_4 = 1.21E\text{-}15 \left[\sum_i f_{ai} \lambda^2_{ai} - \sum_j f_{bj} \lambda^2_{bj} \right] \quad (\lambda \text{ in } \mu)$

notes: V is the relative velocity between atom and perturber. (cm/s)

N_H, N_{he} are number densities (cm^{-3})

χ' is the ionisation potential of the perturbed atom.

Z is the effective charge of the perturbed atom

χ_a, χ_b are excitation potentials (eV)

2,4 km s^{-1} (Müller et al 1968) have been suggested for the sun, with many different depth dependances. An approximate value can be found by trial and error until the derived abundance is independant of equivalent width (Garz et al 1969).

Continuing their analysis Blackwell et al found the 'safe' value of W_λ for uncertainties in micro-turbulence was only 35 mÅ for ground state lines.

The deficiency in the line theory that results in the need for a microturbulence parameter may be connected with the assumption of LTE. For giant stars where the pressures are much lower and collisional processes may not be sufficient to maintain equilibrium, turbulent velocities of as much as 6 or even 8 km s^{-1} are required (Tomley et al 1970). The calculation of line profiles in non LTE is a very complex problem requiring accurate atomic data and involving many iterative solutions. Simple approaches (Müller and Mutschlecner 1964) have pointed to little difference between LTE and non LTE in the photospheric abundances, but detailed calculations using non LTE programs such as that of Mihalas and Auer (1972) will not be very instructive until more complete atomic data is available.

To complete the line profile calculation:
Given ℓ_λ the line optical depth t_λ is found from

$$\frac{dt_\lambda}{d\tau_\lambda} = \frac{\kappa_\lambda + \ell_\lambda}{\kappa_\lambda} \qquad (7.9)$$

and the line profile is simply

$$\frac{I^l_\lambda(0,\mu)}{I^c_\lambda(0,\mu)} = \frac{\int_0^\infty B_\lambda(t_\lambda)\, e^{-t_\lambda/\mu}\, dt_\lambda/\mu}{\int_0^\infty B_\lambda(\tau_\lambda)\, e^{-\tau_\lambda/\mu}\, d\tau_\lambda/\mu} \qquad (7.10)$$

where superscripts l, c refer to line and continuum.
A slight modification arises for the case where the disk cannot be resolved. Intensities are then replaced by fluxes obtained by

integrating over the disk.

$$\pi F_\lambda^c(0) = 2\pi \int_{-1}^{1} I_\lambda^c(0,\mu)\,\mu\,d\mu = 2\pi \int_0^\infty B_\lambda(t)\,E_2(t)\,dt \qquad (7.11)$$

and the integrated profile is thus $\pi F_\lambda^1(0) / \pi F_\lambda^c(0)$.

7.4 Observations and Results

In order to obtain realistic abundances, lines with equivalent widths of less than 35mÅ should be used. This is a particularly stiff constraint as there are few such lines in the solar spectrum for which accurate f-values are available. In the past, investigations have of necessity used lines with equivalent widths of between 50 and 150 mÅ. With such strong lines uncertainties in line theory can quite easily lead to changes of 20% in the derived abundance. Weaker lines have been avoided because of uncertain continuum levels and blending troubles. It is only since the introduction of high resolution photoelectric scanning spectrometers that accurate measurements of weak line profiles have become possible.

A spectrometer of the low-noise type described in Chapter 5 has been used to scan various parts of the solar spectrum. This instrument was installed together with a coelostat on the Gornergrat (3090m) in Switzerland. Data collection was performed using a PDP-8 processing computer. It was shown by Blackwell et al (1967) that, using the technique already described in Chapter 5, noise levels of less than 0.01% can be readily achieved using this instrument. In order to investigate the possibility of using weak lines for a solar abundance analysis, scans containing useful Ti I lines were selected from a large series obtained in 1970-72 by B.S. Collins at the Gornergrat. As thby are recorded on paper tape they are particularly suitable for computer-assisted investigations of weak features.

A typical Gornergrat scan is shown in Fig. 7.2. Each scan consists of 750 points covering about 7-10 Å. A continuum can be inserted either by judgement or by referring to the higher resolution spectra of Delbouille et al (1973). The feature of interest can then be isolated on a visual display and magnified as required. Using a program kindly supplied by A.D. Petford it is then possible to examine blending effects quantitatively. Fig. 7.3 shows the same Ti I feature with a wing inserted by on-line manipulation of the displayed profile. Insofar as it is possible to magnify the profile more readily and examine synthetic profiles quantitatively, this method is superior to planimetering tracings (even from Delbouille's atlas), which is a slow tedious process and particularly susceptible to human error.

In choosing a line list from these measured in the furnace, all lines with equivalent widths greater than 50 mÅ were first discarded because of the damping and microturbulence uncertainties that would be involved. The remaining 19 lines were examined using the above programme and were ruthlessly whittled down to 12 by stipulating that the measured equivalent width should be reproducible to 2% for suitable alternative synthetic profiles. This constraint is necessary because the present version of STARLINE is not capable of dealing directly with blends although it is proposed to incorporate this into the program in the near future. It has already been shown (Warren 1970) that useful information can be extracted from blends provided the wavelengths of the components are known to an accuracy better than their Doppler halfwidths.

For convenience the lines were classified according to strength:

I	$W_\lambda < 7.5$	mÅ	(2 lines)
II	$7.5 \leqslant W_\lambda \leqslant 35$	mÅ	(8 lines)
III	$35 < W_\lambda \leqslant 50$	mÅ	(2 lines)

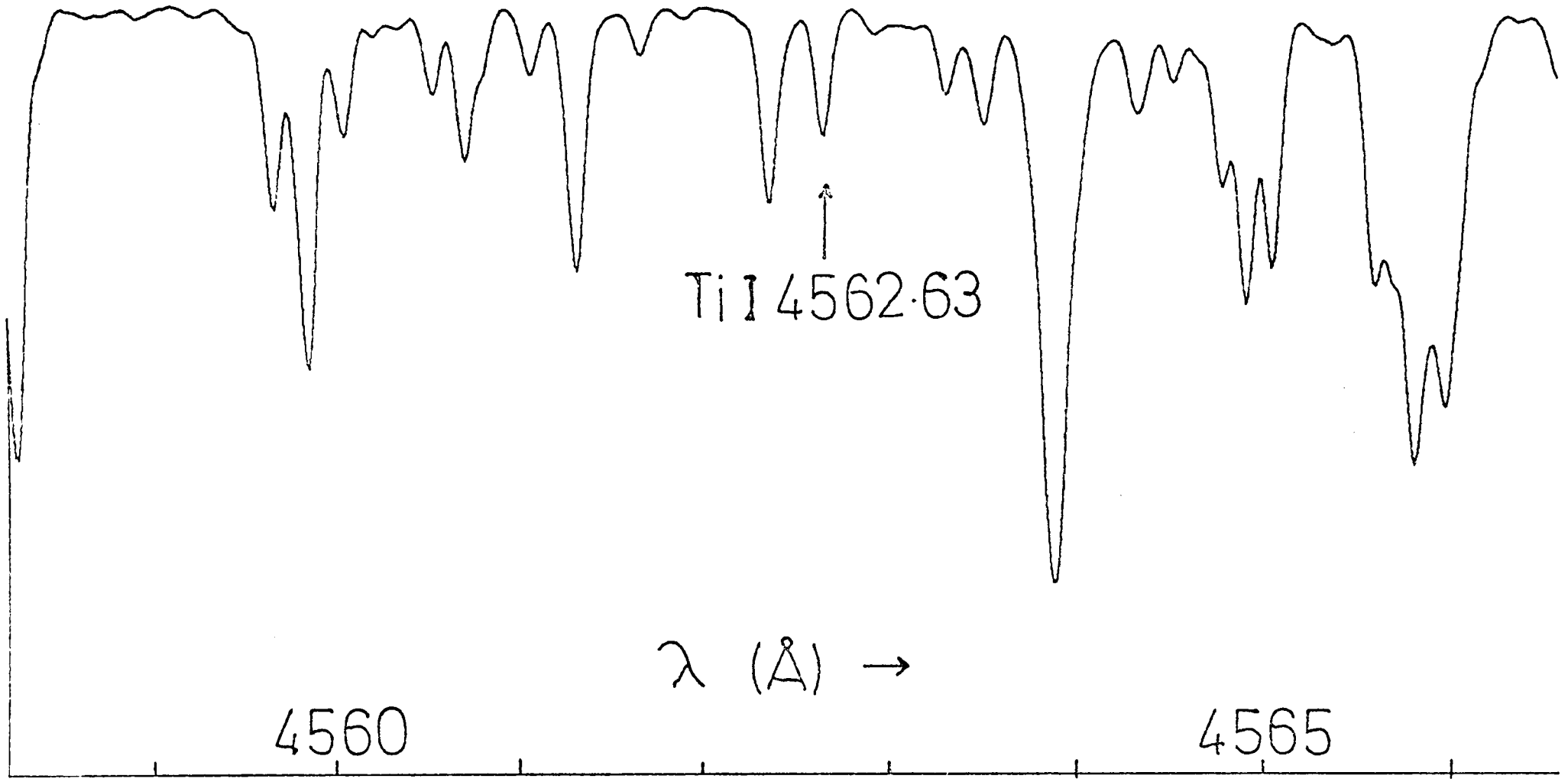

Figure 7.2

A typical low-noise solar scan

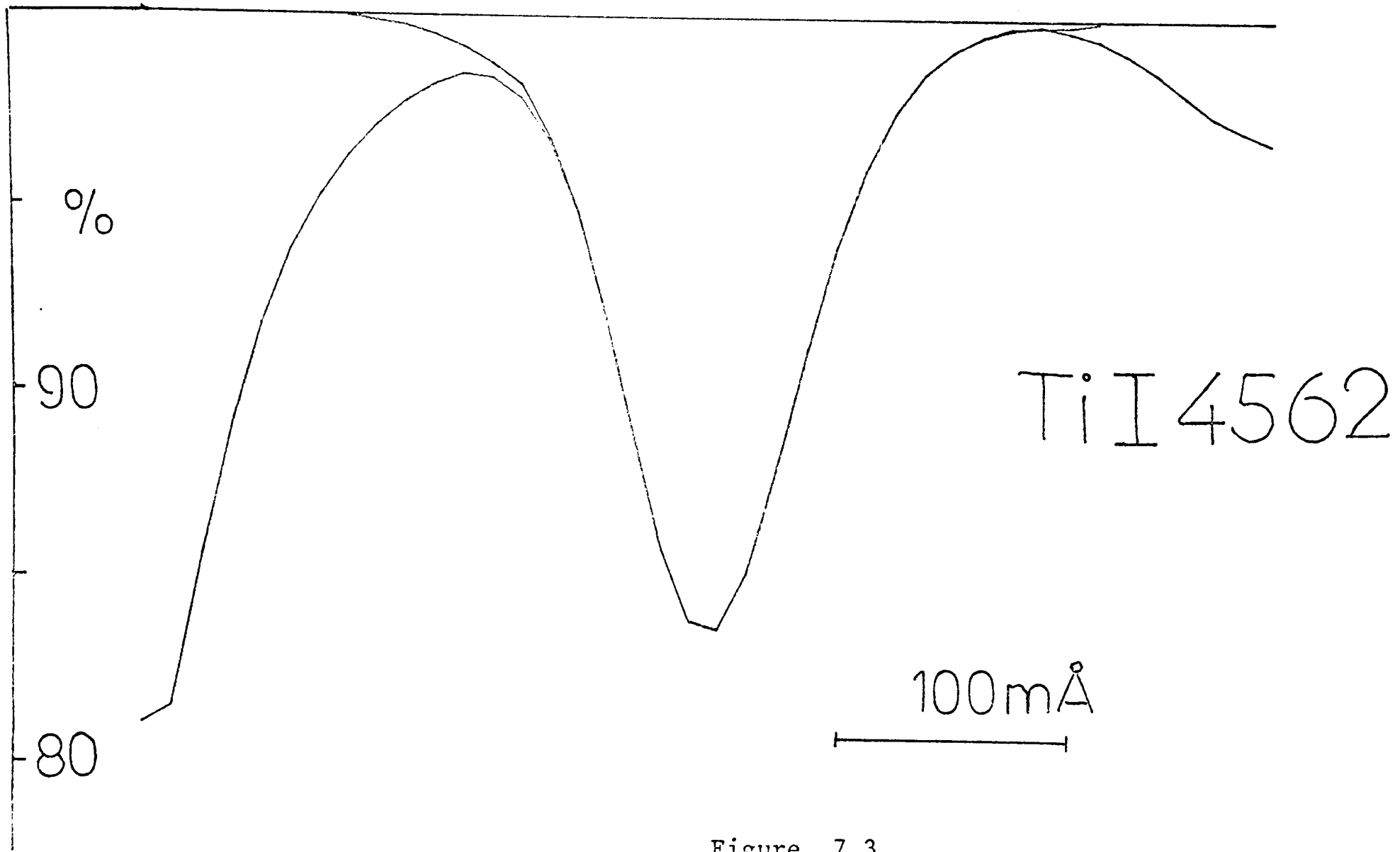

Figure 7.3

A demonstration of the line fitting program mentioned in the text.

Class III lines represent those for which abundance uncertainties of at least 10% can be expected. Class I lines have been included purely to test the versatility of this method. Normally such weak lines would be excluded as uncertainties in the continuum level alone could change their equivalent widths by at least 10%. Class II lines form the basic material for this analysis and it is later shown that uncertainties in line theory produce a negligible effect on abundance interpretations from these lines.

With STARLINE a full curve of growth analysis was performed for each line and the abundance found by interpolating with the observed equivalent width. For the Class III lines microturbulent velocities of 1.5 and 2.0 km s^{-1} were used with collision damping enhancement factors of 1.0 and 1.3 in γ_6 and γ_{6he}. Natural damping was inserted at its classical value and Stark broadening was ignored. Deridder and Rensbergen (1974) have shown the latter two assumptions are reasonable for photospheric analyses. For the other lines nominal values of 1.5 km s^{-1} for the microturbulence and 1.3 for the enhancement were adopted. The author does not attach any physical significance to these values, which were included purely to demonstrate the uncertainties involved.

Fig. 7.4 clearly shows that Class II lines are virtually independent of damping. The curve of growth for Ti I λ6126 Å (1 eV) for enhancements of 1 and 6.3 in γ_6 and γ_{6he} (corresponding to x1 and x100 in c_6) is different by only 1.6% at the observed equivalent width. This corresponds to only 0.010dex(2.3%) in the abundance.

A similar investigation for microturbulence is given in Fig. 7.5 which shows the same curve of growth for v_t = 1.5 and 2.0 km s^{-1}. This time the abundance uncertainty is 0.012dex(2.5%). Thus allowing for a 2% error in the observed equivalent width, Class II abundances should test the relative oscillator strengths

Figure 7.4

Effects of damping on the solar curve of growth

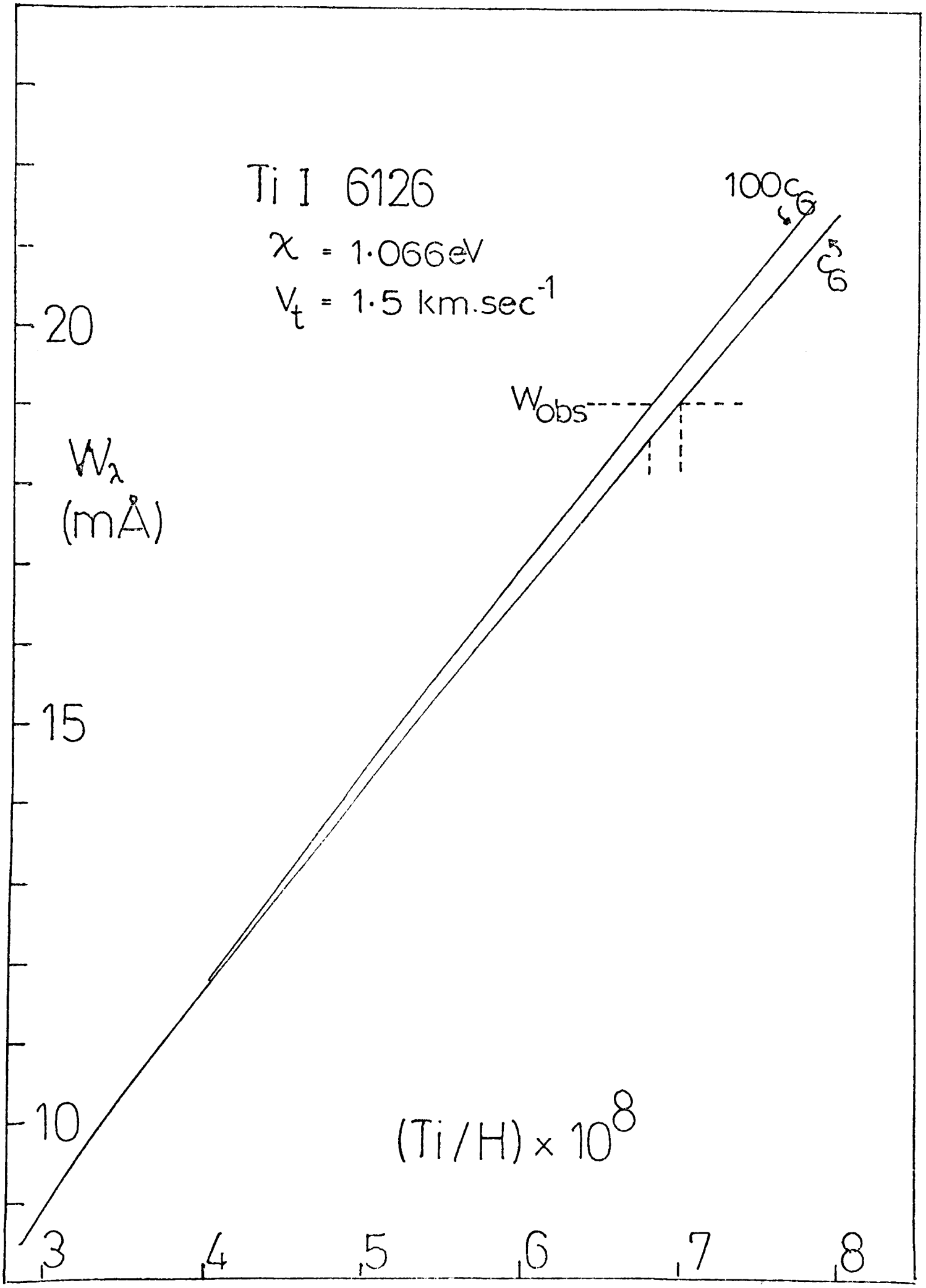

Figure 7.5

Effects of microturbulence on the solar curve of growth

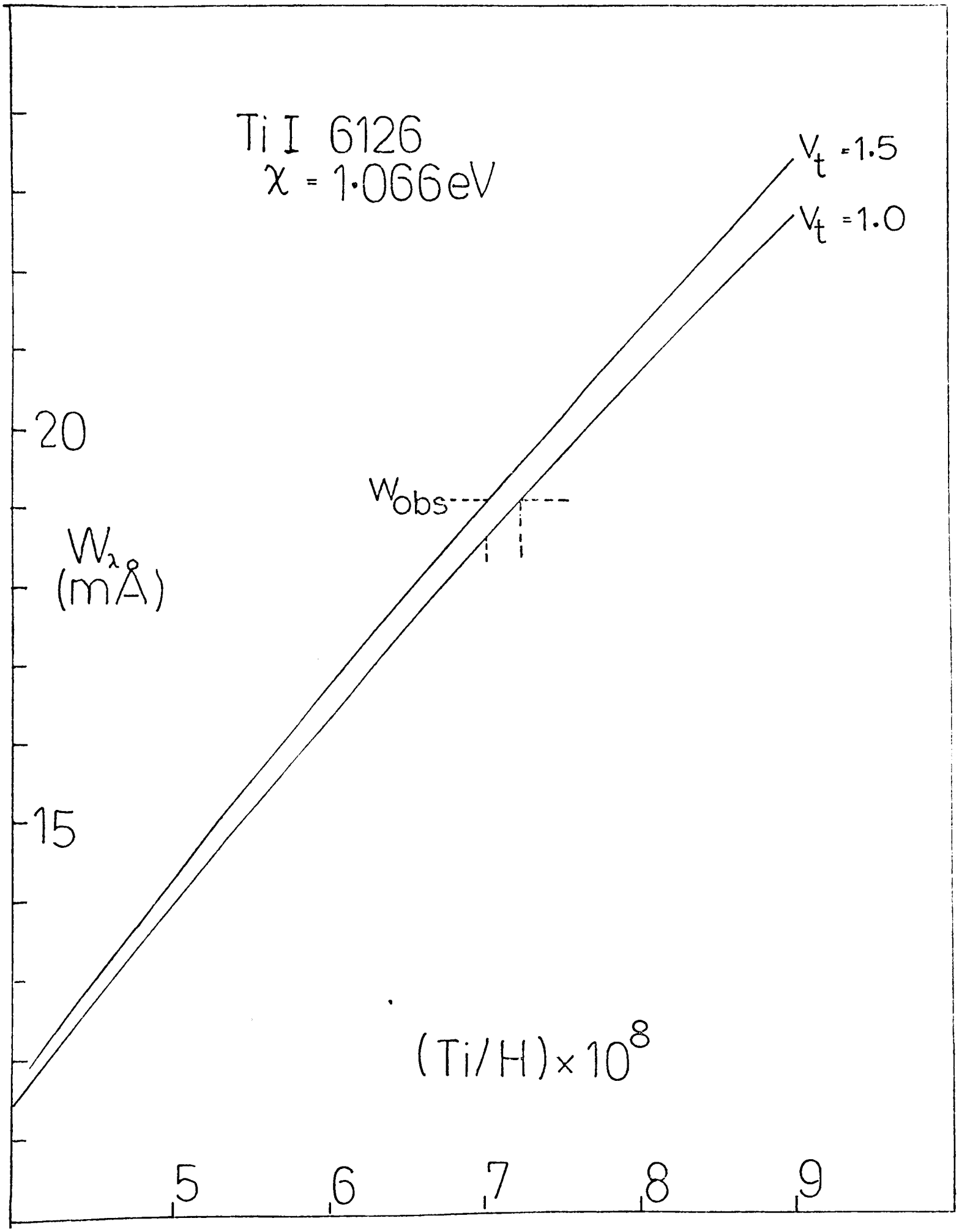

to at least 0.02dex(4.5%).

The result of the analysis is given in Table 7.3. The Utrecht equivalent width (Moore et al 1966) differs significantly from that measured here for both strong and weak lines thus possibly demonstrating that blending extraction from poor resolution spectra is not necessarily easier with strong lines. The Gornergrat values have been corrected for scattered light in accordance with extensive comparisons made with the results of the Kitt Peak double-pass spectrometer (Pierce 1969).

It is of interest to determine whether the resulting abundances are sensitive to the solar model. Fig. 7.6 shows the curve of growth for HSRA and the model of Elste (1968). An investigation of the contribution functions (essentially the variation of ζ_λ with depth) revealed that all lines form in the region $0.1 < \tau_{5000} < 1$ where the temperature difference between these models is 110 degrees. The difference in the calculated equivalent widths is disturbingly large ($\sim$7% at 20 mÅ) and would lead to an abundance 0.04(10%) less for this particular line.

7.5 Discussion

It is gratifying to note that the abundance variations over the 12 lines are not very large, indicating that none of the f-values used are seriously in error. The abundances for the class II lines vary by only $\pm$ 0.03 dex thus justifying the error analysis of the last chapter. Although only $\frac{1}{3}$ of the total lines studied in the furnace were included in this abundance analysis, they cover a wide range of excitation and the author sees no reason why the entire relative scale should not be accurate to the same amount.

The results for the weakest lines are 0.07dex higher than those of class II suggesting a rough overestimation of 20% in their equivalent widths. It is nevertheless a compliment to the

Table 7.3

Results of the solar Ti analysis

Class	λ	χ	Utrecht	Grat	log N(Ti)
I	5366.65	0.818	2.5	2.2	4.87
	5389.18	0.813	5	4.6	4.88
II	4715.30	0.048	11	8.8	4.83
	4926.16	0.818	5.5	5.1	4.83
	5009.65	0.021	24	26.8	4.79
	5045.45	0.848	10	8.0	4.85
	5295.78	1.066	10	11.2	4.80
	5460.51	0.048	8.5	8.2	4.80
	6064.63	1.046	7	7.8	4.83
	6126.22	1.066	20	19.1	4.84
III	5152.20	0.021	38	40.5	4.76 - 4.80
	5866.46	1.066	40	46.5	4.80

Mean values:

Class I: 4.88

Class II: 4.82 $\pm$ 0.02 (std.dev)

Class III: 4.80

Notes: Col 1: Strength classification (see text)

2: Wavelength in Ångstroms

3: Excitation potential of lower level in eV

4: Equivalent width in mÅ from Moore *et al* (1966)

5: Gornergrat equivalent width after 3% scattered light correction.

6: Abundance relative to log N(H) = 12.00

Figure 7.6

Curves of growth for 2 solar models

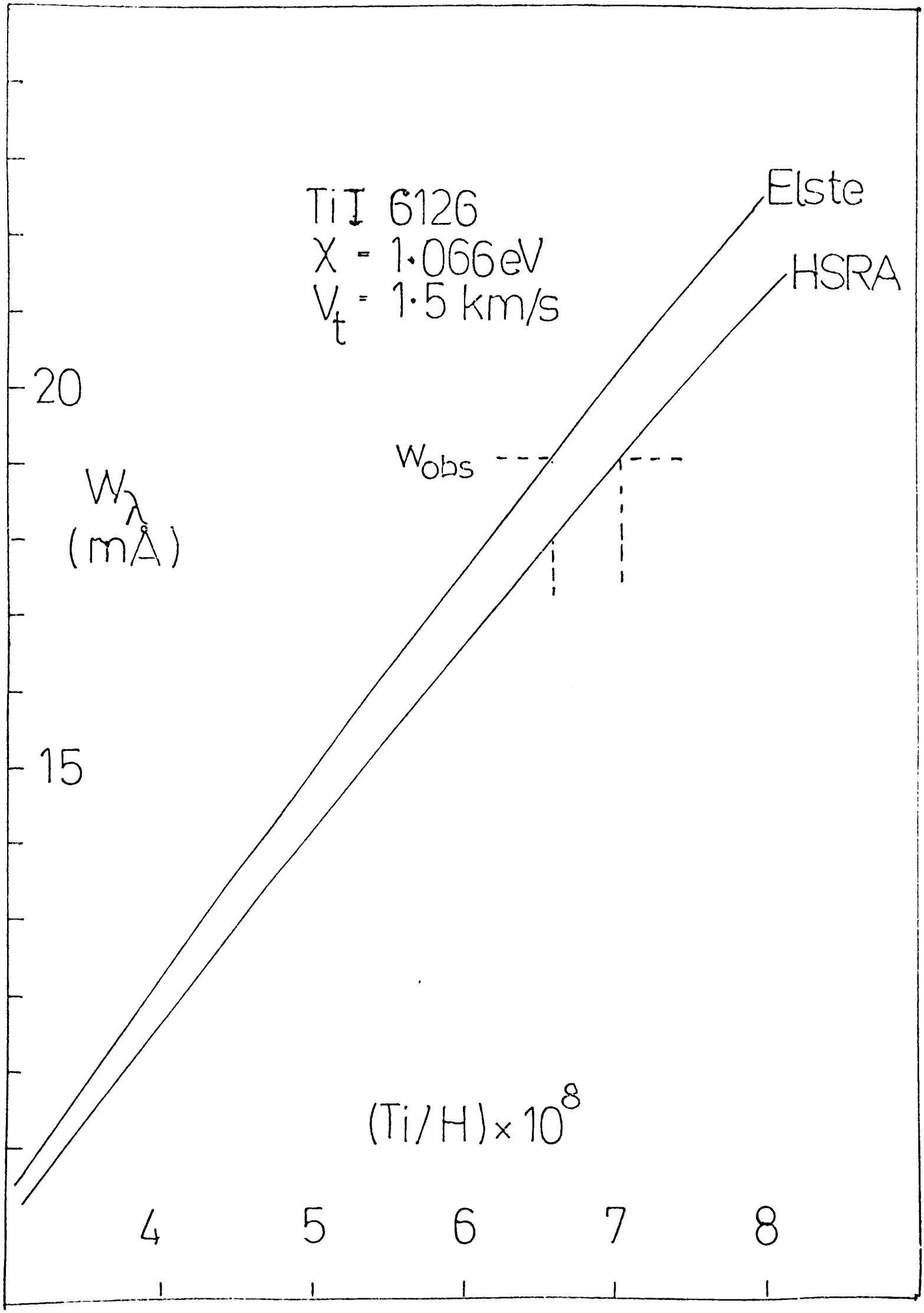

low-noise spectrometer that a realistic abundance can be obtained from a line of only 2mÅ; Minnaert would indeed be surprised! With only two results it is hardly possible to comment further on the accuracy of working with such weak lines.

The error bar on the class III results, arising principly from uncertainties in microturbulence, shows that investigations using these lines will be inaccurate. The final abundance has therefore been based solely on class II lines.

The error bar in the absolute scale is $\pm$ 0.03dex, and as this is much larger than the variation in the results it is claimed that:-

$$\log\ n(\mathrm{Ti}) = -4.81 \pm 0.08$$

on the log n(H) = 12.00 scale

The previous determinations of the solar titanium abundance are summarised in Table 7.4. It is seen that the author's value is slightly higher than that obtained by Goldberg et al (GMA 1962) and Müller and Mutschlecner (MM, 1964) though is in rough agreement with the recent work of Wolnik (1973) and Grevesse (1970), Wolnik's value is merely a slight shift of Grevesse's abundance to an absolute scale consistent with his shock tube measurements. As this scale is in itself only accurate to $\pm$ 0.08dex (see Table 6.7) the author disputes his reduced abundance error of $\pm$ 0.05dex.

Wolnik's absolute scale is 0.23dex lower than the author's (cf. table 6.7), implying that a repeat of the author's abundance analysis with his f-values would give an abundance of about 4.58, in rough agreement with the early work of GMA and MM. It must be appreciated however, that these early investigations used crude semi-empirical models based on incomplete solar observations, and an approximate theory of weighting functions valid only for weak lines (see Aller 1963 p. 363). The standard of the photometry was

Table 7.4

The Solar Ti abundance

Reference	log N(Ti)	Remarks
Aller(1953)	4.78	Compiled from classical curves of growth by Minnaert, Unsold and Menzel
Pecker(1959)	5.68	Non LTE, f_{rel} from King, f_{abs} from sumrule.
Goldberg et al(1960)	4.68	LTE, selected f_{rel}, f_{abs} from sumrule.
Muller & Mutschlecner (1964)	4.58 (4.78)	Non LTE investigation across solar disk, f_{abs} from C&B, ()= f_{abs} from sumrule
Warner(1968)	4.50	Ti II, f_{rel} from arc measurements made absolute from sumrule.
Unsold(1968)	4.68	Average of Goldberg & Muller with f_{abs} correction.
Grevesse(1970)	4.73 (4.33)	Ti I using Tatum f_{abs} (Ti II using Warner f_{abs})
Wolnik & Berthel(1973)	4.78 ± 0.05	Re-analysis of Grevesse using f_{abs} of Wolnik & Berthel
Ellis(1974)	4.81 ± 0.08	

Notes: Abundances are on the H=12.00 scale
f_{rel} refers to relative oscillator strengths
f_{abs} refers to absolute oscillator strengths
C&B means Corliss & Bozman(1962)

of course also much worse. As it has been demonstrated that the Ti abundance is particularly sensitive to temperature variations, it is unlikely that these early results are accurate to more than a factor 2 (0.30dex).

Grevesse used the f-values of Tatum (1961b) who has himself stated that his scale is only 'approximately absolute'. Wolnik finds his absolute scale agrees with Tatum's however. On the author's scale Grevesse's value would be about 4.90 which is rather high.

Apart from Pecker's (1959) surprising result, crude non LTE investigations have given values roughly consistent with LTE. This was originally confirmed to some extent by Warner's observation that n(Ti I) $\sim$ n(Ti II). However Wolnik has shown Warner's Ti II f-values are 0.50dex too low. This has the effect of bringing Grevesse Ti II abundance up to 4.33 in excellent agreement with the author's value for Ti I.

As the author's investigation is the only one restricted to weak lines, utilising reliable f-values and the latest solar model, he suggests his value is, at present, the most accurate available.

CHAPTER 8

ABSOLUTE ABUNDANCES FOR ARCTURUS

8.1 Introduction

These Arcturus abundances have been determined using the same line theory and methods detailed in the last chapter. The theory may be considerably unsound however, for strong lines, which are formed in low density regions where LTE may not be valid. Another difference here is that the lower temperature reduces the thermal broadening, and consequently the effect of microturbulence on the curve of growth is increased. Although Griffin's Arcturus Atlas is outstanding in comparison to other stellar spectra, it cannot match the low-noise solar spectra and consequently accurate measurements of weak lines (which would avoid microturbulence uncertainties) will be difficult. It is therefore necessary to use stronger lines whose equivalent widths can be accurately measured and to assume, or to determine separately, a value for the microturbulence. This velocity can also be used in determining the surface gravity (see Chapter 4) to produce a refined model for Arcturus.

The results presented here use f-values determined with the Oxford furnace. The original titanium list was closely tailored to the Arcturus analysis and several good quality lines are included. The iron list has been constructed for other purposes however, and thus only a few lines are presently applicable in this study. These latter f-values (Blackwell et al 1974a) have been placed on an absolute scale by referring to an atomic beam absorption result of Bell and Tubbs (1970). Using a more refined model and a considerably extended line list, a more complete analysis will soon be possible. In particular LTE in Arcturus can be scrutinised by determining Ti II and Fe II f-values from a solar analysis, where LTE is perhaps a

more reasonable assumption.

Despite the preliminary nature of this investigation it is the first time Arcturus has been studied with absolute f-values and without reference to another star, and the accuracy of the abundances is shown to at least equal that of other published values. Because Ti and Fe are synthesised in the later stages of stellar evolution, their abundances are useful indicators of the metallicity of the interstellar medium where the star formed. Arcturus is thought to be representative of a large number of high velocity stars in the solar neighbourhood and these results will be of use in theories of galactic evolution as well as for those of nucleosynthesis.

8.2 Observations

Equivalent widths have been measured, with a planimeter, for all reasonably unblended lines in the Griffin atlas that have Oxford f-values. Equivalent widths are particularly amenable for abundance interpretations as they are independent of large-scale macroturbulent velocity fields. In a spectrum synthesis program such as that developed by Bell, and used for an Arcturus analysis by Upson II (1973), uncertainties in velocity fields will seriously affect profile interpretations. Equivalent widths are often independent of instrumental effects. Griffin (1969b) however has demonstrated that excessive noise in the extended wings of an instrumental profile could alter weak equivalent widths by as much as 10%. Fortunately it has been satisfactorily demonstrated (Warren 1970, and see Blackwell et al 1971) that such effects are neglibible in the Arcturus atlas.

The accuracy of these equivalent widths is determined by the noise level and continuum position rather than the accuracy with which one can planimeter. For lines of 50-200 m Å with an adopted noise level of 2% an accuracy of about 3% is claimed.

8.3 The microturbulent velocity

There is no observational evidence for interpreting the micro-

turbulence parameter as a true velocity field and it was suggested in Chapter 7 that the increased value incorporated in line analyses of giants could be a non LTE effect. The consequence of the parameter is an increased linear portion of the curve of growth which, for cool stars, is quite short because of the reduced thermal velocity. At 4400°K the most probable thermal velocity for a titanium atom is only 1.1 km sec^{-1} and the effect of various microturbulent velocities is shown in Fig. 8.1. As a rough example, to ascertain the abundance of titanium from this line, one would require it to be weaker than 30 mÅ, or alternatively at 50 mÅ one needs the microturbulence, v_t, to an accuracy of $\pm$ 0.15 km sec^{-1}. As a weak line analysis of Arcturus is not yet possible, it is essential that the existence and effects of v_t be explored. Fortunately the effects of damping are considerably reduced at these low densities.

The microturbulence has previously been estimated from the extent of the linear part of the curve of growth, and also from the line profiles (where it is likely to be confused with other velocities). The former method is commonly used differentially with respect to the sun whose microturbulence is quite uncertain (from 0.5 km sec^{-1} to 2.4 km sec^{-1}) and the spread of values for K giants obtained in this way is even more. Glebocki (1972) found v_t = 1.1 km sec^{-1} (less than most solar values) though his curves of growth are of poor quality. Helfer and Wallerstein (1968) found a value of 2.5 km sec^{-1} satisfied the curves of growth of 20 K giants and this value was selected by Williams (1971ab) for his narrow-band survey of many K giants

For Arcturus, Griffin and Griffin (1967) determined a value of 2.1 from the Fe and Ti curves of growth, though they had to use gf-values from Corliss and Bozman. Warren (1970) assumed a value of 2.0 for a differential analysis with ξ Peg; Upson II (1973) and Simon (1971) use this value for investigating line profiles.

Here v_t is determined by a method involving the curve of

Figure 8.1

Effects of microturbulence on the Arcturus curve of growth

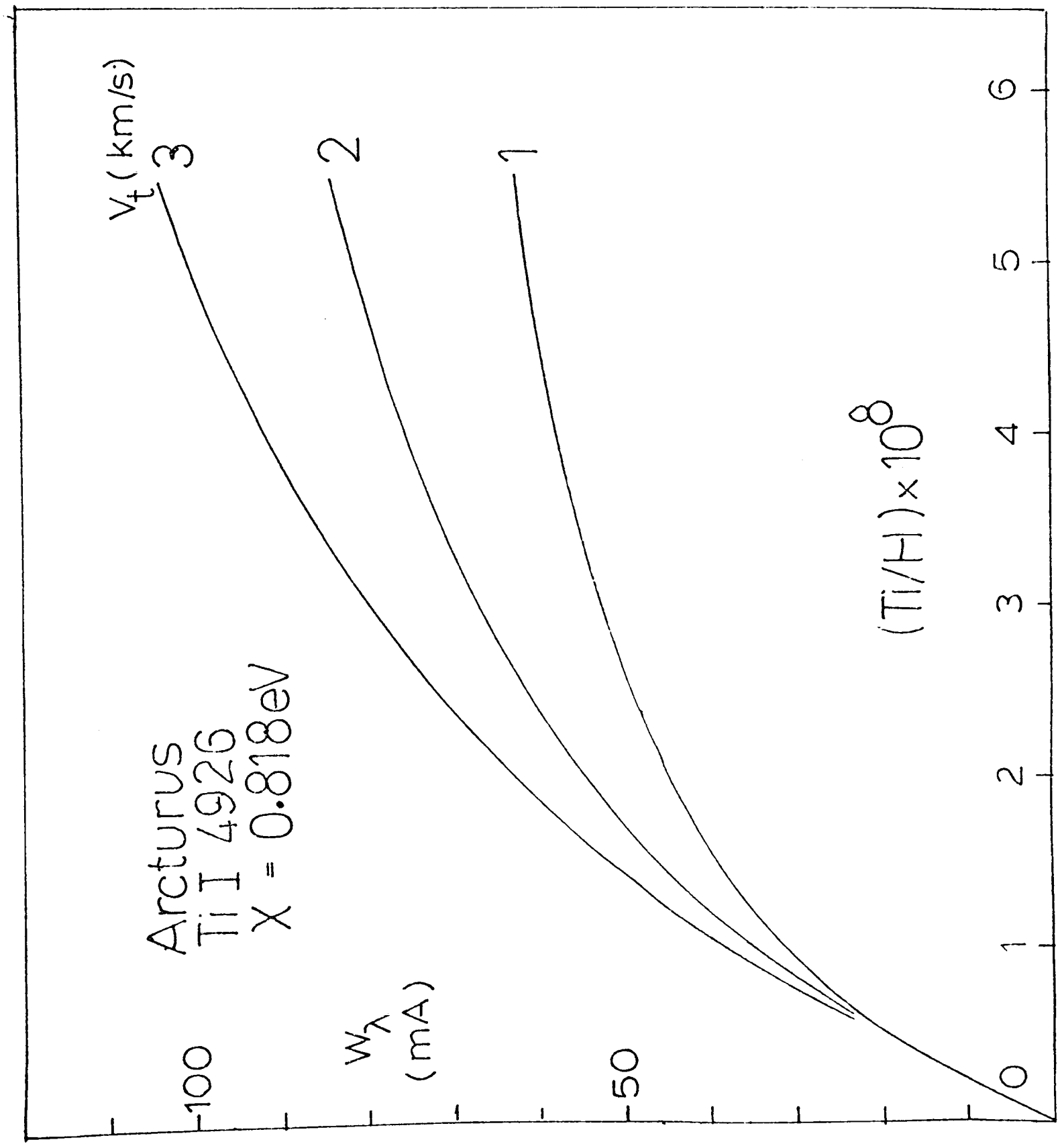

growth. It is assumed at the outset that there is no depth dependance or variation in v_t amongst different elements. The results are sensitive to the depth-dependences but it is felt there is precious little evidence for one botching parameter without extending the degree of freedom still further. v_t is therefore regarded as a fudge-factor.

Firstly curves of growth for several strong ($W_\lambda \sim 200$mÅ) Fe I lines with Oxford f-values were constructed using STARLINE. These saturated lines lie on the flat part of the curve of growth where abundance effects are minimised. Assuming a spread of 0.50dex in the abundance and a realistic variation in damping constants, a preliminary range of $1.6 \leqslant v_t \leqslant 2.5$ km/sec was established. With a grid of turbulence values from 1 to 3 km/sec, curves of growth were then constructed for all lines in the Arcturus line list, and abundances were derived for each v_t. Garz et al (1969) determined the solar v_t by stipulating that the abundance should be independent of equivalent width. A simplified version of this is to plot derived abundance against v_t and hope that a single abundance and microturbulence will emerge. Such a N-v_t diagram is shown in Fig. 8.2. The gradient dN/dv_t depends on the position of the line on its curve of growth; for saturated lines the gradient will be largest, whereas the gradient will be less for weak lines. The value deduced from this diagram is based on 5 intersecting lines out of a possible 9. Ideally the method requires the use of stronger lines situated on the 'arch' of the curve of growth where dN/dv_t is changing, but in this study such lines are either seriously blended or do not have good f-values. From this a value of $1.9 \leqslant v_t \leqslant 2.3$ is deduced. A preliminary abundance of log n(Ti) = 4.39 ± 0.05 can be deduced from these 5 lines.

The adopted value, taken as $v_t = 2.1 \pm 0.2$ km sec^{-1} is consistent with other values for Arcturus and similar stars. It is quite evident that a value below 1.8 km sec^{-1}, such as that reported by Glebocki, would lead to absurd abundance variations from line to line.

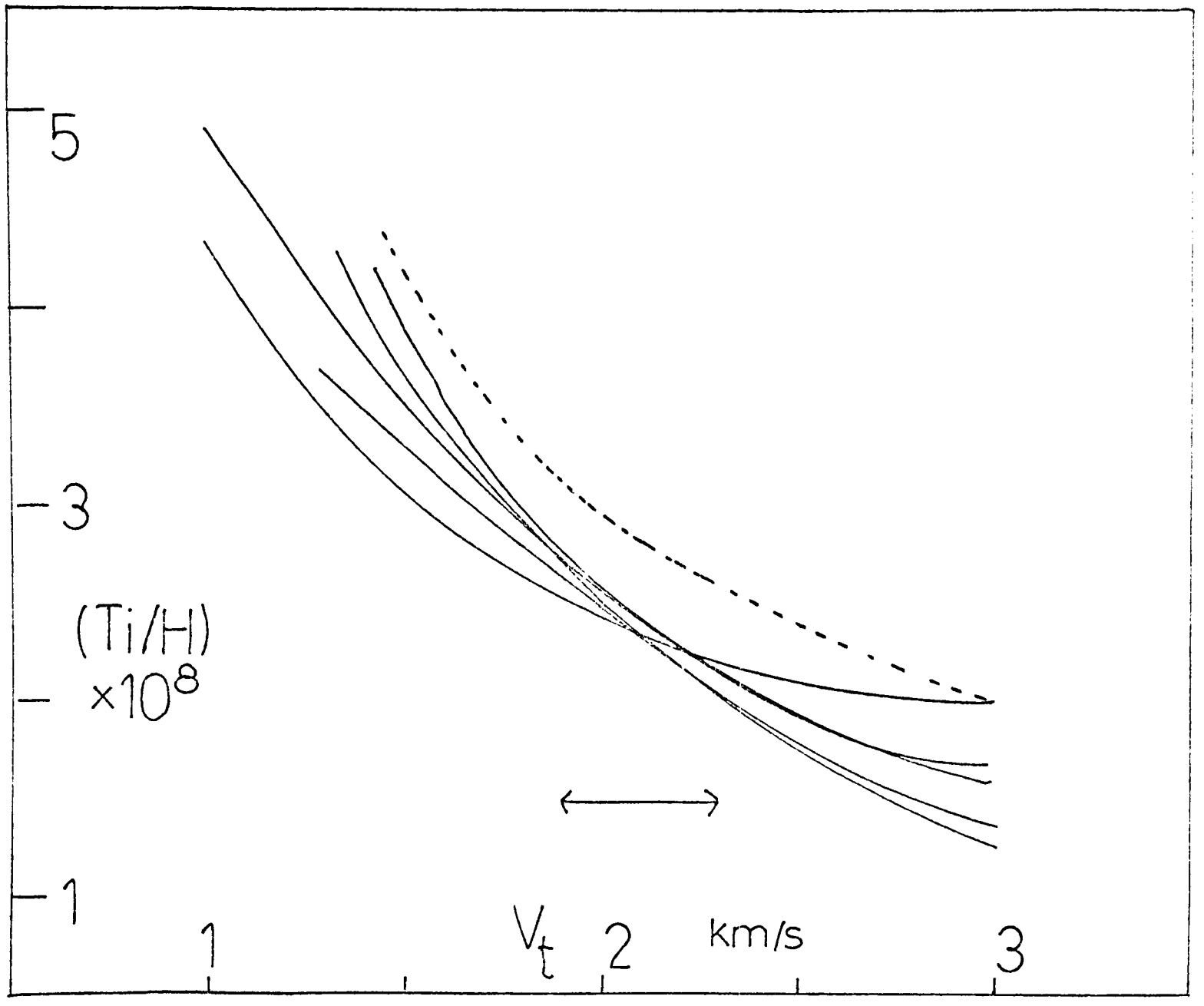

Figure 8.2

Determination of the microturbulence - a N-v_t diagram

8.4 Abundance results and errors

The final abundance results with the adopted v_t are given in Table 8.1. There does not seem to be any significant correlation between abundance and equivalent width which, within the scatter, implies the microturbulence is about right. It is now possible to test the Ti I f-values by comparing solar and Arcturus abundances. The scatter in the ratio Arcturus/Sun (see Table 8.1) demonstrates the variation of the abundances in both analyses cannot be purely due to errors in the relative f-values. The Ti I abundances agree to within $\pm$ 0.06dex (15%) apart from the line at λ6064.63 Å which requires a reduction of about 15 mÅ in equivalent width. This spread is twice that observed in the solar analysis and is attributed to poorer data and possible uncertainties in the model. The mean value for titanium is 4.42 $\pm$ 0.04, which (for those who insist on referring to the sun), using the author's solar abundance (Chapter 7) implies $[Ti/H]$ =-0.39. The iron analysis has a similar spread and the mean value of 7.27 $\pm$ 0.05 becomes $[Fe/H]$ = -0.33 after using the solar iron abundance of Garz et al. The implication of these values and the comparisons with other published results are postponed until the next section.

These results contain errors from nearly every chapter in this thesis, and a detailed analysis would require a full investigation for each line. To arrive at a crude figure, the possible errors are considered individually.

i) T_e : The above analysis was performed with the model at 4400° K (Table 4.12). Curves of growth constructed with the hotter model at 4500° K(Table 4.3) gave abundances consistently higher by about 0.08dex. Since T_e = 4450 $\pm$ 50° K these results are strictly 0.04dex too low.

ii) log g: As there is no indication of the error on the adopted value of log g = 1.7, it is difficult to estimate the uncertainty in these abundances. To demonstrate the effect: changing

Table 8.1

Abundances in Arcturus

	λ	χ	W_λ	log N	[N]
TiI	4617.27	1.749	130	4.45	
	4675.12	1.066	92	4.40	
	4715.30	0.048	126	4.51	-0.32
	5238.58	0.848	104	4.46	
	5295.79	1.066	87	4.42	-0.38
	5426.51	0.048	54	4.38	
	5460.51	0.048	119	4.43	-0.37
	6064.63	1.046	128	4.60*	-0.23
	6126.22	1.066	130	4.41	-0.43
FeI	4389.24	0.052	185	7.30	
	4427.30	0.052	218	7.23	
	5110.41	0.000	195	7.32	
	5127.78	0.052	64	7.23	

Mean values: n(Ti) = 4.43 $\pm$ 0.04

n(Fe) = 7.27 $\pm$ 0.05

relative to H=12.00

*ignored

from log g = 1.7 to 2.0 the electron pressure at $\tau = 0.1$ increases by 30% (see Fig. 4.13), thus the neutral abundance would increase and the derived total abundance would have to be lowered by 0.12dex.

iii) v_t : The error here will affect lines on the flat part of the curve of growth quite seriously. For weak lines the error of $\pm$ 0.2 km sec^{-1} gives about $\pm$ 0.05 dex in derived abundance.

iv) Equivalent width : On the linear portion this error transfers directly i.e. 3% or about $\pm$ 0.013dex.

v) f-values : Again it is assumed that for Ti the error in the relative scale (0.03dex) is negligible in comparison with that of the absolute scale (0.08dex). The Fe f-values are known on an absolute scale to less than 0.01 however, and the relative error of 0.03 will dominate.

Taking into account all these errors gives a rough uncertainty of $\pm$ 0.15dex (40%), for Ti and $\pm$ 0.10dex (26%) for Fe, which is possibly discouraging considering differential abundance analyses are canonically quoted to a factor two (e.g. Pagel 1972). Although the author does not dispute differential error analyses he would stress, firstly, the relatively large error introduced by the models. Many workers do not seem to appreciate that their models may be based on very inaccurate estimates of T_e and log g (see Chapter 4). Secondly, although the error in the author's result is dominated by that in the absolute f-values needed for this absolute analysis, even larger errors could be introduced in analyses between stars of different types where residual curve of growth effects would enter.

To summarise therefore, in Arcturus:-

$\log n(Ti) = 4.42 \pm 0.15$

$\log n(Fe) = 7.27 \pm 0.10$

on the H = 12.00 scale,

Using solar abundances referred to above, these imply

$$\left[\text{Ti/H}\right] = -0.39 \pm 0.07$$

$$\left[\text{Fe/H}\right] = -0.33 \pm 0.10$$

8.5 Discussion

These results agree broadly with other metal abundances for Arcturus collated in Table 8.2. The older analyses seem closer than the more recent investigations, which point to a larger deficiency, especially for iron. Griffin and Griffin (1967) determined T_e = 4163° from Willstrop's scans and it has already been noted that this value will be too low and uncertain by at least $\pm$ 250 deg. A re-adjustment of their results gives $\left[\text{M/H}\right] = -0.4 \pm 0.2$. Holweger's (1971) results, confirmed by van Paradijs (1974), agree well with the author's for titanium though his iron abundance is rather lower. These analyses are based on models constructed for T_e = 4250°, which would seem to be a favourite value for Arcturus (see Linsky and Ayres 1973), yet strong evidence has been presented in favour of a higher temperature. The increased abundances here are mainly attributed to this revision in T_e for Arcturus. The only remaining puzzle is why Williams (1971a), whose T_e is nearly the same as that adopted here, obtains the largest iron deficiency of all. Comparing these narrow-band results with other detailed analyses, the author notes a consistent lowering of between 0 and 0.3dex for his iron abundance. Williams claims his result is accurate to 'a factor two' ($\pm$ 0.15dex) yet that error is not sufficient to match the author's result.

Simple empirical curves of growth will always lead to poor abundance estimates as they require mean values for temperature and pressure. Differential curves of growth constructed from model atmospheres avoid these stratification problems although the curve is not unique for lines of differing excitation. Cayrel and Cayrel (1963) demonstrated that the actual $T(\tau)$ employed in such a differential analysis matters little provided it is the same in both

Table 8.2

Metal abundances in Arcturus

Reference	[Fe / H]	[Ti / H]
Griffin & Griffin(1967)	-0.48	-0.52
Holweger(1971)	-0.65	-0.40
Williams(1971)	-0.77	
Ellis(1974)	-0.33	-0.39

Notes:

Holweger's results are confirmed to within ± 0.05 dex by van Paradijs(1974).

Williams' analysis is with narrow-band photometry.

stars. This useful fact makes it more reliable to compare K giants with Arcturus rather than with the sun, where $T(\tau)$ will not be homologous because of convective and backwarming effects.

Of course, differential analyses avoid f-values, and an alternative approach to that used here would be to compare Arcturus and the sun separately using relative f-values. In this case the abundance uncertainty would not be less however because although absolute f-values are avoided, uncertainties in the solar analysis are automatically transferred. The few lines in Table 8.1 for which this has effectively been done indicate that the error on the final [Ti/H] is much less than the quoted $\pm$ 0.07dex.

The higher T_e is further justified by Simon's (1971) failure to fit the H line profiles using various models at 4250°; he wanted to raise the temperature but felt this would be unreasonable. Also, Upson II (1973) reports that his N abundance, [N/H] = -0.50, is too low for normal CNO production in a star of this luminosity and temperature (see Iben 1967). He assumed T_e = 4100° which gives a luminosity of 170 $L_\odot$, whereas at the new T_e the luminosity becomes 240 $L_\odot$ which may be sufficient to allow destruction of N^{14} by the reactions:-

$$N^{14} + \alpha \rightarrow F^{18} + \gamma$$

$$F^{18} \rightarrow O^{18} + e^{+} + \nu$$

This would result in a high O abundance, which is in fact observed ([O/H] = -0.25, Upson II, 1973). Related to the CNO bicycle is the anomalously low C^{12}/C^{13} ratio of 7 reported for Arcturus by several observers (Geballe et al 1972, Greene 1970, Upson II 1973) which is also inconsistent with normal nuclear processing (Truran 1972). It is suggested that experimenting with hotter models might help to resolve some of these uncertainties. The new Te and L place Arcturus on the Population I giant branch in the Te-L diagram (Faulkner and Cannon 1973) corresponding to a mass of about 1.5M implying g = 50 is not far wrong.

Arcturus is a high velocity star (Roman 1955, Wodley et al 1970) and the metal deficiency agrees with the theory of Galactic evolution proposed by Eggen et al (1962). More recent observations (Helfer 1969, Williams 1971a) show that high velocity stars simply show a broader iron abundance distribution corresponding to poor interstellar mixing and different regions of formation. Eggen (1971) has suggested that Arcturus is typical of a large number of kinematically associated stars called the 'Arcturus group'. Several other members of this group are K giants, though all are too faint for fine analyses. Thus although Arcturus is now essentially to be regarded as a standard source for other K giant analyses, the abundances of this remarkable star will always be of interest for their own sake.

CHAPTER 9

NUCLEOSYNTHESIS AND THE IRON-PEAK

"Metals and alloys Her chore
raising telescopes.....
towards Her All Encompassed Eye"

from "God? She's Black" by
Gregory Corso (1962)

9.1 Introduction

This thesis would not be complete without a brief discussion of theories accounting for the origin of those elements that have been studied here. Observed abundances are an essential test for these theories, and future work can only be properly coordinated if both results are regularly brought together.

Nucleosynthesis theories have changed remarkably over the last ten years and the colourful history has been summarised by Arnett (1973). Nevertheless there is a need for a less technical review of calculations accounting for nuclei in the iron peak, with possibly more emphasis placed on the role of stellar abundance investigations.

The theoretical aspects of this chapter are largely in the nature of a review; a more complete (though less uptodate) version has already been given (Ellis 1972). Broadly speaking, the changes in the iron-peak theories are purely in the gradual removal of mathematical and physical assumptions introduced nearly 30 years ago. Using the high speed computer it is now possible to follow a time-dependent supernova calculation whereas earlier investigators resorted to various forms of statistical equilibrium.

9.2 Theories of nucleosynthesis

It will always be difficult for the observational astronomer to allow the existence of a 'cosmic abundance distribution' against which

nucleosynthesis theories can be tested. Even the author's results reveal abundance variations and uncertainties of a factor two, and the literature is full of even larger anomalies. There is therefore certainly no reason why the solar system abundances should be regarded as typically cosmic. It is nevertheless customary to separate the larger variations and say that, providing an explanation can be found for these, it seems evident that many stars in the Galactic disk do have solar abundances to within a factor 3 (Pagel 1968, 1974).

A unique form for the abundance curve suggests two possibilities. Either some or all of the elements were created together primordially, and were subsequently distributed in space to form galaxies and stars, or that the majority of the elements were synthesised in many sites spread over the universe e.g. stars. In the latter case the possible existence of a cosmic abundance distribution would suggest the processes and physical conditions in the sites have not varied a great deal.

The high abundance of hydrogen and its simple nuclear structure suggests it is the building block from which heavier elements are constructed. The necessary nuclear fusion can only occur at high temperatures and densities because of the Coulomb barrier to charged particles. Although such conditions may have occurred during the initial 'big-bang' it is now believed that only a few of the lightest nuclei can have been formed primordially. These theories, of historical interest only as far as the iron-peak is concerned, were collected by Alpher and Hermann (1953), and the problems are summarised by Peebles (1968).

In an attempt to overcome the problems associated with the above theories, Wagoner et al (1967) suggested supermassive objects ($\sim 10^6$ $M_\odot$) when exploding in 'little bands' would reach very high temperatures long enough for synthesis of iron group elements. Fowler (1968) later showed that the form of the abundance curve so produced is quite different from that observed and that most heavy elements are produced to only 1% of their solar abundances. Nevertheless, provided such

objects can have existed, this is of interest because it corresponds to the metal content of the oldest Population II objects in the Galaxy.

The stellar theory of nucleosynthesis was developed by Hoyle and others (Hoyle 1946, 1954, Burbidge et al 1957 hereafter B^2FH). The mass of a nucleus is less than that of its constituent nucleons and the binding energy per nucleon rises rapidly with increasing atomic weight A, peaks at A = 56, and then declines gradually (see Tayler 1972 p.68). This partially explains the existence of the iron peak as a region of high stability. It also means that all fusion reactions up to here will be exoergic.

B^2FH proposed that all elements are synthesised during various evolutionary stages in stellar interiors, and are ejected by mechanisms such as mass loss, supernovae etc. The interstellar medium is then enriched with heavy elements which are present in the atmospheres of subsequent stellar generations. A total of 8 distinct processes were invoked, forming a chain reaction. Each process ends when its fuel supply in the core is depleted. The star collapses igniting the next fuel, though previous fuels may continue to burn in shells surrounding the core. The iron-peak was attributed to an e(for equilibrium) process occurring during a final supernova stage of the star's evolution.

Although it has been necessary to modify several of these processes, the basic framework is still the same. Of particular importance for subsequent discussion was the discovery by Cameron (1959ab) that C^{12} and O^{16} could ignite by fusion reactions at temperatures of 10^9 K. Under normal hydrostatic conditions, C & O-burning do not produce enough of the elements in the mass range $20 \leqslant A \leqslant 32$ and the relevance of Cameron's discovery was not realised until several years later. During a supernova explosion C^{12} and O^{16} will be subjected to far higher temperatures, either as products of helium burning in a degenerate core, or in the envelope of a highly evolved star as a shock wave passes. This explosive burning of carbon and oxygen gives satisfactory agreement with the observed abundances for most isotopes in the mass range $12 \leqslant A \leqslant 40$ but of greater importance for this chapter, it has prompted similar explosive calculations for Si^{28}.

9.3 The approach to nuclear statistical equilibrium

At sufficiently high temperatures and densities, reactions will become as likely as their inverses and if such an equilibrium can be attained the resulting abundances can be calculated without using any reaction rates. The earliest application of such a statistical equilibrium was in the primordial theories discussed earlier (Klein et al 1947). The first application in a stellar interior, during a high temperature phase was made by Hoyle (1946, 1954).

In a true equilibrium between all species the final abundances are described by the temperature T and the density ρ. By restricting the equilibrium to the exchange of protons(p) and neutrons(n) between heavier elements, B^{2}FH attributed the iron-peak to such an e-process. In this case the p/n ratio is regarded as a constant parameter, written now in the form of a neutron excess η

$$\eta = (n + p) / (n - p) \qquad (9.1)$$

At $T_9 = 3.73$ (the notation X_n indicates X in units of 10^n) and $\eta = 0.07$, B^{2}FH found the predicted abundances agreed with the preliminary solar abundances of Goldberg et al (1960) to within a factor 2 in the mass range $50 \leqslant A \leqslant 62$. Outside this range the e-process abundances fall short of the observed values and other processes were invoked.

In later calculations (Cameron 1963, Clifford and Tayler 1965) the nature of the equilibrium was carefully reconsidered. A true equilibrium cannot be established because of the significant neutrino energy loss at such high temperatures. Nevertheless if the time-scale of this phase is long enough for a crude balance between decays and inverse decays, a quasi-equilibrium(QE) is possible. Although the arithmetic becomes slightly more involved, detailed reaction networks can still be avoided and by virtue of its simplicity QE calculations

are still favoured today by several investigators (Michaud and Fowler 1972).

The possible criticism of the QE approximation as used by Clifford and Tayler lies with the discovery by Stothers and Chiu (1962) that the maximum stellar timescale permitted at these temperatures is only 0.3 years. Would this be long enough for establishing QE? Calculations by Gilbert et al (1966, 1968) revealed that a more realistic approach would be to allow partial processing of seed nuclei. This technique of 'incomplete burning' has been performed by Bodansky et al (1968) with Si^{28}. They refer to their QE as 'Si-burning QE' though this is perhaps a misnomer as (unlike C & O) Si cannot burn by fusion reactions because of the large Coulomb barrier. At high temperatures it is photodissociated and rearranged to form heavier nuclei in the mass range $23 \leqslant A \leqslant 62$.

Viz: $2Si^{28} \rightarrow Si^{28} + 7\alpha \rightarrow Ni^{56}$

Bodansky et al found good agreement with observations provided only 35% of the Si^{28} was processed. This arbitrary freezing of the QE allows for any timescale problems as the star expands and cools during the supernova explosion. It also effectively introduces a fourth free parameter. It was realised at the time that a more accurate description would be to calculate the reaction network at every instant thus accounting for different reactions freezing out at different instants.

Such rigorous 'explosive' calculations have only been possible with the recent measurements of many heavy nuclei reaction rates mainly by Fowler and his crew (Fowler 1974). A fast large-storage computer is another essential for these calculations. They will eventually provide the most accurate solutions though, unlike the equilibrium methods, they rely on models of evolved objects (Arnett 1969b) which are presently not very well defined. Thus in some ways QE

calculations may be more realistic at the moment.

The first explosive calculations were performed by Arnett and Truran (1969) and Arnett et al (1971). It is generally assumed that the expansion in the explosion is adiabatic in which case the temperature and density at any instant are given by:

$$\rho(t) = \rho_i \exp(-t/\tau_{hd})$$
$$T(t) = T_i (\rho(t)/\rho_i)^{1/3} \qquad (9.2)$$

where $\tau_{hd} = \chi' \rho_i^{-1/2}$ is the hydrodynamical timescale which can be ajusted using a scale-factor χ'. Subscripts i refer to initial values.

Calculations have been performed with regions of pure C^{12}, O^{16} and Si^{28} and the results are summarised by Arnett (1973). Explosive C-burning produces good agreement for the mass range $12 \lesssim A \lesssim 28$, though in the heavier region $28 \lesssim A \lesssim 62$ it is necessary to combine the results of separate burnings of O^{16} and Si^{28}. In this case the number of free parameters is greatly increased and good agreement is encouraging yet not particularly remarkable.

A major difficulty in synthesing the iron-peak is that all explosive burnings give a peak at Ni^{56} instead of at Fe^{56}. The important isotopes Ca^{44}, Ti^{48} and Fe^{56} are also seriously underproduced. On the other hand the old equilibrium calculations match Fe^{56} quite well but fail in the region $28 \lesssim A \lesssim 44$. For these reasons it has now become fashionable to invoke both processes, attributing the e-process (or its equivalent) to a pre-supernova stage, and the explosive Si-burning to the actual event. Table 9.1 gives the parameters used in the most recent calculations (Woosley et al 1974) which accounts for nearly all isotopes in the mass range $28 \lesssim A \lesssim 62$ to within a factor 3.

Table 9.1

Parameters for origin of the nuclei

$28 \leqslant A \leqslant 62$ (Woosley *et al* 1974)

Process	T_9	ρ_5	X
Explosive O^{16}	3.6	2	1.00
Explosive Si^{28}	4.7	200	4.45
e-process(complete)	5.5	200	4.45

Notes:

Col 1: Processes are combined to account for all nuclei.

Col 3: Densities in cgs

Col 4: Timescale according to

$$\tau_{hd} = 446 X e^{-\frac{1}{2}} \text{ secs}$$

All processes have a neutron excess of 0.002

All values are initial starting values.

An important feature of all the nucleosynthesis calculations is the sensitivity of the final results on η. Evidence for the consistency of the explosive theories is provided by the constant value of η = 0.002 required for matching the results of C,O and Si-burning with the solar system abundances. The neutron excess in a typical observed composition is determined mainly by the isotopes of C, N, and O, which in a second generation star are produced by H-burning in the 'CNO-bi-cycle' (Tayler 1972 p. 34). For a Population I object the resulting excess is quite close to 0.002 implying that the 'father stars' of the solar-system material were Population I objects. In older stars η would be much less and so one would expect the abundance of certain n-rich nuclei e.g. Na^{23} to be reduced; this is in fact observed (Oke and Greenstein 1966).

The justification of T_i and ρ_i on a stellar model is discussed in the next section. Apart from this, the most important problem concerning the origin of the iron peak is the reinstated e-process necessary to explain the high abundance of Fe^{56}. Arnett (1969a) suggested this might be avoided by a decay of the form

$$Ni^{56} \rightarrow Fe^{56} + \gamma$$

In the decay a characteristic gamma-ray spectrum would be radiated. Its detection both in individual objects (Clayton et al 1969) and in the universal background (Clayton and Woosley 1969) would place explosive nucleosynthesis on a firmer observational basis. Regarding possible time-scale difficulties connected with the e-process, Michaud and Fowler (1972) showed quasi-equilibrium might be possible if there is a prolonged pre-supernova central temperature in excess of $4.5\ 10^{9°}$K. The role of the equilibrium approximations is thus now uncertain. Yet the e-process is employed quite regularly even in most recent calculations. Heinebach (1972) has found good agreement with observations by combining many e-processes. Clayton and Woosley

(1969) obtain satisfactory results using a high η e-process ($\eta \sim 0.07$) though there is no observational backing for such a value.

The resulting picture is thus one of slight confusion. Initially the e-process was regarded as a 'poor man's' approach to explosive calculations, yet as these in turn fail to describe every feature observed in the iron-peak, the e-process has been reinvoked. Without adequate models of highly evolved stars however, it is not certain that calculations involving equilibrium or QE are physically realistic. As there are so many other experimental uncertainties, both in reaction rates and in observed abundances, it is perhaps foolhardy and premature to assign every discrepancy to deficiencies in the theory.

9.4 Supernova models

In this section the evolution of a massive star is described, and possible supernova mechanisms are discussed, though the emphasis is on heavy element production rather than on detailed stellar models.

The motivation of the studies of explosive nucleosynthesis was the discovery by Schwarzschild and Härm (1962) that at the end of H-burning in a low mass star, the core is a partially degenerate gas. Contraction raises the central temperature, and consequently any thermonuclear reaction rate increases enormously whereas the gas pressure remains more or less the same. This explosive condition is referred to as the 'Helium-flash' because the ignition of helium triggers off the explosion.

Helium is not a particularly energetic fuel, and the degeneracy may be removed after the flash, in which case the star returns to hydrostatic equilibrium. Degenerate cores of C^{12} and O^{16} may however give flashes that are sufficiently violent to disrupt the star (Arnett 1969b). The nucleosynthesis accompanying the explosion considerably exceeds that during the hydrostatic burning.

The stage at which a star blows up depends on the onset of

degeneracy in the core, which in turn depends on the core mass. Heavier stars will generally witness more forms of hydrostatic burning, though at each successive stage the evolution becomes more rapid because of increased neutrino losses. If the star is sufficiently massive to survive ignition of helium, C and O-burning, it will be able to burn Silicon, though the timescale at such temperatures renders hydrostatic calculations unrealistic. There cannot be a Si-flash incidentally as Si-burning is a disintegration procedure. A rise in temperature at the end of Si-burning is thought to lead to the destruction of iron-peak elements by reactions like:

$$Fe^{56} \rightarrow 13\,\alpha + 4n$$

These highly endoergic reactions require further temperature rises. The extraordinary luminosity of the supernova is then attributed to the neutrinos which, at such high temperatures, transport large amounts of energy to the outer layers blowing them off to expose the hot interior. The star disrupts, leaving perhaps a collapsing remnant.

This massive-supernova model (proposed by Fowler and Hoyle 1964) has several restrictions. Firstly if the core mass $M_c < 2M_\odot$ the star will not proceed this far along the evolutionary track. Arnett (1967ab) also points out that if $M_c > 4\ M_\odot$ neutrino deposition will be ineffective. The mean free path for electron-neutrino scattering in the high densities of such massive cores is two orders of magnitude less than the core radius. Such stars will continue to collapse after the endoergic reactions and may become black holes (about which one need say no more). Though this model requires $2 \leqslant M_c/M_\odot \leqslant 4$ it hardly restricts the total stellar mass at all.

During such explosions, nucleosynthesis can occur both in the core at the time of explosion, and also in the envelope where shock waves impose extremely high temperatures and densities for short periods

($\sim$ 1/100th sec.) (Colgate and White 1966). Detailed calculations by Truran (1969) show that the evolution of C,O shells is so fast that all the outer layers can be accurately represented by pure Si^{28}. The resulting abundances may then be almost as described by Woosley et al (1974).

Perhaps the greatest uncertainties in understanding Galactic element production are the masses of the objects involved, and the proportion of processed and unprocessed material ejected. If the central density exceeds 10^9 gm cm^{-3} Arnett and Truran (1969) found that an 'embarrassing overproduction' of iron-peak elements results, and they would restrict explosions to stars with total masses between 20 and 40 $M_\odot$. The fact that a star does not produce the correct mix of heavy elements does not however prevent it from doing so.

Another uncertainty in evolutionary calculations is the supernova frequency. As no-one has suggested a heavy element producer that is anywhere near as efficient as a supernova it may be useful to equate the solar share of ejected material with the heavy element fraction observed in the solar system. Allowing for unprocessed material (Arnett and Clayton 1970) gives:

$$M_{ej} \sim 0.35\, M_\odot / f_s \qquad (9.3)$$

$$\text{i.e.} \qquad f_s^{-1} \sim 3\, M_{ej} / M_\odot \quad \text{years} \qquad (9.4)$$

where f_s, the supernova frequency is at the moment regarded as time-independent; M_{ej} is the total ejected mass per event.

Observationally $f_s \sim 1/350\ yr^{-1}$ (Zwicky 1969), a figure based on 3 Galactic and 200 extragalactic events observed upto 1967. This implies an improbable 120 $M_\odot$ is ejected in each event, whereas a more realistic result of 9 - 17 $M_\odot$ corresponds to about one event every 25 - 50 years (Katgert and Oort 1967). Normally astronomers wouldn't

worry about a factor 3 but it is often suggested that the present rate of $1/50\ yr^{-1}$ is sufficient to account for the heavy element production (Tayler 1972). Zwicky and other observers feel particularly strongly however that the supernova frequency is considerably less, despite interstellar obscurration and difficulties detecting extragalactic events. It is probably that f_s was considerably higher in the past; this would then be consistent with the observations (Helfer 1969) that the oldest disk stars have near solar abundances, indicating that a sizeable proportion of the supernova processing occured in a short period after the origin of the Galaxy.

9.5 The role of stellar abundances

Predicted iron-peak abundances are conventionally compared with the observed abundances of Cameron (1963, 1974). These come from studies of meteoritic and lunar samples however, and therefore represent a very localised abundance distribution. Stellar and solar abundances are usually excluded in these tables for two reasons.

Firstly, uncertainties in f-values and spectral interpretations apparently render stellar abundances inadequate (Arnett 1973). This excuse is surely outdated. Figure 9.1 shows the remarkable change in the solar abundance of iron-group elements with respect to Cameron's values since 1960. The remaining differences are not significant as far as nucleosynthesis is concerned, and can partly be attributed to the inhomogeneity of the non-solar samples. This thesis has already shown that the abundance uncertainty in cooler stars in only twice that in the sun, and since a large part of this error is due to presently inadequate models, the prospect for greater accuracy is encouraging. For hotter stars with accurate angular diameters and realistic models, the main limitation is the uncertainty in the f-values which is rapidly decreasing.

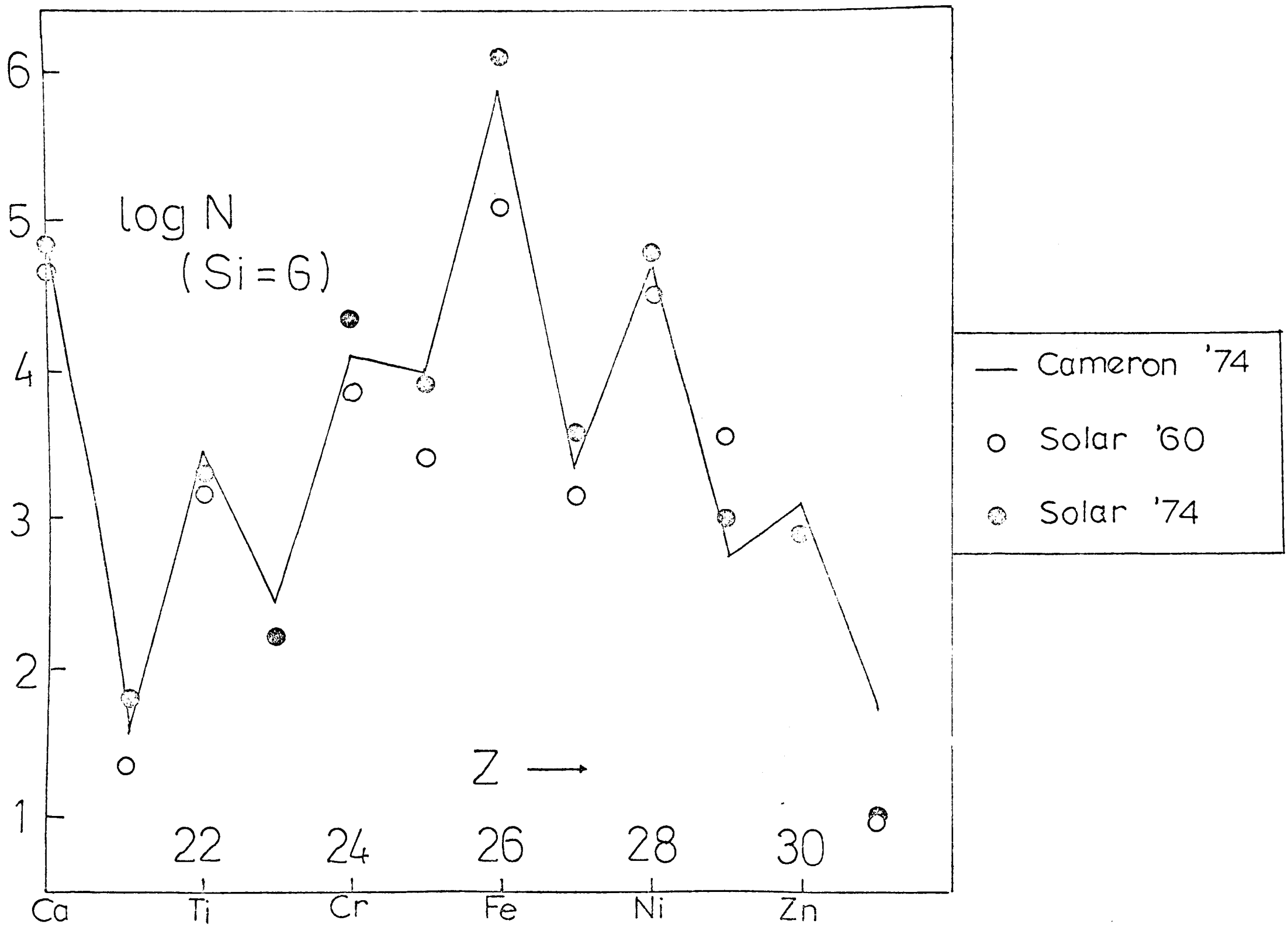

Figure 9.1 Revision of the solar iron-peak abundances

The second criticism of stellar abundances is that they fail to offer direct isotope ratios. Exciting developments are being made in millimetre-wave studies (Jefferts et al 1974) and cosmic ray astronomy (Cowsik and Price 1971), and reference has already been made to the use of gamma-ray investigations. Despite the alternative methods which are capable of producing isotopic abundances, spectroscopy utilises many other branches of stellar physics and by studying stellar structure and evolution it is possible to provide a firmer base for the nucleosynthesis theories.

Further information is derived from the abundance variations from one star to another. Variations of light element abundances are thought to be due to mixing of products synthesised locally, for example, by the CNO-cycle (Wallerstein 1968). Heavy element variations were originally attributed to poor observational interpretations (Unsöld 1969) though this hypothesis is now wearing a bit thin. There is little doubt for example, that the Arcturus/solar deficiencies are real. The variations can of course be attributed to time and spatial variations in the metal content of the inter-stellar medium (Talbot and Arnett 1970, Powell 1972).

Several distinct nuclear processes are needed to explain the solar-system abundances, though at present they can all occur in one evolved object. It may eventually be necessary to combine products from different objects, in which case the concept of a cosmic abundance distribution will need modification, and the spatial abundance variations discussed above will be of great interest. Observationally we should attack the abundance problem in as many ways as possible, though as stars are the major constituents of this Galaxy, thought to be the only significant nuclear processors, we must continue to investigate them as much as possible.

CHAPTER 10

CONCLUSIONS

Although narrow and intermediate-band photometry offer exciting prospects for rapid abundance investigations of many stars, detailed analyses are still important. There is an urgent need for a good cool standard star with which other cool stars can be quickly but accurately compared using simple differential techniques. Arcturus is a suitable choice and is of special interest because deviations from LTE might be expected in this giant. As f-values are rapidly becoming more reliable, it is perhaps time that abundances were determined by a line-by-line method rather than by assuming a single curve of growth. For standard stars it is particularly desirable that analyses be performed without recourse to solar measurements.

This absolute analysis of Arcturus, though preliminary in several aspects, brings to light many new problems and possibilities. For cool stars the greatest uncertainty at present is in the determination of parameters necessary for constructing model atmospheres. It is generally found that:

1) Angular diameter measurements are unlikely to achieve the accuracy necessary for determinations of T_e from the total flux. The only solution is to compare the relative energy distribution with a grid of model atmospheres. Other methods usually involve undesirable equilibrium assumptions.

2) Determinations of T_e from the shape of the flux curve are limited by the unrealistic nature of the available model atmospheres. Serious flux discrepancies below 5000Å are noted and are attributed to inaccurate opacities and possibly to an underestimation of line and band effects.

3) A reasonable estimate of T_e could come from the H^- bump at 1.6μ though earth-based measurements here are unreliable.

4) A good gravity-indicator for cool stars is badly needed. An indicator independent of abundance and equilibrium assumptions has been suggested (see 4.5c) and it is proposed that gravities of many late-type stars could be found this way.

5) Serious errors may result when using scaled models for investigating cool stellar atmospheres.

Oscillator strengths can now be measured accurately by several methods though few results are available for weak lines of astrophysical interest. The absorption method is possibly the best for relative measurements of such lines, and with the Oxford furnace a relative accuracy of $\pm$0.03dex(7%) is easily attained; using refinements it is possible to reduce this error to $\pm$0.01dex. Absolute scales are still too uncertain however, and more lifetime measurements for iron-group species are needed, particularly for the neutral atoms.

The solar Ti analysis has demonstrated the internal consistency of the Oxford f-values, and also shows how it is possible to avoid uncertainties in damping and microturbulence by restricting abundance work to weak lines carefully measured from low noise spectra. For cooler stars however, the increased noise level and decreased thermal broadening makes it essential to investigate the effects of microturbulence. This is unfortunate for there is little justification for the existence of this parameter, and its determination is not straightforward. For the case of Arcturus, in the final abundances, the source of the greatest error lies with T_e and g, thus emphasising the points made above. With an improved model an increased accuracy of $\pm$0.05dex in the absolute abundance will be possible.

The origin of the iron-peak is now fairly well understood in terms of explosive theories of nucleosynthesis, though the equilibrium processes have been re-introduced to account for otherwise unexplained features. The nuclear equilibrium has not been physically justified

however, and it is suggested that the discrepancies might relate to poor experimental data rather than to incomplete theories. Gamma ray investigations could be crucial in settling this problem.

Stellar analyses are soon likely to be regarded as 'old fashioned' because of exciting alternative methods for examining products of nucleosynthesis. Stellar abundances are vital however for studies of the structure and evolution of stars and galaxies. It is hoped that these Arcturus abundances will provide the necessary stepping-stone to a wealth of knowledge concerning cool stars.

Acknowledgements

I should like to express gratitude to my supervisor Professor Blackwell for help, advice and encouragement during the last 3 years. He has always provided time for discussing my problems and I have enjoyed this collaboration a great deal.

Thanks is also due to Mr. (shortly Dr.) P.G. Craven for stimulating discussions about many aspects of this work. In particular, he is responsible for leading me from the lost labyrinths of FORTRAN to the nirvana of Algol68.

Regarding the various instruments I have used, I thank Mr. R.B. Willis for helping with the Israeli measurements and Dr. P.A. Ibbetson for building electronic components for both the scanner and the furnace. I also thank members of the workshop for their devoted help, particularly Mr. Eric Adnams who stood by most capably when operating the furnace during the 3-day week.

In my computing I must thank both Oxford and London University computing laboratories for large allocations of time and store. The ATLAS runs would not have been possible without the help of Bob Carruthers and Dr. Jim Argyros.

Finally I would like to thank my wife for feeding the cats and washing up whilst this thesis was being written.

The work was supported by a grant from the Science Research Council and also by a Graduate Award from Wolfson College.

References

Alexander D.,Johnson H.R. 1973; Ap. J. 176, 629
Allen C.W. 1934; Comm. Sol. Phys. Obs. Mem. 5
Allen C.W. 1973; Astrophysical Quantities, Third Edition
Athlone Press(London)
Allen C.W.,Asaad A.S. 1957; M.N.R.A.S. 117, 36
Aller L.H. 1953; Atmospheres of Sun & Stars,First Edition
Ronald Press(New York)
Aller L.H. 1963; Atmospheres of Sun & Stars,Second Edition
Ronald Press(New York)
Alpher R.A.,Hermann R.C. 1953; Ann. Rev. Nucl. Sci. 2, 1
Andersen T.,Roberts J.,Sørenson G. 1973; Ap. J. 181, 567
Arnett W.D. 1967a; Canadn.Jrnl. Phys. 45, 1621
Arnett W.D. 1967b; Canadn.Jrnl. Phys. 45, 2953
Arnett W.D. 1969a; Ap. J. 157, 1369
Arnett W.D. 1969b; Astrophys. Space Sci. 5, 180
Arnett W.D. 1973; Ann. Rev. Astron. Astrophys. 11,
Arnett W.D.,Clayton D.D. 1970; Nature 227, 780
Arnett W.D.,Truran J.W. 1969; Ap. J. 157, 339
Arnett W.D.,Truran J.W.,Woosley S.E. 1971; Ap. J. 165, 87
Auman J. 1967; Ap. J. Suppl. 14, 171
Auman J. 1969a; Ap. J. 157, 799
Auman J. 1969b; Low Luminosity Stars(ed. Kumar),p483
Gordon & Breach(New York)
Avrett E.H.,Krook M. 1963; Ap. J. 137, 874
Bahner K. 1963; Ap. J. 138, 1314
Bashkin S. 1964; Nuclear Instr. Methods 28, 88
Bashkin S. 1968; Proceedings First Conference Beam-Foil
Spectroscopy, Tucson,Arizona 1967
Gordon & Breach(New York)
Bashkin S. 1974; Proceedings Third Conference Beam-Foil
Spectroscopy, Tucson, Arizona 1972
Gordon & Breach(New York), in print.

Bates D.R.,Damgaard A. 1949; Phil. Trans. Roy. Soc.(Ser A) 242, 101

Bell G.D.,Davis M.H.,King R.B.,Routley P.B. 1958; Ap. J. 127, 775

Bell G.D., Tubbs E.F. 1970; Ap. J. 159, 1093

Bell R.A. 1972; M.N.R.A.S. 159, 349

Bennett W.R.jr. 1961; Advances in Quantum Mechanics(ed. Singer) p28, Columbia Univ. Press(New York)

Bethe H.A.,Salpeter E.E. 1957; Handbuch der Physik(ed. Flugge) p88, Springer-Verlag(Berlin)

Biermann R. 1948; Zeit. f. Ap. 25, 135

Blackwell D.E.,Calamai G.,Willis R.B. 1972; M.N.R.A.S. 160, 121

Blackwell D.E.,Collins B.S. 1972; M.N.R.A.S. 157,255

Blackwell D.E.,Ibbetson P.A.,Petford A.D. 1974a; M.N.R.A.S.(in preparation)

Blackwell D.E.,Petford A.D.,Mallia E.A. 1967; M.N.R.A.S. 136, 365

Blackwell D.E.,Petford A.D.,Collins B.S.,Ibbetson P.A.,Mallia E.A.,Smith G.,Emerson D. 1971; Solar.Physics 19, 264

Bodansky D.,Clayton D.D.,Fowler W.A. 1968; Ap.J. Suppl. 16, 299

Boni 1968; J.Q.S.R.T. 8, 1385

Boyarchuk M.E.,Boyarchuk A.A. 1960; Izv. Krymskoi Astrof. Observ. 22, 234

Brossel J.,Bitter 1952; Phys. Rev. 86, 308

Burbidge E.M.,Burbidge G.,Fowler W.A.,Hoyle F. 1957; Reviews Mod. Phys. 29, 547 ("B^2FH")

Cameron A.G.W. 1959a; Ap. J. 130, 429

Cameron A.G.W. 1959b; Ap. J. 130, 895

Cameron A.G.W. 1963; Nuclear Astrophysics (Yale University)

Cameron A.G.W. 1968; Origin & Distribution of the Elements (ed. Ahrens) p125, Pergamon Press(London)

Cameron A.G.W. 1974; Space Sci. Rev. 15, 121

Carbon D. 1974; Ap. J. 187, 135

Carbon D.,Gingerich O. 1969; Theory and Observation of Normal Stellar Atmospheres,(ed. Gingerich), p377, MIT Press(Mass.)

Carbon D.,Gingerich O.,Latham D.W. 1969; Low Luminosity Stars(ed.Kulmar),p435,Gordon & Breach(NY).

Carnahan B.,Luther H.A.,Wilkes J.O.1969; Applied Numer. Methods,p240,Wiley & Son(New York)

Cayrel G.,Cayrel R.1963; Ap. J. 137, 431

Chandrasekhar S. 1936; M.N.R.A.S. 96, 21

Chandrasekhar S. 1950; Radiative Transfer,Oxford University Press(Oxford)

Channappa 1965; Proc. Phys. Soc. 86, 1145

Clayton D.D.,Colgate S.A.,Fishman G.J.1969; Ap. J. 155, 75

Clayton D.D.,Woosley S. 1969; Ap. J. 157, 1381

Clifford F.E.,Tayler R.J. 1965; Memoirs R.A.S. 69, 21

Colgate S.A.,White R.H. 1966; Ap. J. 143, 626

Collins B.S. 1970; Thesis, University of Oxford,England

Collins B.S.,Blackwell D.E.,Petford A.D. 1970; Applied Optics 9, 1606

Connes P.,Connes J.,Montgomery E.F.,Edmonds F.N.jr. 1969; Ap. J. Suppl. 19, 1

Conti P.S.,Greenstein J.L.,Spinrad H.,Wallerstein G,Vardya M.S. 1967; Ap. J. 148, 165

Corliss C.H.,Bozman W.R.1962; NBS Monograph Number 53

Corney A. 1970; Adv.Electr. Elec. Phys. 29, 115

Cowley C.R.,Elste G.H.,Allen R.H.1969; Ap. J. 158, 1177

Cowsik R.,Price P.B. 1971; Physics Today 24, 30

Cox J.P.,Guili R.T. 1968; Principles of Stellar Structure, Gordon & Breach(New York)

Crossley R.J.S. 1969; Adv. Atomic. Mol. Phys. 5, 237

Czerny M, Turner A.F. 1930; Zeit. f. Phys. 61, 792

Dalgarno A. 1962; private communication to Gingerich(1964)

Dalgarno A.,Williams D.A. 1962; Ap. J. 136, 690

Darius J. 1974; private communication

Delbouille L.,Neven L.,Roland G. 1973; Photometric Atlas

of the Solar Spectrum(Liege University)
Demstroder W. 1962; Zeit. f. Phys. 166, 42
Deridder G.,Rensbergen W. 1974; Solar Physics 34, 77
Edmonds F.N.jr. 1973; P.A.S.P. 85, 24
Eggen O.J. 1971; P.A.S.P. 83, 271
Eggen O.J.,Lyndon-Belle D.,Sandage A.R. 1962; Ap. J. 136, 748
Ellis R.S. 1972; Johnson Memorial Essay, University of Oxford
Elste G. 1968; Solar Physics 3, 106
Faulkner D.J.,Cannon R.D. 1973; Ap. J. 80, 435
Faÿ T.,Johnson H.R. 1973; Ap. J. 181, 851
Foster E.W. 1964; Rep. Prog. Phys. 27, 469
Fowler J.W. 1974; Ap. J. 188, 295
Fowler W.A. 1968; Origin & Distribution of Elements(ed. Ahrens),p3, Pergamon Press(London)
Fowler W.A. 1974; Q.J.R.A.S. 15, 82
Fowler W.A.,Hoyle F. 1964; Ap. J. Suppl. 9, 201
Foy R. 1972; Astron. Astrophys. 18, 26
Fromm 1966; Physics Fluids 9, 828
Garstang R.H. 1955; Vistas in Astronomy(ed.Beer), Volume 1, Pergamon Press(London)
Garz T.,Holweger H.,Kock M.,Richter J. 1969; Astron. Astrophys. 2, 446
Garz T.,Kock M. 1969; Astron. Astrophys. 2, 274
Gasson R. 1966; Thesis, University of Cambridge,England
Gehrz R.D.,Woolf N.J. 1971; Ap. J. 165, 285
Gezari D.Y.,Labeyrie A.,Stachnik R.V. 1973; Ap. J. Lett. 173, L1
Gilbert A.,Truran J.W.,Cameron A.G.W. 1966; Canadn. Jrnl. Phys. 44, 151
Gilbert A.,Truran J.W.,Cameron A.G.W. 1968; Nucleosynthesis, Gordon & Breach(New York)
Gillett F.C.,Low F.J.,Stein W.A. 1968; Ap. J. 154, 677
Gillett F.C.,Merrill K.M.,Stein W.A. 1971; Ap. J. 164, 83

Gingerich O. 1961; Thesis, University of Harvard, USA
Gingerich O. 1964; Proceedings First Harvard-Smithsonian Conference on Stellar Atmospheres(1963) S.A.O. Special Report No. 167
Gingerich O.,de Jager C. 1968; Solar Physics 3, 5
Gingerich O.,Noyes R.W.,Kalkofen W.,Cuny Y. 1971; Solar Physics 18, 347
Gleballe T.R.,Wollman E.R.,Rank D.M. 1972; Ap. J. Lett. 177, L27
Glebocki R. 1972; Acta Astron. 22, 141
Goldberg L.,Müller E.A.,Aller L.H. 1960; Ap. J. Suppl. 5,1
Gottlieb D.M.,Bell R.A. 1969; Astron. Astrophys. 19, 434
Grasdalen G.L.,Huber M.,Parkinson W.H. 1968; Harvard Coll. Obs. Shock Tube Sp. Lab. Report No. 27
Greene T.F. 1970; Ap. J. 161, 365
Grevesse N. 1970; Memoires Soc. Roy. Sci. Liège 39, 1
Griffin R.,Griffin R.F. 1967; M.N.R.A.S. 137, 253
Griffin R.F. 1964; M.N.R.A.S. 128, 187
Griffin R.F. 1968; A Photometric Atlas of the Spectrum of Arcturus, Cambridge Phil. Soc. (Cambridge)
Griffin R.F. 1969a; M.N.R.A.S. 143, 319
Griffin R.F. 1969b; M.N.R.A.S. 143, 349
Griffin R.F. 1969c; M.N.R.A.S. 143, 361
Griffin R.F.,Redman R.O. 1960; M.N.R.A.S. 120, 287
Gurtovenko E.A.,Fedorenko L.U. 1969; Solar Physics 6, 465
Hanbury-Brown R.,Davis J.,Lake R.J.W.,Thompson R.J. 1974; M.N.R.A.S. 167, 475
Harris D.L.III,Strand K.A.,Worley C.E. 1963; Stars & Stellar Systems Vol 3 p273, Chicago Press
Hayes D.S. 1970; Ap. J. 159, 165
Hefferlin R. 1960; Ap. J. 132, 259
Heinebach K. 1972; Thesis, Rice University, Texas USA
van der Held E.F.M. 1931; Zeit. f. Phys. 130, 100
Helfer H.L. 1969; Astron. J. 74, 1155

Helfer H.L.,Wallerstein G. 1968; Ap. J. Suppl. 16, 1
Heron S.,McWhirter R.W.P.,Rhoderick E.H. 1956; Proc. Roy. Soc. London A234, 565
Hese A. 1972; Zeit. Naturforsch 27a, 188
Hickock F.R.,Morton D. 1968; Ap. J. 152, 203
Holweger H. 1971; private communication
Holzberlein T.M. 1964; Rev. Sci. Instr. 35, 1041
Hoyle F. 1946; M.N.R.A.S. 106, 354
Hoyle F. 1954; Ap. J. Suppl. 1, 121
Hoyle F.,Wickramasinghe N.C. 1962; M.N.R.A.S. 124, 417
Iben I. 1967; Ann. Rev. Astron. Astrophys. 4,193
Jeffert K.B.,Penzias A.A.,Wilson R.W. 1974; in preparation
Johnson H.L. 1962; Ap. J. 135, 303
Johnson H.L. 1963; Ap. J. 136, 1135
Johnson H.L. 1964; Bol. Obs. Ton. y Tacubaya 3, 305
Johnson H.L. 1965; Ap. J. 141, 940
Johnson H.L. 1968; Stars & Stellar Systems 7, 167 (Chicago)
Johnson H.L.,Mendez M.E. 1970; Astron. J. 75, 785
Johnson H.L.,Mitchell R.I.,Iriate B.,Wisniewski W.Z. 1966; Lunar Plan. Lab. Commun. 4, 99
Johnson H.L.,Mitchell R.I.,Latham A.B. 1967; Lunar Plan. Lab. Commun. 6, 85
Johnson H. R. 1973; Ap. J. 180, 81
Jones O.C. 1964; Jnl. Sci. Instr. 41, 653
Karsas W.J.,Latter R. 1961; Ap. J. Suppl. 6, 167
Katgert P.,Oort J.H. 1967; Bull. Astron. Inst. Neth. 19, 239
Keenan P.G.,Morgan W.W. 1951; Astrophysics(ed. Hynek), p12 McGraw-Hill(New York)
Kharitonov A.V.,Knyazeva L.N. 1969; Soviet A.J. 11, 598
King A.S.,King R.B. 1935; Ap. J. 82, 377
King A.S.,King R.B. 1938; Ap. J. 87, 24
King I. 1952; Ap. J. 115, 580
Klein O.,Beskov F.,Treffenberg L. 1947; Arkiv. Mat. Astron. Fysik 34a, 13

Klemt O. 1973; Astron. Astrophys. 29, 419
Komarov N.S.,Pozigun V.A. 1970; Soviet A.J. 14, 440
Kopfermann H.,Wessel G. 1951; Zeit. f. Phys. 130, 100
Kuhn H.G.,Vaughan J.M. 1963; Proc. Roy. Soc. London A277, 297
Kuiper G.P. 1938; Ap. J. 88, 429
Kurucz R.L. 1969; Ap. J. 156, 235
Kurucz R.L. 1970; S.A.O. Special Report 309 (ATLAS)
Kurucz R.L. 1974; Solar Physics 34, 17
Labs D.,Neckel H., 1967; Zeit. f. Ap. 65, 133
Labs D.,Neckel H. 1970; Solar Physics 15, 79
Lambert D.L.,Pagel B.E.J. 1968; M.N.R.A.S. 141, 299
Laporte O.,Wilkerson T.D. 1960; J.O.S.A. 50, 1293
Lawrence G.M. 1965; J.Q.S.R.T. 5, 359
Lee R.D. 1969; NBS Technical Report No. 483, p1
Linsky J.,Ayres T. 1973; Ap. J. 180, 473
Many 1946; Phys. Rev. 70, 511
Martinson I. 1970; Proceedings Second Conference Beam foil Spectroscopy,Lysekil Sweden 1970, North Holland Publishing Co.
McLure R.D. 1973; I.A.U. Symposium 50, 163
Menzel D.H. 1936; Ap. J. 84, 462
Michaud G.,Fowler W.A. 1972; Ap. J. 173, 157
Michelson A.A., Pease F.G. 1921; Ap. J. 53, 249
Mihalas D. 1966; Ap. J. Suppl. 13, 1
Mihalas D. 1969; Methods in Computational Physics 7, 1
Mihalas D. 1970; Stellar Atmospheres, Freeman & Co.(New York)
Mihalas D.,Auer L.H. 1972; Kitt Peak Contributions 555
Miles B.M.,Wiese W.L. 1970; NBS Special Publication 320
Mitchell A.C.G.,Zemansky M.W. 1961; Resonance Radiation & Excited Atoms, Cambridge Univ.Press(London)
Mitchell R.I.,Johnson H.L. 1969; Lunar Pl.Lab. Comm. 8, 1
Mitrofanova L.S. 1952; Izv. Pulkova Observ. 19, 149
Moore C.E. 1949; Atomic Energy Levels Vol I, NBS Circular 467

Moore C.E.,Minnaert M.G.J.,Houtgast J. 1966; The Solar Spectrum, NBS Monograph 61

Morgan T. 1970; Thesis, University of Indiana,USA

Morgan W.W., Keenan P.C. 1973; Ann. Rev. Astron. Astrophys. 11, 29

Morozova N.G.,Startsev G.P. 1964; Opt. i. Spek. USSR, 17, 174

Morton D.,Mihalas D. 1965; Ap. J. 142, 253

Müller E.A.,Bashek B.,Holweger H. 1968; Solar Physics 3, 125

Müller E.A.,Mutschlecner J.P. 1964; Ap. J. Suppl. 9, 1

Münch G. 1946; Ap. J. 104, 87

Münch G, Unsöld A. 1962; Ap. J. 135, 711

Mutschlecner J.P.,Keller C. 1970; Solar Physics 14, 294

Mutschlecner J.P.,Keller C. 1972; Solar Physics 22, 70

Natta A.,Ranieri M. 1972; Astroph. Space Sci. 17, 390

Naqvi 1964; J.Q.S.R.T. 4, 597

Nesmayanov A.N. 1963; Vapour Pressure of Elements, Publ. No. USSR, Infosearch London

Neckel T. 1967; Landessternewarte Heidelberg-Konigstübe Veroffentlichungen 19, 1

Noyes R.W., Kalkofen W. 1970; Solar Physics 15, 120

Oke J.B. 1965; Ap. J. 140, 689

Oke J.B.,Greenstein J.L. 1966; I.A.U. Symposium 26, 348

Oke J.B.,Schild R.E. 1970; Ap. J. 161, 1015

Osborn W. 1973; I.A.U. Symposium 50, 176

Ostrovsky Y.I.,Parchevskii G.P.,Penkin N.P. 1956; Opt. i. Spek. 1, 821

Ostrovsky Y.I.,Penkin N.P. 1957; Optical Transition Probabilities,Israel Translation Prog. Sci. 1, 332

Pagel B.E.J. 1964; Roy. Obs. Bull. 55

Pagel B.E.J. 1968; Q.J.R.A.S. 9, 401

Pagel B.E.J. 1972; Observatory 92, 240

Pagel B.E.J. 1974; Space Sci. Rev. 15, 1

Pagel B.E.J.,Tomkin J. 1969; Q.J.R.A.S. 10, 194
van Paradijs J. 1974;Conference on Origin & Distribution of Elements,Cambridge England 1974,(in print)
Parkinson W.H.,Reeves E.M. 1970; Solar Physics 10, 342
Peach J. 1966; Thesis, University of Oxford, England
Peach J. 1969; M.N.R.A.S. 144, 171
Pease F.G. 1931; Erg. d. exakte Naturwissenschaft 10, 84
Pecker J.C. 1959; Ann. d'Ap. 22, 594
Peebles P.J.E. 1968; Origin & Distribution of Elements (ed. Ahrens), Pergamon Press(London)
Peytremann E. 1974; Astron. Astrophys. 33, 203
Peytremann E.,Avrett E.H. 1974; in preparation(see Peytremann 1974)
Peytremann E.,Parson S.B. 1973; Ap. J. 180, 71
Pierce J. 1969; private communication
Powell A.L.T. 1972; M.N.R.A.S. 155, 483
Prokof'ev V.K. 1969; Izv. Krymskoi Astrof. Observ. 39, 1 English transl. from National Lending Library, Boston Spa,Yorks. England,(ref. RTS 7072)
Querci J.,Querci M.,Kunde V. 1971; Astron. Astrophys. 15, 256
Reinke P. 1967; Zeit. f. Ap. 66, 234
Rohrlich P. 1948; Phys. Rev. 74, 1381
Roman N.G. 1955; Ap. J. Suppl. 2, 198
Rozhdestvenskii D. 1912; Ann. Phys. Leipzig 39, 307
Schild R.E. 1971; Ap. J. 166, 95
Schwarzschild D.,Harm R. 1962; Ap. J. 136 ,158
Siddall J. 1969; Thesis, University of Oxford, England
Simon T. 1971; P.A.S.P. 83, 607
Solomon P.M.,Stein W. 1966; Ap. J. 144, 825
Somerville W.B. 1964; Ap. J. 139, 192
Spinrad H.,Taylor B.J. 1969; Ap. J. 157, 1279
Spinrad H.,Wing R. 1969; Ann. Rev. Astron. Astrophys. 7, 249
Spinrad H.,Wing R. 1970; Ap. J. 159, 973

Stebbins J.,Huffer C.M.,Whitford A.E. 1940; Ap. J. 92, 193
van Stekelenburg L.H.M. 1948; Physica 14, 169
Stewart , Rotenberg 1965; Phys. Rev. 140, A1508
Stickland D.J. 1970; Observatory 90, 206
Stickland D.J. 1971; M.N.R.A.S. 153, 501
Stothers R.,Chiu H.Y. 1962; Ap. J. 135, 963
Strom S.E.,Kurucz R.L. 1966; J.Q.S.R.T. 6, 591
Strømgren B. 1973; I.A.U. Symposium 50, 141
Suess H.E.,Urey H.G. 1956; Rev. Mod. Phys. 28, 58
Takens R.J. 1970; Astron. Astrophys. 5, 244
Talbot R.,Arnett W.D. 1970; Ap. J. 170, 409
Tatum J.B. 1961a; M.N.R.A.S. 122, 311
Tatum J.B. 1961b; Commun. Univ. London Obs. 41
Tayler R.J. 1972; Origin of the Chemical Elements,
Wykenham Science Series
Tomley L.J.,Wallerstein G.,Wolff S.G. 1970; Astron. Astrophys 9, 384
Travis L.D.,Matsushima S. 1968; Ap. J. 154, 689
Truran J.W. 1969; Supernova Conference Proceedings, p117
Gordon & Breach(New York)
Truran J.W. 1972; Proceedings of Conference Red Giants,
Bloomington Ind.(to be published)
Underhill A. 1972; Vistas in Astronomy(ed.Beer),Vol. 13, 169
Pergamon Press(London)
Unsöld A. 1955; Physik der Sternatmospharen,Springer(Berlin)
Unsöld A. 1968; The New Cosmos, Heidelberg Press
Unsöld A. 1969; Science 165, 1015
Upson W.L. II 1973; Thesis, University of Maryland,USA
Vardya M.S. 1970; Ann. Rev. Astron. Astrophys. 8, 87
Wagoner R.V.,Fowler W.A.,Hoyle F. 1967; Ap. J. 148, 3
Walker R.G. 1969; Phil.Trans. Royal Soc.(Ser. A) 264, 209
Wallerstein G. 1968; Science 162, 625

Warner B. 1968; M.N.R.A.S. 138, 143
Warren P.R. 1970; Thesis, University of Cambridge,England
Wegner G. 1974; in preparation
Whaling W.,King R.B.,Martinez-Garcia M. 1969; Ap. J. 158, 389
Wickramasinghe N.C. 1967; Interstellar Grains, Chapman & Hall(London)
Williams P.M. 1970; Thesis, University of Cambridge,England
Williams P.M. 1971a; M.N.R.A.S. 153, 171
Williams P.M. 1971b; M.N.R.A.S. 155, 215
Williams P.M. 1972; M.N.R.A.S. 158, 361
Willis R.B. 1975?; Thesis in preparation,University of Oxford, England
Willstrop R.V. 1965; Memoirs R.A.S. 69, 83
Wilson O.C.,Bappu M.K.V. 1957; Ap. J. 125, 661
Wolnik S.J.,Berthel R.O. 1973; Ap. J. 179, 665
Woodward P.M., Bond S.G. 1972; Algol 68-R Users Guide, HMSO
Woolley R.v.d.R.,Epps E.A.,Penston M.J.,Pockock S.B. 1970; Royal Obs. Ann. 5
Woolley R.v.d.R.,Stibbs D.W.N. 1953; Outer Layers of a Star, Oxford Univ. Press(Oxford)
Woolff N.J.,Ney E.P. 1968; Ap. J. Lett. 155, L18
Woosley S.E.,Arnett W.D.,Clayton D.D. 1974; Ap. J. Suppl. 26, 231
Worrall G.,Wilson A.M. 1972; Nature 236, 15
Yamashita Y. 1962; P.A.S.J. 14, 390
Ziock K. 1957; Zeit. f. Phys. 147, 99
Zwicky F. 1969; Supernova Conference Proceedings,p1 Gordon & Breach(New York)